A fluorescence microscopy image showing several organoids. The organoids are composed of numerous cells, each stained with different fluorescent dyes, resulting in a variety of colors including blue, green, yellow, orange, and red. The organoids are arranged in a somewhat vertical, descending pattern from the top left towards the bottom right. The background is black, making the colorful cells stand out.

CONSTRUCTING
ROADMAPS
TOWARDS
FUNCTIONAL
CELL TYPES
USING
ORGANOIDS

.....

JOEP BEUMER

CONSTRUCTING ROADMAPS TOWARDS FUNCTIONAL CELL TYPES USING ORGANIDS

Shaping and changing the functions of the intestine

Joep Beumer

ISBN: 978-94-93197-02-2

Author: Joep Beumer

Cover: Joep Beumer

Printed by: Off Page, Amsterdam

The research described in this thesis was performed at the Hubrecht Institute, Utrecht, The Netherlands, in the lab of Prof. Dr. Hans Clevers.

© All rights reserved. No part of this thesis may be reproduced, stored or transmitted in any form by any means without prior permission of the author. The copyright of the publications remains with the publishers.

Printing of this thesis was financially supported by U-Protein Express, Sanbio, Stemcell Technologies and Peprotech.

**CONSTRUCTING ROADMAPS TOWARDS FUNCTIONAL
CELL TYPES USING ORGANOID**

Shaping and changing the functions of the intestine

**RECONSTRUEREN VAN DE WEG NAAR FUNCTIONELE
CELTYPEN MET BEHULP VAN ORGANOÏDEN**

De vorming en het aanpassen van de diverse functies van de darm

(met een samenvatting in het Nederlands)

Proefschrift

ter verkrijging van de graad van doctor aan de
Universiteit Utrecht
op gezag van de
rector magnificus, prof.dr. H.R.B.M. Kummeling,
ingevolge het besluit van het college voor promoties
in het openbaar te verdedigen op

donderdag 10 september 2020 des ochtends te 9.15 uur

door

Joep Beumer
geboren op 3 oktober 1992
te Ommen

PROMOTOR

Prof. dr. J.C. Clevers

TABLE OF CONTENTS

Scope of the thesis		7
Chapter 1	Regulation and plasticity of intestinal stem cells during homeostasis and regeneration	13
Chapter 2	New concepts in enteroendocrine cell biology	41
Chapter 3	Induced quiescence of Lgr5+ stem cells in intestinal organoids enables differentiation of hormone-producing enteroendocrine cells	59
Chapter 4	Enteroendocrine cells switch hormone expression along the crypt-to-villus BMP signaling gradient	99
Chapter 5	Specialization of human goblet cells and enterocytes along the crypt-villus axis	125
Chapter 6	High resolution mRNA and secretome atlas of human enteroendocrine cells	141
Chapter 7	Snake venom gland organoids	189
Chapter 8	Summarizing discussion	237
Appendix	Nederlandse samenvatting	249
	Curriculum vitae	255
	List of publications	256
	Dankwoord	258

SCOPE OF THE THESIS



SCOPE OF THE THESIS

The vast majority of the tissues in animals have the capacity to repair damage and constantly do so during normal wearing and tearing. Most visible are the hairs and pieces of skin we lose every day. This ability to regenerate comes from resident adult stem cells. These are defined by their ability to unlimitedly self-renew and to produce all the cell types of the corresponding organ. The champion of all mammalian adult stem cells is found in the intestine, where stem cells divide each day to ensure that all cells of the epithelium are renewed every 4 to 7 days. Signals that control the balance between self-renewal and differentiation into the different cell types are crucial to prevent tumorigenesis. An emerging tool to study these developmental cues are organoids, three-dimensional cultures derived from adult stem cells that form miniature versions of the organ these are derived from. Organoids are amendable to high throughput screens and genetic engineering, and are therefore particularly useful to fill gaps in the understanding of homeostasis of multiple tissues. An example of such a gap is the development and functioning of intestinal enteroendocrine cells (EECs), a cell type that constitutes just 1% of the intestine but still makes it the largest endocrine organ. These cells control important physiological processes such as appetite and insulin release, and are attractive therapeutic targets for metabolic diseases. Their rarity renders *in vivo* investigations impractical. Another example where organoids can come to rescue is in species where genetic engineering like in mice is impossible. For example, the snake venom gland is such a system where any tractable model system is lacking. Snake venom constitutes a rich resource of potential therapeutics, which only have been partly mined. One of the most potent diabetes drug has been isolated from the venom of the lizard Gila monster: exendin-4, a homologue of the EEC hormone GLP-1 that is resistant to degradation. On the other hand, snakebite still kills over 100.000 people every year globally.

In this thesis, we have employed organoids to answer basic developmental questions on how the intestine produces the constituent lineages with their diverse functions. We identify extensive specialization of cell types along the crypt-villus axis that is BMP regulated. We gain new insights in how EECs are generated, use organoids to study their functioning in-depth and provide an organoid-based system where the different EEC subtypes can be efficiently generated and tracked. Venom gland organoids are presented as the first reptilian organoid culture. These systems will allow studying cells which are inaccessible and hard to study in their cognate animal source.

The first two chapters present review studies describing literature background on the main topics of this thesis. **Chapter 1** reviews the signaling pathways in controlling intestinal homeostasis, and how these balance proliferation and differentiation towards the different lineages. Particular attention is given to an emerging concept at that time: the omnipresent stem cell potential among intestinal progenitor cells, and how this is exploited during damage. **Chapter 2** focuses on the hormone-producing enteroendocrine cells. Their function, development and tools to study these rare but important cells are highlighted.

Chapter 3 investigates cell cycle control of intestinal stem cells using organoids. We find that loss of EGF signaling halts proliferation in intestinal stem cells, without inducing their

differentiation. Quiescent stem cells are biased towards generation of EECs when these re-enter the cell cycle, uncovering a link between fate and cell division speed of intestinal stem cells. Additional loss of Notch and Wnt signals generates a high-purity culture of EECs in organoids.

In **Chapters 4 and 5**, we report on a BMP-regulated specialization of intestinal cell types along the crypt-villus axis. EECs switch their hormone profile during their journey from crypt to villus in a BMP-dependent manner (Chapter 4). A similar functional switch controlled by BMP signaling occurs in goblet cells and enterocytes (Chapter 5). We find that human enterocytes express genes related to carbohydrate metabolism in the bottom of the villus, while specializing to BMP-regulated lipid metabolism and chylomicron synthesis in the tip of the villus. Blocking the BMP gradient *in vivo* could reset these zoned functional programs, providing therapeutic opportunities for multiple metabolic diseases.

In **Chapter 6**, we build an extensive biobank of human organoids that allows efficient EEC generation combined with fluorescent tagging of 10 different hormones. Using this biobank, we provide an in-depth analysis of the transcriptome and secreted products of human EECs. We find novel intestinal hormones and highlight key differences between mouse EECs and human EECs.

Chapter 7 closes with the generation of the first reptilian organoid system, derived from the snake venom gland. We show this system is able to produce snake venom *in vitro*, and utilize it to assess cellular heterogeneity of the organ. We find that the snake venom gland contains different cells producing different combinations of toxins, as well as cells that specialize in the production of protective factors against their own venom.

Chapter 8 concludes all the previous chapters, and discusses these in a broader context of current literature. We highlight therapeutic implications and future prospects.

CHAPTER

REGULATION AND PLASTICITY OF INTESTINAL STEM CELLS DURING HOMEOSTASIS AND REGENERATION

Published in Development
doi: 10.1242/dev.133132

SUMMARY

The intestinal epithelium is the fastest renewing tissue in mammals and has a large flexibility to adapt to different types of damage. Lgr5⁺ Crypt Base Columnar (CBC) cells act as stem cells during homeostasis and are essential during regeneration. Upon perturbation, the activity of CBCs is dynamically regulated to maintain homeostasis while multiple dedicated progenitor cell populations can reverse to the stem cell state upon damage, adding another layer of compensatory mechanisms to facilitate regeneration. Here, we review our current understanding of how intestinal stem and progenitor cells contribute to homeostasis and regeneration, and the different signaling pathways that regulate their behavior. Nutritional state and inflammation have been recently identified as upstream regulators of stem cell activity in the mammalian intestine, and we further explore how these systemic signals can influence homeostasis and regeneration.

Joep Beumer^{1,2} and Hans Clevers^{1,2,*}

¹ Hubrecht Institute, Royal Netherlands Academy of Arts and Sciences (KNAW) and UMC Utrecht, 3584 CT Utrecht, The Netherlands.

² Cancer genomics Netherlands, University Medical Center Utrecht, 3584CX, Utrecht, The Netherlands

* Corresponding author: Hans Clevers; h.clevers@hubrecht.eu

INTRODUCTION

The intestinal epithelium is organized in modules termed crypt-villus units. Villi are surface-extending protrusions into the intestinal lumen that are covered by differentiated cell types. Intestinal stem cells (called crypt-base columnar cells, or CBCs) are easily identifiable by their slender morphology and localization at the crypt base, intermingled with the much larger, granule-containing and post-mitotic Paneth cell (see Figure 1). CBCs divide each day to produce rapidly proliferating daughter cells that move up the wall of the crypt onto the flanks of the villus, sometimes referred to as the intestinal ‘conveyor belt’. At the villus tips, mature cells undergo apoptosis and are shed in the lumen, sometimes referred to as the intestinal ‘conveyor belt’.

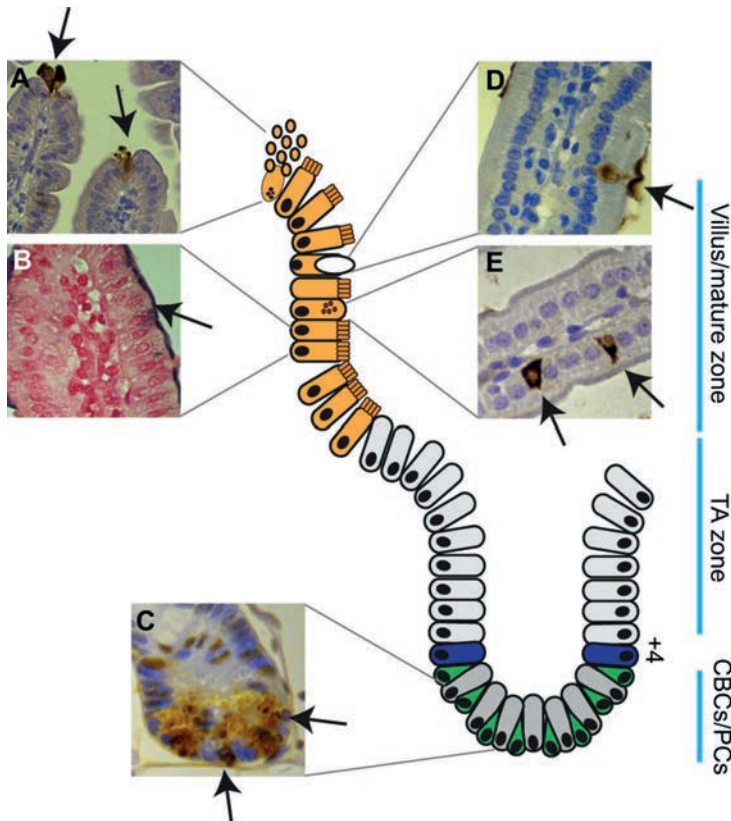


Figure 1. The intestinal crypt-villus unit. A-E) Cross section of the murine small intestine. The epithelium is organized in units of crypt-villi. Stem cells and transit amplifying cells in the crypt proliferate continuously to renew mature cells in the villi. At the tip of villi (A), mature cells undergo apoptosis and are shed in the lumen, stained by cleaved caspase-3 (brown, arrows). The brush border on the apical surface of the enterocytes (B) can be visualized by alkaline phosphatase staining (black, arrow). Paneth cells (C) at the crypt bottom stained by Lysozyme (brown, arrows). Goblet cell (D) stained by Mucin-2 (brown, arrow). Enteroendocrine cells (E) stained by Chromogranin-A (brown, arrow). Orange indicates differentiated cells in villi, light grey indicates transit-amplifying progenitor cells, blue indicates the +4 cell position, green indicates CBCs, dark grey indicates PCs. TA, transit-amplifying; CBCs, crypt base columnar cells; PCs, Paneth cells.

are continuously lost by undergoing apoptosis, 4-5 days after their birth. Only the stem cells in the crypt retain long-term self-renewing ability. A second population of non-dividing stem cells has been suggested to exist at the so-called +4 position, 4 cell diameters above the base of the crypt and directly adjacent to the CBC/Paneth region. Within the intestine, two major differentiated epithelial lineages are distinguished: 1) the enterocyte or absorptive lineage, responsible for absorbing nutrients, and 2) the secretory lineage (see Figure 2). The latter consists of Paneth cells that act as niche cells for stem cells and secrete antimicrobial molecules, the mucus-secreting Goblet cells, a variety of hormone-producing enteroendocrine cells and the mechanosensing Tuft cells (Clevers, 2013). The intestinal epithelium is exposed to a hostile luminal environment, which may explain its high turnover rate of 4-5 days, the highest among mammalian tissues.

Different extrinsic or intrinsic causes can upset the homeostatic self-renewal, and/or result in overt damage. Under such circumstances, the epithelium displays an impressive regenerative response. For instance, a 12 Gy dose of irradiation causes hematopoietic failure, yet still triggers

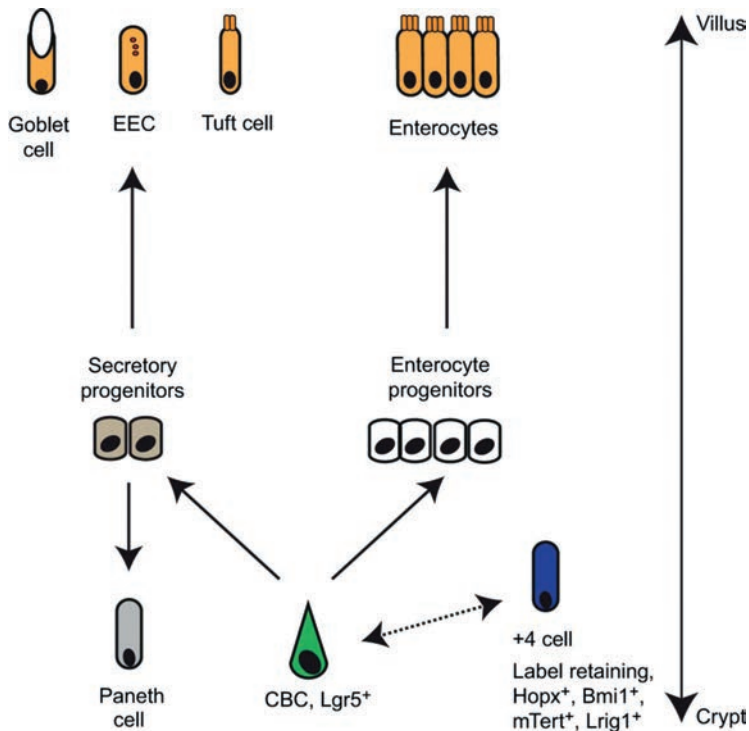


Figure 2. Stem cells and differentiated progeny in the intestine. Crypt base columnar cells (green, CBCs) are intestinal stem cells that generate all major intestinal lineages, including secretory cells and enterocytes (orange). Paneth cells are the exception of the differentiated lineage, and do not migrate upwards. +4 cells (blue), marked by Hopx, mTert Bmi1 and Lrig1 or identified as label retaining, have been proposed as a second stem cell population. The double-headed arrow on the right indicates relative position of the cells along the crypt-villus axis.

an effective regenerative response in the intestine, classically involving hyperproliferation of non-differentiated crypt cells, as well as crypt fission – the process by which one crypt produces two crypts - to repopulate the epithelium (Withers and Elkind, 1970). This response is illustrative of the adaptive capacity of the intestine. Flexibility in the regenerative response also occurs upon surgical resection and acute inflammation (Cordero and Sansom, 2012). Regeneration is generally believed to be facilitated by stem cells, and multiple strategies can be conceived that could facilitate such a flexible response to injury (see Figure 3). Firstly, separate stem cell populations may exist in a two-stem cell model that either act during homeostasis or are activated during damage. The CBC stem cells that fuel intestinal renewal during homeostasis are rapidly dividing. A separate non-dividing, or quiescent, population of ‘reserve’ stem cells has been proposed to co-exist, i.e. the intestinal ‘+4’ stem cell. Such non-dividing reserve stem cells could be less radiosensitive, and may divide only when the actively dividing stem cells are challenged (Li and Clevers, 2010). A second scenario could be that the activity of a single stem cell population is adaptively controlled upon injury. Indeed, inflammation increases the activity of intestinal stem cells (ISCs) in a cell-autonomous manner (Lindemans et al., 2015). Similarly, calorie restriction can impinge on stem cell activity, for example by augmenting the function of Paneth cells which indirectly increases the number of CBCs (Richmond et al., 2015; Yilmaz

I
II
III
IV
V
VI
VII
VIII
&

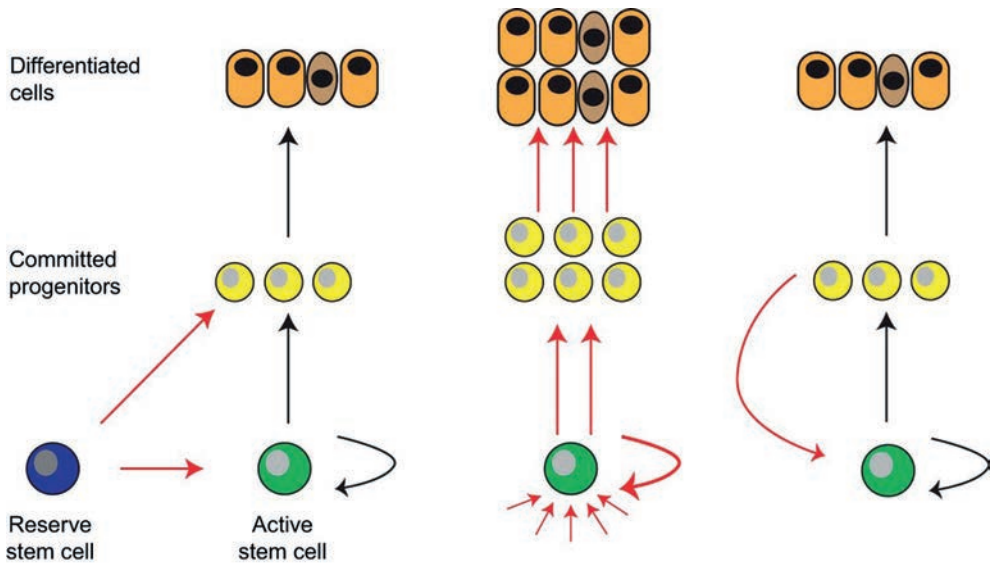


Figure 3. Models of regeneration in the intestine. A variety of possible scenarios exist for intestinal regeneration. In the first, actively dividing stem cells (green) are responsible for intestinal renewal during homeostasis, producing committed progenitor cells (yellow), which produce differentiated cells (orange). A coexisting quiescent, reserve population of stem cells (blue) is activated upon injury, and might contribute directly to the generation of progeny or active stem cells (red arrows). In the second scenario, niche and inflammatory signals (red arrows, bottom) can directly enhance stem cell activity to promote a regenerative response. In the third scenario, committed progenitor cells retain stem cell potential and can revert to the stem cell state in response to perturbations (red arrow).

et al., 2012). In a third model committed progenitor cells could regain stem cell potential by reverting to a stem cell state. Such plasticity could be termed ‘reverse’ stem cell potential (vs. ‘reserve’ stem cells), and by its very nature would exist in a non-stem cell population (Buczacki et al., 2013; Tetteh et al., 2016; van Es et al., 2012a). The capacity to dedifferentiate has been identified in a variety of multicellular organisms, pointing to a potentially universal mechanism for regeneration (Sánchez Alvarado and Yamanaka, 2014), and has been described for mammalian endodermal tissues like the lung (Hogan et al., 2014).

In this review, we discuss the range of cellular responses that enable the intestine to adapt to different perturbations, with a focus on stem and progenitor cell dynamics. We will first give a general overview of the identification of intestinal stem cells. Next, we will review the requirement for different signaling pathways to maintain homeostasis, both under normal physiological conditions as well as in response to injury. We focus on recent advances in the understanding of how dynamics in stem cell activity occur including how specific stressors such as inflammation or nutritional deprivation may directly impact on stem cell behavior.

THE QUEST FOR THE INTESTINAL STEM CELLS

Radioactive nucleotide labeling studies have been used to show that intestinal proliferation is restricted to crypts, and that cells after their generation (with the exception of Paneth cells) move upward towards the villus tips to eventually self-sacrifice (Clevers, 2013). This conveyor-belt model of intestinal renewal and cell migration suggests that the cells that drive homeostatic renewal reside at the crypt bottom. The CBC stem cells were originally identified by Cheng and Leblond and are located at the crypt base, interspersed between Paneth cells (see Figure 1; Cheng and Leblond, 1974). Functional evidence to definitively identify crypt stem cells, like in other epithelial tissues, had to await the identification of specific marker genes and the development of lineage tracing technology, as the golden standard for assessing stem cell potential (Kretschmar and Watt, 2012). Leucine-rich repeat containing G-protein coupled receptor 5 (*Lgr5*), a target gene of the Wnt signaling pathway, was identified as marker of CBCs (Barker et al., 2007). With the generation of appropriate *Lgr5* knock-in alleles, murine CBCs were shown to generate all differentiated cell types of the intestine over long time periods (see Figure 2). Surprisingly at the time, they were observed to be rapidly dividing, with an average cell cycle time of 21.5 hours (Schepers et al., 2011). Single *Lgr5*⁺ cells can be isolated from mouse intestine and under defined culture conditions can form mini-guts; miniature intestines with crypt-villus domains that containing all the mature intestinal cell types (Sato et al., 2009). Therefore, CBCs fulfill the defining criteria of stem cells, namely multipotency and the capacity to self-renew.

Stem cells are generally believed to be slowly cycling/quiescent in order to protect genome integrity. The rapid cell division rate of CBCs challenges this belief, building upon the idea that quiescence might not be a defining hallmark of stem cells (Clevers, 2015). However, a second stem cell population has been proposed to exist alongside CBCs. Potten and colleagues identified DNA label-retaining cells at the +4 position, 4 cells above the base of the crypt (see

Figure 1; Potten et al., 1974). *Bmi1*, *Lrig1*, *Hopx* and *mTert* have been described as markers of these cells (see Figure 2; Montgomery et al., 2011; Powell et al., 2012; Sangiorgi and Capecchi, 2008; Takeda et al., 2011). +4 cells are insensitive to injury and lineage-tracing experiments based on these markers show increased stem cell activity upon damage, suggesting that these cells are reserve stem cells capable of replacing CBCs in the injury setting (Montgomery et al., 2011). The study of +4 cells became complicated when it was found that these marker genes were broadly expressed at the transcript level, including in CBCs (Grün et al., 2015; Li et al., 2014; Muñoz et al., 2012). Lengner and colleagues subsequently showed that the *Bmi1*-CreER and *Hopx*-CreER proteins are more specifically localized than the corresponding mRNA transcripts, and that these reporters - based on transcriptional profiling - can identify cells that are largely distinct from those marked by *Lgr5*⁺ cells (Li et al., 2014). Moreover, lineage tracing from *Hopx*-CreER and subsequent single cell profiling demonstrated that *Hopx*⁺ and *Bmi1*⁺ cells can generate CBCs during homeostasis (Li et al., 2014), suggesting a bona fide separate stem cell population (Figure 2). However, using the original experimental conditions, our lab has shown that lineage tracing from the *Bmi1* locus initiates with equal efficiency along the entire crypt axis, including in CBCs (Muñoz et al., 2012). It is clear that +4 cells as defined by each of these markers require more attention to unequivocally demonstrate their homeostatic stem cell potential, and their relation to CBCs.

SIGNALING PATHWAYS THAT REGULATE INTESTINAL STEM CELLS

The activity of CBCs is tightly controlled by signaling molecules that derive from the epithelium, and mesenchymal cells outside the epithelial crypt-villus unit depicted in Figure 1. Mesenchymal cells are vital components of the intestinal niche, and include fibroblasts, immune cells, enteric neurons and capillaries. These cells have been shown to secrete a wide variety of growth factors and cytokines that together with epithelial signals control proliferation and differentiation of CBCs (Powell et al., 2011). Perturbations such as irradiation, toxins, chemotherapy, inflammation and nutritional deprivation can all induce rewiring of signaling pathways to modulate CBC activity and compensate for cellular loss in order to accommodate regeneration. In this section, we summarise and discuss the main signaling pathways that are involved in the regulation of intestinal stem cell activity in homeostasis and upon injury (Table 1).

Wnt

The Wnt pathway is essential for the maintenance of intestinal stem cells. When Wnt ligands bind to the Frizzled-LRP5/6 receptor complex, the cytoplasmic APC destruction complex is inhibited, leading to accumulation of the key mediator of Wnt signals: β -catenin. β -catenin translocates to the nucleus and acts as a transcriptional co-factor for T-cell factor (TCF) transcription factors, inducing transcription of Wnt target genes (Clevers and Nusse, 2012). Inactivating mutations in *Tcf4/Tcf712*, one of the downstream transcription factors of the Wnt pathway, prevent the formation of proliferative crypts in neonatal mice (Korinek et al., 1998). In

Table 1. Summary of signaling pathways involved in dynamic control of ISC activity

Signaling pathway	Role in ISC dynamics	Evidence	Reference
Wnt	Stem cell maintenance	TCF4 inactivation causes loss of stem cells in mice	(Korinek et al., 1998; van Es et al., 2012b)
		Overexpression of Dkk1 in mice causes loss of crypts in mice	(Kuhnert et al., 2004; Pinto et al., 2003)
	Regeneration	APC inactivation confers stem cells with a competitive advantage in mice	(Snippert et al., 2014; Vermeulen et al., 2013)
		FAK deletion prevents regenerative proliferation after intestinal injury in mice	(Ashton et al., 2010)
		Wnt5a deficient murine crypts show abnormal regenerative response with prolonged proliferation	(Miyoshi et al., 2013)
		Rspodin1 administration improves regeneration in mice	(Kim et al., 2005; Zhou et al., 2013)
Notch	Stem cell maintenance	Inhibition of Notch through γ -secretase causes stem cell conversion towards secretory lineages	(Milano et al., 2004; van Es et al., 2010)
	Inhibition of secretory fate	Inactivation of Notch effectors Hes1, Hes3 and Hes5 in the intestine causes increased secretory formation in mice: Ueo 2012	(Ueo et al., 2012)
EGF/EphB	Stem cell proliferation	Proliferation is reduced in mouse intestinal crypts lacking EphB2/3	(Holmberg et al., 2006)
	Regeneration	Loss of Lrig1 causes activation of ErbB signaling and expansion of the intestinal crypt in mice.	(Wong et al., 2012)
		Doxorubicin treatment induces EGF-ligand/BMP inhibitor expression in sub-epithelial tissue in mice, although its relevance remains to be determined	(Seiler et al., 2015)
BMP	Stem cell differentiation	BMP inhibition by transgenic noggin overexpression, or conditional loss of Bmpr1a, causes formation of ectopic crypts in mice?	(Haramis, 2004; He et al., 2004)
	Regeneration	BMP ligand expression is increased in Drosophila gut after injury and limits stem cell expansion, Doxorubicin treatment induces EGF-ligand/BMP inhibitor expression in sub-epithelial tissue in mice although its relevance remains to be determined	(Guo et al., 2013) (Seiler et al., 2015)
Hippo	Stem cell proliferation	Yorki overexpression increases stem cell proliferation in Drosophila	(Karpowicz et al., 2010)
	Regeneration	Knockdown of YAP/TAZ in mouse crypts suppresses proliferation	(Imajo et al., 2014)
		YAP deletion interferes with regeneration in DSS-induced colitis in mice, shown by reduced proliferation and increased mortality.	(Cai et al., 2010)
		YAP deletion interferes with regeneration after irradiation in mice indicated by reduced proliferation.	(Gregorieff et al., 2015)
		YAP/TAZ deletion impairs organoid formation .	(Azzolin et al., 2014; Gregorieff et al., 2015)

the adult intestine, ubiquitous deletion of Tcf4 using a Villin-CreERT2 transgenic model caused rapid loss of Lgr5+ CBCs (van Es et al., 2012b). Similarly, mice with an intestinal overexpression of the secreted Wnt inhibitor Dickkopf 1 (Dkk1) showed loss of crypts and decreased epithelial proliferation (Kuhnert et al., 2004; Pinto et al., 2003). CBC-specific activation of the Wnt pathway by inactivating mutations in APC stabilizes β -catenin and confers stem cells with a competitive advantage over their wild-type counterparts resulting in the rapid formation of adenomas (Barker et al., 2009; Snippert et al., 2014; Vermeulen et al., 2013).

Wnt ligands are redundantly expressed in epithelial Paneth cells and in the mesenchyme surrounding the crypt (Farin et al., 2012; Kabiri et al., 2014). Paneth cell-derived Wnt3 is essential to maintain proper growth of cultured epithelial 3D intestinal organoids, but can be depleted *in vivo* without a phenotype. This is because, in the latter, the mesenchyme acts as alternative source of Wnt, whereas *in vitro* the mesenchyme was not present (Farin et al., 2012). Indeed, Wnt3 knockout intestinal organoids can be rescued by co-culturing them with mesenchyme. Removal of Foxl1-expressing peri-cryptal mesenchymal cells *in vivo* causes loss of Wnt activity, and of proliferation, in crypts (Aoki et al., 2016). This recent study work identifies the mesenchyme as a critical component of the CBC niche, though it remains to be determined whether Wnt itself or another signal is non-redundant with the Paneth cell niche function.

Activation of the Wnt pathway is restricted to the lower crypt, and forms a signaling gradient along the crypt axis (Batlle et al., 2002; Muñoz et al., 2012). Different strategies for Wnt-controlled growth and patterning have been proposed, with both long-distance and local signaling activity observed (Mikels and Nusse, 2006). In *Drosophila* larvae, Wnt is expressed by a narrow stripe of cells in the imaginal discs and forms a long-distance gradient into the prospective wing. Tethering of the *Drosophila* Wnt ligand Wingless to the membrane of the producing cell does not, however, disturb normal wing development (Alexandre et al., 2014). Surprisingly, in the mammalian intestinal crypt, Paneth cell-produced Wnt3 does not freely diffuse, but is bound to the neighboring stem cell membranes as visualized by an HA-tagged Wnt3 allele (Farin et al., 2016). Binding to the membrane occurs directly through Frizzled, the cognitive Wnt receptor, and transfer of Wnt3 from Paneth cells to neighboring cells depends on direct cell-to-cell contact. When proliferation is inhibited in intestinal organoids, the Wnt gradient in the crypts collapses, implying that Wnt spreads through proliferative dilution of Wnt-binding membranes (Farin et al., 2016). It is tempting to speculate that the coupling between cell cycle activity and the concentration of a crucial stem cell niche signal is part of a functional feedback loop. When proliferation is overstimulated, rapid dilution of Wnt might lead to loss of CBCs or of their transit-amplifying (TA) cells. This protective feedback could explain why intestinal oncogenesis is virtually always initiated by mutations in the Wnt pathway (Morin et al., 1997). Indeed, recent work indicates that BRAF mutations cause loss of CBCs, which could be reversed by activating the Wnt pathway by exogenous Wnt ligands *in vitro* or β -catenin mutations *in vivo* (Riemer et al., 2015). Vice versa, a decrease in CBC proliferation in the event of injury or other perturbations could lead to a large CBC-bound pool of Wnt that stimulates proliferation or symmetric stem cell expansion during subsequent regeneration.

I

II

III

IV

V

VI

VII

VIII

&

Wnt signaling is a crucial mediator of regeneration (Cordero and Sansom, 2012). Deletion of the Wnt target gene *c-Myc* impedes regeneration by causing massive crypt loss following 14 Gy irradiation (Ashton et al., 2010). Downstream of Wnt/*c-Myc*, focal adhesion kinase (FAK) is upregulated following irradiation (Ashton et al., 2010). FAK is essential for maintaining Wnt-driven proliferation during regeneration, and suppresses apoptosis by activating AKT/mTOR signaling (Ashton et al., 2010). Non-canonical Wnt signaling also seems to partly mediate regenerative responses in the colon (Miyoshi et al., 2013). After mechanical injury, one of the transcripts enriched in wound beds compared to normal epithelium is *Wnt5a*, a non-canonical Wnt ligand. *Wnt5a* is expressed by stroma surrounding the site of injury, and lack of *Wnt5a* causes a failure to develop new crypts at the wounding site. *Wnt5a* has been shown to limit the proliferation of crypt cells after injury in a TGF- β dependent manner (Miyoshi et al., 2013), however it remains unclear whether cell cycle inhibition is a functionally relevant element of the *Wnt5a*-mediated regenerative response, or whether *Wnt5a* has additional effects.

Multiple studies have found that enhancing Wnt signaling can stimulate recovery after intestinal damage. Administration of the Wnt agonist R-spondin1 improves recovery after chemoradiotherapy in mice (Kim et al., 2005). E3 ligases and Wnt targets RNF43 and ZNRF3 can downregulate Frizzled receptors, thereby effectively inhibiting the Wnt pathway (Hao et al., 2012; Koo et al., 2012). R-spondin short circuits this negative feedback by binding to its receptor *Lgr5*, and together these associate with and inhibit RNF43/ZNFR3 (Hao et al., 2012; Koo et al., 2012). The effect of R-spondin1 on regeneration can be further improved by simultaneous treatment with *Slit2* (Zhou et al., 2013). *Slit2* is expressed by CBCs, along with its receptor *Roundabout 1* (*Robo1*). Knockout of *Robo1* decreases the number of CBCs, suggesting that a *Robo1/Slit2* signaling axis is important for CBC maintenance (Zhou et al., 2013). Simultaneous administration of R-spondin1 and *Slit2* expands the number of *Lgr5+* cells, and synergistically acts to stimulate intestinal recovery, thereby preventing lethality of mice treated with chemoradiotherapy. It remains unclear whether *Slit2* is a potentiator of Wnt signaling in a similar manner to R-spondin1 in this regenerative context. *Slit2* is overexpressed in some intestinal cancers, and has been found to downregulate E-cadherin, thereby possibly releasing β -catenin and activating Wnt signaling (Zhang et al., 2015). Paradoxically, signaling through *Slit2/Robo2* decreases β -catenin in mammary stem cells, limiting stem cell self-renewal (Harburg et al., 2014). Future studies are clearly required to dissect downstream targets of *Slit2* activity in intestinal regeneration. Taken together, current evidence implies a large therapeutic opportunity for Wnt signal enhancement in promoting gastrointestinal recovery, for example upon chemotherapy.

Notch

The Notch signaling pathway depends on a cell presenting a Notch ligand to an adjacent Notch-expressing cell. When the Notch receptor binds its ligand, the Notch intracellular domain (NICD) is released by proteolysis. NICD subsequently translocates to the nucleus where it activates target genes through the transcription factor RBP-J. Paneth cells express Notch ligands

Delta-like 1 and 4 (Dll1 and Dll4) and present these ligands to adjacent CBCs (Sato et al., 2011). Notch inhibition causes rapid conversion of all proliferative crypt cells including the intestinal stem cells (ISCs) into goblet cells (Milano et al., 2004; van Es et al., 2005; van Es et al., 2010). Notch signaling activates expression of Hes family transcription factors including Hes1, that repress the helix-loop-helix transcription factor Math1/Atoh1. Similar to Notch inhibition, induction of Math1/Atoh1 in turn promotes differentiation towards a secretory fate (Ueo et al., 2012), whereas loss of Atoh1 results in an absence of secretory cells (Shroyer et al., 2007). Therefore, Notch acts as a binary switch through lateral inhibition, promoting CBCs to undergo Atoh1-dependent secretory differentiation when inactivated. Secretory progenitors express Dll1 (van Es et al., 2012a) and suppress a secretory fate in their neighbors, driving the fate of these cells towards the enterocyte lineage.

EGF

Epidermal growth factor (EGF) is a crucial component of the intestinal organoid culture (Sato et al., 2009). The EGF receptor (EGFR) is highly expressed in CBCs, while its ligands are expressed by Paneth cells (Sato et al., 2011). The activity of ErbB signaling is controlled by the negative regulator Lrig1, a transmembrane protein, which is co-expressed with Lgr5 in CBCs (Wong et al., 2012). Loss of Lrig1 causes enhanced receptor activation and a concomitant rapid expansion of crypts and stem cell numbers. It is currently unknown at which level Lrig1 affects ErbB signaling. These lines of evidence illustrate the importance of this pathway as an inductive signal for stem cell proliferation. Although the role of EGFR/ErbB signaling for ISC proliferation is clearly established, it is not known if it is a prerequisite for CBC identity.

BMP

Bone morphogenic protein (BMP) signaling acts as inducer of differentiation in the crypt. Mesenchyme surrounding CBCs create a BMP-low environment by secreting BMP inhibitors (Kosinski et al., 2007), while BMP ligands expressed in villi create a BMP-high environment that promotes differentiation. Consistent with this, transgenic expression of the BMP inhibitor Noggin leads to excessive crypt formation (Haramis, 2004). Moreover, the BMP inhibitor Noggin is an essential ingredient of the organoid culture medium (Sato et al., 2009), as without it stem cells undergo differentiation. Similarly, conditional inactivation of the BMP receptor *Bmpr1a* in mice elevates Wnt signaling activity and causes a rapid expansion of the stem cell compartment (He et al., 2004). These phenotypes are reminiscent of patients with juvenile polyposis who carry inactivating mutations in the BMP pathway (Howe et al., 2001). In the *Drosophila* midgut, BMP is induced upon injury and acts directly on ISCs to limit their expansion (Guo et al., 2013). In the murine intestine, the BMP inhibitor Chordin-like 2 is upregulated together with EGF ligand Amphiregulin in sub-epithelial tissues after treatment with the chemotherapeutic doxorubicin (Seiler et al., 2015). This upregulation occurs in concert with an increase in ISC proliferation. The requirement of differential BMP or EGF signaling during regeneration remains to be assessed in future studies.

I

II

III

IV

V

VI

VII

VIII

&

Hippo

The Hippo signaling pathway is a key player in the regulation of organ size and has been shown to act as an interpreter of mechanical cues (Varelas, 2014). Recent studies indicate a role for Hippo signaling in intestinal homeostasis and regeneration, although its exact function remains controversial (Li and Clevers, 2013). Upon Hippo pathway activation, a kinase cascade consisting of MST1/2 and LAT1/2 kinases phosphorylates and inactivates YAP and TAZ through their cytoplasmic translocation. YAP and TAZ are final effector proteins of the pathway acting as co-activators of TEAD transcription factors (Pan, 2010).

During homeostasis, YAP is expressed throughout the intestinal crypt (Cai et al., 2010). Genetic inhibition of the Hippo pathway increases ISC proliferation in *Drosophila* (Karpowicz et al., 2010). Imajo and colleagues report similar proliferative effects after YAP activation in the murine intestine (Imajo et al., 2014). However, overexpression of YAP-S127A, a phospho-deficient mutant that readily translocates to the nucleus, decreased proliferation and inhibited Wnt signaling *in vivo* (Barry et al., 2013). These paradoxical observations can be reconciled by postulating separate cytoplasmic and nuclear functions of YAP/TAZ. YAP/TAZ have been shown to directly bind to Axin and inhibit Wnt signaling in an overexpression system (Azzolin et al., 2014; Imajo et al., 2014). In this scenario, YAP/TAZ would thus act as part of the β -catenin destruction complex in HEK cells, and mediate the recruitment of the β -catenin E3 ligase β -TrCP, targeting it for destruction (Azzolin et al., 2014). Wnt/Lrp6 can displace YAP/TAZ from the destruction complex, inducing both YAP/TAZ nuclear translocation and β -catenin stabilization. When Wnt is inactive, YAP/TAZ is both sequestered by the destruction complex and forms an active part of it by recruiting β -TrCP. In APC knockout mice, crypts become hyperplastic and produce adenomas due to overactivation of the Wnt pathway. This phenotype is reversed by the additional double knockout of YAP/TAZ, preventing APC loss-induced lethality in mice (Azzolin et al., 2014). These observations fit a model in which Hippo and Wnt act in a concerted manner, with YAP/TAZ forming part of the Wnt response. Strikingly, the Wnt signature (high ectopic expression of Wnt targets such as Lef1 and CD44) is still present in the APC/YAP/TAZ mutant compared to APC-only loss (Azzolin et al., 2014). Knockdown of YAP/TAZ *in vivo* similarly does not affect the β -catenin/TCF4 gene signature (Imajo et al., 2014). These observations indicate that YAP/TAZ promote their own transcriptional program, or control other pathways, complementary to Wnt transcriptional targets. Indeed, YAP has been shown to activate EGF signaling independent of its interaction with the Wnt pathway, which is critical for the progression of APC-mutant adenomas (Gregorieff et al., 2015).

The role of Hippo signaling during regeneration has been extensively studied. Upon induction of colitis using dextran sodium sulfate (DSS), YAP is initially downregulated (Cai et al., 2010). After withdrawal of DSS, YAP is dramatically increased during the regenerative phase. An intestinal knockout of YAP does not cause a phenotype during homeostasis, but interferes with regeneration in DSS-induced colitis (Cai et al., 2010). A similar dependence on YAP for regeneration was recently reported by Gregorieff and colleagues (Gregorieff et al., 2015). After irradiation, YAP nuclear localization increased after 2 days and returned to a predominantly cytoplasmic localization after 4 days. Knockout of YAP in CBCs caused increased apoptosis

upon irradiation and a delayed regenerative response. In the absence of YAP, irradiation-induced recovery promotes a conversion of crypt cells to Paneth cells, which is a Wnt-dependent phenomenon (Gregorieff et al., 2015). In organoids, which mimic some aspects of regeneration, YAP deletion has been shown to result in a drastic decrease in crypt formation. Decreasing Wnt activity reverses the increase in Paneth cells, and restores the number of crypts in these YAP-deficient organoids (Gregorieff et al., 2015). In contrast, overexpression of YAP interferes with organoid formation by decreasing Paneth cell numbers and Wnt activity (Barry et al., 2013). This suggests that YAP acts in a narrow window by keeping Wnt in check during regeneration, thus preventing CBC exhaustion. High Wnt activity sensitizes CBCs to p53-induced apoptosis, which could explain increased apoptosis upon irradiation when YAP is lost (Tao et al., 2015). In further support of this model, R-spondin injection in YAP knockout mice leads to a much larger increase in intestinal Wnt target gene expression - with a concomitant increase in CBCs - than observed in wild-type mice (Barry et al., 2013). Besides regulating Wnt, YAP also apparently controls a transcriptional program required for regeneration. One of the YAP-dependent upregulated genes during regeneration is *Ereg*, an EGFR ligand (Gregorieff et al., 2015). Formation of YAP-deficient organoids is rescued by exogenous *Ereg* to a similar extent as inhibition of the Wnt pathway. Hippo signaling thus impacts on both EGF and Wnt signaling to control regeneration after irradiation.

The intricate - and still somewhat confusing - connection between Hippo and Wnt signaling could partly account for high nuclear β -catenin in the bottom of the crypt. YAP is nuclear in regions with active Wnt signaling, and cytoplasmic where Wnt is inactive (Barry et al., 2013). The 3D architecture of the bottom crypt, which is curved, has unique mechanical properties. Possibly as a consequence, YAP/TAZ expression at the crypt bottom is nuclear, compared to upper crypt- and villus regions, where Hippo is active and YAP/TAZ are located in the cytoplasm. In these areas, YAP/TAZ may actively block Wnt signaling. Interestingly, YAP/TAZ are also Wnt targets (Konsavage et al., 2012), and can thus impose a negative feedback on Wnt signaling by inhibiting β -catenin. A comparable negative feedback loop in the Wnt pathway has been described above, by the E3 ligases RNF43 and ZNRF3 that can downregulate Frizzled receptors (Hao et al., 2012; Koo et al., 2012). Negative feedback signaling on the Wnt pathway is a crucial part of the regenerative response and functions to preventing overactivation (Gregorieff et al., 2015).

NUTRITIONAL STATE AND INFLAMMATION AS REGENERATIVE CUES

Nutritional state regulates intestinal stem cell activity

Nutritional state and inflammation have been described as upstream regulators of ICSs in the *Drosophila* gut (Jiang and Edgar, 2011). In snakes that are fed after a prolonged fasting period, a large amount of energy is directed to restoring the intestinal mucosa, underscoring the important link between nutritional status and intestinal homeostasis (Secor et al., 1994). The role of different stressors such as fasting, prolonged caloric restriction or nutrient availability

I

II

III

IV

V

VI

VII

VIII

&

have also recently been investigated in mammalian intestinal regeneration (see Figure 4A). Prolonged fasting has been shown to cause atrophy in the rat intestine, whereby the length and number of villi decreased (Dunel-Erb et al., 2001). Within 3 days after re-feeding, the intestinal mucosa in the rats recovered and villi were restored to normal numbers. Prolonged fasting or caloric restriction has also been shown to impinge directly on CBC activity and indirectly on the CBC niche. In mice that are calorie-restricted, villi shorten and contain fewer enterocytes, and total intestinal mass decreases (Yilmaz et al., 2012). Paradoxically, CBC proliferation and number increases, while cell cycle activity in the transit amplifying cell compartment decreases. Calorie restriction lowers mTOR activity in Paneth cells, which boosts both the number of Paneth cells together with their function as the CBC niche cell, the latter presumably being dependent on the Paneth cell-secreted paracrine factor cyclic ADP-ribose (Yilmaz et al., 2012). When Paneth cells from calorie-restricted mice are combined with CBCs from fed mice, organoids form more efficiently. This suggests that calorie restriction increases CBCs at least in part non-cell autonomously by hyperactivating the niche. In line with this, calorie-restricted mice resist irradiation better than their controls (Yilmaz et al., 2012).

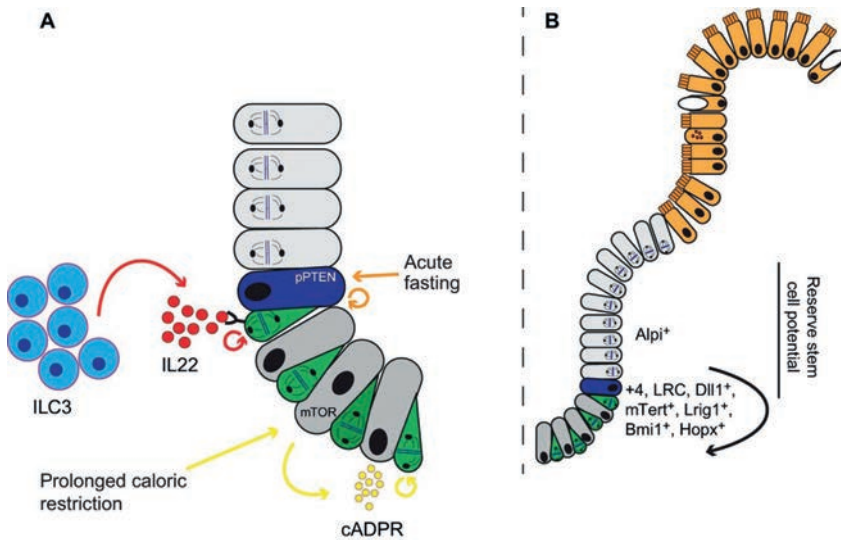


Figure 4. Regenerative adaptations in the intestinal stem cell compartment. Different regenerative adaptations exist in the intestinal epithelium. Left panel: Proliferative cells, CBCs (green) and transit-amplifying cells, are indicated by mitotic spindles. ILC3 cells (blue) secrete IL22 that directly increases the proliferation of CBCs that express the IL22-receptor (red arrows). Nutritional stimuli can target CBCs non-cell autonomously. Prolonged caloric restriction (yellow arrows) augments the function of Paneth cells (grey) by inhibiting mTOR signaling. Paneth cells then secrete cyclic-ADPR (cADPR) that increases CBC self-renewal. Acute fasting (orange arrows) increases phospho-PTEN (pPTEN) levels in mTERT⁺ cells (blue), directly activating their proliferation after re-feeding. B) CBCs are the active stem cells that reside in the crypt bottom. Stem cell potential however is present along the whole crypt in dedicated Alpi⁺ cells (light grey) and cells in the +4 position (blue) that can be called upon to revert to *bona fide* intestinal stem cells during injury (black arrow).

Interestingly, a high-fat diet can increase ISC activity despite a decrease in Paneth cell number (Beyaz et al., 2016). Mice on a high-fat diet resist irradiation better than control mice, and crypts derived from these mice initiate organoid cultures more efficiently. The high-fat diet increases Wnt activity in ISCs dependent on the nuclear receptor PPARdelta. Moreover, Notch ligand Jag1 and Jag2 expression is observed in CBCs in mice on a high-fat diet (Beyaz et al., 2016). It is possible that ISCs resist a decrease in Paneth cells by becoming independent of the niche, through expressing their own Notch ligands. These data indicate that dietary composition can promote CBC activity directly, although it is surprising that a high-fat diet and low calorie intake seem to cause similar phenotypes. Moreover, it remains to be established whether increased CBC activity is functionally relevant upon high intake of dietary fats.

Acute fasting has been shown to increase the inactive form of PTEN, pPTEN, in mTert expressing cells (Richmond et al., 2015). mTert has been reported as marker of reserve stem cells (Montgomery et al., 2011), although it is present in Lgr5+ cells at the transcript level (Itzkovitz et al., 2012; Schepers et al., 2011). The number of mTERT-GFP+ cells increases 4-fold upon fasting, and lineage tracing from mTERT-CreER increases accordingly in re-fed mice compared to control. This indicates activation of these cells as reserve stem cells, although the number label crypts originating from mTERT+ cells is still rare (Richmond et al., 2015). Interestingly, lineage tracing from Lgr5 is decreased after re-feeding suggesting inactivation or loss of these cells (Richmond et al., 2015), an important difference with increased CBC proliferation and number during prolonged caloric restriction (Yilmaz et al., 2012). PTEN is a known negative regulator of AKT-mTOR signaling. When mice are fed after a 48h fasting period, pPTEN persists in crypt cells with concomitant higher levels of active pAkt and mTOR target phospho-S6 (Richmond et al., 2015). Future studies will address the relevance of increased pAkt-mTOR signaling for recovery during re-feeding.

Inflammatory cues regulate intestinal stem cell activity

The regulation of CBC activity described so far occurs through local niche signals derived from the epithelium and mesenchyme. However, a recent seminal study by Lindemans and colleagues showed how inflammatory signals can also affect CBC behavior (Lindemans et al., 2015). This has previously been described in the *Drosophila* gut, where cytokines are secreted by enterocytes in the event of injury or infection, and activate Jak/Stat signaling in ISCs to stimulate their proliferation (Jiang et al., 2009). The mammalian intestine contains group 3 innate lymphoid cells (ILC3s), cells from the lymphoid lineage that lack antigen receptors. ILC3s reside in close proximity to intestinal crypts and are potent producers of Interleukin 22 (IL-22). IL-22 has previously been shown to be upregulated after injury and to support subsequent epithelial regeneration (Hanash et al., 2012; Sonnenberg and Artis, 2015; Zenewicz et al., 2007). Furthermore, IL-22 supports intestinal regeneration *in vivo* in a graft-versus-host disease context (Lindemans et al., 2015). In intestinal organoids, IL-22 increases the phosphorylation of signal transducer and activator of transcription (Stat3) in CBCs and promotes proliferation, while Wnt, Notch and EGF activities remain unchanged (Lindemans et al., 2015). Irradiated organoids upregulate IL-22 receptor, and show a higher rate of survival when treated with IL-22.

I

II

III

IV

V

VI

VII

VIII

&

IL-22-driven intestinal recovery occurs in the absence of Paneth cells, suggesting that it acts by directly targeting CBCs. Indeed, IL-22-driven intestinal recovery depends on the presence of CBCs. When Lgr5⁺ cells are depleted using diphtheria toxin in Lgr5-DTR-EGFP organoids, IL-22 fails to increase organoid size after irradiation (Lindemans et al., 2015). Pro-inflammatory signals such as IL-22 can also contribute to carcinogenesis (Kirchberger et al., 2013) and are effectively counteracted by sequestering proteins like IL-22 binding protein (IL-22BP) (Balzola et al., 2013).

Another recent study implies that inflammatory signals can affect symmetric division of intestinal stem cells to prevent excessive expansion during repair (Bu et al., 2016). CBCs predominantly undergo symmetric cell divisions while competing for niche space; through neutral competition clones eventually are either lost or take over the crypt in a stochastic fashion (Snippert et al., 2010). Inflammatory signals can, however, enforce asymmetric cell divisions in CBCs. In DSS-induced colitis, the number of asymmetric cell divisions of Lgr5-GFP⁺ cells increases from 2% to 13% (Bu et al., 2016). Shen and colleagues propose that asymmetric stem cell divisions are essential to prevent inflammation-induced increase of stem cell numbers (Bu et al., 2016). Deletion of miR34-a in intestinal organoids reverses this increase in asymmetric cell division following treatment with TNF-alpha, causing a concomitant, rapid expansion of stem cell numbers. miR34-a is a microRNA that negatively regulates the Notch receptor and its negative regulator Numb. By both having a negative and indirect positive effect on Notch, miR34-a installs robust bimodal rather than graded Notch activity, being high in CBCs and low in their offspring (Bu et al., 2016). Deletion of Numb disrupts the binary Notch activity, creating a population of cells with intermediate Notch levels that express both stem cell and differentiated markers. It has been previously reported that miR-34a is a cell fate determinant that promotes differentiation after stem cell division (Bu et al., 2013). Altering the expression of miR-34a can shift the balance between self-renewal and differentiation in stem cells (Bu et al., 2013). It remains to be established how differential miR34-a and Notch activity are able to switch CBCs from dividing symmetrically to asymmetrically during inflammation. Future studies may utilize the multi-lineage Cre reporters such as Rosa-Confetti (Snippert et al., 2010) to assess whether miR34-a controls symmetric cell division *in vivo*. Upon loss of miR34-a, drift towards clonality is expected to be delayed if stem cell divisions would preferentially become asymmetric. In summary, these studies add the immune system as 'external' regulator of CBC activity by acting independent of the local niche.

PROGENITOR CELL PLASTICITY

Lgr5⁺ cells can be selectively removed in Lgr5DTR-EGFP mice that express the diphtheria toxin receptor under control of the Lgr5 promoter (Tian et al., 2012). For at least a week, depletion of CBCs does not disturb homeostasis, which is suggestive of an alternative stem cell, or alternatively a non-stem cell source that can gain stem cell potential (Tian et al., 2012). Plasticity among progenitors would provide a large alternative source of stem cell potential (see Figure 4B).

Dedifferentiation of committed progenitors

As previously discussed, the +4 cells described by Potten and colleagues have been proposed as quiescent, reserve stem cells in the intestine (Li and Clevers, 2010). Reserve stem cell capacity of secretory progenitors has been specifically assessed using a Dll1-GFP-IRES-CREERT2 knockin mouse (van Es et al., 2012a). Delta-like 1 (Dll1) is a Notch ligand expressed in secretory progenitors, and tracing indicates that these cells indeed produce the entire repertoire of secretory cell types during homeostasis. Destruction of Lgr5 stem cells by irradiation can induce reversion of the committed secretory state to a stem cell state, whereby intestinal crypts are fully labeled after Dll1 tracing (van Es et al., 2012a).

Winton and colleagues have examined the reserve stem cell capacity of non-dividing cells more broadly. For this, they developed an inducible histone 2B-YFP (H2B-YFP) knockin mouse (Buczacki et al., 2013). As expected, the long-lived Paneth cells retain the histone label for up to 8 weeks. Interestingly, a second population of label-retaining cells expresses markers of the enteroendocrine lineage, as well as the CBC marker Lgr5 and the proposed quiescent stem cell markers Bmi1 and mTert. These LRCs thus have a combined enteroendocrine and stem cell signature, and reside predominantly at the +4 position. To assess the fate of these LRCs during homeostasis and injury, an ingenious lineage tracing strategy was used to trace cells based on their quiescence: Cre-recombinase was expressed as two fragments, one part produced ubiquitously from the Rosa26 locus and another part inducibly, fused to Histone-2B. Binding of these two fragments was dependent on a dimerizing agent (Buczacki et al., 2013). Lineage tracing of the cells that were histone label-retaining for up to 2 weeks showed that these cells could revert to the stem cell state upon injury. Moreover, H2B-YFP⁺ cells could form organoids when isolated and stimulated with the niche signal Wnt3, further indicative of their capacity to act as stem cells. In support of these findings, quiescent Lgr5-low cells have been identified as secretory progenitors in a KI67-RFP knockin mouse model (Basak et al., 2014).

Taken together, these studies imply that the non-dividing cells observed by Potten at the +4 location are secretory progenitors that retain ‘facultative’ stem cell potential upon injury, and may exclude the existence of genuine ‘professional’ quiescent stem cells (Table 2). When CBCs are lost, progenitor cells fall back in the stem cell niche and revert to stemness, likely through contact with Paneth cells and the availability of a potent Wnt source. Location in the stem cell zone itself is indeed linked to stemness, with Lgr5⁺ CBC stem cells located at the border of the niche displaying a survival disadvantage over other CBCs residing in the bottom of the crypt (Ritsma et al., 2014).

Secretory progenitors retain stem cell potential though only comprise a small part of the committed progenitor population. The majority of the intestinal epithelium consists of absorptive enterocytes, and their crypt progenitors are abundant and highly proliferative. If these cells could also act as stem cells when returning into the niche, the pool of ‘reserve stem cell potential’ would be much larger. To analyze if potential stem cells exist among enterocyte progenitors, Tetteh and colleagues generated a Alpi-IRES-CreERT2 knockin mouse, based on Alkaline phosphatase (Alpi), which has been widely used as marker for enterocytes and

I

II

III

IV

V

VI

VII

VIII

&

Table 2. Intestinal cell types that demonstrate stem cell potential upon injury

Cell type	Marker (s)	Summary of studies	Reference
Secretory progenitor	Dll1	Dll1+ cells produce all secretory cells during homeostasis and regain stemness upon damage	(van Es et al., 2012a)
Enterocyte progenitor	Alpi	Alpi+ produce enterocytes during homeostasis and regain stemness upon damage	(Tetteh et al., 2016)
Label retaining cells	H2B-retaining, Lgr5GFP ^{low} Ki67 ^{low}	Non-dividing early stem cell daughters with low Lgr5 expression are secretory progenitors that retain stemness	(Basak et al., 2014; Buczacki et al., 2013)
“Reserve” stem cells	Bmi1, Hopx, mTERT, Lrig1	Bmi1, Hopx, mTERT and Lrig1 mark the +4 cell, which shows stem cell potential upon lineage tracing.	(Montgomery et al., 2011; Powell et al., 2012; Sangiorgi and Capecchi, 2008; Takeda et al., 2011)

their progenitors (Tetteh et al., 2016). Clones derived from Alpi-expressing cells indeed only contained enterocytes, and were entirely lost within days at the top of the villus under physiological conditions (Tetteh et al., 2016). 15 hours after tracing, the ‘lowest’ Alpi+ cells were found around the +8 position counted from the crypt base, and did not co-express secretory markers. Upon ablation of Lgr5+ CBCs, Alpi+ cells contributed extensively to long-term tracing and produced all differentiated cell types, suggesting that these progenitors can readily regain stem cell potential, similar to secretory progenitor cells. Strikingly, ablation of CBCs two to three days after labeling Alpi+ cells still resulted in rare tracing events. The ‘lowest’ Alpi+ cells at these time points were already exiting the crypts. Apparently these cells still can act as stem cells, albeit rarely. It is likely that for these cells to return to the stem cell niche, a collapse of the entire crypt is required.

CONCLUSION

In this Review, we have summarised the role of different signaling pathways during crypt homeostasis and regeneration, with a particular focus on cellular dynamics within the intestinal stem cell compartment. An important question remains as to what the upstream regulators are of these signaling pathways in the injury setting. How is damage sensed and translated into the production of regenerative signals? A model that directly links injury to regenerative signals was described in the freshwater polyp Hydra. Here, cells undergoing apoptosis secrete Wnt3 to promote cell division of neighboring cells (Galliot, 2013). *In vitro* models like organoids represent simple systems that may help to dissect signals that restore homeostasis after injury (Huch and Koo, 2015; Clevers, 2016) Organoids can be damaged chemically or mechanically, or can be irradiated to establish models of regeneration. Co-cultures with mesenchyme or immune cells would then be valuable for the identification of non-epithelial derived signals that confer adaptability to damage.

All progenitor cells in the intestinal crypts display a high level of plasticity upon damage, and have been shown to dedifferentiate to stem cells in mouse models where CBCs were artificially removed. The inherent capacity of these cells to switch fates is likely to be related to their open chromatin structure (Kim et al., 2014). But does intestinal regeneration really depend on plasticity among progenitor cells? Winton and colleagues have shown how label-retaining cells can dedifferentiate in response to different kinds of perturbations, for example treatment with hydroxyurea, doxorubicin or irradiation. This dedifferentiation is a rare event and its efficiency differs depending on the type of injury (see Figure 4E in Buckzacki et al., 2013). Simultaneous depletion of CBCs and 6 Gy irradiation, the latter normally well tolerated in mice, causes rapid crypt loss and disruption of the epithelial architecture (Metcalf et al., 2014). This suggests that potential stem cells are radiosensitive and irreversibly affected, impairing their ability to revert to the stem cell state. Nevertheless, CBCs are also indispensable for irradiation-induced damage, which is a remarkable observation given their high proliferative activity. It has been previously found that CBCs indeed are very good at repairing their genome after irradiation, and do so by the low error prone homologous recombination (Hua et al., 2012). Future work will focus on teasing out the events in which regeneration is primarily driven by the differential activity of CBCs, and those in which the reserve stem cell pool of committed progenitor cells is called into action.

ACKNOWLEDGEMENTS

We thank Kim Boonekamp and Onur Basak for discussions and critically reading the manuscript, and Harry Begthel for providing immunohistochemistry figures.

I

II

III

IV

V

VI

VII

VIII

&

REFERENCES

- Alexandre, C., Baena-Lopez, A. and Vincent, J.-P. (2014). Patterning and growth control by membrane-tethered Wingless. *Nature* 505, 180–185.
- Aoki, R., Shoshkes-Carmel, M., Gao, N., Shin, S., May, C. L., Golson, M. L., Zahm, A. M., Ray, M., Wisner, C. L., Wright, C. V. E., et al. (2016). Foxl1-expressing mesenchymal cells constitute the intestinal stem cell niche. *Cell Mol Gastroenterol Hepatol.* 2, 175–188.
- Ashton, G. H., Morton, J. P., Myant, K., Phesse, T. J., Ridgway, R. A., Marsh, V., Wilkins, J. A., Athineos, D., Muncan, V., Kemp, R., et al. (2010). Focal Adhesion Kinase is required for intestinal regeneration and tumorigenesis downstream of Wnt/c-Myc signaling. *Dev. Cell* 19, 259–269.
- Azzolin, L., Panciera, T., Soligo, S., Enzo, E., Bicciato, S., Dupont, S., Bresolin, S., Frasson, C., Basso, G., Guzzardo, V., et al. (2014). YAP/TAZ incorporation in the β -catenin destruction complex orchestrates the Wnt response. *Cell* 158, 157–170.
- Balzola, F., Cullen, G., Ho, G. T., Hoentjen, F. and Russell, R. K. (2013). IL-22BP is regulated by the inflammasome and modulates tumorigenesis in the intestine. *Inflamm. Bowel Dis. Monit.* 13, 108–109.
- Barker, N., van Es, J. H., Kuipers, J., Kujala, P., van den Born, M., Cozijnsen, M., Haegbarth, A., Korving, J., Begthel, H., Peters, P. J., et al. (2007). Identification of stem cells in small intestine and colon by marker gene *Lgr5*. *Nature* 449, 1003–1007.
- Barker, N., Ridgway, R. A., van Es, J. H., van de Wetering, M., Begthel, H., van den Born, M., Danenberg, E., Clarke, A. R., Sansom, O. J. and Clevers, H. (2009). Crypt stem cells as the cells-of-origin of intestinal cancer. *Nature* 457, 608–611.
- Barry, E. R., Morikawa, T., Butler, B. L., Shrestha, K., de la Rosa, R., Yan, K. S., Fuchs, C. S., Magness, S. T., Smits, R., Ogino, S., et al. (2013). Restriction of intestinal stem cell expansion and the regenerative response by YAP. *Nature* 493, 106–110.
- Basak, O., van de Born, M., Korving, J., Beumer, J., van der Elst, S., van Es, J. H. and Clevers, H. (2014). Mapping early fate determination in *Lgr5+* crypt stem cells using a novel *Ki67-RFP* allele. *EMBO J.* 33, 1–12.
- Battle, E., Henderson, J. T., Beghtel, H., Van den Born, M. M. W., Sancho, E., Huls, G., Meeldijk, J., Robertson, J., Van de Wetering, M., Pawson, T., et al. (2002). β -catenin and TCF mediate cell positioning in the intestinal epithelium by controlling the expression of *EphB/EphrinB*. *Cell* 111, 251–263.
- Beyaz, S., Mana, M. D., Roper, J., Kedrin, D., Saadatpour, A., Hong, S.-J., Bauer-Rowe, K. E., Xifaras, M. E., Akkad, A., Arias, E., et al. (2016). High-fat diet enhances stemness and tumorigenicity of intestinal progenitors. *Nature* 531, 53–58.
- Bu, P., Chen, K. Y., Chen, J. H., Wang, L., Walters, J., Shin, Y. J., Goerger, J. P., Sun, J., Witherspoon, M., Rakhilin, N., et al. (2013). A microRNA miR-34a-regulated bimodal switch targets notch in colon cancer stem cells. *Cell Stem Cell* 12, 602–615.
- Bu, P., Wang, L., Chen, K.-Y., Srinivasan, T., Murthy, P. K. L., Tung, K.-L., Varanko, A. K., Chen, H. J., Ai, Y., King, S., et al. (2016). A miR-34a-Numb feedforward loop triggered by inflammation regulates asymmetric stem cell division in intestine and colon cancer. *Cell Stem Cell* 18, 189–202.
- Buczacki, S. J. a, Zecchini, H. I., Nicholson, A. M., Russell, R., Vermeulen, L., Kemp, R. and Winton, D. J. (2013). Intestinal label-retaining cells are secretory precursors expressing *Lgr5*. *Nature* 495, 65–69.
- Cai, J., Zhang, N., Zheng, Y., De Wilde, R. F., Maitra, A. and Pan, D. (2010). The Hippo signaling pathway restricts the oncogenic potential of an intestinal regeneration program. *Genes Dev.* 24, 2383–2388.

- Cheng, H. and Leblond, C. (1974). Origin, differentiation and renewal of the four main epithelial cell types in the mouse small intestine. V. Unitarian theory of the origin of the four epithelial cell types. *Am J Anat* 141, 537–561.
- Clevers, H. (2013). The intestinal crypt, a prototype stem cell compartment. *Cell* 154, 274–284.
- Clevers, B. H. (2015). What is an adult stem cell? *Science* (80-.). 350, 4–6.
- Clevers, H. and Nusse, R. (2012). Wnt/B-catenin signaling and disease. *Cell* 149, 1192–1205.
- Cordero, J. B. and Sansom, O. J. (2012). Wnt signalling and its role in stem cell-driven intestinal regeneration and hyperplasia. *Acta Physiol.* 204, 137–143.
- Dunel-Erb, S., Chevalier, C., Laurent, P., Bach, A., Decrock, F. and Le Maho, Y. (2001). Restoration of the jejunal mucosa in rats refed after prolonged fasting. *Comp. Biochem. Physiol. - A Mol. Integr. Physiol.* 129, 933–947.
- Farin, H. F., Van Es, J. H. and Clevers, H. (2012). Redundant sources of Wnt regulate intestinal stem cells and promote formation of paneth cells. *Gastroenterology* 143, 1518–1529.
- Farin, H. F., Jordens, I., Mosa, M. H., Basak, O., Korving, J., Tauriello, D. V. F., de Punder, K., Angers, S., Peters, P. J., Maurice, M. M., et al. (2016). Visualization of a short-range Wnt gradient in the intestinal stem-cell niche. *Nature* 530, 340–343.
- Galliot, B. (2013). Injury-induced asymmetric cell death as a driving force for head regeneration in *Hydra*. *Dev. Genes Evol.* 223, 39–52.
- Gregorieff, A., Liu, Y., Inanlou, M. R., Khomchuk, Y. and Wrana, J. L. (2015). Yap-dependent reprogramming of *Lgr5+* stem cells drives intestinal regeneration and cancer. *Nature* 526, 715–718.
- Grün, D., Lyubimova, A., Kester, L., Wiebrands, K., Basak, O., Sasaki, N., Clevers, H. and van Oudenaarden, A. (2015). Single-cell messenger RNA sequencing reveals rare intestinal cell types. *Nature* 525, 251–5.
- Guo, Z., Driver, I. and Ohlstein, B. (2013). Injury-induced BMP signaling negatively regulates *Drosophila* midgut homeostasis. *J. Cell Biol.* 201, 945–961.
- Hanash, A. M., Dudakov, J. A., Hua, G., O'Connor, M. H., Young, L. F., Singer, N. V., West, M. L., Jenq, R. R., Holland, A. M., Kappel, L. W., et al. (2012). Interleukin-22 protects intestinal stem cells from immune-mediated tissue damage and regulates sensitivity to graft versus host disease. *Immunity* 37, 339–350.
- Hao, H.-X., Xie, Y., Zhang, Y., Charlat, O., Oster, E., Avello, M., Lei, H., Mickanin, C., Liu, D., Ruffner, H., et al. (2012). *ZNRF3* promotes Wnt receptor turnover in an R-spondin-sensitive manner. *Nature* 485, 195–200.
- Haramis, A.-P. G. (2004). De novo crypt formation and Juvenile Polyposis on BMP inhibition in mouse intestine. *Science* (80-.). 303, 1684–1686.
- Harburg, G., Compton, J., Liu, W., Iwai, N., Zada, S., Marlow, R., Strickland, P., Zeng, Y. A. and Hinck, L. (2014). *SLIT/ROBO2* signaling promotes mammary stem cell senescence by inhibiting wnt signaling. *Stem Cell Reports* 3, 385–393.
- He, X. C., Zhang, J., Tong, W.-G., Tawfik, O., Ross, J., Scoville, D. H., Tian, Q., Zeng, X., He, X., Wiedemann, L. M., et al. (2004). BMP signaling inhibits intestinal stem cell self-renewal through suppression of Wnt-beta-catenin signaling. *Nat Genet* 36, 1117–1121.
- Hogan, B. L. M., Barkauskas, C. E., Chapman, H. A., Epstein, J. A., Jain, R., Hsia, C. C. W., Niklason, L., Calle, E., Le, A., Randell, S. H., et al. (2014). Repair and regeneration of the respiratory system: Complexity, plasticity, and mechanisms of lung stem cell function. *Cell Stem Cell* 15, 123–138.

- Holmberg, J., Genander, M., Halford, M. M., Anner??n, C., Sondell, M., Chumley, M. J., Silvany, R. E., Henkemeyer, M. and Fris??n, J. (2006). EphB Receptors Coordinate Migration and Proliferation in the Intestinal Stem Cell Niche. *Cell* 125, 1151–1163.
- Howe, J. R., Bair, J. L., Sayed, M. G., Anderson, M. E., Mitros, F. a, Petersen, G. M., Velculescu, V. E., Traverso, G. and Vogelstein, B. (2001). Germline mutations of the gene encoding bone morphogenetic protein receptor 1A in juvenile polyposis. *Nat. Genet.* 28, 184–187.
- Hua, G., Thin, T. H., Feldman, R., Haimovitz-Friedman, A., Clevers, H., Fuks, Z. and Kolesnick, R. (2012). Crypt base columnar stem cells in small intestines of mice are radioresistant. *Gastroenterology* 143, 1266–1276.
- Huch, M. and Koo, B. (2015). Modeling mouse and human development using organoid cultures. *Development* 142, 3113–25.
- Imajo, M., Ebisuya, M. and Nishida, E. (2014). Dual role of YAP and TAZ in renewal of the intestinal epithelium. *Nat. Cell Biol.* 17, 7–19.
- Izkovitz, S., Lyubimova, A., Blat, I. C., Maynard, M., van Es, J., Lees, J., Jacks, T., Clevers, H. and van Oudenaarden, A. (2012). Single-molecule transcript counting of stem-cell markers in the mouse intestine. *Nat. Cell Biol.* 14, 106–14.
- Jiang, H. and Edgar, B. A. (2011). Intestinal stem cells in the adult *Drosophila* midgut. *Exp. Cell Res.* 317, 2780–2788.
- Jiang, H., Patel, P. H., Kohlmaier, A., Grenley, M. O., McEwen, D. G. and Edgar, B. A. (2009). Cytokine/Jak/Stat signaling mediates regeneration and homeostasis in the *drosophila* midgut. *Cell* 137, 1343–1355.
- Kabiri, Z., Greicius, G., Madan, B., Biechele, S., Zhong, Z., Zaribafzadeh, H., Edison, Aliyev, J., Wu, Y., Bunte, R., et al. (2014). Stroma provides an intestinal stem cell niche in the absence of epithelial Wnts. *Development* 141, 2206–15.
- Karpowicz, P., Perez, J. and Perrimon, N. (2010). The Hippo tumor suppressor pathway regulates intestinal stem cell regeneration. *Development* 137, 4135–4145.
- Kim, K.-A., Kakitani, M., Zhao, J., Oshima, T., Tang, T., Binnerts, M., Liu, Y., Boyle, B., Park, E., Emtage, P., et al. (2005). Mitogenic influence of human R-Spondin1 on the intestinal epithelium. *Science* (80-.). 309, 1256–1259.
- Kim, T.-H., Li, F., Ferreiro-Neira, I., Ho, L.-L., Luyten, A., Nalapareddy, K., Long, H., Verzi, M. and Shivdasani, R. A. (2014). Broadly permissive intestinal chromatin underlies lateral inhibition and cell plasticity. *Nature* 506, 511–515.
- Kirchberger, S., Royston, D. J., Boulard, O., Thornton, E., Franchini, F., Szabady, R. L., Harrison, O. and Powrie, F. (2013). Innate lymphoid cells sustain colon cancer through production of interleukin-22 in a mouse model. *J. Exp. Med.* 210, 917–931.
- Konsavage, W. M., Kyler, S. L., Rennoll, S. A., Jin, G. and Yochum, G. S. (2012). Wnt / β -Catenin signaling regulates Yes-associated Protein (YAP) gene expression in colorectal carcinoma cells. 287, 11730–11739.
- Koo, B. K., Spit, M., Jordens, I., Low, T. Y., Stange, D. E., van de Wetering, M., van Es, J. H., Mohammed, S., Heck, A. J., Maurice, M. M., et al. (2012). Tumour suppressor RNF43 is a stem-cell E3 ligase that induces endocytosis of Wnt receptors. *Nature* 488, 665–669.
- Korinek, V., Barker, N., Willert, K., Molenaar, M., Roose, J., Wagenaar, G., Markman, M., Lamers, W., Destree, O. and Clevers, H. (1998). Two members of the Tcf family implicated in Wnt/beta-catenin signaling during embryogenesis in the mouse. *Mol. Cell. Biol.* 18, 1248–56.

- Kosinski, C., Li, V. S. W., Chan, A. S. Y., Zhang, J., Ho, C., Tsui, W. Y., Chan, T. L., Mifflin, R. C., Powell, D. W., Yuen, S. T., et al. (2007). Gene expression patterns of human colon tops and basal crypts and BMP antagonists as intestinal stem cell niche factors. *Proc. Natl. Acad. Sci. U. S. A.* 104, 15418–15423.
- Kretschmar, K. and Watt, F. M. (2012). Lineage tracing. *Cell* 148, 33–45.
- Kuhnert, F., Davis, C. R., Wang, H.-T., Chu, P., Lee, M., Yuan, J., Nusse, R. and Kuo, C. J. (2004). Essential requirement for Wnt signaling in proliferation of adult small intestine and colon revealed by adenoviral expression of Dickkopf-1. *Proc. Natl. Acad. Sci. U. S. A.* 101, 266–71.
- Li, L. and Clevers, H. (2010). Coexistence of quiescent and active adult stem cells in mammals. *Science* 327, 542–545.
- Li, V. S. W. and Clevers, H. (2013). Intestinal regeneration: YAP-tumor suppressor and oncoprotein? *Curr. Biol.* 23, R110–R112.
- Li, N., Yousefi, M., Nakauka-Ddamba, A., Jain, R., Tobias, J., Epstein, J. A., Jensen, S. T. and Lengner, C. J. (2014). Single-cell analysis of proxy reporter allele-marked epithelial cells establishes intestinal stem cell hierarchy. *Stem Cell Reports* 3, 876–891.
- Lindemans, C. A., Calafiore, M., Mertelsmann, A. M., O'Connor, M. H., Dudakov, J. A., Jenq, R. R., Velardi, E., Young, L. F., Smith, O. M., Lawrence, G., et al. (2015). Interleukin-22 promotes intestinal-stem-cell-mediated epithelial regeneration. *Nature* 528, 560–564.
- Metcalf, C., Kljavin, N. M., Ybarra, R. and De Sauvage, F. J. (2014). Lgr5+ stem cells are indispensable for radiation-induced intestinal regeneration. *Cell Stem Cell* 14, 149–159.
- Mikels, A. J. and Nusse, R. (2006). Wnts as ligands: processing, secretion and reception. *Oncogene* 25, 7461–7468.
- Milano, J., McKay, J., Dagenais, C., Foster-Brown, L., Pognan, F., Gadiant, R., Jacobs, R. T., Zacco, A., Greenberg, B. and Ciaccio, P. J. (2004). Modulation of Notch processing by γ -secretase inhibitors causes intestinal goblet cell metaplasia and induction of genes known to specify gut secretory lineage differentiation. *Toxicol. Sci.* 82, 341–358.
- Miyoshi, H., Ajima, R., Luo, C. T., Yamaguchi, T. P. and Stappenbeck, T. S. (2013). Wnt5a potentiates TGF- β signaling to promote colonic crypt regeneration after tissue injury. *Cell* 154, 108–113.
- Montgomery, R. K., Carlone, D. L., Richmond, C. a, Farilla, L., Kranendonk, M. E. G., Henderson, D. E., Baffour-Awuah, N. Y., Ambruzs, D. M., Fogli, L. K., Algra, S., et al. (2011). Mouse telomerase reverse transcriptase (mTert) expression marks slowly cycling intestinal stem cells. *Proc. Natl. Acad. Sci. U. S. A.* 108, 179–184.
- Morin, P., Sparks, A. B., Korinek, V., Barker, N., Clevers, H., Vogelstein, B. and Kinzler, K. W. (1997). Activation of beta-catenin-Tcf signaling in colon cancer by mutations in beta-catenin or APC. *Science* (80-.). 275, 1787–1790.
- Muñoz, J., Stange, D. E., Schepers, A. G., van de Wetering, M., Koo, B.-K., Itzkovitz, S., Volckmann, R., Kung, K. S., Koster, J., Radulescu, S., et al. (2012). The Lgr5 intestinal stem cell signature: robust expression of proposed quiescent “+4” cell markers. *EMBO J.* 31, 3079–3091.
- Pan, D. (2010). The hippo signaling pathway in development and cancer. *Dev. Cell* 19, 491–505.
- Pinto, D., Gregorieff, A., Begthel, H. and Clevers, H. (2003). Canonical Wnt signals are essential for homeostasis of the intestinal epithelium. *Development* 130, 1709–1713.

I

II

III

IV

V

VI

VII

VIII

&

- Potten, C., Kovacs, L. and Hamilton, E. (1974). Continuous labelling studies on mouse skin and intestine. *Cell Tissue Kinet.* 7, 271–283.
- Powell, D. W., Pinchuk, I. V., Saada, J. I., Chen, X. and Mifflin, R. C. (2011). Mesenchymal cells of the intestinal lamina propria. *Annu Rev Physiol* 73, 213–237.
- Powell, A. E., Wang, Y., Li, Y., Poulin, E. J., Means, A. L., Washington, M. K., Higginbotham, J. N., Juchheim, A., Prasad, N., Levy, S. E., et al. (2012). The pan-ErbB negative regulator Irig1 is an intestinal stem cell marker that functions as a tumor suppressor. *Cell* 149, 146–158.
- Richmond, C. A., Shah, M. S., Deary, L. T., Trotier, D. C., Thomas, H., Ambruzs, D. M., Jiang, L., Whiles, B. B., Rickner, H. D., Montgomery, R. K., et al. (2015). Dormant intestinal stem cells are regulated by PTEN and nutritional Status. *Cell Rep.* 13, 2403–2411.
- Riemer, P., Sreekumar, A., Reinke, S., Rad, R., Schäfer, R., Sers, C., Bläker, H., Herrmann, B. G. and Morkel, M. (2015). Transgenic expression of oncogenic BRAF induces loss of stem cells in the mouse intestine, which is antagonized by β -catenin activity. *Oncogene* 34, 3164–3175.
- Ritsma, L., Ellenbroek, S. I. J., Zomer, A., Snippert, H. J., de Sauvage, F. J., Simons, B. D., Clevers, H. and van Rheenen, J. (2014). Intestinal crypt homeostasis revealed at single-stem-cell level by in vivo live imaging. *Nature* 507, 362–365.
- Sánchez Alvarado, A. and Yamanaka, S. (2014). Rethinking differentiation: Stem cells, regeneration, and plasticity. *Cell* 157, 110–119.
- Sangiorgi, E. and Capecchi, M. R. (2008). *Bmi1* is expressed in vivo in intestinal stem cells. *Nat. Genet.* 40, 915–920.
- Sato, T., Vries, R. G., Snippert, H. J., van de Wetering, M., Barker, N., Stange, D. E., van Es, J. H., Abo, A., Kujala, P., Peters, P. J., et al. (2009). Single *Lgr5* stem cells build crypt-villus structures in vitro without a mesenchymal niche. *Nature* 459, 262–265.
- Sato, T., van Es, J. H., Snippert, H. J., Stange, D. E., Vries, R. G., van den Born, M., Barker, N., Shroyer, N. F., van de Wetering, M. and Clevers, H. (2011). Paneth cells constitute the niche for *Lgr5* stem cells in intestinal crypts. *Nature* 469, 415–418.
- Schepers, A. G., Vries, R., van den Born, M., van de Wetering, M. and Clevers, H. (2011). *Lgr5* intestinal stem cells have high telomerase activity and randomly segregate their chromosomes. *EMBO J.* 30, 1104–1109.
- Secor, S. M., Stein, E. D. and Diamond, J. (1994). Rapid up-regulation of snake intestine in response to feeding - a new model of intestinal adaptation. *Am. J. Physiol.* 266, G695–G705.
- Seiler, K. M., Schenhals, E. L., von Furstenberg, R. J., Allena, B. K., Smith, B. J., Scaria, D., Bresler, M. N., Dekaney, C. M. and Henning, S. J. (2015). Tissue underlying the intestinal epithelium elicits proliferation of intestinal stem cells following cytotoxic damage. *Cell Tissue Res.* 427–438.
- Shroyer, N. F., Helmuth, M. A., Wang, V. Y. C., Antalffy, B., Henning, S. J. and Zoghbi, H. Y. (2007). Intestine-specific ablation of Mouse atonal homolog 1 (*Math1*) reveals a role in cellular homeostasis. *Gastroenterology* 132, 2478–2488.
- Snippert, H. J., van der Flier, L. G., Sato, T., van Es, J. H., van den Born, M., Kroon-Veenboer, C., Barker, N., Klein, A. M., van Rheenen, J., Simons, B. D., et al. (2010). Intestinal crypt homeostasis results from neutral competition between symmetrically dividing *Lgr5* stem cells. *Cell* 143, 134–144.
- Snippert, H. J., Schepers, A. G., Van Es, J. H., Simons, B. D. and Clevers, H. (2014). Biased competition between *Lgr5* intestinal stem cells driven by oncogenic mutation induces clonal expansion. *EMBO Rep.* 15, 62–69.

- Sonnenberg, G. F. and Artis, D. (2015). Innate lymphoid cells in the initiation, regulation and resolution of inflammation. *Nat. Med.* 21, 698–708.
- Takeda, N., Jain, R., LeBoeuf, M. R., Wang, Q., Lu, M. M. and Epstein, J. A. (2011). Interconversion between intestinal stem cell populations in distinct niches. *Science* 334, 1420–1424.
- Tao, S., Tang, D., Morita, Y., Sperka, T., Omrani, O., Lechel, A., Sakk, V., Kraus, J., Kestler, H. A., Kühl, M., et al. (2015). Wnt activity and basal niche position sensitize intestinal stem and progenitor cells to DNA damage. *EMBO J.* 34, 624–40.
- Tetteh, P. W., Basak, O., Farin, H. F., Wiebrands, K., Kretschmar, K., Begthel, H., van den Born, M., Korving, J., de Sauvage, F., van Es, J. H., et al. (2016). Replacement of Lost Lgr5-Positive Stem Cells through Plasticity of Their Enterocyte-Lineage Daughters. *Cell Stem Cell* 18, 203–213.
- Tian, H., Biehs, B., Warming, S., Leong, K. G., Rangell, L., Klein, O. D. and de Sauvage, F. J. (2012). A reserve stem cell population in small intestine renders Lgr5-positive cells dispensable. *Nature* 482, 120–120.
- Ueo, T., Imayoshi, I., Kobayashi, T., Ohtsuka, T., Seno, H., Nakase, H., Chiba, T. and Kageyama, R. (2012). The role of Hes genes in intestinal development, homeostasis and tumor formation. *Development* 139, 1071–1082.
- van Es, J. H., van Gijn, M. E., Riccio, O., van den Born, M., Vooijs, M., Begthel, H., Cozijnsen, M., Robine, S., Winton, D. J., Radtke, F., et al. (2005). Notch/gamma-secretase inhibition turns proliferative cells in intestinal crypts and adenomas into goblet cells. *Nature* 435, 959–63.
- van Es, J. H., de Geest, N., van de Born, M., Clevers, H. and Hassan, B. A. (2010). Intestinal stem cells lacking the Math1 tumour suppressor are refractory to Notch inhibitors. *Nat. Commun.* 1, 18.
- van Es, J. H., Sato, T., van de Wetering, M., Lyubimova, A., Yee Nee, A. N., Gregorieff, A., Sasaki, N., Zeinstra, L., van den Born, M., Korving, J., et al. (2012a). Dll1+ secretory progenitor cells revert to stem cells upon crypt damage. *Nat. Cell Biol.* 14, 1099–1104.
- van Es, J. H., Haegerbarth, A., Kujala, P., Itzkovitz, S., Koo, B.-K., Boj, S. F., Korving, J., van den Born, M., van Oudenaarden, A., Robine, S., et al. (2012b). A critical role for the Wnt effector Tcf4 in adult intestinal homeostatic self-renewal. *Mol. Cell. Biol.* 32, 1918–27.
- Varelas, X. (2014). The Hippo pathway effectors TAZ and YAP in development, homeostasis and disease. *Development* 141, 1614–1626.
- Vermeulen, L., Morrissey, E., Heijden, M. van der, Nicholson, A. M., Sottoriva, A., Buczacki, S., Kemp, R., Tavaré, S. and Winton, D. J. (2013). Defining Stem Cell Dynamics in Models of Intestinal Tumor Initiation. *Science* (80-.). 342, 995–998.
- Withers, H. and Elkind, M. (1970). Microcolony survival assay for cells of mouse intestinal mucosa exposed to radiation. *Int J Radiat Biol Relat Stud Phys Chem Med.* 17, 261–267.
- Wong, V. W. Y., Stange, D. E., Page, M. E., Buczacki, S., Wabik, A., Itami, S., van de Wetering, M., Poulosom, R., Wright, N. A., Trotter, M. W. B., et al. (2012). Lrig1 controls intestinal stem-cell homeostasis by negative regulation of ErbB signalling. *Nat. Cell Biol.* 14, 401–408.
- Yilmaz, Ö. H., Katajisto, P., Lamming, D. W., Gültekin, Y., Bauer-Rowe, K. E., Sengupta, S., Birsoy, K., Dursun, A., Yilmaz, V. O., Selig, M., et al. (2012). mTORC1 in the Paneth cell niche couples intestinal stem-cell function to calorie intake. *Nature* 486, 490–495.
- Zenewicz, L. A., Yancopoulos, G. D., Valenzuela, D. M., Murphy, A. J., Karow, M. and Flavell, R. A. (2007). Interleukin-22 but Not Interleukin-17 Provides Protection to Hepatocytes during Acute Liver Inflammation. *Immunity* 27, 647–659.

Zhang, Q.-Q., Zhou, D.-L., Lei, Y., Zheng, L., Chen, S.-X., Gou, H.-J., Gu, Q.-L., He, X.-D., Lan, T., Qi, C.-L., et al. (2015). Slit2/Robo1 signaling promotes intestinal tumorigenesis through Src-mediated activation of the Wnt/ β -catenin pathway. *Oncotarget* 6, 3123–35.

Zhou, W.-J., Geng, Z. H., Spence, J. R. and Geng, J.-G. (2013). Induction of intestinal stem cells by R-spondin 1 and Slit2 augments chemoradioprotection. *Nature* 501, 107–111.

CHAPTER
NEW CONCEPTS IN
ENTEROENDOCRINE CELL BIOLOGY



SUMMARY

The recent intersection of endocrinology with single-cell technologies and novel in vitro model systems has generated a tremendous amount of new data in the field of enteroendocrine biology. Here we highlight these recent developments and explore how these findings challenge historical and more recent concepts of lineages and cell types. In particular, the concept of hormonal plasticity, the ability of endocrine cells to produce different hormones in the course of their lifetime, bridges the gap between single-letter nomenclature and observations of multi-hormonal cells. Due to the continuously renewing nature of the intestine, enteroendocrine cells travel in the course of their life through different signaling environments that directly influence their hormonal repertoire and thus cell fate. In this context, we examine how enteroendocrine cell fate is determined and modulated by signaling molecules such as BMPs or location along the gastro-intestinal tract. We analyze advantages and disadvantages of novel in vitro tools, adult stem cell or iPS derived intestinal organoids, that have been crucial for recent findings on enteroendocrine development and plasticity. Finally, we illuminate the future perspectives of the field and discuss how understanding enteroendocrine plasticity can lead to new therapeutic approaches.

ESSENTIAL POINTS

- Enteroendocrine cells are rare hormone producing cells in the gut that control key physiological processes related to food intake by secreting more than 20 different peptides
- Types of secreted hormones change over the lifetime of an individual enteroendocrine cell
- The hormonal repertoire of an individual cell is limited by enteroendocrine lineage (5 lineages total) and gastrointestinal region-specific epigenetic landscape
- Hormone expression within these limits is dynamically controlled by the action of changing morphogen signaling during the migration of cells from crypt to villus.
- Adult and pluripotent stem cell derived organoids represent emerging model systems to assess development and function of enteroendocrine cells

Joep Beumer^{1,2}, Helmuth Gehart^{1,2,*} and Hans Clevers^{2,3*}

¹ Co-first author

² Hubrecht Institute, Royal Netherlands Academy of Arts and Sciences (KNAW) and UMC Utrecht, 3584 CT Utrecht, The Netherlands.

³ Oncode Institute, Hubrecht Institute, 3584 CT Utrecht, The Netherlands.

* Co-corresponding author

INTRODUCTION

The intestinal epithelium is generally associated with nutrient uptake and barrier function. However, it is also the largest endocrine organ in our body. In an average human, around 100 million intestinal endocrine cells, called enteroendocrine cells (EECs), are shed every day and regenerated by newly differentiating cells. Despite the impressive number, EECs only constitute 1% of the intestinal epithelium. These rare cells are scattered throughout the epithelium and produce more than 20 intestinal hormones. Which hormones are produced in an individual cell and which stimulus causes the release depends on the EEC type. Classically EECs are distinguished by the main hormone they secrete: Enterochromaffin (EC) cells (Serotonin, 5-HT), I cells (Cholecystokinin, CCK), K cells (Gastric inhibitory peptide, GIP), L cells (Glucagon-like peptide 1, GLP-1), X cells (Ghrelin, GHRL), S cells (Secretin, SCT), D cells (Somatostatin, SST), and N cells (Neurotensin, NTS) were originally described. However, reports of multihormonal cells, significant regional differences among EECs along the gastrointestinal tract and species specificity testify to the insufficiency of the single letter system (Diwakarla et al., 2017; Haber et al., 2017; Habib et al., 2012). Alternative classification systems describing region, species and detected hormones (e.g. $J_M^{GIP+SST+GCG-PYY}$ for a mouse jejunal EEC) (Drucker, 2016) have been suggested, but have not yet found widespread adoption.

Intestinal hormones serve a wide range of functions. Postprandially released hormones (PYY, 5-HT, CCK, GLP-1, GIP) or hormones released during fasting (GHRL, 5-HT) have direct influence on glucose homeostasis. GLP-1 and GIP, called incretins, potentiate insulin release from pancreatic beta cells in the pancreas (Nauck et al., 1993). In contrast, GHRL release has the opposite effect (Adriaenssens et al., 2016). Intestinal hormones act not only indirectly via the pancreas on blood glucose levels, but also by controlling the flow of nutrients through the intestine. CCK, GLP-1 and PYY, for example delay gastric emptying once nutrients have reached the distal small intestine (Phillips et al., 2015). Finally, gut hormones control metabolic adaptation by controlling behaviour. GHRL is released in anticipation of a meal, whereas postprandially released GLP-1, CCK and PYY induce satiety in the central nervous system (Skibicka and Dickson, 2013; Sun et al., 2019). Although, less established than their metabolic roles, EECs have also been linked to orchestrating mucosal immunity (Gribble and Reimann, 2017; Worthington et al., 2018). Since EECs express receptors for microbial metabolites, secrete cytokines upon stimulation and produce hormones that can act directly on immune cells they are equipped to act as sentinels and coordinators of intestinal immunity. However, the extent of this role has yet to be mechanistically assessed.

Until recently it has been unclear whether the observed diversity in EECs (more than 20 reported cell types) is a product of an equally high number of independent differentiation pathways from the common enteroendocrine progenitor stage. However, advances in endocrine biology, single cell sequencing and organoid technology have partially reconciled the original classification with the observed functional diversity by introducing the concept of hormonal plasticity: the ability of a single EEC to go through various mature stages with differing hormonal repertoire. In this review, we discuss these recent findings and try to synthesize a comprehensive

I

II

III

IV

V

VI

VII

VIII

&

picture of the signals and factors that determine and modulate enteroendocrine fate. Finally, we will highlight the advantages and disadvantages of the enteroendocrine in vitro systems that made these findings possible and discuss the future perspectives of the field.

ENTEROENDOCRINE CELL FATE DETERMINATION

Until the 60s, the large resemblance of EECs to neurons (e.g. the production of neurotransmitters and synapse-like projections) led to a general belief that endocrine epithelial cells stem from neural crest cells migrating into the gut epithelium (Schonhoff et al., 2004). The chromaffin cells of the adrenal medulla, named after their characteristic stain with chrome salts resembling intestinal ECs, are similarly known to derive from the neural crest. The first embryonic lineage tracing techniques refuted this model later. When quail mesoderm was combined with chick endoderm during embryonic development all resulting EEC cells were of chick origin (Andrew et al., 1982). Thus, it was definitively shown that all EECs are of endodermal origin.

In an attempt to establish a common precursor to the differentiated cells of the intestinal epithelium, Cheng and Leblond performed radioactive nucleotide labeling and followed the trace over time (Cheng and Leblond, 1974). This work identified crypt base columnar (CBC) cells, slender cells in between Paneth cells (Fig. 1), passing on their label to all differentiated lineages including EECs (Cheng and Leblond, 1974). Final proof for the stem-cell nature of CBCs was only provided in 2007, when the G-protein coupled receptor *Lgr5* was identified as a marker of CBCs. Lineage tracing based on *Lgr5* expression demonstrated the ability of CBCs to regenerate the whole intestinal epithelium and themselves throughout lifetime (Barker et al., 2007). Single *Lgr5*⁺ CBC cells can be isolated and generate three-dimensional in vitro organoid cultures (discussed later) containing all intestinal cell types including EECs (Sato et al., 2009).

Mechanisms of EEC specification

The intestinal epithelium displays a rapid turnover of 4-5 days, which is highly atypical for an endocrine organ. For example, the endocrine pancreas is largely generated during embryonic development and shows little turnover in adult homeostasis (Puri et al., 2015). Intestinal stem cells, on the other hand, divide continuously at the bottom of crypts, while their differentiating offspring moves in a conveyor belt-like motion upwards to the villus tips, where cells are shed (Fig. 1). Two main branches of differentiated cell types are generated: the absorptive enterocytes and the secretory cells, including mucus-secreting goblet cells, antimicrobial and niche compound producing Paneth cells, and a range of different EECs. A binary switch controlled by Notch signaling maintains a steady balance between secretory and absorptive cells via lateral inhibition. Cells that do not receive Notch signals when leaving the stem cell zone acquire a secretory fate. These secretory progenitors will upregulate Notch ligands and induce Notch activation in all surrounding cells that consequently differentiate to the absorptive fate.

Active Notch signaling stimulates expression of Hairy/enhancer of split 1 (Hes1) (Akazawa et al., 1995; Lee et al., 2002), a potent repressor for the basic helix-loop-helix (bHLH) transcription factors *Atoh1* (also known as *Math1*) and *Neurogenin-3* (*Neurog3*). Whereas the former is

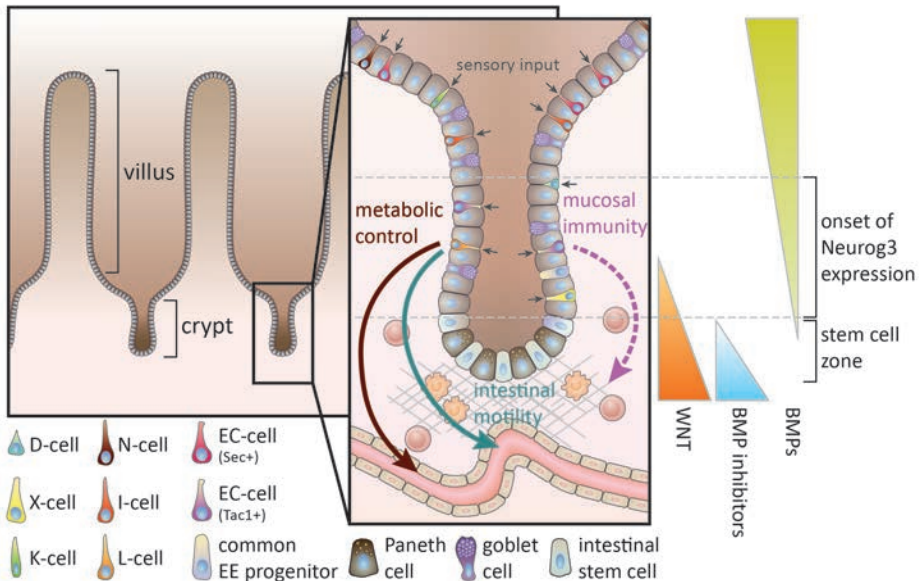


Figure 1. Subtypes and functions of enteroendocrine cells. Enteroendocrine cells (EECs) secrete about 20 different products and identified by a single-letter code based on their principle hormone. Sensory input from the intestinal lumen controls secretion of hormones that regulate metabolism, mucosal immunity and intestinal motility. EECs derive from stem cells at the crypt bottom, when their daughter cells lose Notch signals that allows for the expression of the pro-endocrine transcription factor Neurogenin-3 (Neurog3). Initiation of Neurog3 expression can occur in a wide range of the crypt epithelium, with different exposure levels of the morphogens WNT and BMP.

important for the production of all secretory cells, the latter is the key regulator for EEC cell formation. Mice deficient for Neurog3 completely lack all EEC subtypes in the small and large intestine. Conversely, transgenic overexpression greatly increases the generation of all EEC lineages (Jenny et al., 2002; López-Díaz et al., 2007). In addition to transcriptional regulation, NEUROG3 is also post-transcriptionally regulated by several cyclin-dependent kinases that phosphorylate NEUROG3 and cause its proteasomal degradation (Azzarelli et al., 2017; Krentz et al., 2017). NEUROG3 on the other hand also promotes cell cycle exit by regulating expression of the cell cycle inhibitor *Cdkn1a* (Miyatsuka et al., 2011). A study by the Winton lab followed the fate of particularly slow dividing cells in the intestine and found that these turned indeed into Paneth cells and EECs, but never into Goblet cells (Buczacki et al., 2013). Along the same line, we have found that cell cycle inhibition of intestinal stem cells predispose these to an EEC fate (Basak et al., 2017). These findings corroborate the earlier mechanistic studies and indicates that active proliferation and endocrine fate specification are mutually exclusive.

Another player recently implicated in the regulation of EEC differentiation is mechanical force. EEC progenitors in the gut of fruit flies express the mechanosensor *Piezo*, a membrane-spanning protein that functions as an ion channel responding to forces (He et al., 2018). Stretch forces on the intestinal epithelium cause an increase in cytosolic Ca^{2+} levels specifically in EEC

progenitors that stimulates their differentiation (He et al., 2018). In parallel, Hippo signaling in mammals has been implicated in the regulation of secretory cell differentiation (Gregorieff et al., 2015). The Hippo signaling pathway senses mechanical cues, and when active causes its downstream transcription factor YAP to be translocated from the nucleus. When cellular density is low, Hippo signaling is turned off and YAP translocates to the nucleus to activate target gene expression. Overexpression of YAP blocks the development of secretory cells, including EECs (Petersen et al., 2018).

Although the niche signals driving segregation of EECs from absorptive enterocytes (Notch), Paneth cells (Wnt) and Goblet cells (cell cycle, EGF, mechanical forces) are elucidated (Basak et al., 2017; Mori-Akiyama et al., 2007), the downstream factors causing the different EEC subtypes to be produced are unknown. Transcription factor cascades important for the specification of the EEC lineages have however been well established.

Recent advances in the field of single cell sequencing have enabled researchers to study fate determination of EECs on a single cell level. An intestinal cell atlas by Haber et al. described the diversity of intestinal endocrine cells in the crypt and defined previously unknown endocrine cell populations (Haber et al., 2017). Building on this first single cell dataset, our own work reconstructed the complete developmental trajectory of all EEC subtypes on single-cell level with real-time resolution. To do so, we created a time-resolved Neurog3 reporter mouse (Neurog3Chrono), which combined high temporal resolution with the ability to report even the lowest levels of NEUROG3 expression (Gehart et al., 2019). The cell position within the crypt at the onset of Neurog3 expression is not uniform, but distributed across a broad band along the crypt (Fig. 1). Thus, it is tempting to speculate that the position along the signaling gradients within the crypt play an important role in determining the final lineage of the differentiating cell. By combining the Neurog3Chrono system with single-cell sequencing and functional studies in organoids we were able to determine the order of transcriptional events and key regulators at branching points that determine differentiation from the common enteroendocrine progenitor state to each of the 5 endocrine lineages. Using the real-time resolution of our system, we could show that many presumably mature EEC types are transition stages in the life-time of an individual cell that switches its hormonal repertoire as it moves along the crypt-villus axis.

Hormone plasticity

EECs are usually described as hormone factories with static peptide repertoires, often only a single hormone. This led to the single letter-coding of the EEC subtypes described above. With the advent of more sensitive imaging techniques or transcriptomic measurements, a more complex set of combinations of hormones was identified (Fothergill et al., 2017; Haber et al., 2017). It remained unknown, however, if the vast combinations of hormones represented different cell types transition stages.

First evidence for the latter appeared in the 80s. Radioactive thymidine labeling showed rapid labeling of serotonin-producing cells, while secretin-producing cells were labeled only

after 2 days and were restricted to the villus (Inokuchi et al., 1984, 1985). This led the authors to conclude that the differentiation of secretin-producing cells does not happen before these reach the villus. The Gordon lab in the early 90s more widely characterized crypt-villus heterogeneity of EEC products and for the first time suggested possible lineage relationships between EECs making different hormones in these areas. This extensive immunohistochemical work identified TAC1 and serotonin co-expression in the intestinal crypt, while in the villus tips serotonin overlapped with secretin (Roth and Gordon, 1990). In the villus bottom, rare Tac1, serotonin and secretin triple-positive EECs could be found, suggesting a lineage of EECs undergoing transitions in the produced peptides (Roth and Gordon, 1990). Subsequent work combined hormone staining with BrdU injections to confirm that TAC1+ cells were rapidly generated from dividing progenitors, while secretin+ cells did not appear until 2 days later (Aiken and Roth, 1992). Similarly, GLP-1 was recognized as a typical crypt hormone that follows similar temporal and spatial patterns as TAC1 (Aiken et al., 1994). Functional evidence that individual EECs can dynamically produce different hormone peptides appeared two decades later: Exploiting a diphtheria-toxin receptor driven by the preproglucagon promoter (*Gcg*, precursor for *Glp-1*), the Schwartz lab specifically ablated L-cells defined by *Gcg* expression and followed the loss and reappearance of different hormones (Grunddal et al., 2016). Within 24 hours, the vast majority of GLP-1+ cells were lost, while also a significant but smaller proportion of NTS and PYY positive cells disappeared. Interestingly, GLP-1+ cells reappeared much quicker than PYY- and NTS-producing cells (Grunddal et al., 2016), which indicates that the former may give rise to the latter. The Neurog3Chrono model enabled researchers to follow individual EEC cells over their lifetime, and showed that L-cells indeed upregulate Pyy and Nts after downregulating *Gcg*, 3 days after the initiation of Neurog3-expression (Gehart et al., 2019). The model demonstrated a similar temporal transition for Tac1, serotonin and secretin. Lineage tracing is often used as a golden standard to confirm relationships between cell types (Kretzschmar and Watt, 2012). When TAC1+ cells were traced in the intestinal epithelium, all EECs that produced Serotonin and Secretin in the villus were labeled, even though most stained negative for TAC1 (Beumer et al., 2018). This same tracing experiment yielded no labeling of the other EEC lineages, highlighting the committed nature of EEC subtypes and the inherent limits of plasticity (Beumer et al., 2018).

Different lines of evidence suggest hormone-switching should involve signals unique to the crypt or villus such as morphogens or luminal components, rather than a cell-intrinsic trans-differentiation pathway of the EEC subset. Bjerknes and Cheng described a population of EECs that does not follow the conveyor belt but stays in the crypt after its generation (Bjerknes and Cheng, 1981). These cells failed to express villus hormones such as Secretin, and maintained expression of the crypt-restricted Tac1 or Glp-1 (Aiken and Roth, 1992; Aiken et al., 1994). Using the Neurog3Chrono system, we could show that all EECs remained in the crypt during lineage specification and thus did not move immediately upwards with the conveyor belt. Once functionally mature, the majority of EECs start to move up the crypt villus-axis, while others remain in the crypt for longer periods (Gehart et al., 2019). Interestingly, the observed hormone switching of L- and EC-cells coincided with movement of these populations from

I

II

III

IV

V

VI

VII

VIII

&

the crypt to the villus (Fig. 2). This indicates that the differing environments in crypt and villus could indeed drive hormone switching. Mechanistic insight into this process comes from organoid experiments: EECs *in vitro* in murine intestinal organoids always co-expressed Tac1 and Tph1 (Tryptophan hydroxylase 1, the rate-limiting enzyme for serotonin production) and displayed low secretin levels (Basak et al., 2017; Beumer et al., 2018; Grün et al., 2015). Multiple morphogen gradients exist in the intestinal epithelium along the crypt-villus axis, including WNT, BMP, EGF and hedgehog signals, that are not naturally established in organoids (Beumer and Clevers, 2016). By modulating these pathways in organoids, we identified BMP signaling as the orchestrator of the different patterns of hormone expression in the epithelium (Beumer et al., 2018). BMP signals are high in the intestinal villus and are normally inhibited in organoid cultures to promote stem cell expansion. Activation of the pathway drives hormone switches in individual EECs, such as the repression of Glp-1/Tac1 and induction of Secretin (Beumer et al., 2018). Inhibition of BMP signaling *in vivo* extends the expression of crypt hormones into the villus region, while repressing the expression of the typical villus hormones (Beumer et al., 2018). This makes the BMP signaling pathway an interesting factor in targeted manipulation of EE cell composition in the intestine for therapeutic purposes.

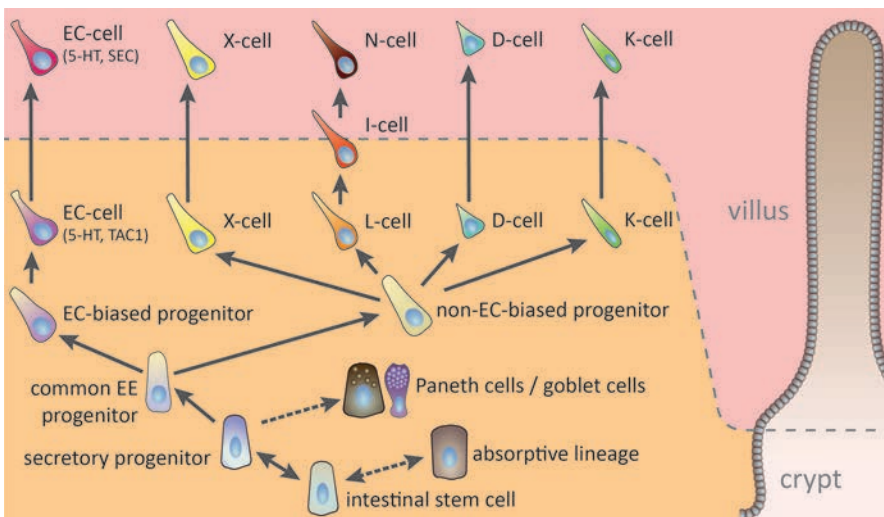


Figure 2. Hormone plasticity among enteroendocrine cells. Intestinal stem cells generate absorptive enterocytes and all secretory cell types, including EECs, Paneth cells and goblet cells. All EECs share a common, Neurog3-positive, progenitor cell. Enterochromaffin cells (ECs) later derive from a separate, EC-biased progenitor, while the other hormone-producing cells share a common progenitor. During the lifetime and migration along the crypt-villus axis, EECs switch their hormone repertoire in response to BMP exposure. BMP signals repress Tac1 in ECs, while inducing Secretin (Sct). Neurotensin-producing N-cells are a BMP-induced state of the Glp-1 producing L-cells. Glp-1 in turn is repressed by BMP signaling.

Heterogeneity along the intestinal tract

The majority of EEC subtypes are not found in constant ratios across the GI tract. The enterochromaffin cells and D-cells are the exception to this rule. L-cells are abundant in the distal SI and almost absent in the duodenum, while GIP and K-cells display the reverse trend (Gunawardene et al., 2011). The underlying mechanisms for these differential hormone programs are currently unknown. One hint can be derived from organoid cultures, that have been found to maintain their location-specific function *in vitro* (Middendorp et al., 2014). For example, the bile acid transporter *Slc10a2* is unique to the ileum, and was accordingly expressed in organoids. This finding was later extended to EECs in mouse and human intestinal organoids, that maintained their native hormone ratio during long-term culture (Basak et al., 2017; Beumer et al., 2018). These observations exclude non-epithelial niche factors or nutrients as potential regulators of regional differences in hormone expression. This leaves differing DNA methylation patterns as likely explanation, since they are generally known to be stable. Indeed, organoid cultures maintained identical DNA methylation patterns compared to the source tissue (Kraiczy et al., 2019). When methylation patterns were disrupted using DNA methyltransferase inhibitors in organoids, ectopic expression of multiple markers that are regionally restricted occurred (Kraiczy et al., 2019). Although, it has not been shown yet, it is likely that the same treatment would reset the EE repertoire of organoids derived from different intestinal regions.

In summary, recent experiments revealed unexpected plasticity within the EEC compartment that is controlled by signaling gradients along the crypt-villus axis. However, this plasticity acts within strict limits imposed by initial lineage specification and regional identity. This results in only 5 distinct cell types of EECs that cannot interconvert, but have the capacity to express a certain cell type-specific set of hormones. Which hormones among this set are expressed in an individual EEC is determined statically by regionally defined epigenetic landscape and dynamically by different environmental cues along the crypt-villus axis. Thus, many of the EEC cell types that have been defined in the past are not distinct states, but individual points in a continuum of potential.

MODEL SYSTEMS FOR THE STUDY OF EEC BIOLOGY

EECs are exceedingly rare, yet highly heterogenous due to hormonal plasticity and regional differences. Multiple model systems have been employed to aid the study of EECs, including hormone reporters to purify populations or follow the effects of genetic or chemical challenges on subsets of EECs. Mouse models have made invaluable contributions to our understanding of the EE system. However, mechanistic understanding of EE fate and function necessitates representative *in vitro* systems that are accessible for functional testing and easily accessible for manipulation such as genome editing.

Cell lines

Cell lines are immortalized by alterations circumventing senescence, such as the introduction of the SV40 antigen, and have been generated from a wide variety of animals. For example,

I

II

III

IV

V

VI

VII

VIII

&

the murine GLUTag cell line was generated from a mouse endocrine tumor, and has been widely used as a model for regulation of GLP-1 secretion (Drucker et al., 1994). The BON cell line is another commonly used model for EEC functioning, that produces serotonin and is derived from a metastatic human carcinoid tumor (Evers et al., 1991). Although these models have been instrumental for early insights in the regulation of EEC function, these cells do not capture the complex features underpinning EEC development and behavior. Cell lines display high proliferation rates, which makes them easy to expand, but inherently non-representative for the anti-proliferative state that is necessary for EEC differentiation in vivo (Solorzano-Vargas et al., 2019). Moreover, cellular interactions between different cell types of the intestinal epithelium are completely absent due to homogenous nature of cell lines. These shortcomings made the development of more complex, but also more representative in vitro systems necessary.

Adult stem cell derived organoids

In the last decade, organoids or “mini-guts” have evolved as alternative to the use of cell lines. Organoids are three-dimensional (3D) cultures that can be grown from a single adult mouse or human stem cell (ASC) and expand indefinitely in a gel-matrix (Fig. 3). These cells are grown

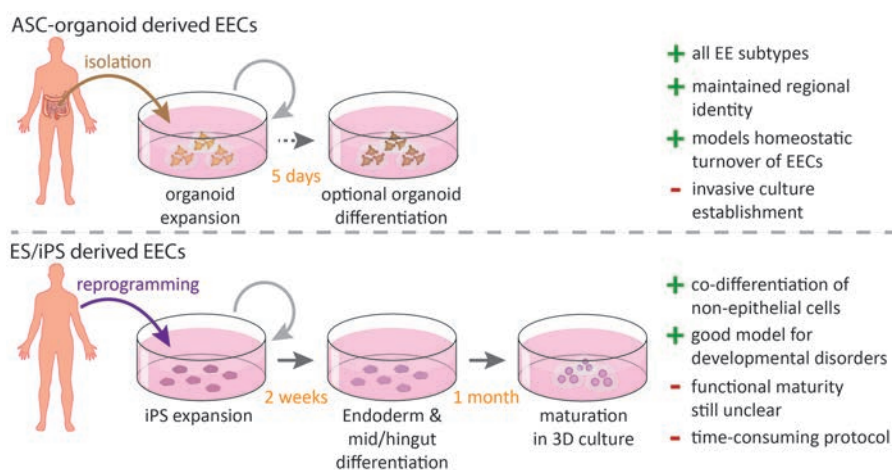


Figure 3. Organoid models for the study of enteroendocrine cells. Adult stem cell (ASC) derived organoids are established from mature tissue, and reflect the region of origin. Thus, only the constituent cell types including EECs of that region of the intestinal tract are generated in culture. Differentiation protocols are generally simple, requiring few growth factor changes and short time windows until maturation. All EEC subtypes can be generated. Embryonic or induced pluripotent stem cells can readily be derived from any adult cell type, and do not require invasive surgeries from the gastrointestinal tract. To generate adult intestine, developmental principles are mimicked that occur during embryonic development. Other cell types that exist alongside the epithelium, such as mesenchyme and enteric neurons, can simultaneously be induced or added, allowing for studying the interaction between these cells and EECs. Diseases that have an embryonic origin can be well studied with this model. The differentiation process from stem cells to EECs is time-consuming, taking more than 1 month, and the maturation level of these cells remains to be assessed.

in defined cocktail of growth factors mimicking the stem cell niche. Mouse small intestinal organoids contain all different intestinal epithelial cell types at near-normal ratios, and are therefore excellent models to study interaction among EECs and with other epithelial cell types (Sato et al., 2009). These organoids can be exposed to different signaling pathway modulators to enrich EECs. For example, the inhibition of WNT, Notch and EGFR/MEK boosted the differentiation of EECs in mouse small intestinal organoids from less than 1% to almost 50% (Basak et al., 2017). These cultures have been valuable to identify developmental regulators of EECs by modulation of certain niche signals – such as BMP signaling - or by loss-of-function experiments using CRISPR Cas9-mediated knockout (Beumer et al., 2018; Gehart et al., 2019). The specific luminal signals that dictate hormone secretion are difficult to distinguish in mice due to the complexity of the diet and microbiome. Organoids allow for a controlled exposure to individual metabolic molecules. Such experiments are essential to untangle effects of different dietary molecules on hormone secretion and to unravel ligand-receptor relationships (Goldspink et al., 2018; Zietek et al., 2015). Finally, ASC-derived organoids have recently also been employed to study the complex interaction between the epithelium and enteric nervous system (ENS) in co-culture experiments (Bellono et al., 2017; Kaelberer et al., 2018a).

Human ASC-derived organoids are more complex to grow than their murine counterparts and require additional activation of Wnt-signaling and inhibition TGF-beta and p38 MAP kinase signaling to expand stem cells (Sato et al., 2011). This necessitates separate expansion and differentiation conditions, since Wnt activation blocks differentiation towards most intestinal lineages (Sato et al., 2011). Multiple differentiation strategies have been employed to generate human EECs in these organoids, such as withdrawing growth factors and inhibition of Notch and MEK signaling (Beumer et al., 2018), or addition of short-chain fatty acids including butyrate (Petersen et al., 2014). Importantly, the differentiation of the human intestinal organoids is an end-point process, that exhausts the stem cell pool and causes a limited lifespan of the resulting cultures of about a week (Sato et al., 2011). To circumvent this limitation, a recent study performed transcriptomic analyses on human intestinal niche ligands and their receptors occurring in the stem cell zone, that could potentially allow both stem cell renewal and differentiation (Fujii et al., 2018). Based on their findings the authors withdrew the p38 inhibitor and added the niche factors IGF-1 and FGF-2 (Fujii et al., 2018). The resulting cultures expanded indefinitely and contained most differentiated cell types including EECs. As this work only assessed these conditions for the human ileum, future studies will have to show whether they are applicable to other parts of the small intestine or colon.

Induced pluripotent stem cell derived organoids

In analogy with ASCs, organoids can be derived from embryonic stem (ES) cells or their synthetic counterparts, induced pluripotent stem cells (iPS) cells, by mimicking the developmental principles that shape the mature tissues in a dish (Clevers, 2016). Endoderm is first specified by treating mouse or human pluripotent stem cells (PSCs) with Activin A, after which the mid/hindgut fate is induced by supplying FGF4 and WNT3A (Spence et al.,

I

II

III

IV

V

VI

VII

VIII

&

2011). (Fig. 3) The resulting spheroid cultures are incubated for one month in the same culture conditions established for mouse small intestinal organoids derived from ASCs (Sato et al., 2009; Spence et al., 2011). During this period, the organoids mature into a columnar epithelium that develops villus-like structures, along with all mature cell types including 1% of the cells being EECs. Subepithelial fibroblasts and smooth muscle cells surround the human intestinal epithelial organoids and are likely derived from a small fraction of mesodermal cells induced after Activin A treatment (Spence et al., 2011). A recent study introduced functional ENS by co-culturing neural crest cells with developing human intestinal organoids, both derived from PSCs (Workman et al., 2017). Upon transplantation of these structures, functional networks of smooth muscle layers and neurons developed that were capable of concerted contraction and relaxation activities (Workman et al., 2017). Although EECs were often found associated with neuronal fibers, physical connection between the two were, in contrast to primary tissue, never found (Workman et al., 2017). This could indicate a lack of maturity of one of the two players, or that these interactions require unknown exogenous factors.

PSC derived intestinal organoids can be forced to differentiate towards EECs with the transient overexpression of *NEUROG3* (Sinagoga et al., 2018; Spence et al., 2011). These EECs can respond to nutrient stimuli, and produce a wide spectrum of hormones. In contrast to PSC-derived organoids, ASC derived organoids have a strict regional identity based on the biopsy location, including the representation of EEC subtypes and hormones of that part of the gut (Basak et al., 2017; Middendorp et al., 2014). The possibilities to induce regional specificity in PSC derived cultures is still very limited. The original protocol to generate human PSC derived organoids generally induced proximal SI hormones, with the notable exception of *CCK* that was not produced (Sinagoga et al., 2018). A short pulse of BMP activation in developing human gut tubes could specify PSC derived cultures towards a more colon-like fate, that showed production of the typical large intestinal hormone *INSL5* in EECs (Múnera et al., 2017). However, the ileal EEC repertoire could not yet be generated through these protocols, and might potentially be achieved by more subtle manipulation of BMP signaling during specification of the different parts of the gut.

The PSC derived model is particularly interesting for disorders that have an origin during embryonic development, and that involve non-epithelial cell types. For example, Hirschsprung's disease is characterized by impaired development of the ENS. Rare mutations in the homeobox-containing transcription factor *PHOX2B* associated with this disease have been successfully introduced in PSCs. Neural crest cells with this mutation were then recombined with intestinal organoids (Workman et al., 2017). This work revealed that developing neural crest cells mutant for *PHOX2B* impaired the development of smooth muscles in the PSC derived intestinal organoids. Similarly, a recent study modeled different mutations in *NEUROG3* that cause a rare inherited EEC deficiency in humans using PSC derived cultures, and showed how these affect the stability and DNA binding activity of the transcription factor (Zhang et al., 2019).

The nature of PSC-based models, capturing the entire embryonic development of adult tissues, makes these exquisitely suitable for the study of disorders that arise in development. The ability to induce non-epithelial cell types on top allows assessing the emergence and

functioning of different interactors with the gut epithelium. ASC derived organoids, on the contrary, are simpler to handle and maturation levels of the constituent cell types have been benchmarked against native tissue. These comparisons have evidenced that ASC organoid EECs are virtually identical to tissue (Gehart et al., 2019), making these organoids ideally suited to study the function and homeostatic turnover of EECs.

CONCLUSIONS & OUTLOOK

New models to study EECs, including intestinal organoids, have greatly increased insights into the developmental phenomena of these enigmatic cells. The novel concept of hormonal plasticity demonstrates the surprising adaptability of the intestinal endocrine system. It reconciles observations of multihormonal cells with lineage tracing data and greatly simplifies the EE lineage tree: there are only 5 different EEC lineages that produce mature cells with gradually changing hormonal profiles. These switches are at least partly imposed by variations in BMP signals during their journey along the crypt-villus axis. Targeting these signals or the migration process would be a new strategy to shape the enteroendocrine landscape for therapeutic purposes.

Although the transcriptional effectors that drive the specification of individual EEC subtypes have been mapped, the signals upstream of these transcription factors remain elusive. Similarly, it is unknown how the stable differences in EEC subtype ratio arise along the GI tract. DNA methylation patterns are strong candidates, but their influence remains to be functionally proven. Indeed, the ability to influence the regional identity of EECs would have great therapeutic value. Bariatric surgery, that bypasses part of the proximal SI, is believed to be successful for glucose management due to rapid delivery of nutrients to the distal SI (Hutch and Sandoval, 2017). GLP-1 is more abundant in the distal SI, and is accordingly increased after bariatric surgery (Hutch and Sandoval, 2017). Inducing a distal SI hormone signature in the proximal SI is expected to have a similar therapeutic outcome.

Finally, the rise of new in vitro systems has opened the opportunity to functionally test decades of knowledge that was generated in the mouse in a human system. Some key differences are obvious and will clearly lead to significant species differences. Mice and humans have different diets, and even produce different hormones in EECs (such as motilin). It is therefore not unlikely that mouse and human EECs generate different hormonal outputs in response to the same nutrient. Thus, human organoids represent attractive targets for the identification of secretagogues with therapeutic value. However, the system is not limited to testing biological molecules and compounds but also compatible with more complex co-culture experiments. Enteric neurons and the microbiome are just two examples of a wide range of interactors that can be assessed in vitro for their ability to regulate gut hormones (Bohórquez et al., 2015; Kaelberer et al., 2018b; Martin et al., 2018). This wealth of new data and availability of new tools holds the potential for a renaissance of enteroendocrine biology, which may see our understanding of a complex differentiation process translated to new therapeutic approaches.

I

II

III

IV

V

VI

VII

VIII

&

REFERENCES

- Adriaenssens, A.E., Svendsen, B., Lam, B.Y.H., Yeo, G.S.H., Holst, J.J., Reimann, F., and Gribble, F.M. (2016). Transcriptomic profiling of pancreatic alpha, beta and delta cell populations identifies delta cells as a principal target for ghrelin in mouse islets. *Diabetologia*.
- Aiken, K.D., and Roth, K.A. (1992). Temporal differentiation and migration of substance P, serotonin, and secretin immunoreactive enteroendocrine cells in the mouse proximal small intestine. *Dev. Dyn.* *194*, 303–310.
- Aiken, K.D., Kisslinger, J.A., and Roth, K.A. (1994). Immunohistochemical studies indicate multiple enteroendocrine cell differentiation pathways in the mouse proximal small intestine. *Dev. Dyn.* *201*, 63–70.
- Akazawa, C., Ishibashi, M., Shimizu, C., Nakanishi, S., and Kageyama, R. (1995). A mammalian helix-loop-helix factor structurally related to the product of *Drosophila* proneural gene *atonal* is a positive transcriptional regulator expressed in the developing nervous system. *J. Biol. Chem.*
- Andrew, A., Kramer, B., and Rawdon, B.B. (1982). The embryonic origin of endocrine cells of the gastrointestinal tract. *Gen. Comp. Endocrinol.* *47*, 249–265.
- Azzarelli, R., Hurley, C., Sznurkowska, M.K., Rulands, S., Hardwick, L., Gamper, I., Ali, F., McCracken, L., Hindley, C., McDuff, F., et al. (2017). Multi-site Neurogenin3 Phosphorylation Controls Pancreatic Endocrine Differentiation. *Dev. Cell* *41*, 274-286.e5.
- Barker, N., van Es, J.H., Kuipers, J., Kujala, P., van den Born, M., Cozijnsen, M., Haegebarth, A., Korving, J., Begthel, H., Peters, P.J., et al. (2007). Identification of stem cells in small intestine and colon by marker gene *Lgr5*. *Nature* *449*, 1003–1007.
- Basak, O., Beumer, J., Wiebrands, K., Seno, H., van Oudenaarden, A., and Clevers, H. (2017). Induced Quiescence of *Lgr5+* Stem Cells in Intestinal Organoids Enables Differentiation of Hormone-Producing Enteroendocrine Cells. *Cell Stem Cell* *20*, 177-190.e4.
- Bellono, N.W., Bayrer, J.R., Leitch, D.B., Castro, J., Zhang, C., O'Donnell, T.A., Brierley, S.M., Ingraham, H.A., and Julius, D. (2017). Enterochromaffin Cells Are Gut Chemosensors that Couple to Sensory Neural Pathways. *Cell* *170*, 185-198.e16.
- Beumer, J., and Clevers, H. (2016). Regulation and plasticity of intestinal stem cells during homeostasis and regeneration. *Development* *143*, 3639–3649.
- Beumer, J., Artegiani, B., Post, Y., Reimann, F., Gribble, F., Nguyen, T.N., Zeng, H., Van den Born, M., Van Es, J.H., and Clevers, H. (2018). Enteroendocrine cells switch hormone expression along the crypt-to-villus BMP signaling gradient. *Nat Cell Biol* *20*.
- Bjerknes, M., and Cheng, H. (1981). The stem-cell zone of the small intestinal epithelium. III. Evidence from columnar, enteroendocrine, and mucous cells in the adult mouse. *Am. J. Anat.* *160*, 77–91.
- Bohórquez, D. V., Shahid, R.A., Erdmann, A., Kreger, A.M., Wang, Y., Calakos, N., Wang, F., and Liddle, R.A. (2015). Neuroepithelial circuit formed by innervation of sensory enteroendocrine cells. *J. Clin. Invest.* *125*, 782–786.
- Buczacki, S.J. a, Zecchini, H.I., Nicholson, A.M., Russell, R., Vermeulen, L., Kemp, R., and Winton, D.J. (2013). Intestinal label-retaining cells are secretory precursors expressing *Lgr5*. *Nature* *495*, 65–69.
- Cheng, H., and Leblond, C. (1974). Origin, differentiation and renewal of the four main epithelial cell types in the mouse small intestine. V. Unitarian theory of the origin of the four epithelial cell types. *Am J Anat* *141*, 537–561.
- Clevers, H. (2016). Modeling Development and Disease with Organoids. *Cell*.

- Diwakarla, S., Fothergill, L.J., Fakhry, J., Callaghan, B., and Furness, J.B. (2017). Heterogeneity of enterochromaffin cells within the gastrointestinal tract. *Neurogastroenterol. Motil.*
- Drucker, D.J. (2016). Evolving concepts and translational relevance of enteroendocrine cell biology. *J. Clin. Endocrinol. Metab.*
- Drucker, D.J., Jin, T., Asa, S.L., Young, T.A., and Brubaker, P.L. (1994). Activation of proglucagon gene transcription by protein kinase-A in a novel mouse enteroendocrine cell line. *Mol. Endocrinol.* 8, 1646–1655.
- Evers, B.M., Townsend, C.M., Upp, J.R., Allen, E., Hurlbut, S.C., Kim, S.W., Rajaraman, S., Singh, P., Reubi, J.C., and Thompson, J.C. (1991). Establishment and characterization of a human carcinoid in nude mice and effect of various agents on tumor growth. *Gastroenterology.*
- Fothergill, L.J., Callaghan, B., Hunne, B., Bravo, D.M., and Furness, J.B. (2017). Costorage of enteroendocrine hormones evaluated at the cell and subcellular levels in male mice. *Endocrinology* 158, 2113–2123.
- Fujii, M., Matano, M., Toshimitsu, K., Takano, A., Mikami, Y., Nishikori, S., Sugimoto, S., and Sato, T. (2018). Human Intestinal Organoids Maintain Self-Renewal Capacity and Cellular Diversity in Niche-Inspired Culture Condition. *Cell Stem Cell* 23, 787–793.e6.
- Gehart, H., van Es, J.H., Hamer, K., Beumer, J., Kretschmar, K., Dekkers, J.F., Rios, A., and Clevers, H. (2019). Identification of Enteroendocrine Regulators by Real-Time Single-Cell Differentiation Mapping. *Cell.*
- Goldspink, D.A., Lu, V.B., Billing, L.J., Larraufie, P., Tolhurst, G., Gribble, F.M., and Reimann, F. (2018). Mechanistic insights into the detection of free fatty and bile acids by ileal glucagon-like peptide-1 secreting cells. *Mol. Metab.* 7, 90–101.
- Gregorieff, A., Liu, Y., Inanlou, M.R., Khomchuk, Y., and Wrana, J.L. (2015). Yap-dependent reprogramming of Lgr5+ stem cells drives intestinal regeneration and cancer. *Nature* 526, 715–718.
- Gribble, F.M., and Reimann, F. (2017). Signalling in the gut endocrine axis. *Physiol. Behav.*
- Grün, D., Lyubimova, A., Kester, L., Wiebrands, K., Basak, O., Sasaki, N., Clevers, H., and van Oudenaarden, A. (2015). Single-cell messenger RNA sequencing reveals rare intestinal cell types. *Nature* 525, 251–255.
- Grunddal, K. V., Ratner, C.F., Svendsen, B., Sommer, F., Engelstoft, M.S., Madsen, A.N., Pedersen, J., Nøhr, M.K., Egerod, K.L., Nawrocki, A.R., et al. (2016). Neurotensin is coexpressed, coreleased, and acts together with GLP-1 and PYY in enteroendocrine control of metabolism. *Endocrinology* 157, 176–194.
- Gunawardene, A.R., Corfe, B.M., and Staton, C.A. (2011). Classification and functions of enteroendocrine cells of the lower gastrointestinal tract. *Int. J. Exp. Pathol.* 92, 219–231.
- Haber, A.L., Biton, M., Rogel, N., Herbst, R.H., Shekhar, K., Smillie, C., Burgin, G., Delorey, T.M., Howitt, M.R., Katz, Y., et al. (2017). A single-cell survey of the small intestinal epithelium. *Nature* 551, 333–339.
- Habib, A.M., Richards, P., Cairns, L.S., Rogers, G.J., Bannon, C.A.M., Parker, H.E., Morley, T.C.E., Yeo, G.S.H., Reimann, F., and Gribble, F.M. (2012). Overlap of endocrine hormone expression in the mouse intestine revealed by transcriptional profiling and flow cytometry. *Endocrinology* 153, 3054–3065.
- He, L., Si, G., Huang, J., Samuel, A.D.T., and Perrimon, N. (2018). Mechanical regulation of stem-cell differentiation by the stretch-activated Piezo channel. *Nature* 555, 103–106.
- Hutch, C.R., and Sandoval, D. (2017). The role of GLP-1 in the metabolic success of bariatric surgery. *Endocrinology.*
- Inokuchi, H., Azuma, T., Kawai, K., Takeuchi, Y., and Sano, Y. (1984). Serotonin immunohistochemistry reveals immature EC cells. *Histochemistry* 80, 517–518.

I

II

III

IV

V

VI

VII

VIII

&

- Inokuchi, H., Fujimoto, S., Hattori, T., and Kawai, K. (1985). Tritiated thymidine radioautographic study on the origin and renewal of secretin cells in the rat duodenum. *Gastroenterology* 89, 1014–1020.
- Jenny, M., Uhl, C., Roche, C., Duluc, I., Guillermin, V., Guillemot, F., Jensen, J., Kedinger, M., and Gradwohl, G. (2002). Neurogenin3 is differentially required for endocrine cell fate specification in the intestinal and gastric epithelium. *EMBO J.* 21, 6338–6347.
- Kaelberer, M.M., Buchanan, K.L., Klein, M.E., Barth, B.B., Montoya, M.M., Shen, X., and Bohórquez, D. V (2018a). A gut-brain neural circuit for nutrient sensory transduction. *Science* (80-.). 361, eaat5236.
- Kaelberer, M.M., Buchanan, K.L., Klein, M.E., Barth, B.B., Montoya, M.M., Shen, X., and Bohórquez, D. V (2018b). A gut-brain neural circuit for nutrient sensory transduction. *Science* (80-.). 361, eaat5236.
- Kraczy, J., Nayak, K.M., Howell, K.J., Ross, A., Forbester, J., Salvestrini, C., Mustata, R., Perkins, S., Andersson-Rolf, A., Leenen, E., et al. (2019). DNA methylation defines regional identity of human intestinal epithelial organoids and undergoes dynamic changes during development. *Gut*.
- Krentz, N.A.J., van Hoof, D., Li, Z., Watanabe, A., Tang, M., Nian, C., German, M.S., and Lynn, F.C. (2017). Phosphorylation of NEUROG3 Links Endocrine Differentiation to the Cell Cycle in Pancreatic Progenitors. *Dev. Cell* 41, 129-142.e6.
- Kretschmar, K., and Watt, F.M. (2012). Lineage tracing. *Cell* 148, 33–45.
- Lee, C.S., Perreault, N., Brestelli, J.E., and Kaestner, K.H. (2002). Neurogenin 3 is essential for the proper specification of gastric enteroendocrine cells and the maintenance of gastric epithelial cell identity. *Genes Dev.*
- López-Díaz, L., Jain, R.N., Keeley, T.M., VanDussen, K.L., Brunkan, C.S., Gumucio, D.L., and Samuelson, L.C. (2007). Intestinal Neurogenin 3 directs differentiation of a bipotential secretory progenitor to endocrine cell rather than goblet cell fate. *Dev. Biol.*
- Martin, C.R., Osadchiy, V., Kalani, A., and Mayer, E.A. (2018). The Brain-Gut-Microbiome Axis. *CMGH*.
- Middendorp, S., Schneeberger, K., Wiegerinck, C.L., Mokry, M., Akkerman, R.D.L., Van Wijngaarden, S., Clevers, H., and Nieuwenhuis, E.E.S. (2014). Adult stem cells in the small intestine are intrinsically programmed with their location-specific function. *Stem Cells*.
- Miyatsuka, T., Kosaka, Y., Kim, H., and German, M.S. (2011). Neurogenin3 inhibits proliferation in endocrine progenitors by inducing Cdkn1a. *Proc. Natl. Acad. Sci. U. S. A.*
- Mori-Akiyama, Y., van den Born, M., van Es, J.H., Hamilton, S.R., Adams, H.P., Zhang, J., Clevers, H., and de Crombrughe, B. (2007). SOX9 Is Required for the Differentiation of Paneth Cells in the Intestinal Epithelium. *Gastroenterology* 133, 539–546.
- Múnera, J.O., Sundaram, N., Rankin, S.A., Hill, D., Watson, C., Mahe, M., Vallance, J.E., Shroyer, N.F., Sinagoga, K.L., Zarzoso-Lacoste, A., et al. (2017). Differentiation of Human Pluripotent Stem Cells into Colonic Organoids via Transient Activation of BMP Signaling. *Cell Stem Cell*.
- Nauck, M.A., Heimesaat, M.M., Orskov, C., Holst, J.J., Ebert, R., and Creutzfeldt, W. (1993). Preserved incretin activity of glucagon-like peptide 1 [7-36 amide] but not of synthetic human gastric inhibitory polypeptide in patients with type- 2 diabetes mellitus. *J. Clin. Invest.*
- Petersen, N., Reimann, F., Bartfeld, S., Farin, H.F., Ringnalda, F.C., Vries, R.G.J., Van Den Brink, S., Clevers, H., Gribble, F.M., and De Koning, E.J.P. (2014). Generation of I cells in mouse and human small intestine organoids. *Diabetes*.
- Petersen, N., Frimurer, T.M., Pedersen, M.T., Kristoffer, L., Albrechtsen, N.J.W., Holst, J.J., Grapin-botton, A., Kim, B., and Schwartz, T.W. (2018). Inhibiting RHOA Signaling in Mice Increases Glucose Tolerance and Numbers of Enteroendocrine and Other Secretory Cells in the Intestine. *Gastroenterology*.

- Phillips, L.K., Deane, A.M., Jones, K.L., Rayner, C.K., and Horowitz, M. (2015). Gastric emptying and glycaemia in health and diabetes mellitus. *Nat. Rev. Endocrinol.*
- Puri, S., Foliás, A.E., and Hebrok, M. (2015). Plasticity and dedifferentiation within the pancreas: Development, homeostasis, and disease. *Cell Stem Cell.*
- Roth, K. a, and Gordon, J.I. (1990). Spatial differentiation of the intestinal epithelium: analysis of enteroendocrine cells containing immunoreactive serotonin, secretin, and substance P in normal and transgenic mice. *Proc. Natl. Acad. Sci. U. S. A.* 87, 6408–6412.
- Sato, T., Vries, R.G., Snippert, H.J., van de Wetering, M., Barker, N., Stange, D.E., van Es, J.H., Abo, A., Kujala, P., Peters, P.J., et al. (2009). Single Lgr5 stem cells build crypt-villus structures in vitro without a mesenchymal niche. *Nature* 459, 262–265.
- Sato, T., Stange, D.E., Ferrante, M., Vries, R.G.J., Van Es, J.H., Van Den Brink, S., Van Houdt, W.J., Pronk, A., Van Gorp, J., Siersema, P.D., et al. (2011). Long-term expansion of epithelial organoids from human colon, adenoma, adenocarcinoma, and Barrett’s epithelium. *Gastroenterology* 141, 1762–1772.
- Schonhoff, S.E., Giel-Moloney, M., and Leiter, A.B. (2004). Minireview: Development and differentiation of gut endocrine cells. *Endocrinology* 145, 2639–2644.
- Sinagoga, K.L., McCauley, H.A., Múnera, J.O., Reynolds, N.A., Enriquez, J.R., Watson, C., Yang, H.C., Helmraath, M.A., and Wells, J.M. (2018). Deriving functional human enteroendocrine cells from pluripotent stem cells. *Development.*
- Skibicka, K.P., and Dickson, S.L. (2013). Enteroendocrine hormones - Central effects on behavior. *Curr. Opin. Pharmacol.*
- Solorzano-Vargas, R.S., Bjercknes, M., Wu, S.V., Wang, J., Stelzner, M., Dunn, J.C.Y., Dhawan, S., Cheng, H., Georgia, S., and Martín, M.G. (2019). The cellular regulators PTEN and BMI1 help mediate NEUROGENIN-3’induced cell cycle arrest. *J. Biol. Chem.* jbc.RA119.008926.
- Spence, J.R., Mayhew, C.N., Rankin, S.A., Kuhar, M.F., Vallance, J.E., Tolle, K., Hoskins, E.E., Kalinichenko, V. V., Wells, S.I., Zorn, A.M., et al. (2011). Directed differentiation of human pluripotent stem cells into intestinal tissue in vitro. *Nature.*
- Sun, E.W.L., Martin, A.M., Young, R.L., and Keating, D.J. (2019). The regulation of peripheral metabolism by gut-derived hormones. *Front. Endocrinol. (Lausanne).*
- Workman, M.J., Mahe, M.M., Trisno, S., Poling, H.M., Watson, C.L., Sundaram, N., Chang, C.F., Schiesser, J., Aubert, P., Stanley, E.G., et al. (2017). Engineered human pluripotent-stem-cell-derived intestinal tissues with a functional enteric nervous system. *Nat. Med.*
- Worthington, J.J., Reimann, F., and Gribble, F.M. (2018). Enteroendocrine cells-sensory sentinels of the intestinal environment and orchestrators of mucosal immunity. *Mucosal Immunol.*
- Zhang, X., McGrath, P.S., Salomone, J., Rahal, M., McCauley, H.A., Schweitzer, J., Kovall, R., Gebelein, B., and Wells, J.M. (2019). A Comprehensive Structure-Function Study of Neurogenin3 Disease-Causing Alleles during Human Pancreas and Intestinal Organoid Development. *Dev. Cell.*
- Zietek, T., Rath, E., Haller, D., and Daniel, H. (2015). Intestinal organoids for assessing nutrient transport, sensing and incretin secretion. *Sci. Rep.* 5.

I

II

III

IV

V

VI

VII

VIII

&

CHAPTER

**INDUCED QUIESCENCE OF LGR5+ STEM
CELLS IN INTESTINAL ORGANOIDS
ENABLES DIFFERENTIATION
OF HORMONE-PRODUCING
ENTEROENDOCRINE CELLS**



SUMMARY

Lgr5+ adult intestinal stem cells are highly proliferative throughout life. Single Lgr5+ stem cells can be cultured into three-dimensional organoids containing all intestinal epithelial cell types at near-normal ratios. Conditions to generate the main cell types (enterocyte, goblet cells, Paneth cells, and M cells) are well established, but signals to induce the spectrum of hormone-producing enteroendocrine cells (EECs) have remained elusive. Here, we induce Lgr5+ stem cell quiescence in vitro by blocking epidermal growth factor receptor (EGFR) or mitogen-associated protein kinase (MAPK) signaling pathways in organoids and show that their quiescent state is readily reverted. Quiescent Lgr5+ stem cells acquire a distinct molecular signature biased toward EEC differentiation. Indeed, combined inhibition of Wnt, Notch, and MAPK pathways efficiently generates a diversity of EEC hormone-expressing subtypes in vitro. Our observations uncouple Wnt-dependent stem cell maintenance from EGF-dependent proliferation and provide an approach for the study of the elusive EECs in a defined environment.

Onur Basak^{1,3}, Joep Beumer^{1,3}, Kay Wiebrands^{1,3}, Hiroshi Seno²,
Alexander van Oudenaarden¹, Hans Clevers^{1,*}

¹Hubrecht Institute, Royal Netherlands Academy of Arts and Sciences (KNAW), and University Medical Center Utrecht, Uppsalalaan 8, 3584 CT, Utrecht, The Netherlands

²Department of Gastroenterology and Hepatology, Kyoto University Graduate School of Medicine, Kyoto, Japan

³These authors contributed equally to this work

* Corresponding author: Hans Clevers; h.clevers@hubrecht.eu

INTRODUCTION

Lgr5+ stem cells self-renew constantly throughout life at the base of intestinal crypts (Clevers, 2013). Active Notch signaling in rapidly dividing daughters specifies an enterocyte fate. Alternatively, some daughters upregulate Notch ligands (i.e., Dll1 and Dll4) immediately after leaving the crypt base niche, concomitant with an exit from the cell cycle (van Es et al., 2012). The latter cells represent secretory progenitors that give rise to Paneth, goblet, and enteroendocrine cells (EECs).

Murine Lgr5+ intestinal stem cells divide on average every 21.5 hr (Schepers et al., 2011). A reserve stem cell population has been shown to reside above the Paneth cells at the “+4” position (Montgomery et al., 2011, Muñoz et al., 2012, Potten et al., 1978, Powell et al., 2012, Sangiorgi and Capecchi, 2008, Schepers et al., 2011, Takeda et al., 2011, Yan et al., 2012). These cells are generally non-proliferative and can replace lost Lgr5+ stem cells. An elegant lineage-tracing strategy identified these label-retaining cells as non-cycling secretory progenitors (Buczacki et al., 2013). Indeed, these secretory progenitors and the +4 cells share several molecular markers, including Hopx, Bmi1, Lrig, and Tert expression (Montgomery et al., 2011, Muñoz et al., 2012, Powell et al., 2012, Schepers et al., 2011, Takeda et al., 2011, Yan et al., 2012). Moreover, dissection of Lgr5+ crypt populations with distinct cell-cycle features suggests that Lgr5^{low} cells with slow cell-cycle kinetics are secretory precursors (Basak et al., 2014). The presence and identity of “professional” quiescent intestinal stem cells has remained elusive.

Traditionally known as defensive units against microbial infections, Paneth cells also act as part of the niche for the juxtaposed Lgr5+ stem cells by secreting Wnt3 and epidermal growth factor (EGF) and by presenting the Notch ligands Dll1 and Dll4 (Pellegrinet et al., 2011, Sato et al., 2011). Mesenchyme surrounding the crypts also contributes to the niche by secreting Wnt2b as well as several BMP inhibitors (Aoki et al., 2016, Farin et al., 2012).

The murine intestinal organoid culture system (Sato et al., 2009) generates all principle cell types of the intestinal epithelium, including Lgr5+ stem cells. The system is based on substitution of in vivo niche components (i.e., the Wnt agonist R-spondin-1, EGF, and the BMP inhibitor Noggin). Matrigel mimics the extracellular matrix and provides the structural basis for self-organization. R-spondin-1 is a critical component that, through interaction with its Lgr4 and 5 receptors, amplifies the Wnt3 signal emanating from Paneth cells (de Lau et al., 2011).

Organoids can be programmed to produce relatively pure populations of most epithelial cell types. High-Wnt and high-Notch conditions favoring expansion of Lgr5+ stem cells can be mimicked by the addition of the GSK3 inhibitor CHIR99021 combined with the histone deacetylase (HDAC) inhibitor valproic acid (Yin et al., 2014). Enterocytes appear under conditions of Wnt inhibition and Notch activation (Yin et al., 2014). The addition of Rank ligand promotes the fate of M cells, which cover Peyer’s patches and transport luminal antigens via transcytosis (de Lau et al., 2012). Notch inhibition generally induces secretory fates. In the absence of Wnt, secretory goblet cells are formed (van Es et al., 2005), while in the presence of Wnt, Paneth cells appear (van Es et al., 2012, Yin et al., 2014).

I

II

III

IV

V

VI

VII

VIII

&

EECs are rare, hormone-secreting cells that are also generated from *Lgr5*⁺ stem cells (Barker et al., 2007). Hormones expressed by EECs regulate a wide variety of physiological responses, including gastric emptying, release of pancreatic enzymes, blood glucose levels, and appetite and mood changes. Most commonly, subtypes are distinguished based on their secreted hormones and include somatostatin⁺ (Sst) D-cells, gastric inhibitory polypeptide⁺ (Gip) K-cells, secretin⁺ (Sct) S-cells, cholecystokinin (Cck) I-cells, glucagon-like protein 1⁺ (GLP-1) L-cells, neurotensin⁺ (Nts) N-cells, and serotonin-producing enterochromaffin cells (Gunawardene et al., 2011). However, a single EEC may express multiple hormones at varying levels, underscoring a high level of heterogeneity (Egerod et al., 2012). In a recent single-cell-sequencing approach, we demonstrated that organoids faithfully generate the various EEC types and identified three additional subtypes of EECs: *Tac1*/*Cck*⁺, *Ucn3*⁺, and *Alb*/*Afp*⁺ (Grün et al., 2015). G-protein-coupled taste receptors have been identified as regulators of hormone secretion in these cells (Janssen and Depoortere, 2013). Indeed, EECs can have direct luminal contact and sense the intestinal content with microvilli. Other EECs, the so-called closed-type cells, are not exposed to the lumen (Janssen and Depoortere, 2013). Their basal process (of varying length) may form synaptic contacts with enteric neurons to connect to the nervous system. While EECs clearly play crucial roles in controlling various aspects of intestinal function and organismal metabolism, their scarcity has posed a hurdle to their in-depth study. Here, we explore methods to program organoids toward EEC fates *in vitro*.

RESULTS

Inhibition of EGFR Signaling Abolishes Proliferation of *Lgr5*⁺ Stem Cells and Induces Their Quiescence

To understand how mouse *Lgr5*⁺ stem cells are kept in cycle, we manipulated key signaling pathways active in the crypt niche. The *Lgr5*^{GFPDTR} allele (Tian et al., 2011) is never silenced in *Lgr5*⁺ cells (see below) and is well suited for flow-cytometry-based quantification of *Lgr5*⁺ cell numbers. Combining flow cytometric analysis of *Lgr5*^{GFPDTR/+} organoids with antibody staining against KI67, a marker of cycling cells in all cell-cycle phases, confirmed that the overwhelming majority (94.1% ± 2.1%) of the *Lgr5*⁺ cells cycle in ENR (EGF, Noggin and R-spondin-1) medium (Figures S1A and S1C). Wnt signaling is reported to induce cell-cycle progression through cyclin D₂ and c-Myc expression (Myant and Sansom, 2011). We inhibited Wnt signaling using two independent methods: (1) withdrawal of R-spondin1 from the culture medium and (2) IWP-2 treatment which inhibits Wnt3 secretion by Paneth cells (Figure S1A). R-spondin-1 withdrawal caused rapid loss of *Lgr5*^{GFPDTR} expression (Figure S1A). IWP2 treatment (iWnt) poses a slower Wnt inhibition that depends on dilution of ligands through proliferation (Farin et al., 2016). *Lgr5*^{GFPDTR} expression was gradually downregulated while stem cells differentiated into KI67⁺ *Lgr5*⁻ cells upon iWnt treatment (Figures S1A and S1B). Yet, the remaining *Lgr5*^{GFPDTR}⁺ cells maintained KI67 expression (63.5% ± 2.8% vs. 94.4% ± 2.1% in control; Figure S1C). Withdrawal of the BMP inhibitor Noggin or addition of the Notch inhibitor DAPT (iNotch) both induced a rapid decrease in *Lgr5*^{GFPDTR}⁺ cell numbers (Figure

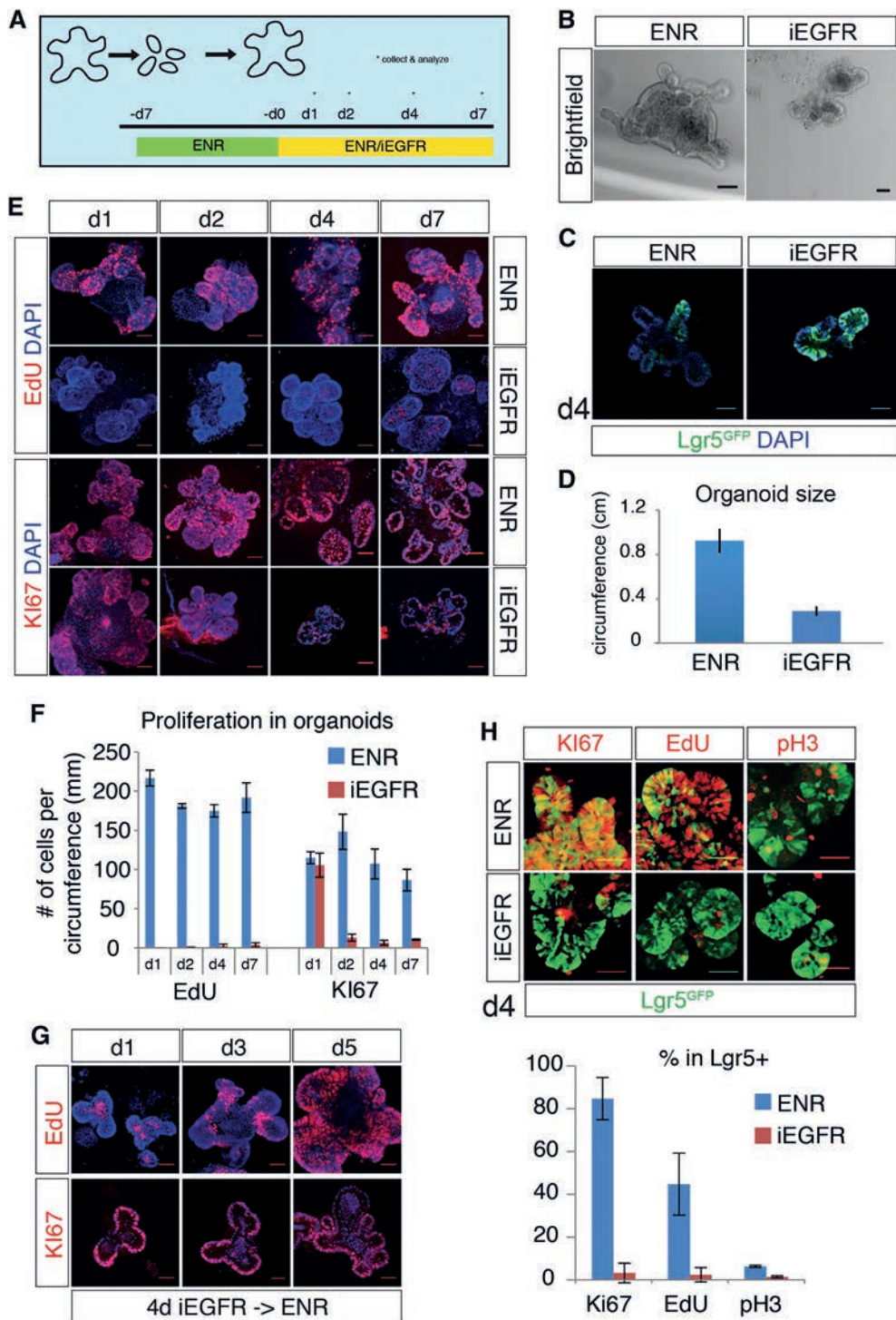
S1A) but did not affect proliferation of the remaining $Lgr5^{GFPDTR+}$ cells ($82.3\% \pm 1.4\%$ in Noggin withdrawal and $45.1\% \pm 10\%$ in iNotch) (Figure S1C). Next, we inhibited EGF receptor (EGFR) signaling using gefitinib accompanied by withdrawal of EGF from the culture medium (iEGFR). While $Lgr5^{GFPDTR}$ expression persisted (Figures S1A and S1D), the $Lgr5^{GFPDTR+}$ cells eventually lost KI67 expression ($13.1\% \pm 1.0\%$ remaining KI67+ cells) indicative of cell-cycle exit (Figures S1C and S1D). After 4 days of iEGFR treatment, $Lgr5^{GFPDTR+}$ cells comprised $44.4\% \pm 0.8\%$ (vs. $13.6\% \pm 6.5\%$ in control) of the organoids when analyzed by fluorescence-activated cell sorting (FACS) (Figures S1A and S1D).

We then focused on the early events associated with EGFR inhibition (Figure 1A). Despite extensive apoptosis of the differentiated compartments of the organoid, buds resembling crypt structures survived iEGFR treatment for at least a week (Figures 1B and S2B). Fluorescent microscopy analysis using both $Lgr5^{GFPiresCreER/+}$ (Figure S2A) and $Lgr5^{GFPDTR/+}$ (Figure S2B) organoids confirmed that these buds contained $Lgr5+$ cells. Of note, the $Lgr5^{GFPiresCreER}$ allele is well suited for lineage tracing and is the strongest GFP-expressing $Lgr5$ allele, yet it is stochastically silenced in some cells (Barker et al., 2007). We noticed that GFP levels increased upon iEGFR treatment (Figures S2A and S2B). The $Rosa^{TCF-CFP}$ Wnt signal reporter allele (Serup et al., 2012) revealed that increased $Lgr5$ reporter expression coincided with high Wnt activity (Figure S2B). Confocal microscopy revealed that the cellular bridges connecting buds in normal organoid cultures (ENR) slowly converted into cellular debris in iEGFR cultures (Figure 1B). Typically, iEGFR cultures contained round, crypt-like bud structures with many $Lgr5+$ cells intermingled with $Lgr5-$ cells (Figure 1C). We also noticed that organoids in iEGFR cultures were considerably smaller than controls (Figures 1C and 1D). Thus, iEGFR treatment results in smaller organoids mostly consisting of crypt-like buds with high Wnt signal strength and $Lgr5$ expression.

Next, we analyzed proliferation of organoids using immunofluorescence and confocal microscopy. The KI67 protein persisted for the first 24 hr but was lost from 48 hr onward (Figures 1E and 1F). Using a short pulse of ethynyldeoxyuridine (EdU) as a measure of S phase cells, we found that iEGFR lead to a rapid halt in DNA replication as early as 24 hr, which persisted for at least a week (Figures 1E and 1F). Consistent with exit from S phase and eventually from the cell cycle, labeling the DNA content of iEGFR-treated organoids using Hoechst DNA staining confirmed that all cells were in G_0/G_1 phase (Figure S2C). 4 days after iEGFR treatment, reconstitution of EGF signaling induced rapid cell-cycle entry within 24 hr (KI67+) and progression to the S phase within 48 hr (EdU+) (Figures 1G and S2D). Figure 1H further illustrates that $Lgr5+$ cells in iEGFR-treated organoids lacked the cell-cycle marker KI67 and the M phase marker pH3 and did not incorporate EdU, excluding that rare dividing cells persisted during iEGFR treatment (Figure 1H). Altogether, our results reveal that iEGFR treatment abolishes proliferation of organoids and induces generation of quiescent $Lgr5+$ cells.

Stem Cell Potential Is Maintained in Reactivated $Lgr5+$ Intestinal Stem Cells

To test whether quiescent $Lgr5+$ cells maintain stem cell potential, we used $Lgr5^{GFPiresCreER/+}$ $Rosa^{LacZ/YFP}$ mice to lineage-trace $Lgr5+$ cells (Figure S2E). CreER induction using 4-OH tamoxifen



(Tmx) led to rapid recombination of the *Rosa^{LacZ}* allele. Cre reporter that could be visualized by X-Gal staining (blue precipitate in Figure S2E). Quiescent *Lgr5⁺* cells generated upon 4 days of iEGFR treatment. Tmx was introduced to the medium during the last day of the treatment and removed when *Egf* signaling was reactivated. Labeled and reactivated quiescent *Lgr5⁺* cells gave rise to organoids entirely labeled with X-Gal, as visualized two passages after Tmx induction. As control, labeled *Dclk1^{GFPiresCreER}Rosa^{LacZ}* cells (marking tuft cells) did not generate new organoids consistent with their differentiated nature (the rare blue cells are persisting Tuft cells). Since only stem cells can generate new organoids in intestinal organoid cultures (Sato et al., 2009), these findings indicated that quiescent *Lgr5⁺* cells generated by EGFR inhibition retain their stemness.

To evaluate the cellular composition of iEGFR-treated organoids, we performed immunofluorescence analysis. Quantification of the number of marker-positive cells per organoid revealed that absolute numbers of LYZ+ Paneth cells and CHGA+ EECs were not significantly increased after 4 days in iEGFR (Figure 2A). Mucin-2 (MUC2) immunostaining revealed that a comparable amount of goblet cells were present following iEGFR treatment (Figure S2F). Tuft cells (intestinal M-cells) are rare mechanosensory cells involved in response to parasitic invasion (Howitt et al., 2016). Apical actin bundles that are revealed by acetylated tubulin and F-actin (Phalloidin) staining distinguishes Tuft cells (Höfer and Drenckhahn, 1996). The number of Tuft cells per organoid increased upon iEGFR treatment (Figure 2B). We corroborated these results using the *Dclk1^{GFPiresCreER}* allele (Nakanishi et al., 2013), revealing that iEGFR treatment increased the absolute number of *Dclk1⁺* Tuft cells 3.2-fold (11.3 ± 6.6 in ENR and 35.8 ± 8.8 in iEGFR; Figure 2B). GFP-marked cells almost invariably contained acetylated tubulin bundles confirming the specificity of the *Dclk1* allele (Figure 2B). The absence of EEC, Paneth cell, and Tuft cell markers in *Lgr5^{GFPiresCreER}⁺* cells argued against upregulation of *Lgr5* in differentiated cells (Figure S2G). Thus, continuous EGFR inhibition drives *Lgr5⁺* cells into

- ❖ **Figure 1. EGFR inhibition induces cell cycle exit in intestinal organoids.** (A) Experimental setup for panels B-H. Organoids were treated with either EGFR inhibitor Gefitinib in the absence of EGF (iEGFR) or DMSO in standard ENR medium (control) one week after plating in BME. Samples were collected 1 (d1), 2 (d2), 4 (d4) or 7 (d7) days after the treatment. (B) Brightfield images of intestinal organoids after 4 days of iEGFR treatment or culture in control (ENR) medium. Crypts and differentiated units are visible in ENR, while iEGFR treated organoids mainly contain crypt-like structures that are placed closer to each other. (C) GFP fluorescence of *Lgr5^{GFPiresCreER/+}* (green) organoids shows that *Lgr5⁺* cells persist following iEGFR treatment. (D) Quantification of circumference of organoids after 4 days of iEGFR treatment or in control cultures. (E) Analysis of the cell cycle in intestinal organoids. EdU was administered 1h prior to the sacrifice. Control (ENR) organoids continuously incorporate EdU (upper panels) and express KI67 (lower panels), while iEGFR treated organoids exit the cell cycle over time. (F) Quantification of E. (G) Analysis of the cell cycle of iEGFR treated organoids following reintroduction of EGF in the culture medium. KI67 expression and EdU incorporation were analysed 1 (d1), 3 (d3) or 5 (d5) days after replating in ENR. (H) *Lgr5^{GFPiresCreER/+}* cells exit the cell cycle upon 4 days of iEGFR treatment. Phospho-histone H3 (pH3) staining was used to visualize M phase. The graph at the bottom shows the quantification. DAPI is used to visualize the nuclei. Scale bars, 50 μ m. Error bars represent SD. All fluorescent images are confocal sections. B and C are optical sections. E, G and H are 3D reconstructions. See also Figure S1 and S2.

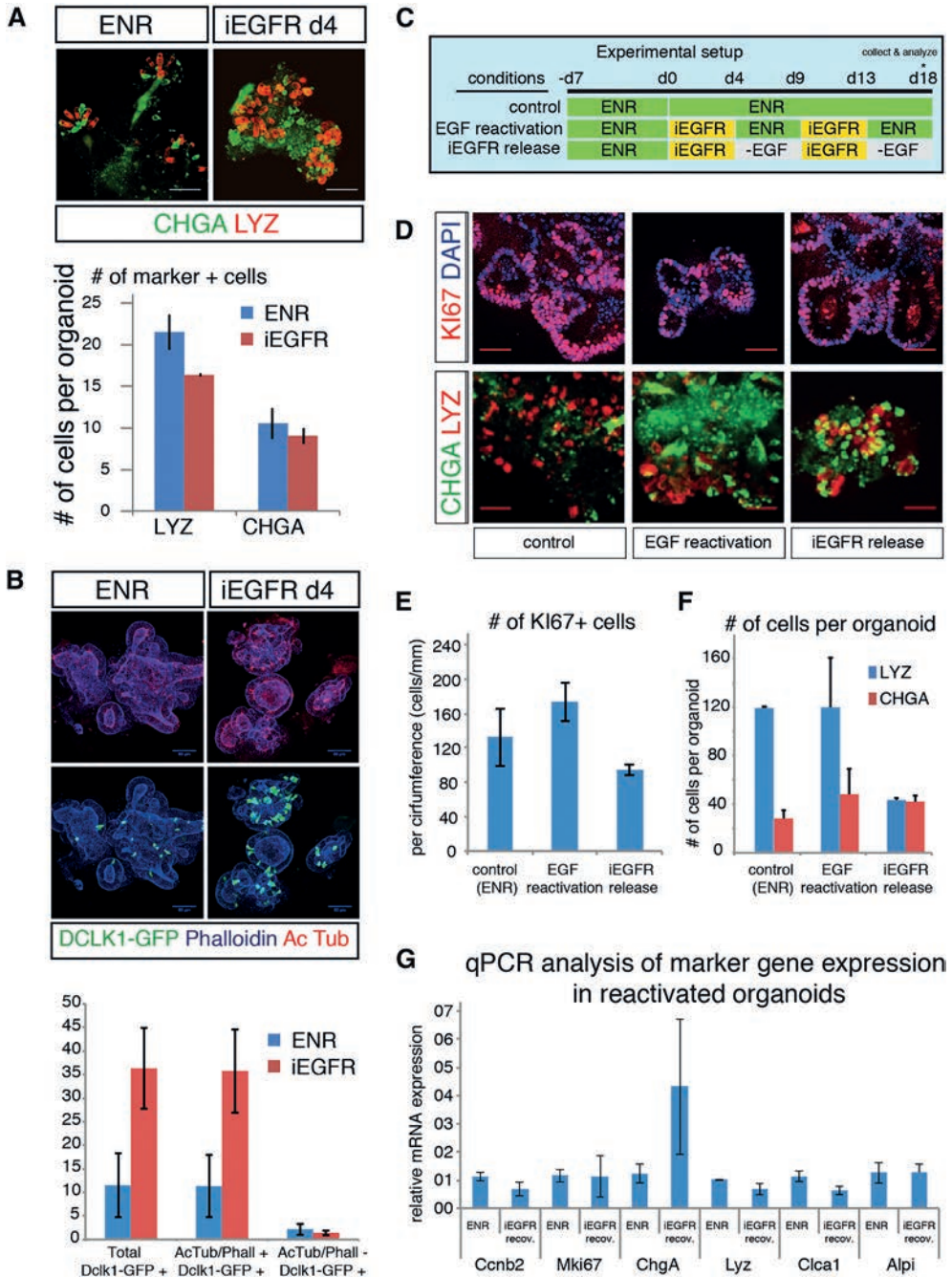


Figure 2. Differentiation status of EGFR inhibited and reactivated organoids indicate lineage bias towards enteroendocrine cells. (A) Marker analysis of enteroendocrine cells (CHGA, green) and Paneth cells (LYZ, red) indicates that both cell types remain unchanged after 4 days of EGFR inhibition (iEGFR) (B) Tuft cell numbers, quantified using DCLK1^{GFP} expression or with their characteristic apical actin bundles (visualised by Phalloidin and acetylated Tubulin staining) are increased after iEGFR treatment. ▶

quiescence and leads to a loss of proliferating cells. However, this treatment provokes no change in the absolute number of differentiated cells, with the exception of inducing an increase in Tuft cell numbers.

Next, we asked whether stem cells could survive repeated cycles of cell-cycle exit and entry (Figure 2C). Upon EGFR reactivation followed by washout and the addition of EGF, proliferation was restored to control levels (Figures 2C–2E). Some proliferation was even restored in the absence of exogenous EGF, likely due to endogenous EGF secreted by Paneth cells (Figures 2C–2E). These findings indicated that iEGFR-induced quiescence is reversible and that quiescent stem cells maintain their self-renewal potential.

While the absolute number of LYZ+ Paneth cells was not changed upon EGFR reactivation compared to the controls, CHGA+ EEC numbers were somewhat increased (Figures 2D and 2F). Similarly, absolute numbers of CHGA+ cells were higher in the absence of exogenous EGF, even though organoid size was considerably smaller compared to control organoids (Figures 2D, 2E, and S2H).

To corroborate these findings, we analyzed marker gene expression for key cell types in reactivated organoids using qPCR (Figure 2G; Table S5). After 1 week of reactivation, expression of proliferation markers *Ki67* and *Ccnb2* were restored to control levels. Moreover, lineage markers for Paneth cells (*Lyz*), Goblet cells (*Gob5*), and enterocytes (*Alpi*) were restored to near-normal ratios. Expression of the EEC marker *Chga* was elevated upon reactivation (Figure 2G). Thus, all lineages could be generated from reactivated *Lgr5+* cells, suggesting that EEC generation is enhanced by reduced EGF/EGFR signaling.

MAPK Signaling Downstream of EGFR Controls Intestinal Stem Cell Proliferation

Mitogen-associated protein kinase (MAPK) signaling is a major downstream target of EGFR signaling pathway and regulates cell-cycle progression. MAPK kinase (MEK) phosphorylates MAPK (ERK) to induce its nuclear localization and activation. Phosphatidylinositol 3-kinase (PI3K)/AKT pathway is also downstream of EGFR and is, for instance, implicated in neuroendocrine tumors (Banck et al., 2013). To quantify changes in ERK phosphorylation

- ▶ Graph shows quantification. (C) Experimental paradigm used to assess proliferation and differentiation potential of reactivated quiescent stem cells. Organoids were treated with EGFR inhibitor and subsequently replated in ENR medium (repeated iEGFR) or medium without EGF (repeated -EGF) to recover in two consecutive rounds. (D) Proliferation (*Ki67* expression) is restored after recovery from the second iEGFR treatment, indicating cell cycle inhibition is reversible. Enteroendocrine cells (CHGA+), but not Paneth cells (LYZ), were increased after consecutive iEGFR treatment. This was more pronounced after repeated -EGF. (E-F) Quantification of D. (E) The number of *Ki67+* cells normalized to the circumference of the quantified sections. (F) Quantification of the absolute number of CHGA+ and LYZ+ cells per organoid. (G) Quantitative PCR analysis of lineage markers in reactivated organoids that were cultured for 1 week in ENR following 4 days of iEGFR treatment. Scale bars, 50 μ m. Error bars represent SD. All fluorescent pictures are 3D reconstructions confocal images, except for top panels in D that show optical confocal sections. See also Figure S2.

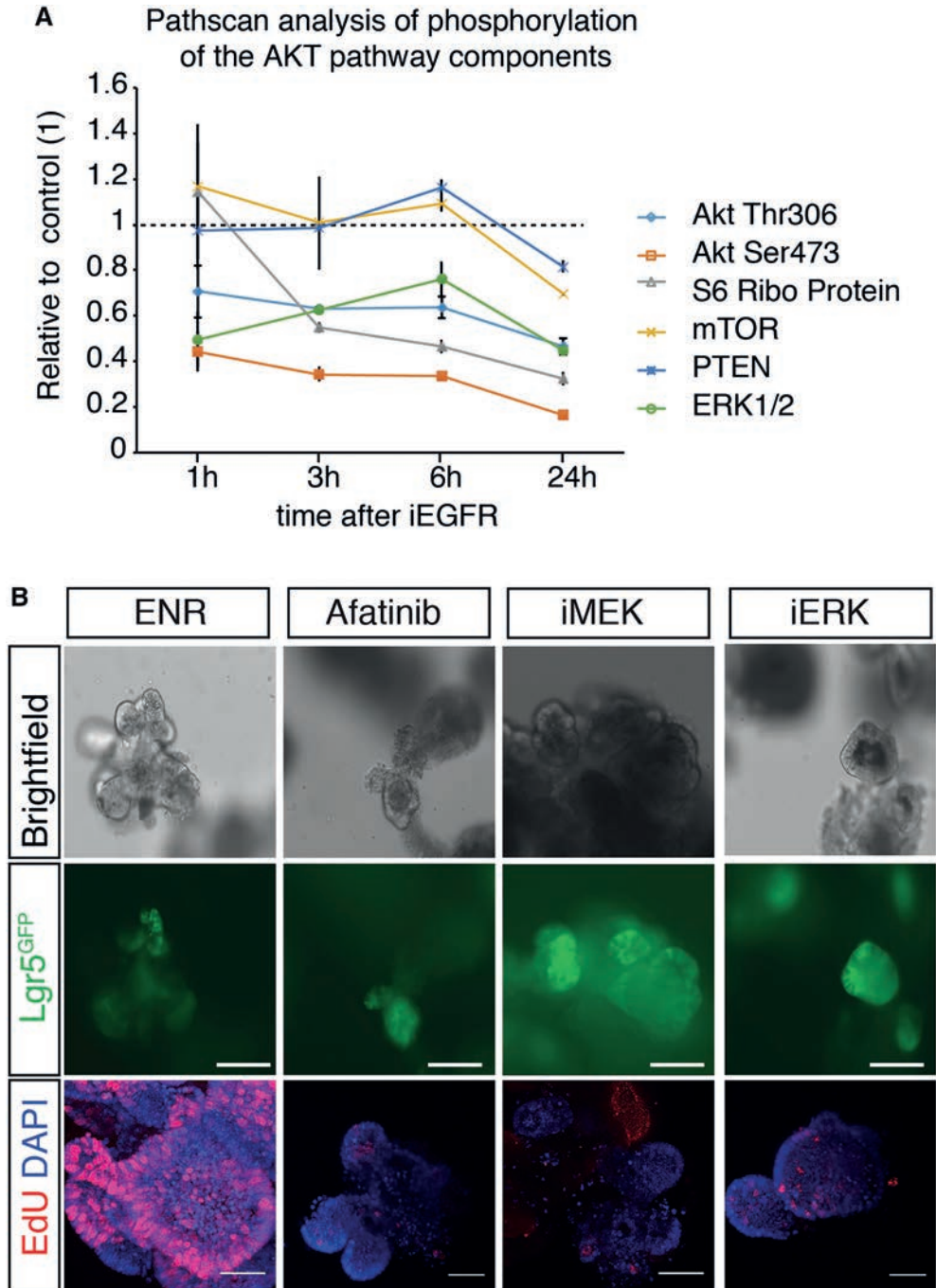


Figure 3. EGFR signalling induced cell cycle exit is mediated by MAPK signalling pathway. (A) Pathscan^R analysis of EGFR inhibited organoids. Akt and ERK pathways are effectively inhibited after 1h of EGFR inhibition, which is maintained over 24 hours. (B) Single inhibition of Mek (iMek) or Erk (iErk) as well as simultaneous inhibition of EGFR and ErbB-2 using Afatinib yields similar results to Gefitinib induced

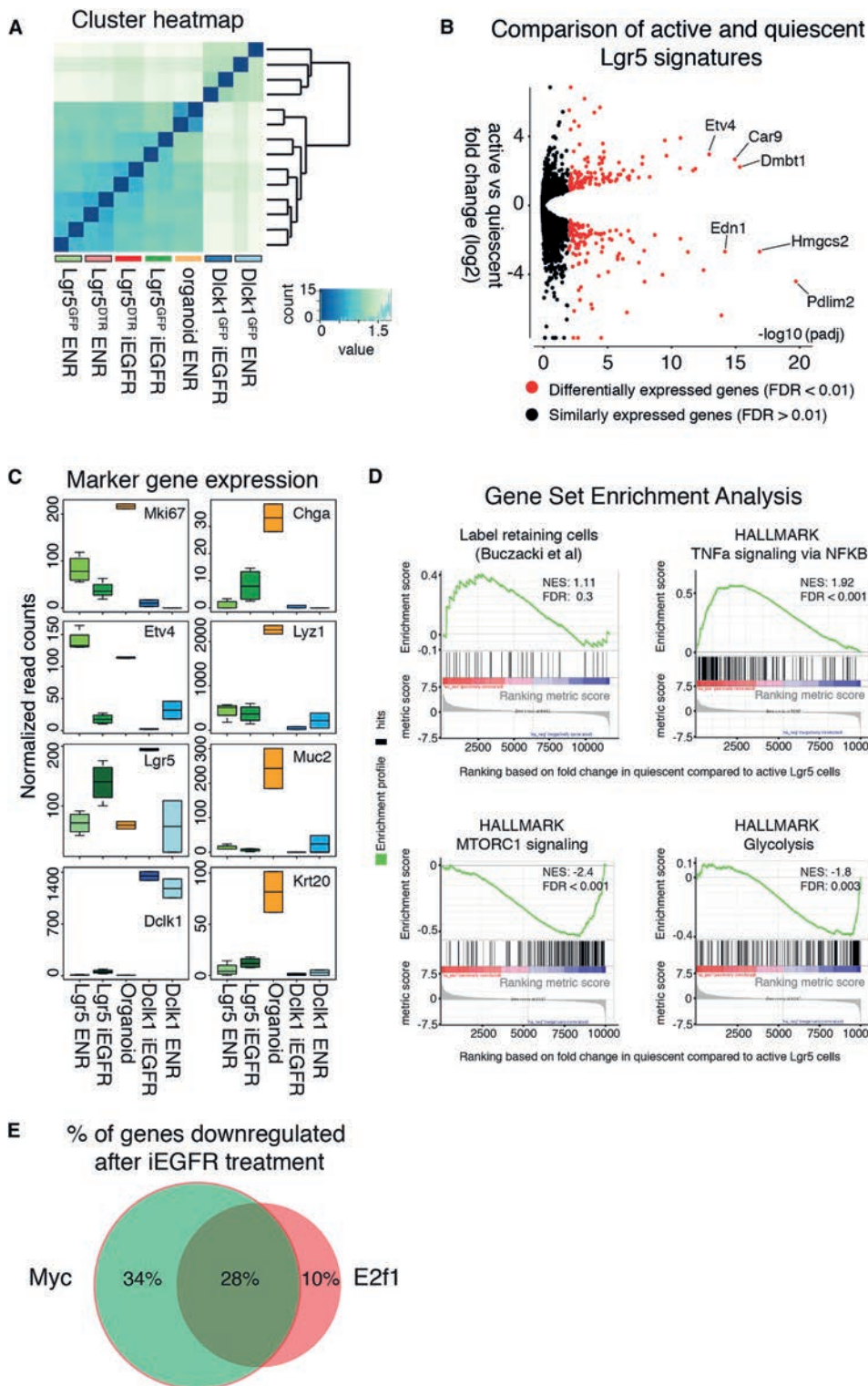
and AKT pathway activation, we used PathScan array analysis (Figures 3A and S3A). Phosphorylation of both ERK/2 and AKT at Thr306 and Ser473 was reduced as early as 1 hr after iEGFR treatment of organoids and remained low 24 hr after treatment (Figure 3A). S6 ribosomal protein phosphorylation, a target of AKT signaling, dropped after 3 hr, while mTOR and PTEN phosphorylation was reduced only after 24 hr (Figure 3A).

To evaluate the temporal change of ERK phosphorylation upon iEGFR treatment, we performed immunohistochemistry. iEGFR reduced ERK phosphorylation as early as 1 hr after treatment, consistent with the PathScan results (Figure S3B). However, we observed a gradual and partial recovery in phospho-ERK (pERK) levels within 48 hr, despite continuing quiescence (Figure S3B). Thus, we asked whether MEK/ERK signaling is essential for cell-cycle progression of intestinal stem cells using small inhibitors for either MEK (PD0325901; Meki) or ERK (SCH772984; Erki). Both inhibitors induced quiescence of Lgr5+ cells, implying that the ERK pathway downstream of EGFR is required for proliferation of Lgr5+ cells (Figure 3B). The use of afatinib, which inhibits both EGFR and ErbB2, yielded similar results (Figure 3B). These results indicated that inhibition of MAPK signaling could induce a reversible quiescent state in intestinal organoid stem cells, similar to iEGFR treatment. These data implied that decreased MAPK/ERK signaling suffices for cell-cycle exit of Lgr5+ cells.

RNA Sequencing Reveals the Molecular Signature of Quiescent Lgr5+ Stem Cells

To better understand the molecular characteristics of quiescent Lgr5+ cells, we performed bulk RNA sequencing on FACS-isolated control (DMSO) and quiescent (iEGFR treatment, day 4) Lgr5+ stem cells. We included both Lgr5^{GFPiresCreER/+} (n = 2) and Lgr5^{GFPDTR/+} (n = 2) organoids in our study to observe potential differences in Lgr5 reporter expression. We also included sorted Tuft cells (using the Dclk1^{GFPiresCreER/+} allele) for comparison. Whole control organoids cultures were sequenced as a reference population. Hierarchical clustering and principal-component analysis (PCA) revealed that quiescent Lgr5+ cells were more similar to active Lgr5+ stem cells than to whole organoids or Tuft cells (Figures 4A and S4A). Differential gene expression analysis between active and quiescent Lgr5+ cells revealed 533 differentially regulated genes, 290 of which were enriched in quiescent Lgr5+ cells (false discovery rate [FDR] <0.01 Figures 4B and S4B; Table S1). Transcriptional targets of the Erk pathway (Etv4 [7.7×, p-adj < 0.001] and Etv5 [7.7×, p-adj < 0.001]) were downregulated in quiescent Lgr5+ stem cells, confirming efficient Erk inhibition (Figures 4C and S4B). Similarly, several cell-cycle-associated genes, such as Ccnb1 (2.1×, p-adj < 0.005) and Ccnb2 (1.9×, p-adj < 0.05), were decreased, consistent with cell-cycle arrest (Figure S4B). Gene Ontology (GO) analysis of the genes downregulated upon iEGFR treatment confirmed a clear loss of cell-cycle-associated genes (Figure S4C). In line with

- ▶ EGFR inhibition. EdU is added to the culture medium 1 hour before the sacrifice. Middle panels show endogenous GFP expression from the Lgr5^{GFPiresCreER} allele. DAPI is used to visualize the nuclei in lower panels. Scale bars, 50 μm. Error bars represent SD. See also Figure S3.



our reporter expression, we observed a significant increase in some of the well-known Wnt target genes, including *Rnf43* (2.3×, $p\text{-adj} < 0.005$) and *Lgr5* (2×, $p\text{-adj} < 0.05$) (Figure S4B). We also noticed a strong increase of members of the AP-1 family of transcription factors (*Junb*, *Fos*, and *Fosb*) in quiescent *Lgr5*⁺ cells (Figures 4C and S4B). Early markers for Paneth cells (*Lyz1*), enterocytes (*Alpi1*), and goblet cells (*Muc2*) remained unchanged (Figure 4C). *Chga*, expressed by EECs and their precursors, was 7.3-fold higher in quiescent compared to active *Lgr5*⁺ stem cells (Figure 4C). Similarly, while *Dclk1* (6×, $p\text{-adj} < 0.05$) and some other Tuft cell markers increased upon iEGFR treatment, their levels were significantly lower in quiescent *Lgr5*⁺ cells than in Tuft cells (Figure 4C). These results confirmed our confocal analysis and highlighted key molecular changes in *Lgr5*⁺ stem cells upon quiescence entry.

The increase in per cell-*Chga* expression as well as the high CHGA⁺ cell numbers generated in the absence of EGF (Figures 3D and 3F) were reminiscent of the label-retaining secretory precursors (LRCs) described by Winton and colleagues (Buczacki et al., 2013). Indeed, gene set enrichment analysis (GSEA) revealed that the LRC signature is more similar to quiescent than to active *Lgr5*⁺ stem cells (Figure 4D; see STAR Methods). 12 out of 37 of the LRC genes were in the core enrichment group and included the EEC-related genes *Chga*, *Chgb*, *Cldn4*, *Gip*, and *Ghrl2* (Table S2). Next, we analyzed the distribution of the “hallmarks” gene sets provided on the GSEA dataset (Figures 4D and S4D; Table S3). Analysis revealed an enrichment of “E2F targets” and “MYC targets V1 and V2” in active stem cells (Figure S4D). X2K transcription factor target analysis confirmed that 72% of the genes downregulated after iEGFR were targets of either MYC (62%) or E2F1 (38%) (Figure 4E). In addition, mTORC1-associated genes were downregulated upon EGFR inhibition (Figure 4D). The analysis also revealed a metabolic shift upon quiescence entry; genes associated with glycolysis, oxidative phosphorylation, and cholesterol metabolism were downregulated in quiescent stem cells (Figures 4D and S4D). On the other hand, quiescent stem cells were enriched in genes associated with tumor necrosis factor α (TNF- α) signaling via nuclear factor κ B (NF- κ B), interferon gamma response genes, and JAK-STAT3 signaling (Figure 4D; Table S3). In brief, GSEA analysis suggested that loss of proliferation might be driven by decreased of MYC/E2F1 activity. Quiescent stem cells

- ◀ **Figure 4. RNA sequencing identifies key molecular differences between quiescent and active *Lgr5*⁺ stem cells.** (A) Hierarchical clustering of the whole transcript of sorted *Lgr5*⁺ cells using the *Lgr5*^{GFPDTR/+} (*Lgr5*^{DTR}), *Lgr5*^{GFPiresCreER/+} (*Lgr5*^{GFP}) and Tuft cells using the *Dclk1*^{GFPiresCreER/+} (*Dclk1*) organoids cultured in control medium (ENR) or upon EGFR inhibition (iEGFR) based on Pearson’s correlation. Control organoids were added as a reference. Colours indicate Pearson correlation. (B) Volcano plot comparing active and quiescent *Lgr5* signatures. x-axis shows adjusted p value (q value, in $-\log_{10}$) and y axis shows fold change (in \log_2). Each dots represents a gene; differentially expressed genes (False discovery rate < 0.01) are in red. (C) Boxplots displaying normalized expression values of marker genes. (D) Gene set enrichment analysis (GSEA). Fold change in gene expression in quiescent and active *Lgr5*⁺ stem cells are compared. Green line shows enrichment profile. Black bars show where genes from a given gene set are located (hit). (E) Expression2kinase (X2K) analysis showing key transcription factors targeting the active *Lgr5*⁺ stem cell signature. Error bars indicate SD. See also Figure S4 and Tables S1-S3.

downregulate several metabolic pathways and upregulate a signature related to TNF- α and JAK-STAT3 signaling (Figures 4D and S4D).

Combined Inhibition of the Wnt, Notch, and EGFR/MAPK Pathways Induces EEC Fate

We next aimed to establish a protocol for EEC differentiation. Inhibition of Notch signaling by DAPT treatment (iNotch) led to a large increase in the number of LYZ⁺ Paneth cells (Figure 5A). Inhibition of Wnt secretion using IWP-2 (iWnt) in combination with iNotch abolished Paneth cell differentiation and induced EECs and goblet cells (Figure 5A). iEGFR treatment spared both Paneth cells and EECs (Figure 5A). Combined inhibition of WNT/Notch/EGFR pathways (iWnt/iNotch/iEGFR) resulted in a massive increase in EECs while inhibiting Paneth cell differentiation (Figure 5A). Similarly, inhibiting Mek together with Wnt and Notch signaling pathways (iWnt/iNotch/iMek) increased CHGA⁺ EEC numbers (Figure 5C). qPCR analysis confirmed that goblet cell differentiation induced by iWnt/iNotch treatment is countered by both iEGFR and iMek treatments (Figure S5A).

We used cleaved caspase-3 staining to evaluate cell death in these organoids. Only rare apoptotic cells were visible in the “crypt domain” of both standard and iWnt/iNotch/iMek-treated (24 hr) organoids. Similar to the controls, apoptosis was restricted to the “villus domain” upon iWnt/iNotch/iMek treatment (Figure S5D). These results implied that EECs are generated by altered cell-fate choice rather than massive apoptosis of remaining cell types.

We further analyzed the expression of EEC-related genes in differentiated organoids (Figure S5A). Expression of the pan-EEC marker *Chga* was 25-fold higher in iWnt/iNotch/iEGFR-treated organoids and over 100-fold higher in iWnt/iNotch/iMek-treated organoids (Figure S5A). Concordantly, expression of *Sst* (55 \times), *Gip* (14 \times), *Sct* (5 \times), cholecystokinin (15 \times), and glucagon (*Gcg/Proglucagon*, 4 \times) mRNA were upregulated upon iWnt/iNotch/iEGFR treatment, following a similar trend to iWnt/iNotch/iMek treatment (Figure S5A). *Nts* was the sole hormone analyzed that was expressed at control levels. Thus, our protocol generated high numbers of most subtypes of EECs (Egerod et al., 2012).

To visualize hormone production at the protein level, we used immunofluorescence (Figure 5B). We focused on the iWnt/iNotch/iMek condition, which yielded the highest CHGA⁺ cell numbers among the conditions tested (Figures 5C and 5D). The different EEC subtypes are rare in normal intestinal organoid cultures (Figure 5C). iWnt/iNotch/iMek treatment resulted in a robust increase in the number of CHGA, NTS, SEROTONIN, GIP, SCT, SST, and CCK⁺ cells (Figures 5C and 5D; Table S5). This implied that EECs induced in our culture system are functionally mature.

Regional Identity of Intestinal Organoids Determines EEC Heterogeneity

The intestinal tract displays regional differences in EEC subtype representation. We asked whether the regional origin of organoid cultures affects the EEC subtypes generated. Of note, a previous study demonstrated that gut organoids retain at least some aspects of their regional

identity upon long-term culture (Middendorp et al., 2014). We established organoids from four different regions (duodenum to ileum) of the intestinal tract and analyzed EEC-related gene expression upon iWnt/iNotch/iMek using qPCR. iWnt/iNotch/iMek treatment induced Chga expression in all cultures when compared to standard culture conditions (Figure 5E). Nts- and Gcg-expressing cells predominantly reside in the distal small intestine (SI) region, whereas Gip-expressing cells follow the opposite trend (Drucker and Nauck, 2006, Kitabgi and Freychet, 1978, Parker et al., 2009). Consistently, Nts and Gcg expression was much more strongly upregulated in the distal than the proximal organoids (Figure 5E). Conversely, while all regions upregulated Gip upon iWnt/iNotch/iMek treatment, levels were higher in organoids of a proximal origin. Organoids from all regions efficiently expressed Sst and Sct upon differentiation (Figure 5E). We conclude that while our induction protocol is applicable to organoids from all intestinal regions, the regional source of organoids affects the outcome in terms of specific EEC subtypes.

As the PI3K/Akt/mTOR pathway is reduced upon iEGFR and may also affect EEC differentiation, we inhibited mTOR signaling using Azd8055 (iTOR) (Figure S5B). Inhibition of iTOR on a iWnt/iNotch background did not further increase CHGA+ cell numbers. On the contrary, iTOR treatment abrogated the increase in CHGA+ cell numbers when combined with iWnt/iNotch/iEGFR treatment (Figure S5B). qPCR analysis revealed decreases in Chga, Sst, Gip, Sct, Cck, and Gcg upon iTOR treatment (Figure S5C). Thus, while its levels are reduced upon iEGFR treatment, iTOR signaling is required for efficient generation of EECs by our induction protocol.

To better characterize the quiescent stem cell (iMek and iEGFR) and EEC (iWnt/iNotch, iWnt/iNotch/iEGFR, and iWnt/iNotch/iMek) induction protocols, we performed RNA sequencing on bulk cultures at 6 hr and 96 hr (Figure 6A). PCA and hierarchical clustering revealed three distinct groups (Figures 6A and S6A). First, all organoids treated for 6h clustered together with untreated organoids isolated at 6 hr and 96 hr. iMek- and iEGFR-treated organoids clustered closely together in PCA space, consistent with the notion that both induce quiescent Lgr5+ stem cells. iWnt/iNotch, iWnt/iNotch/iEGFR, and iWnt/iNotch/iMek cultures were distinct at 96 hr (Figures 6A and S6A). Separate samples from the same treatment group clustered closely together, confirming the reproducibility of the treatments (Figures 6A and S6A). Expression of the Erk target gene *Etv4* is lost at 6 hr in both iMek (7.2-fold; FDR < 0.001) and iEGFR (4.6-fold; FDR < 0.005), confirming efficient inhibition.

Next, we used our dataset to directly compare the effects of iEGFR and iMek treatments. We measured the number of differentially expressed genes (FDR < 0.01) to visualize the differences between samples. At both 6 hr and 96 hr, iEGFR (1,440 and 1,307 differentially expressed genes at 6 hr and 96 hr, respectively) and iMek (1,147 and 1,631 differentially expressed genes at 6 hr and 96 hr, respectively) treatments induced massive changes of the transcriptomes of the organoids (Figure S6B, red dots indicate differentially expressed gene). Transcriptomes of iMek- and iEGFR-treated cultures were almost identical at both time points (5 and 88 differentially expressed genes at 6 hr and 96 hr, respectively). iWnt/iNotch/iEGFR (3,847 differentially expressed genes) and iWnt/iNotch/iMek (3,166 differentially expressed genes)

I

II

III

IV

V

VI

VII

VIII

&

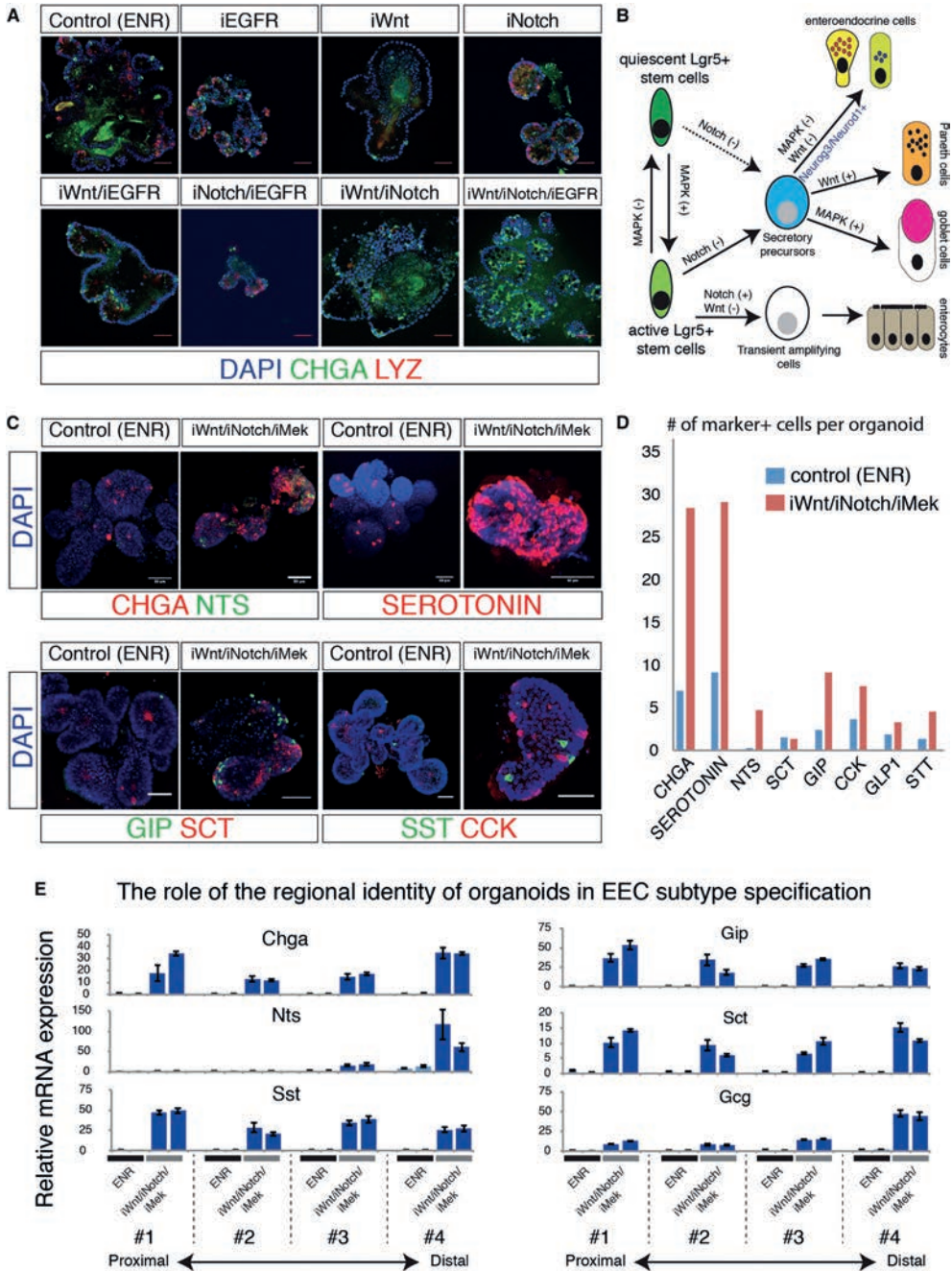


Figure 5. Derivation of a high purity EEC culture. (A) Marker analysis of enteroendocrine cells (CHGA, green) and Paneth cells (LYZ, red). Organoids were treated for 4 days with Notch inhibitor DAPT (iNotch), inhibitor of Wnt secretion IWP-2 (iWnt), Gefitinib (iEGFR) or a combination of these treatments. DMSO is used as a control. Images show optical sections. (B) Model shows critical signalling pathways manipulated in organoids for directed differentiation of intestinal stem cells. (C) Inhibition of Mek signalling (iMek) ▶

treatments were drastically different from controls at 96 hr. While organoids subjected to both treatments clustered together at 96 hr (Figure S6A), 267 genes were differentially expressed between EEC cultures differentiated with iWnt/iNotch/iEGFR versus iWnt/iNotch/iMek treatments. Most noticeable genes were goblet cell-related factors, such as *Clca1* (2.4-fold, $p < 0.001$) and *Zg16* (2.5-fold, $p < 0.001$; Figure 6B). In conclusion, while iEGFR and iMek treatments can be used interchangeably in the context of quiescent stem cell induction, iMek is more efficient in countering goblet cell differentiation.

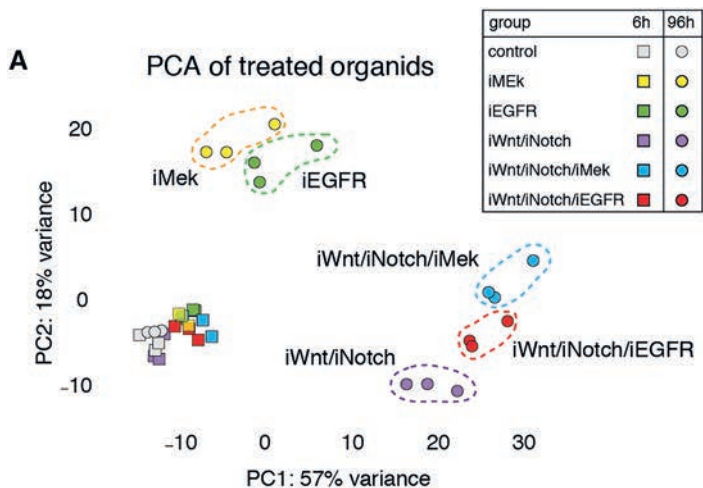
Next, we scrutinized EEC differentiation. At 96 hr, *Chga* and *Chgb* expression were highly elevated in iWnt/iNotch/iEGFR and iWnt/iNotch/iMek treatments (Figure 6B). Similarly, most EEC genes, including *Gip*, *Sst*, *Sct*, *Tac1*, *Tph1*, and *Reg4*, were increased in both conditions. We noticed that expression of *Cck*, *Gcg*, *Ghrl*, and *Reg3a* was upregulated in iWnt/iNotch and not further enhanced by the addition of iEGFR and iMek (Figure 6B). *Nts* expression was not enriched following our EEC differentiation protocols, most likely because duodenum organoids were used. Even so, NTS was clearly expressed by rare cells (Figures 5D and 6B). In brief, both iWnt/iNotch/iEGFR and iWnt/iNotch/iMek conditions efficiently induce generation of multiple EEC subtypes, even though the ratio of the subtypes generated is different.

Single-Cell Sequencing Reveals Heterogeneous EECs in Reactivated Cultures

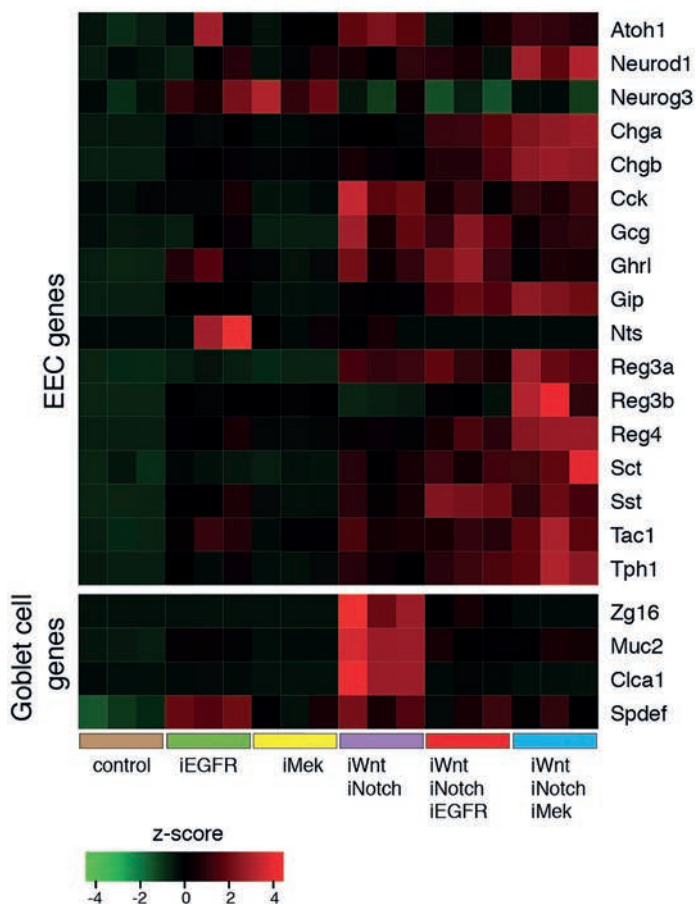
We previously used single-cell sequencing to reveal EEC subtypes *in vivo* (Grün et al., 2015). To elucidate the cellular composition of induced organoids and the extent of heterogeneity in hormone expression, we performed single-cell RNA sequencing (Figure 7). We sorted live single cells (without additional markers) from iWnt/iNotch/iEGFR- and iWnt/iNotch/iMek-treated organoids. Among the 289 cells that passed our filtering, we identified a cluster of 94 cells as enterocytes enriched in *Aldob* (4.9×, $p\text{-adj} < 0.001$), *Apoa1* (12.6×, $p\text{-adj} < 0.001$), and *Alpi* (5.6×, $p\text{-adj} < 0.001$) (Figures S7A and S7B). These were interpreted as surviving post-mitotic enterocytes and were excluded from further analysis. Cells derived from both iWnt/iNotch/iEGFR- and iWnt/iNotch/iMek-treated organoids were distributed similarly in t-distributed stochastic neighbor embedding (t-SNE) space and were analyzed together (Figure S7C).

Using RaceID2 (Grün et al., 2016), we identified 12 distinct clusters of cells (Figures 7A and 7B). k-medoids clustering of the Pearson correlation of cellular transcriptomes revealed a clear separation between clusters as well as possible heterogeneity within clusters (e.g., 7 and 8, Figure 7A). Differential gene expression analysis revealed signature genes for each

- ▶ together with Wnt and Notch signalling pathways (iWnt/iNotch/iMek) similarly increases enteroendocrine cell numbers (CHGA+). Neurotensin (NTS), Serotonin, Gastric inhibitory protein (GIP), Secretin (SCT), Somatostatin (SST) and cholecystokinin (CCK) positive cell numbers dramatically increase. Representative 3D reconstruction confocal images are shown. (D) Quantification of the number of enteroendocrine cell markers per organoid upon iWnt/iNotch/iMek treatment. (E) Regional identity of organoids is maintained in terms of enteroendocrine cell subtypes. Organoids were isolated from proximal-to-distal (#1-#4) small intestine. Distal organoids have higher levels of *Nts* and *Gcg* levels, while *Gip* is enriched proximally. Scale bars, 50 μm . Error bars indicate SD. See also Figure S5 and Table S5.



B Expression of key EEC and Goblet cell genes after 96h of treatment



cluster, which we used to classify cell types (Table S4). The most prominent clusters (“3” [53 cells] and “4” [35 cells]) expressed the pan-EEC markers *Chga* and *Chgb* (Figures 7C and S7D). *Chga* and *Reg4* expression formed a gradient, both being higher in cluster 4. Hormonal production in these *Chgb* high clusters was best defined by *Tac1* and *Tph1* expression, both markers of enterochromaffin cells (Figures 7B, 7C, and S7D). *Tac1* encodes for the hormone substance P, while *Tph1* encodes for the rate-limiting enzyme in serotonin synthesis (Egerod et al., 2012, Grün et al., 2015). Substance P and serotonin may act as neurotransmitters exciting the connected enteric neurons (Latorre et al., 2016). The other clusters displayed relatively low levels of *Chga* and *Chgb* transcripts but included cells expressing peptide hormones (Figures 7C and S7D). Cluster 2 (21 cells) was marked by *Gip* expression (74×) that is expressed by K-cells. *Fabp5* was also highly enriched in this cluster (12.6×), consistent with its role in *Gip* secretion (Shibue et al., 2015). Members of cluster 5 (nine cells) expressed very high levels of *Sst* (182×), identifying them as D-cells (Figure 7C). Ghrelin (*Ghrl*) expression was present in more than one cluster but was highest in cluster 6 (19×, three cells). We also noticed that *Islet1* (*Isl-1*; 9.7×) was co-expressed with *Ghrl* in these cells. *Islet1* plays an important role in cell fate specification, and its loss leads to impaired glucose homeostasis (Terry et al., 2014). Cells in cluster 7 (18 cells) all highly expressed *Cck* (55.7×).

One of the early inducers of EEC differentiation is neurogenin-3 (*Neurog3*), which is followed by *Neurod1*. *Neurog3* (5.2×) expression was highest in cluster 9 (six cells) and in some cells of cluster 3 that were most similar to cluster 9. Virtually all EEC clusters contained *Neurod1*-expressing cells (Figure 7B). Given the temporal expression of these transcription factors, we propose that cluster 9 represents EEC progenitors, which through *Neurod1* generate a panel of EECs. Cluster 1 (18 cells) was enriched in goblet cell- and Paneth cell-related genes, such as *Agr2* (33×), *Muc2* (26×), *Ttf3* (23×), and *Defa24* (28×). Despite the filtering, some enterocyte-like cells expressing *Aldob* and *Mt1/2* remained (cluster 8, seven cells). *Dclk1* and *Trpm5* expression identified cluster 10 (15 cells) as Tuft cells (Figures 7B and S7C). In total, 145/289 cells (50% of all cells) analyzed were EECs or their progenitors, confirming the efficiency of our induction protocol.

Since multiple hormones can be co-expressed in the same cell, we addressed the heterogeneity of hormone expression at the single-cell level (Figure 7C). Focusing on EEC-related gene expression, we identified occasional expression of multiple different hormones in a single cell (Figure 7B). This was in line with our previous report on EECs from freshly isolated intestinal epithelium (Grün et al., 2015). A prominent example is cluster 7, where *Cck*⁺ cells also expressed *Gcg* (28.2×), *Ghrl* (5.3×), or *Pyy* (11.4×). Consistently, I-cells have been reported to co-express



- ◀ **Figure 6. Characterization of organoids following different induction regimens using RNA sequencing.** (A) Principal component analysis (PCA) of the transcriptomes of samples treated with iMek, iEGFR, iWnt/iNotch, iWnt/iNotch/iEGFR, iWnt/iNotch/iMek and DMSO treated controls. Samples were analysed after 6 (6h, square) or 96 (96h, circle) hours of treatment. (B) Heat map showing the expression of key genes related to enteroendocrine (EEC) and goblet cells at 96h. Colour code shows the z-score for each gene along the whole dataset. See also Figure S6.

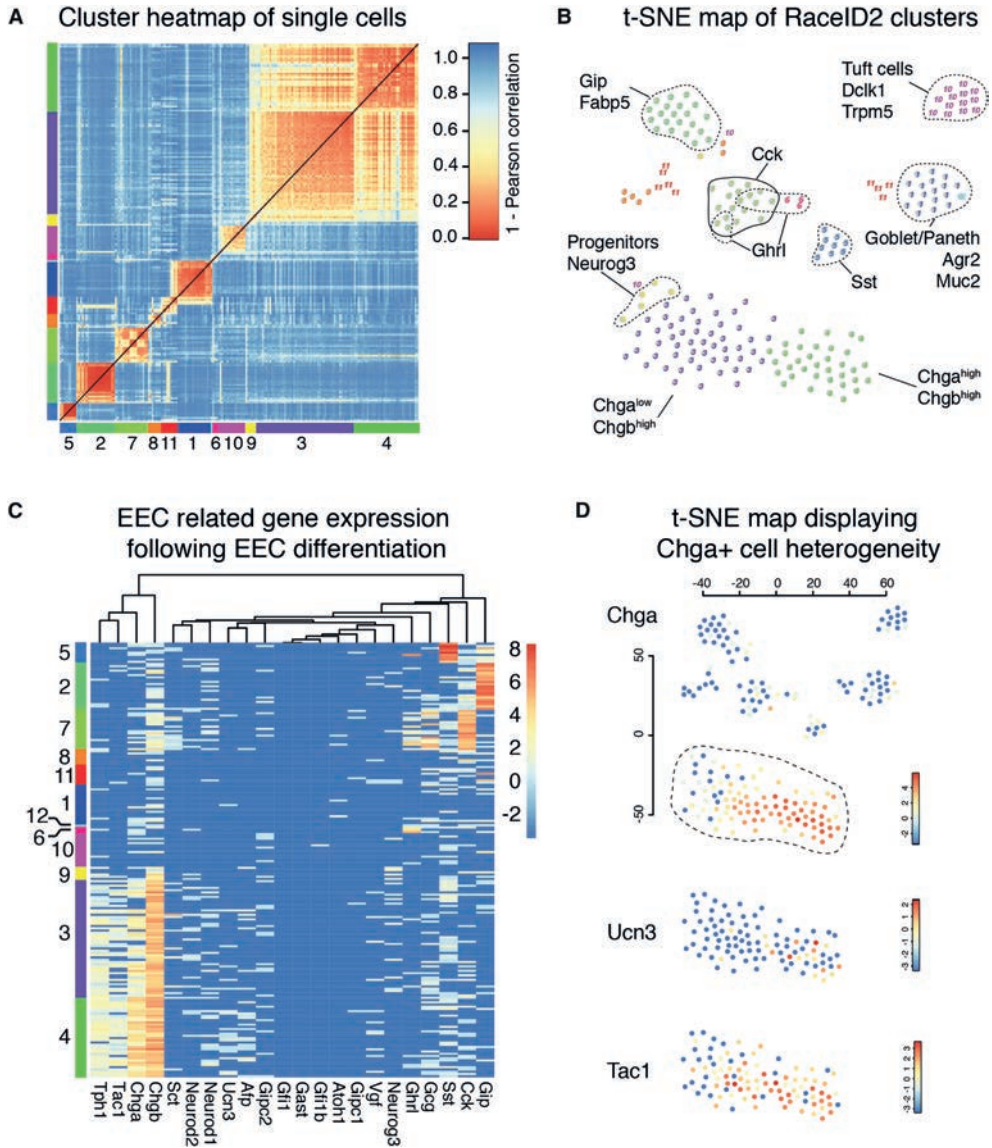


Figure 7. Single cell transcriptome profiling reveals heterogeneity among induced EECs. (A) Heatmap displaying k-medoids clustering of Pearson’s correlation of the whole transcriptome of individual live organoid cells from iWnt/iNotch/iEGFR and iWnt/iNotch/iMek experiments after filtering. Numbers indicates clusters. The colours code for Pearson’s correlation. (B) t-SNE map depicting individual cells and cluster numbers assigned by RaceID2. (C) Heat map displaying the log2 transformed color-coded transcript counts of respective genes related to the enteroendocrine lineage. (D) t-SNE map displaying the heterogeneous expression of Ecn3 and Tac1 transcripts by Chga high cells. See also Figure S7and Table S4.

Cck with other hormones at varying levels (Egerod et al., 2012). Transcriptomes of Sst+ cells were more homogeneous, co-expressing low levels of Gip and Cck, while one cell co-expressed Ghrl only. We previously reported partial overlap between Cck+ and Tac1+ cells (Grün et al., 2015). Consistently, some of the Tac1+ cells in clusters 3 and 4 expressed low levels of Cck (Figures 6B and 6C). Similar to their in vivo counterparts, EECs induced with our protocol contained Chga+ Tac1+ Ucn3+, Chga+ Tac1+ Ucn3-, and Chga+ Tac1- Ucn3- cells (Figure 7D). Thus, EECs generated in our cultures recapitulate EEC heterogeneity seen in the intestinal epithelium in vivo. Taken together, our single-cell analysis indicated that the protocol induces EEC fates in ~50% of organoid cells based on marker gene expression.

DISCUSSION

Here, we identify EGF signaling as an indispensable driver of Lgr5+ stem cell proliferation in organoids. Under conditions where Wnt signaling is untouched but EGF signaling is blocked, actively dividing Lgr5+ stem cells convert into quiescent Lgr5+ cells that retain expression of various Wnt target genes. This cellular state can be maintained for up to a week. Yet, the simple restoration of EGF signaling converts the quiescent cells back into their normal active stem cell state. In organoids as well as in crypts, Lgr5+ cells are always the direct neighbors of the Wnt3-secreting Paneth cells (Sato et al., 2011). In this setting, Wnt3 does not diffuse over distances, but is loaded directly onto the Lgr5+ stem cells (Farin et al., 2016). The quiescent Lgr5+ stem cells remain juxtaposed to the Paneth cells in iEGFR treated organoids and are thus exposed to high local Wnt signals. Indeed, three independent Wnt target gene alleles as well as gene expression analyses confirmed robust Wnt signaling upon EGFR inhibition. In sum, our results show that maintenance of stem cell fate requires Wnt, but not EGF, whereas stem cell proliferation depends on the combination of Wnt and EGF. Whether quiescent stem cells are more competent to remain in the niche when in competition with dividing stem cells remains an open question.

Previous studies have identified quiescent cells located close to the zone of differentiation at the +4 position with stem cell potential (Clevers, 2013). We have reported the existence ofDll1+ secretory precursors at this position (van Es et al., 2012). Using a histone label retention assay, Doug Winton's group identified a chromatin-label-retaining population with secretory differentiation potential. These LRCs share a signature with crypt base columnar cells (CBCs), including the expression of Lgr5, but express significant levels of some of the secretory lineage genes, such as Chga (Buczacki et al., 2013). Taken together, these secretory precursors represent transient states yet can de-differentiate into stem cells when the need arises and can thus be considered facultative stem cells (Buczacki et al., 2013, van Es et al., 2012). A similar situation exists for the abundant enterocyte precursors in the crypt (Tetteh et al., 2016).

We noticed a slight bias of quiescent Lgr5+ cells (induced in culture) toward expression of EEC markers, such as Chga, which made them reminiscent of the in vivo Lgr5+-label-retaining cells identified by Doug Winton. EGFR signaling has been shown to be essential for the production of goblet cells (Heuberger et al., 2014). Our current data show that simultaneous

I

II

III

IV

V

VI

VII

VIII

&

inhibition of enterocyte, Paneth, and goblet cell fate by inhibiting Notch, Wnt, and EGFR signaling, respectively, is the key to the generation of EECs.

This culture system may yield answers toward some of the major outstanding questions about the biology of the enigmatic EECs. It is unclear what signals drive the fate specification of the different subtypes of EECs. It is not known if the physiological processes that are controlled by specific EEC subtypes in turn feed back into the formation of the pertinent subtypes of EECs. Little is known about the triggers that lead to secretion of hormones beyond the identification of a handful of receptors and their ligands (Janssen and Depoortere, 2013). EEC-derived hormones have been implied in conditions of major importance such as depression, glucose insensitivity/diabetes, and obesity (Latorre et al., 2016). A detailed mechanistic understanding of the biology of EECs can be derived using this culture system and may yield insights with broad therapeutic impact.

A detailed description of the materials and methods used in the study is given in the STAR Methods.

CONTACT FOR REAGENT AND RESOURCE SHARING

Requests for reagents should be directed to Prof. Hans Clevers at h.clevers@hubrecht.eu.

EXPERIMENTAL MODEL AND SUBJECT DETAILS

Mouse Strains Used to Initiate Organoid Cultures

Primary organoid cultures used in this study were derived from $Lgr5^{GFPiresCreER/+}$ (Barker et al., 2007), $Lgr5^{GFPDTR/+}$ (Tian et al., 2011), $Dcl1^{GFPiresCreER/+}$ (Nakanishi et al., 2013) and $Rosa^{TCF-CFP/+}$ ($Gt(ROSA)26Sor^{tm10.1(Tcf/Lef-CFP)Mgn}$) mice (Serup et al., 2012). For lineage tracing experiments, organoids were derived from the $Lgr5^{GFPiresCreER/+};Rosa^{LacZ/YFP}$ and $Dcl1^{GFPiresCreER/+};Rosa^{LacZ/+}$ mice. All mice were bred on a C57BL/6 background. All animal procedures and experiments were performed in accordance with national animal welfare laws under a project license obtained from the Dutch Government, and were reviewed by the Animal Ethics Committee of the Royal Netherlands Academy of Arts and Sciences (KNAW). All rodents are housed in a barrier facility in conventional cages and are changed without using a change stations. All personnel entering the barrier must wear protective clothing (including head caps, special clogs). All animals are received directly from approved vendors (Charles River) or generated in house. Animals arriving from other sources must pass the GDL –quarantine for screening or by embryo-transfer. After screening these SPF mice are housed in micro isolator cages and are transferred to the Hubrecht laboratory.

METHOD DETAILS

Organoid Culture

The basic culture medium (advanced Dulbecco's modified Eagle's medium/F12 supplemented with penicillin/streptomycin, 10 mM HEPES, Glutamax, B27 [Life Technologies, Carlsbad, CA])

and 1 mM N-acetylcysteine [Sigma]) was supplemented with 50 ng/ml murine recombinant epidermal growth factor (EGF; Peptotech, Hamburg, Germany), R-spondin1 (conditioned medium, 5% final volume), and Noggin (conditioned medium, 5% final volume), called "ENR" medium. Conditioned media were produced using HEK293T cells stably transfected with HA-mouse Rspo1-Fc (gift from Calvin Kuo, Stanford University) or after transient transfection with mouse Noggin-Fc expression vector. Advanced Dulbecco's modified Eagle's medium/F12 supplemented with penicillin/streptomycin, and Glutamax was conditioned for 1 week.

Organoids were derived from the duodenum of the *Lgr5^{GFPiresCreER/+}* (Barker et al., 2007), *Lgr5^{GFPDTR/+}* (Tian et al., 2011), *Dclk1^{GFPiresCreER/+}* (Nakanishi et al., 2013) and *Rosa^{TCF-CFP/+}* (*Gt(ROSA)26Sor^{tm10.1(Tcf/Lef-CFP)Mgn}*) mice (Serup et al., 2012). For experiment displayed in Figure 5E, organoids were derived from 4 different regions spanning the proximal-distal axis of the intestine. For lineage tracing experiments, organoids were derived from the *Lgr5^{GFPiresCreER/+};Rosa^{LacZ/YFP}* and *Dclk1^{GFPiresCreER/+};Rosa^{LacZ/+}* mice.

Organoids were plated in BME (Trevigen) and treated with the EGFR inhibitor Gefitinib (5 μ M; Santa Cruz Biotechnology), EGFR and ErbB-2 inhibitor Afatinib (10 μ M, Selleckchem), MEK inhibitor PD0325901 (5 μ M; Sigma Aldrich) or ERK inhibitor SCH772984 (10 μ M, Selleckchem) while EGF was withdrawn from the medium. Wnt secretion was inhibited with IWP-2 (1,5 μ M; Stemgent) and Notch with DAPT (10 μ M, Sigma Aldrich). All treatments were performed on organoids 5-7 days after passaging. For EGFR reactivation experiments, organoids were replated in fresh BME and ENR medium to make sure EGFR inhibitor is washed away. For the repeated EGF withdrawal experiment in Figures 2C-2E, EGF was omitted in the medium during reactivation. For mTOR inhibition, Azd8055 (Selleckchem) was added to the medium at 0.1mM concentration. For induction of Cre-ER activity, organoids were treated overnight with 4-OH tamoxifen (1 μ M). All control organoids were treated with similar concentrations of the compound dissolvent, dimethyl sulfoxide (DMSO). During treatments, cells were imaged using an EVOS microscope (Electron Microscopy Sciences).

For the induction of enteroendocrine differentiation, cells were either cultured in standard culture conditions (ENR). 5 days after plating in BME, medium was removed and organoids were washed with PBS before re-embedding in BME. The cocktail for EEC differentiation included: IWP2 (1,5 μ M; Stemgent), DAPT (10 μ M, Sigma Aldrich) and MEK inhibitor PD0325901 (1 μ M; Sigma Aldrich) or Gefitinib (5 μ M; Santa Cruz Biotechnology).

Immunostainings

Whole organoids were collected by gently dissolving the BME in ice-cold PBS, and subsequently fixed overnight at 4°C in 4% paraformaldehyde (Sigma). Next, organoids were permeabilized and blocked in PBS containing 0,5% Triton X-100 (Sigma) and 2% normal donkey serum (Jackson ImmunoResearch) for 30 min at room temperature. Organoids were incubated for 2 hr at room temperature in blocking buffer containing primary antibodies. Primary antibodies used were rabbit anti-Lysozyme (1:500; DAKO), goat anti-Chromogranin A (1:500; Santa Cruz), mouse anti-Ki67 (1:250; BD PharMingen), rabbit anti-phospho-Histone 3 (pH3 Ser10,

1:1000; Millipore), mouse anti-Cytokeratin 20 (1:1000; Dako), goat anti-Cholestocystokin (sc-21617,1:100; Santa Cruz), rabbit anti-Neurotensin (sc-20806,1:100; Santa Cruz), goat anti-Secretin (sc-26630,1:100; Santa Cruz), goat anti-Somatostatin (sc-7819, 1:100; Santa Cruz), goat anti-Serotonin (ab66047, 1:1000, Abcam), rabbit anti-Gastric inhibitory polypeptide (ab22624-50, 1:500, Abcam) and mouse anti-acetylated tubulin (1:100; Santa Cruz). Organoids were incubated with the corresponding secondary antibodies Alexa488, 568 and 647 conjugated anti-rabbit, anti-goat and anti-mouse (1:1000; Molecular Probes), in blocking buffer containing DAPI (1:1000, Invitrogen), or with Alexa 647 conjugated Phalloidin (Thermo Fisher scientific, 1:2000). EdU incorporation was visualized using the Click-iT Assay Kit (Thermo Fisher), after 1 hr pre-incubation with EdU (10 μ M). LacZ staining was performed as previously described (Barker et al., 2007). Alexa 647 conjugated Phalloidin (Thermo Fisher scientific, 1:2000) was added together with the secondary antibodies. Sections were embedded in Vectashield (Vector Labs) and imaged using a Sp5 and Sp8 confocal microscope (Leica). Image analysis was performed using ImageJ software.

FACS Sorting

For FACS analysis of Lgr5 and KI67 expression, Lgr5^{GFPDTR/+} organoids were first dissociated into single cells through mechanical disruption, after 15 min of Trypsin treatment at 37°C (TrypLE Express; Life Technologies). Single cells were fixed on ice using 4% paraformaldehyde for 30 min, and washed 3 times in PBS. Cells were permeabilized in PBS containing 0,5% Triton X-100 for 30 min, and were stained with an eFluor-660 conjugated rat anti-KI67 (1:1000; eBioscience) antibody for 30 min on ice. For cell cycle analysis, cells were stained in 1 μ g/ml Hoechst 33342 (ThermoFisher). Subsequently, stained cells were analyzed on a BD FACS Calibur (BD Biosciences).

For RNA-sequencing analysis in Figures 4 and 7, organoids were dissociated and immediately sorted using a BD FACS Aria (BD Biosciences). For bulk sequencing experiments in Figure 4, up to 5000 cells were sorted in Trizol in eppendorf tubes. For single cell sequencing experiment, cells were sorted as single cells into 384-well plates containing ERCC spike-ins (Agilent), RT primers (Hashimshony et al., 2012) and dNTP (Promega).

RNA Isolation

For RNA-sequencing of sorted cells in bulk, cells were sorted into Trizol (Life Technologies) and total RNA was isolated according to the manufacturer's instructions, with the following alterations. RNA was precipitated overnight at -20°C, with 2 μ g glycogen (Life Technologies). No additional RNA isolation step was used for cells sorted into 384-wells. For quantitative PCR analysis, RNA was isolated from organoids using the RNeasy kit (QIAGEN) as instructed in the manufacturers protocol. For bulk sequencing experiment described in Figure 6, organoids were treated in triplicate for 6 or 96 hr in 48-well plates, collected and washed in PBS. RNA was isolated using Trizol as described above. 10 ng RNA was used as starting material for sequencing reactions.

Quantitative PCR

PCR analysis was performed using the SYBR-Green and Bio-Rad systems as described (Muñoz et al., 2012). PCR reactions were performed in triplicate with a standard curve for every primer. Changes in expression were calculated using CFX manager software (Bio-Rad). Primers were designed using the NCBI primer design tool.

Single-Cell and Bulk Sequencing

RNA samples were prepared using a modified version of the CEL-seq protocol as described previously (Grün et al., 2015, Hashimshony et al., 2012). RNA pellets were dissolved in primer mix and incubated for 2 min at 70°C. Cells sorted into 384-well were directly lysed at 65°C for 5 min. cDNA libraries were sequenced on an Illumina NextSeq500 using 75-bp paired-end sequencing. Data processing is described below.

PathScan Analysis

Organoids that were Gefitinib treated for 1h, 3h, 6h or 24h were collected in ice cold DMEM in medium, and lysed according to manufacture instructions (PathScan Akt Signaling Antibody Array Kit with chemoluminescent, Cell Signaling Technology). Lysates were processed according to protocol. Readout of chemoluminescent readout was performed on ImageQuant LAS 4000 (GE Healthcare Life Sciences). Signal intensities were quantified using ImageJ software. Quantification was performed by calculating intensity of each antigen signal relative to independent time point specific control antigens.

QUANTIFICATION AND STATISTICAL DETAILS

Analysis of RNA-Sequencing Data

Paired-end reads were quantified as described before (Grün et al., 2015) with the following exceptions. Reads that did not align or aligned to multiple locations were discarded. For analysis of the bulk sequencing, unique molecular identifiers (UMIs) were ignored; instead read counts for each transcript were determined by the number of reads that uniquely mapped to that transcript. This count was divided by the total number of reads that mapped to all transcripts and multiplied by one million to generate the reads-per-million (RPM) count. RPM was used in preference of RPKM because CEL-seq only allows 3' end sequencing. Differential gene expression was evaluated using the DESeq (Anders and Huber, 2010) and Deseq2 (Love et al., 2014) packages in R platform. Cut-offs in Figure 4 used were an adjusted p value < 0,1 and FDR < 0,1 and at least 2-fold difference to the compared population. To prevent samples with no reads disabling ratiometric analysis, all 0 reads were converted into 0,1 reads prior to ratio calculation and log₂ conversion. Gene ontology analysis was performed using the Revigo (Supek et al., 2011) and Gorilla (Eden et al., 2009) software.

I

II

III

IV

V

VI

VII

VIII

&

Single-Cell Data Analysis

Single-cell sequencing data was analyzed as described previously (Grün et al., 2015). In brief, 288 cells sorted from iNotch/iWnt/iMek and 384 cells sorted from iNotch/iWnt/iEGFR treated organoids were sequenced in parallel. Cells with less than 1000 unique reads were discarded and samples were down-sampled. Genes with maximum expression less than 5 following down-sampling were discarded. Exclusion of Enterocytes was achieved by discarding samples with more than 8 transcripts of *Apoa1*.

Gene Set Enrichment Analysis

Gene Set Enrichment Analysis (GSEA) was performed following producers' instructions (<http://software.broadinstitute.org/gsea/>). A ranked list comparing the fold changes between quiescent and active *Lgr5+* stem cells was created and compared to the label retaining cell gene set (Basak et al., 2014, Buczacki et al., 2013) and the 'HALLMARKS' gene set available on the server (<http://software.broadinstitute.org/gsea/>). Expression2kinase (X2K) software was used to identify the transcription factors targeting the active *Lgr5+* stem cell signature (Chen et al., 2012).

DATA AND SOFTWARE AVAILABILITY

Data Resources

The data generated in this paper has been deposited in the Gene Expression Omnibus (GEO) under accession number GEO: GSE80636.

The list of differentially expressed genes between quiescent and active *Lgr5+* stem cells are described in Table S1.

Results of the GSEA analysis using the label retaining cell gene set are described in Table S2. GSEA results for the 'HALLMARKS' gene sets are reported in Table S3.

Differentially expressed genes for each cluster described in the single cell analysis are reported in Table S4.

The qPCR primers used in this study are in Table S5.

AUTHOR CONTRIBUTIONS

O.B., J.B., and H.C. designed the experiments and wrote the manuscript; J.B. performed the cell culture experiments; O.B. and K.W. performed RNA-sequencing experiments under the supervision of A.v.O.; O.B., J.B., and K.W. analyzed the data; J.B. was supervised by O.B. and H.C.; and H.S. contributed the *Dclk1* knockin allele.

ACKNOWLEDGMENTS

The authors would like to express their sincere gratitude to Stieneke van den Brink, Harry Begthel, Mauro Muraro, Stefan van der Elst, and Ewart de Bruijn for their support and excellent technical assistance. We thank Kim Boonekamp and Corina Markodimitraki for critical reading of the manuscript. H.C. is listed as the inventor on several patents related to this work. This work was supported by grants from NWO/ZonMW (114021012), NOW-CAS/ZONMW (116006103), and Friends of the Hubrecht Institute.

I

II

III

IV

V

VI

VII

VIII

&

REFERENCES

- Aoki, R., Shoshkes-Carmel, M., Gao, N., Shin, S., May, C.L., Golson, M.L., Zahm, A.M., Ray, M., Wisner, C.L., Wright, C.V., et al. (2016). Foxl1-expressing mesenchymal cells constitute the intestinal stem cell niche. *Cell. Mol.Gastroenterol. Hepatol.* 2, 175–188.
- Banck, M.S., Kanwar, R., Kulkarni, A.A., Boora, G.K., Metge, F., Kipp, B.R., Zhang, L., Thorland, E.C., Minn, K.T., Tentu, R., et al. (2013). The genomic landscape of small intestine neuroendocrine tumors. *J. Clin. Invest.* 123, 2502–2508.
- Barker, N., van Es, J.H., Kuipers, J., Kujala, P., van den Born, M., Cozijnsen, M., Haegebarth, A., Korving, J., Begthel, H., Peters, P.J., and Clevers, H. (2007). Identification of stem cells in small intestine and colon by marker gene *Lgr5*. *Nature* 449, 1003–1007.
- Basak, O., van de Born, M., Korving, J., Beumer, J., van der Elst, S., van Es, J.H., and Clevers, H. (2014). Mapping early fate determination in *Lgr5+* crypt stem cells using a novel *Ki67-RFP* allele. *EMBO J.* 33, 2057–2068.
- Buczacki, S.J., Zecchini, H.I., Nicholson, A.M., Russell, R., Vermeulen, L., Kemp, R., and Winton, D.J. (2013). Intestinal label-retaining cells are secretory precursors expressing *Lgr5*. *Nature* 495, 65–69.
- Chen, E.Y., Xu, H., Gordonov, S., Lim, M.P., Perkins, M.H., and Ma'ayan, A. (2012). Expression of 2 Kinases: mRNA profiling linked to multiple upstream regulatory layers. *Bioinformatics* 28, 105–111.
- Clevers, H. (2013). The intestinal crypt, a prototype stem cell compartment. *Cell* 154, 274–284.
- de Lau, W., Barker, N., Low, T.Y., Koo, B.K., Li, V.S., Teunissen, H., Kujala, P., Haegebarth, A., Peters, P.J., van de Wetering, M., et al. (2011). *Lgr5* homologues associate with Wnt receptors and mediate R-spondin signalling. *Nature* 476, 293–297.
- de Lau, W., Kujala, P., Schneeberger, K., Middendorp, S., Li, V.S., Barker, N., Martens, A., Hofhuis, F., DeKoter, R.P., Peters, P.J., et al. (2012). Peyer's patch M cells derived from *Lgr5(+)* stem cells require *Spib* and are induced by *RankL* in cultured "miniguts". *Mol. Cell. Biol.* 32, 3639–3647.
- Drucker, D.J., and Nauck, M.A. (2006). The incretin system: glucagon-like peptide-1 receptor agonists and dipeptidyl peptidase-4 inhibitors in type 2 diabetes. *Lancet* 368, 1696–1705.
- Eden, E., Navon, R., Steinfeld, I., Lipson, D., and Yakhini, Z. (2009). GOrilla: a tool for discovery and visualization of enriched GO terms in ranked gene lists. *BMC Bioinformatics* 10, 48.
- Egerod, K.L., Engelstoft, M.S., Grunddal, K.V., Nøhr, M.K., Secher, A., Sakata, I., Pedersen, J., Windeløv, J.A., Füchtbauer, E.M., Olsen, J., et al. (2012). A major lineage of enteroendocrine cells coexpress CCK, secretin, *GIP*, *GLP-1*, *PYY*, and neurotensin but not somatostatin. *Endocrinology* 153, 5782–5795.
- Farin, H.F., Van Es, J.H., and Clevers, H. (2012). Redundant sources of Wnt regulate intestinal stem cells and promote formation of Paneth cells. *Gastroenterology* 143, 1518–1529.
- Farin, H.F., Jordens, I., Mosa, M.H., Basak, O., Korving, J., Tauriello, D.V., de Punder, K., Angers, S., Peters, P.J., Maurice, M.M., and Clevers, H. (2016). Visualization of a short-range Wnt gradient in the intestinal stem-cell niche. *Nature* 530, 340–343.
- Grün, D., Lyubimova, A., Kester, L., Wiebrands, K., Basak, O., Sasaki, N., Clevers, H., and van Oudenaarden, A. (2015). Single-cell messenger RNA sequencing reveals rare intestinal cell types. *Nature* 525, 251–255.
- Grün, D., Muraro, M.J., Boisset, J.C., Wiebrands, K., Lyubimova, A., Dharmadhikari, G., van den Born, M., van Es, J., Jansen, E., Clevers, H., et al. (2016). De novo prediction of stem cell identity using single-cell transcriptome data. *Cell Stem Cell* 19, 266–277.

- Gunawardene, A.R., Corfe, B.M., and Staton, C.A. (2011). Classification and functions of enteroendocrine cells of the lower gastrointestinal tract. *Int. J.Exp. Pathol.* 92, 219–231.
- Hashimshony, T., Wagner, F., Sher, N., and Yanai, I. (2012). CEL-Seq: single-cell RNA-Seq by multiplexed linear amplification. *Cell Rep.* 2, 666–673.
- Heuberger, J., Kosel, F., Qi, J., Grossmann, K.S., Rajewsky, K., and Birchmeier, W. (2014). Shp2/MAPK signaling controls goblet/paneth cell fate decisions in the intestine. *Proc. Natl. Acad. Sci. USA* 111, 3472–3477.
- Höfer, D., and Drenckhahn, D. (1996). Cytoskeletal markers allowing discrimination between brush cells and other epithelial cells of the gut including enteroendocrine cells. *Histochem. Cell Biol.* 105, 405–412.
- Howitt, M.R., Lavoie, S., Michaud, M., Blum, A.M., Tran, S.V., Weinstock, J.V., Gallini, C.A., Redding, K., Margolskee, R.F., Osborne, L.C., et al. (2016). Tuft cells, taste-chemosensory cells, orchestrate parasite type 2 immunity in the gut. *Science* 351, 1329–1333.
- Janssen, S., and Depoortere, I. (2013). Nutrient sensing in the gut: new roads to therapeutics? *Trends Endocrinol. Metab.* 24, 92–100.
- Kitabgi, P., and Freychet, P. (1978). Effects of neurotensin on isolated intestinal smooth muscles. *Eur. J. Pharmacol.* 50, 349–357.
- Latorre, R., Sternini, C., De Giorgio, R., and Greenwood-Van Meerveld, B. (2016). Enteroendocrine cells: a review of their role in brain-gut communication. *Neurogastroenterol. Motil.* 28, 620–630.
- Love, M.I., Huber, W., and Anders, S. (2014). Moderated estimation of fold change and dispersion for RNA-seq data with DESeq2. *Genome Biol.* 15, 550.
- Middendorp, S., Schneeberger, K., Wiegerinck, C.L., Mokry, M., Akkerman, R.D., van Wijngaarden, S., Clevers, H., and Nieuwenhuis, E.E. (2014). Adult stem cells in the small intestine are intrinsically programmed with their location-specific function. *Stem Cells* 32, 1083–1091.
- Montgomery, R.K., Carlone, D.L., Richmond, C.A., Farilla, L., Kranendonk, M.E., Henderson, D.E., Baffour-Awuah, N.Y., Ambruzs, D.M., Fogli, L.K., Algra, S., and Breault, D.T. (2011). Mouse telomerase reverse transcriptase (mTert) expression marks slowly cycling intestinal stem cells. *Proc. Natl. Acad. Sci. USA* 108, 179–184.
- Munöz, J., Stange, D.E., Schepers, A.G., van de Wetering, M., Koo, B.K., Itzkovitz, S., Volckmann, R., Kung, K.S., Koster, J., Radulescu, S., et al. (2012). The Lgr5 intestinal stem cell signature: robust expression of proposed quiescent +4 cell markers. *EMBO J.* 31, 3079–3091.
- Myant, K., and Sansom, O. (2011). Efficient Wnt mediated intestinal hyperproliferation requires the cyclin D2-CDK4/6 complex. *Cell Div.* 6,3.
- Nakanishi, Y., Seno, H., Fukuoka, A., Ueo, T., Yamaga, Y., Maruno, T., Nakanishi, N., Kanda, K., Komekado, H., Kawada, M., et al. (2013). Dclk1 distinguishes between tumor and normal stem cells in the intestine. *Nat. Genet.* 45, 98–103.
- Parker, H.E., Habib, A.M., Rogers, G.J., Gribble, F.M., and Reimann, F. (2009). Nutrient-dependent secretion of glucose-dependent insulinotropic polypeptide from primary murine K cells. *Diabetologia* 52, 289–298.
- Pellegrinet, L., Rodilla, V., Liu, Z., Chen, S., Koch, U., Espinosa, L., Kaestner, K.H., Kopan, R., Lewis, J., and Radtke, F. (2011). Dll1- and dll4-mediated notch signaling are required for homeostasis of intestinal stem cells. *Gastroenterology* 140, 1230–1240.
- Potten, C.S., Hume, W.J., Reid, P., and Cairns, J. (1978). The segregation of DNA in epithelial stem cells. *Cell* 15, 899–906.

I

II

III

IV

V

VI

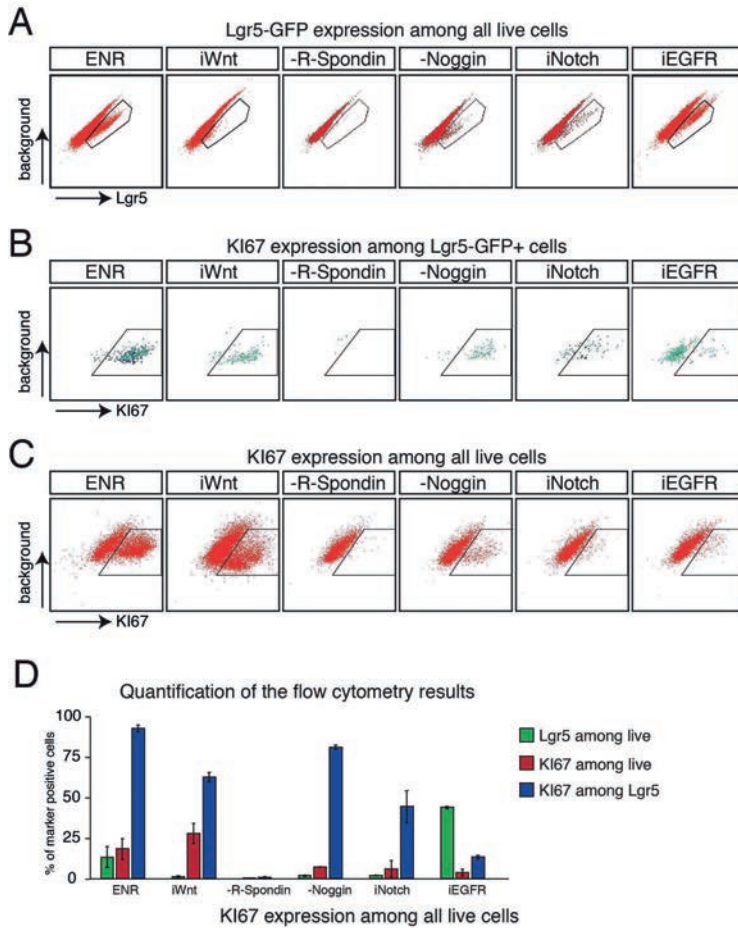
VII

VIII

&

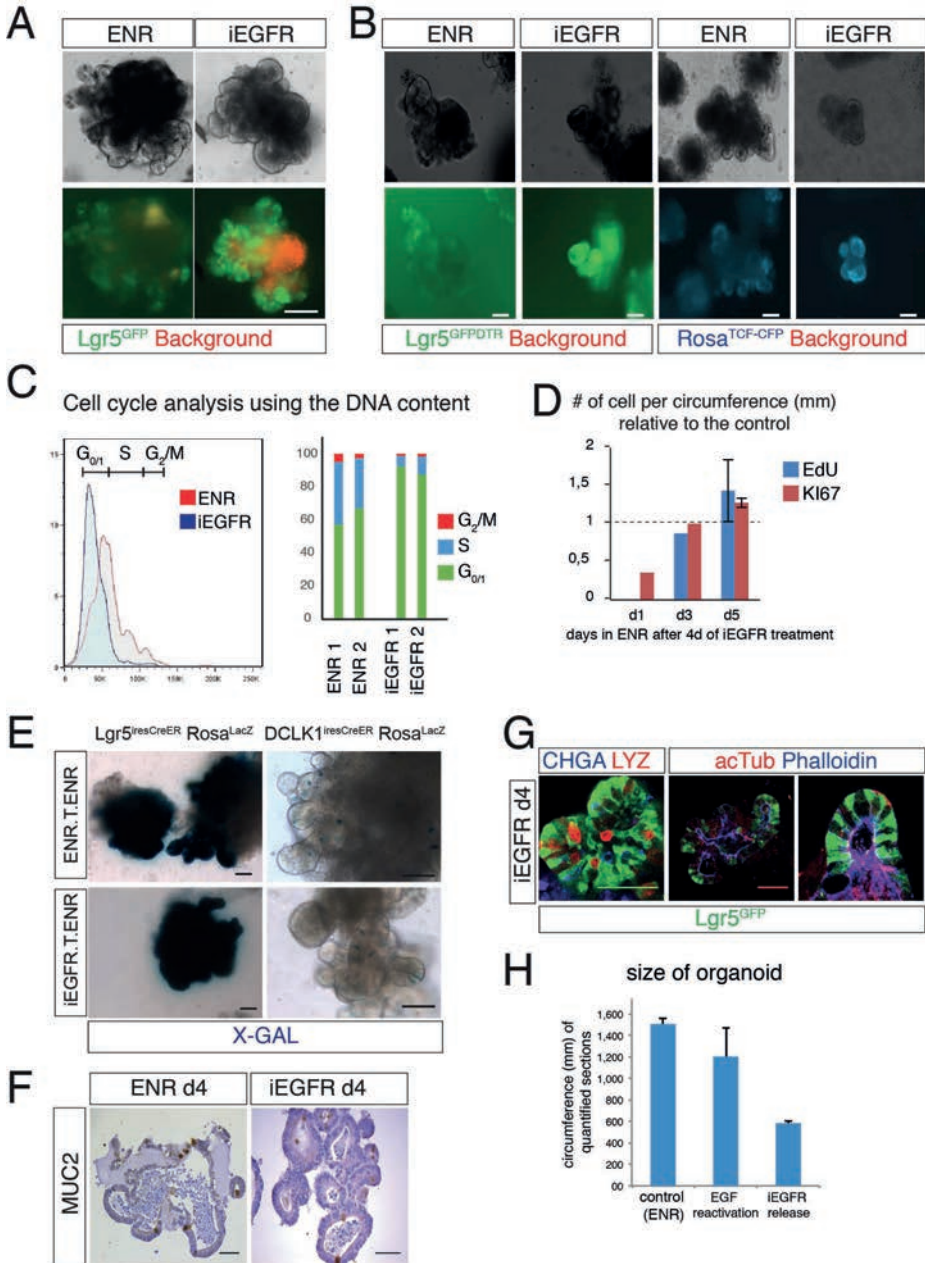
- Powell, A.E., Wang, Y., Li, Y., Poulin, E.J., Means, A.L., Washington, M.K., Higginbotham, J.N., Juchheim, A., Prasad, N., Levy, S.E., et al. (2012). The pan-ErbB negative regulator *Lgr1* is an intestinal stem cell marker that functions as a tumor suppressor. *Cell* 149, 146–158.
- Sangiorgi, E., and Capecchi, M.R. (2008). *Bmi1* is expressed in vivo in intestinal stem cells. *Nat. Genet.* 40, 915–920.
- Sato, T., Vries, R.G., Snippert, H.J., van de Wetering, M., Barker, N., Stange, D.E., van Es, J.H., Abo, A., Kujala, P., Peters, P.J., and Clevers, H. (2009). Single *Lgr5* stem cells build crypt-villus structures in vitro without a mesenchymal niche. *Nature* 459, 262–265.
- Sato, T., van Es, J.H., Snippert, H.J., Stange, D.E., Vries, R.G., van den Born, M., Barker, N., Shroyer, N.F., van de Wetering, M., and Clevers, H. (2011). Paneth cells constitute the niche for *Lgr5* stem cells in intestinal crypts. *Nature* 469, 415–418.
- Schepers, A.G., Vries, R., van den Born, M., van de Wetering, M., and Clevers, H. (2011). *Lgr5* intestinal stem cells have high telomerase activity and randomly segregate their chromosomes. *EMBO J.* 30, 1104–1109.
- Serup, P., Gustavsen, C., Klein, T., Potter, L.A., Lin, R., Mullapudi, N., Wandzioch, E., Hines, A., Davis, A., Bruun, C., et al. (2012). Partial promoter substitutions generating transcriptional sentinels of diverse signaling pathways in embryonic stem cells and mice. *Dis. Model. Mech.* 5, 956–966.
- Shibue, K., Yamane, S., Harada, N., Hamasaki, A., Suzuki, K., Joo, E., Iwasaki, K., Nasteska, D., Harada, T., Hayashi, Y., et al. (2015). Fatty acid-binding protein 5 regulates diet-induced obesity via GLP secretion from enteroendocrine K cells in response to fat ingestion. *Am. J. Physiol. Endocrinol. Metab.* 308, E583–E591.
- Soriano, P. (1999). Generalized *lacZ* expression with the *ROSA26* Cre reporter strain. *Nat. Genet.* 21, 70–71.
- Supek, F., Bosnjak, M., Skunca, N., and Smuc, T. (2011). REVIGO summarizes and visualizes long lists of gene ontology terms. *PLoS ONE* 6, e21800.
- Takeda, N., Jain, R., LeBoeuf, M.R., Wang, Q., Lu, M.M., and Epstein, J.A. (2011). Interconversion between intestinal stem cell populations in distinct niches. *Science* 334, 1420–1424.
- Terry, N.A., Walp, E.R., Lee, R.A., Kaestner, K.H., and May, C.L. (2014). Impaired enteroendocrine development in intestinal-specific *Islet 1* mouse mutants causes impaired glucose homeostasis. *Am. J. Physiol. Gastrointest. Liver Physiol.* 307, G979–G991.
- Tetteh, P.W., Basak, O., Farin, H.F., Wiebrands, K., Kretschmar, K., Begthel, H., van den Born, M., Korving, J., de Sauvage, F., van Es, J.H., et al. (2016). Replacement of lost *Lgr5*-positive stem cells through plasticity of their enterocyte-lineage daughters. *Cell Stem Cell* 18, 203–213.
- Tian, H., Biehs, B., Warming, S., Leong, K.G., Rangell, L., Klein, O.D., and de Sauvage, F.J. (2011). A reserve stem cell population in small intestine renders *Lgr5*-positive cells dispensable. *Nature* 478, 255–259.
- Van Es, J.H., van Gijn, M.E., Riccio, O., van den Born, M., Vooijs, M., Begthel, H., Cozijnsen, M., Robine, S., Winton, D.J., Radtke, F., and Clevers, H. (2005). Notch/ γ -secretase inhibition turns proliferative cells in intestinal crypts and adenomas into goblet cells. *Nature* 435, 959–963.
- Van Es, J.H., Sato, T., van de Wetering, M., Lyubimova, A., Nee, A.N., Gregorieff, A., Sasaki, N., Zeinstra, L., van den Born, M., Korving, J., et al. (2012). *Dll1*+ secretory progenitor cells revert to stem cells upon crypt damage. *Nat. Cell Biol.* 14, 1099–1104.
- Yan, K.S., Chia, L.A., Li, X., Ootani, A., Su, J., Lee, J.Y., Su, N., Luo, Y., Heilshorn, S.C., Amieva, M.R., et al. (2012). The intestinal stem cell markers *Bmi1* and *Lgr5* identify two functionally distinct populations. *Proc. Natl. Acad. Sci. USA* 109, 466–471.
- Yin, X., Farin, H.F., van Es, J.H., Clevers, H., Langer, R., and Karp, J.M. (2014). Niche-independent high-purity cultures of *Lgr5*+ intestinal stem cells and their progeny. *Nat. Methods* 11, 106–112.

SUPPLEMENTARY FIGURES



Supplementary figure 1. The role of niche signalling pathways in proliferation of Lgr5+ cells. (A-C) FACS plots showing the endogenous fluorescence of Lgr5^{GFPDTR/+} organoids in all live cells (A), KI67^{fluor60} immunostaining among Lgr5^{GFPDTR/+} cells (B) or among all live cells (C) on the x axis. Since Lgr5+ cells are lost after R-Spondin1 withdrawal, few KI67+ cells are seen in respective B panel. PL3 channel is used (y axis) to discriminate background. Gates shows positive cells with respect to wild type controls. (D) Quantification of A-C.

I
 II
 III
 IV
 V
 VI
 VII
 VIII
 &



I

II

III

IV

V

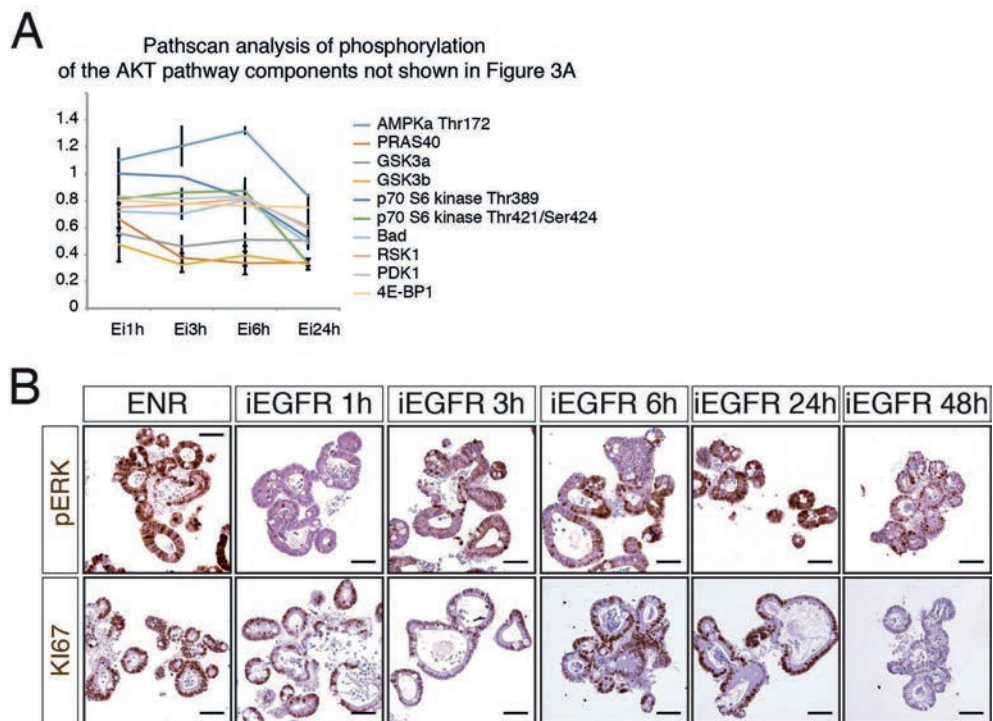
VI

VII

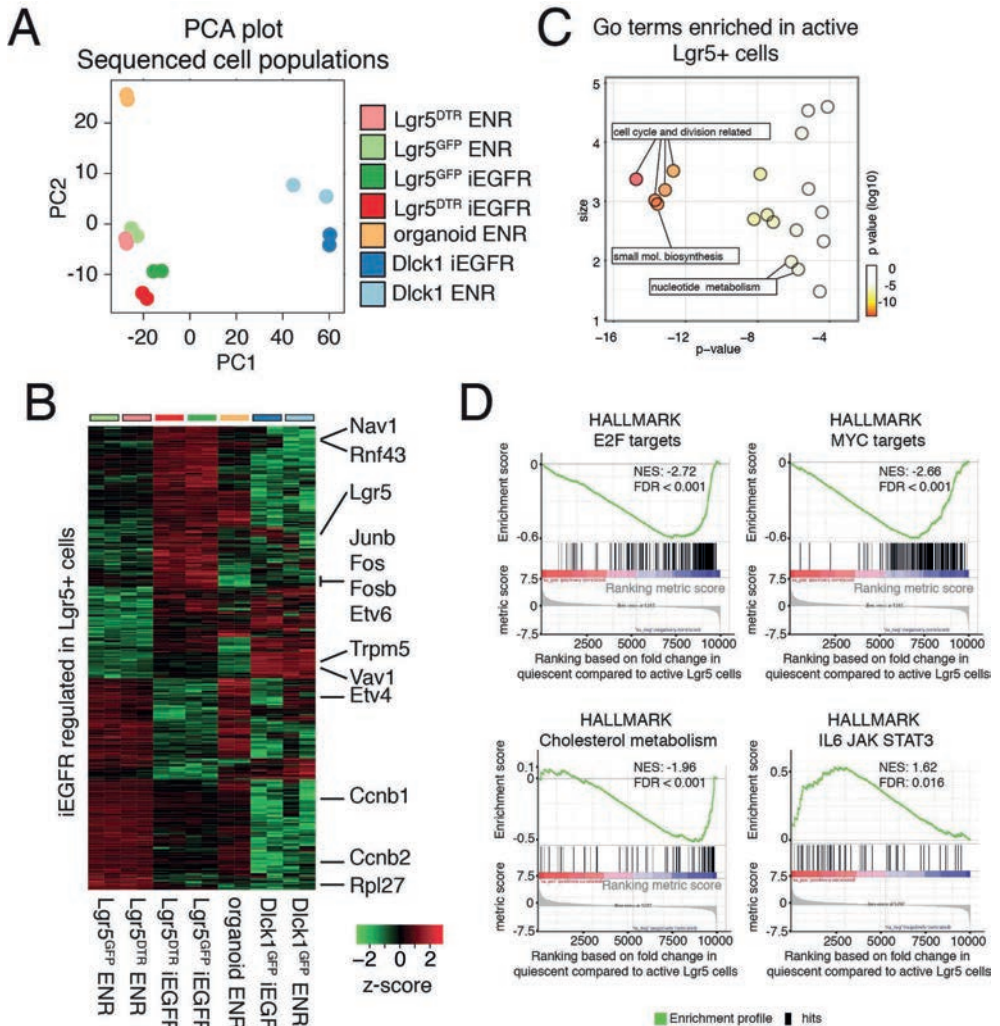
VIII

&

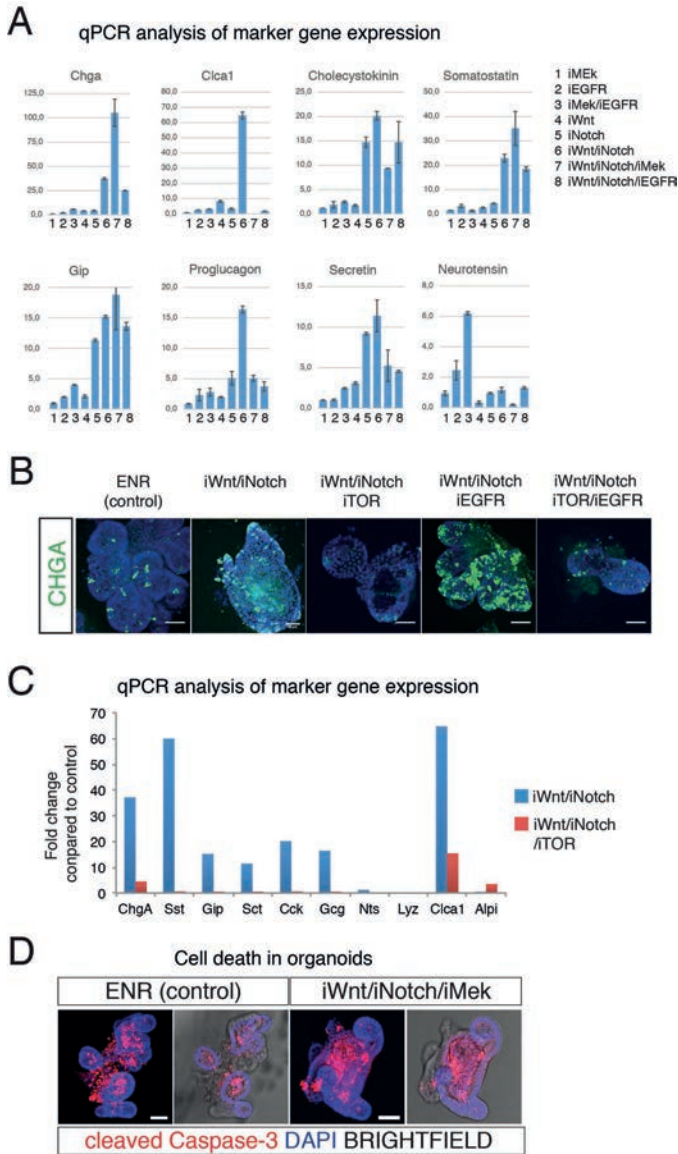
- Supplementary figure 2. EGFR inhibition induces *Lgr5*+ cell quiescence while maintaining self-renewal and multipotency. (A-B) Brightfield (upper) and fluorescent (lower) images in control (ENR) and EGFR inhibited (iEGFR) *Lgr5*^{GFPiresCreER/+} (A, green), *Lgr5*^{GFPDTR/+} (B, green) and *Rosa*^{TCE-CFP/+} (B, blue) organoids. RFP (Red) channel is used to discriminate background. (C) HOECHST analysis of the DNA content of control or iEGFR treated organoids. Bars on the right show quantification of 3 independent experiments. (D) Relative number of marker protein positive cells following reintroduction of EGF signalling for 1 (d1), 3 (d3) or 5 (d5) days compared to respective controls (DMSO treated, same days in culture). Fluorescent images are shown in figure 1G. (E) Lineage tracing iEGFR or control (DMSO) treated *Lgr5*+ or *Dclk1*+ cells. After 4 days of iEGFR treatment in *Lgr5*^{iresCreER}*Rosa*^{LacZ} or *Dclk1*^{iresCreER}*Rosa*^{LacZ} organoids, recombination was induced with 4'OH Tamoxifen (T) for 16 hours and EGF signalling was restored by replating in ENR. X-Gal staining was performed to follow recombined cells (blue) and assess stem cell potential of control (upper panel, ENR.T.ENR) or reactivated quiescent stem cells (lower panel, iEGFR.T.ENR). EGFR reactivated stem cells generate full organoids, indicative of multipotency and cell cycle reactivation. (F) MUC2 antibody staining (brown) on paraffin sections of iEGFR treated organoids and controls. Sections are counterstained using haematoxylin (G) After 4 days of iEGFR treatment; *Lgr5*^{GFP+} stem cells do not express markers of enteroendocrine cells (CHGA, blue), Paneth cells (LYZ, red) or display characteristics of Tuft cells (apical actin bundles stained by Phalloidin, blue or acetylated Tubulin bundles, red). (H) Quantification of the organoid circumference on optical sections of organoids described in figures 2C and 2D. EGFR inhibitor was removed to reactivate organoids, either in the presence (repeated iEGFR) or absence (repeated -EGF) of EGF. EVOS (A, B and E) and confocal (F, optical sections) microscope was used for imaging.



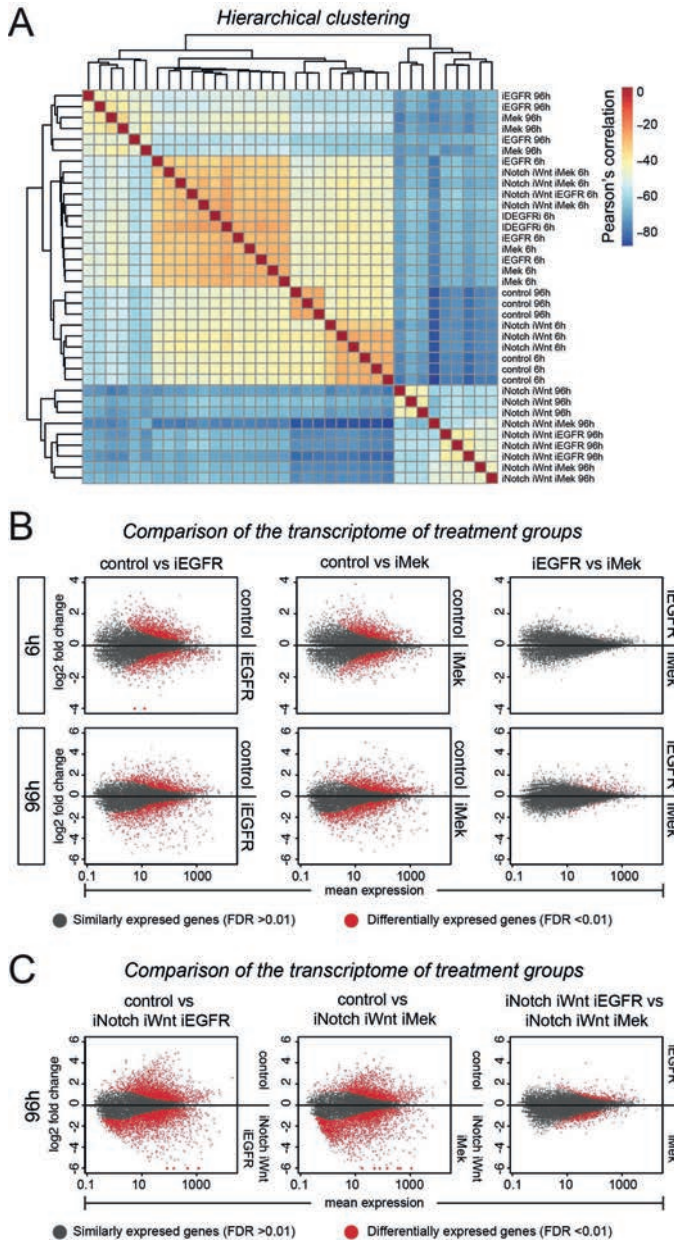
Supplementary figure 3. Downstream effects on MAPK and Akt components after EGFR inhibition. (A) Quantification of the Pathscan[®] analysis of iEGFR treated organoids. Data that is not shown in Figure 3A is displayed. (B) Histological analysis of ERK phosphorylation following EGFR inhibition. A rapid loss in pERK is gradually over 24h, but remains low over 48 hours (upper panels). Lower panels show KI67 staining. Scale bars, 50 μ m. Error bars indicate SD.



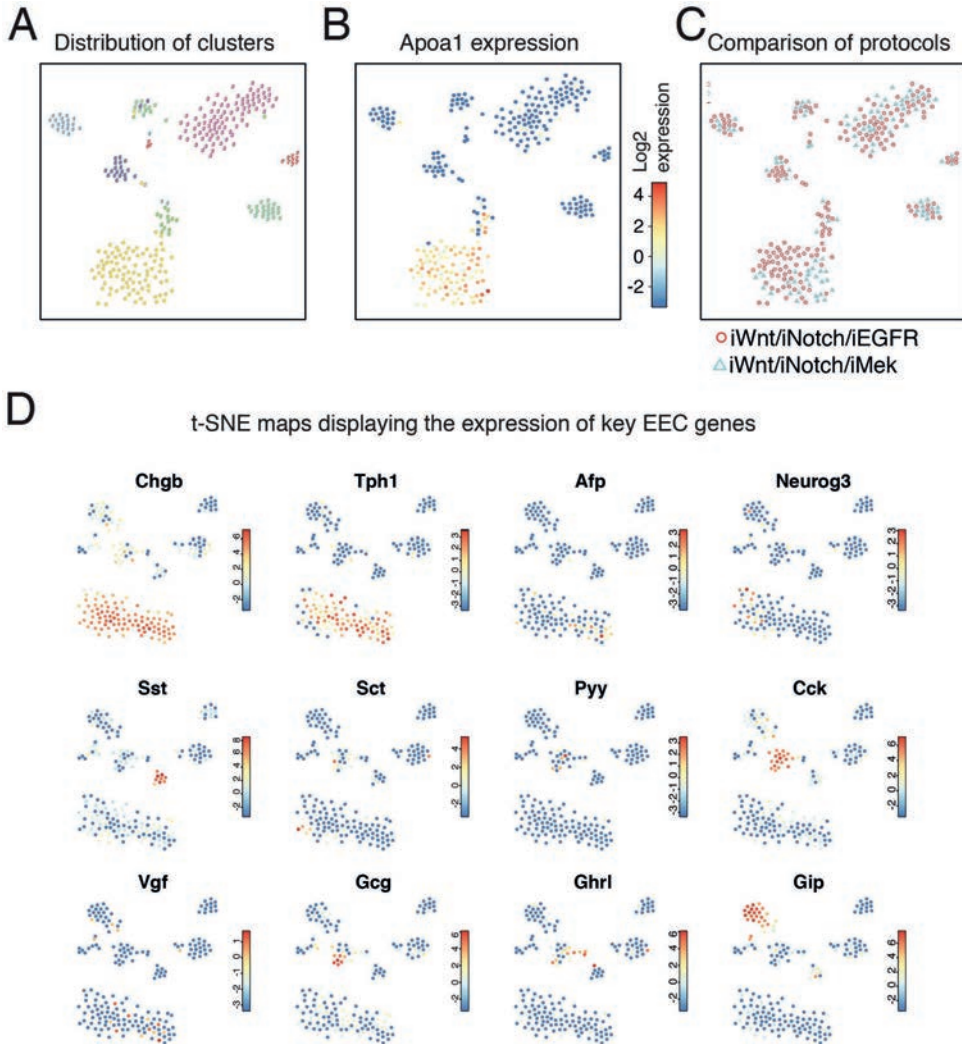
Supplementary figure 4. Molecular features of quiescent and active Lgr5+ stem cells. (A) Principal component analysis (PCA) indicating transcriptome differences between bulk samples in different culturing conditions. (B) Heat map showing the relative expression of genes differentially expressed gene between active and quiescent stem cells. Key genes expressed in stem cells (Nav1, Rnf43, Lgr5), Tuft cells (Trpm5, Vav1), those involved in cell cycle progression (Ccnb1, Ccnb2, Rpl27) and transcription factors (Junb, Fos, Fosb, Etv4) are highlighted. Colours show z-score for each row. (C) Plot displaying Gene Ontology (GO) term enriched in active Lgr5+ stem cells. X-axis shows the relative number of genes related to the GO term, x-axis shows the statistical significance (p-value) for each term. (D) Gene set enrichment analysis (GSEA). Fold change in gene expression in quiescent and active Lgr5+ stem cells are compared. Green line shows enrichment profile. Black bars show where genes from a given gene set are located (hit).



Supplementary figure 5. Enteroendocrine cells are effectively induced in Wnt, Notch and EGFR inhibited organoids. (A) qPCR analysis of organoids for enteroendocrine markers after single Wnt inhibition (iWnt), Notch inhibition (iNotch), EGFR inhibition (iEGFR), MEK inhibition (iMek) or combinations. (B) Confocal sections of organoids stained for enteroendocrine marker CHGA (Green) after combinations of Wnt, Notch, mTOR (iTOR) or EGFR inhibition. iTOR completely attenuates the increase in enteroendocrine cell number observed after iWnt/iNotch/iEGFR treatment. (C) qPCR analysis of enteroendocrine markers in iWnt/iNotch treated organoids, with or without mTOR inhibition. iTOR treatment reverses the increase in enteroendocrine cell markers due to iWnt/iNotch treatment. Scale bars, 50 μ m. (D) Cleaved caspase-3 (red) staining is used to visualize apoptosis in organoids. Most apoptotic figures are shed to the lumen after 1 day of control (ENR) or iWnt/iNotch/iMek treatment. Labelling in the crypts is rare. Images in B and D are 3D reconstruction confocal images. Scale bars, 50 μ m. Error bars indicate SD.



Supplementary figure 6. Characterization of organoids after quiescence or enteroendocrine cell induction using RNA sequencing. (A) Heat map indicating transcriptome similarities between bulk samples in different culturing conditions measured by Pearson's correlation coefficient. Samples are ordered according hierarchical clustering. (B-C) Plots display the comparison of the transcriptome of respective populations. (B) Control, iEGFR and iMek conditions were compared after 6h (upper row) or 96h (lower row) of treatment. (C) Control, iWnt/iNotch/iEGFR and iWnt/iNotch/iMek conditions are compared after 96h of treatment. The y-axis shows the fold change in log₂, the x-axis shows the mean value of the transcripts. Each dot represents a gene. Red dots are differentially expressed between the compared populations (FDR < 0.01).



Supplementary figure 7. Single cell analysis of induced enteroendocrine cells. (A) t-SNE map representation of transcriptome similarities. Colours and numbers indicate RaceID2 clusters. (B) t-SNE map showing \log_2 transformed transcript counts of *Apoa1*, an enterocyte marker. (C) t-SNE map showing the distribution of cells between two different culturing conditions, as indicated. (D) t-SNE map showing \log_2 transformed transcript counts of the key EEC genes indicated. Colours in B and D show normalized expression values.

CHAPTER
ENTEROENDOCRINE CELLS
SWITCH HORMONE EXPRESSION
ALONG THE CRYPT-TO-VILLUS BMP
SIGNALING GRADIENT

IV

SUMMARY

Enteroendocrine cells (EECs) control a wide range of physiological processes linked to metabolism (Furness et al., 2013). We show that EEC hormones are differentially expressed between crypts (e.g. Glp1) and villi (e.g. Secretin). As demonstrated by single-cell mRNA sequencing (scRNAseq) using murine Lgr5⁺ cell-derived organoids, BMP4 signals alter the hormone expression profiles of individual EECs to resemble those found in the villus. Accordingly, BMP4 induces hormone switching of EECs migrating up the crypt-villus axis *in vivo*. Our findings imply that EEC lineages in the small intestine exhibit a more flexible hormone repertoire than previously proposed. We also describe a protocol to generate human EECs in organoids and demonstrate a similar regulation of hormone expression by BMP signalling. These findings establish alternative strategies to target EECs with therapeutically relevant hormone production through BMP modulation

Joep Beumer¹, Benedetta Artegiani^{1,2}, Yorick Post¹, Frank Reimann³,
Fiona Gribble³, Thuc Nghi Nguyen⁴, Hongkui Zheng⁴, Maaïke Van den Born^{1,2},
Johan H. Van Es^{1,2} and Hans Clevers^{1,2*}

¹Hubrecht Institute, Royal Netherlands Academy of Arts and Sciences (KNAW), Uppsalalaan 8, 3584 CT, Utrecht the Netherlands

²Oncode Institute, Utrecht, the Netherlands

³Metabolic Research Laboratories, Wellcome Trust-MRC Institute of Metabolic Science, Addenbrooke's Hospital, Cambridge, UK

⁴Allen Institute for Brain Science, Seattle, WA, USA

* Corresponding author

Intestinal enteroendocrine cells (EECs) constitute the largest hormone-producing organ in mammals and are classified according to their hormone products (Furness et al., 2013). Enterochromaffin cells (ECs) produce Serotonin, a regulator of intestinal motility, and Tachykinin 1 (Tac1, Substance P), a peptide involved in muscle contraction and inflammation (Connor et al.). L-cells produce Glp1, an inducer of insulin release encoded by the Glucagon (Gcg) gene, and can co-express Pyy (Furness et al., 2013). Other EEC subtypes include Gastric inhibitory protein (Gip)-producing K-cells, Somatostatin (Sst)-producing D-cells, Cholecystokinin (Cck)-producing I-cells, Neurotensin (Nts)-producing N-cells and Secretin (Sct)-producing S-cells (Furness et al., 2013). Although this classification suggests well-defined, distinct EEC subtypes, these hormones are often co-expressed suggesting considerable overlap between lineages (Egerod et al., 2012; Haber et al., 2017). As all cell types of the intestinal epithelium, the short-lived EECs are constitutively produced by *Lgr5*⁺ crypt stem cells (Barker et al., 2007). *Lgr5* stem cells can be cultured to generate epithelial organoids that faithfully recapitulate gut epithelial biology (Sato et al., 2009). ScRNAseq has shown that a complete set of EECs subtypes is produced in these mini-guts, including some that had previously gone unnoticed in intact gut (Basak et al., 2017; Grün et al., 2015). However, extrinsic factors that control EEC subtype identity have remained largely unknown.

Previous work has suggested that EECs expressing Tac1 and Glp1 are restricted to crypts, whereas Sct-, Pyy- and Nts-producing EECs are enriched in villi (Grunddal et al., 2016; Roth and Gordon, 1990). In agreement with these studies, we found that ileal L-cells co-express Glp1 and Pyy in the crypt, but mostly lack Glp1 in the villus (Fig. 1a-c, Fig. S1a). Serotonin-producing ECs occurred along the length of the crypt-villus axis, but selectively co-expressed Tac1 in the crypt and Sct in the villus (Fig. 1d-e, Fig. S1a). To address if hormone switching occurs during migration of EECs along the crypt-villus axis, we analyzed intestines from *Tac1^{iresCre} / Rosa^{tdTomato}* mice, an allele which faithfully labels all Tac1⁺/Serotonin⁺ cells in the crypt (Fig. 1f) (Harris et al., 2014). In adult intestines, almost all Serotonin⁺ cells were marked by tdTomato (Fig. 1g). Importantly, >55% of Sct⁺ cells on villi were also traced, while being negative for Tac1 (Fig. 1f-g, S1b). The rarity of tdTomato⁺ cells that were negative for Serotonin suggests that ECs do not lose Serotonin during their lifetime to become single Sct⁺ as previously suggested (Aiken and Roth, 1992; Roth and Gordon, 1990). Serotonin-negative Sct⁺ cells not traced by Tac1 must thus be part of another EEC lineage. EECs producing other hormones, including Cck, Gip and Sst, were only rarely derived from Tac1⁺ progenitors (Fig. 1g, S1b). These data imply lineage relationships between crypt and villus EECs, i.e that Tac1⁺/Sct⁺ ECs on villi derive from Tac1⁺ crypt ECs. This, in turn, suggests that local niche signals can induce shifts in hormone expression.

Multiple signalling gradients exist along the crypt-villus axis, e.g. Wnt levels are high at the crypt base, while BMP is highest at the villus tips (Beumer and Clevers, 2016; Haramis et al., 2004). In murine intestinal organoids, EECs are induced through inhibition of the Wnt, MAPK and Notch signalling pathways, in the presence of the BMP inhibitor Noggin (Basak et al., 2017). We used this differentiation system as a starting point to modulate selected signalling pathways (Basak et al., 2017), while monitoring Sct and Gcg as a proxy of the villus-



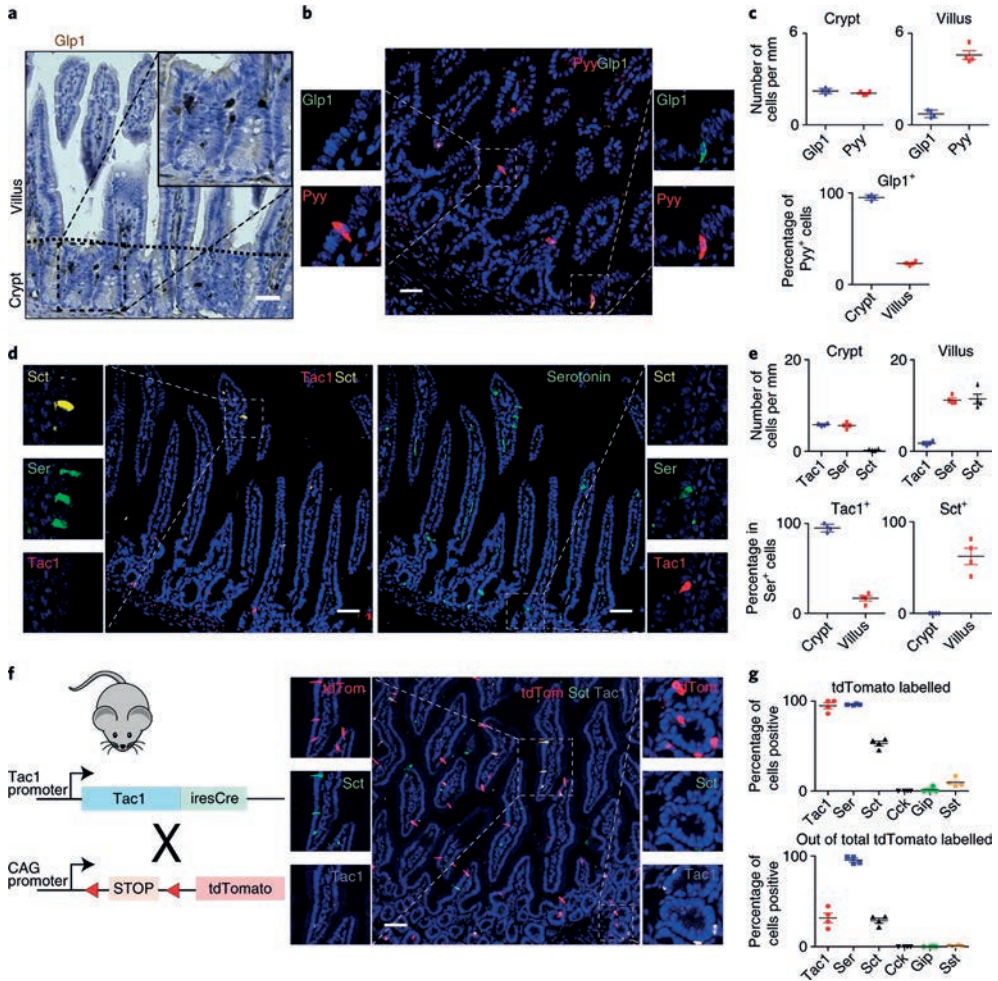


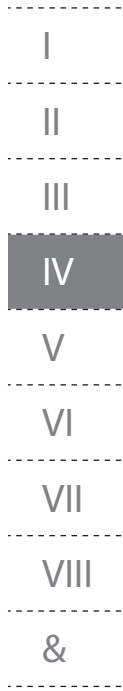
Figure 1. Enteroendocrine cells switch hormone expression while migrating from crypt to villus. **a** and **b**, Immunohistochemical analysis reveals Glp1⁺ cells are enriched in the ileal crypt, where they co-express Pyy. Experiment in (**a**) was repeated two times independently with similar results. **c**, Quantification of **b**. The percentage of Pyy⁺ cells that co-express Glp1 are represented in the lower chart. **d**, ECs express Tac1 in the crypt and Sct in the villus, while Serotonin is produced in both locations. **e**, Quantification of **d**. The percentage of Serotonin⁺ cells that co-express Tac1 or Sct are represented in the lower charts. **f**, Intestine of Tac1^{iresCre}/Rosa^{Aii4} mice reveals that ECs lose Tac1 and gain Sct expression from crypt to villus. **g**, Quantification of (**f**) and Fig S1. The percentages of each hormone that is tdTomato⁺ (upper chart) and of tdTomato⁺ cells that are hormone positive (lower chart) are shown. The mean values are depicted in graphs **c**, **e** and **g**, and error bars present SD for n=4 mice for each experiment. Scale bar is 50 μ m.

and crypt-hormone signatures, respectively. Strikingly, we observed that all ECs in this culture co-expressed Serotonin and Tac1, while Sct was absent (Fig. 2a). This suggests niche signals acting on EECs are dominant over a default, temporal differentiation process. Manipulation of the Wnt, TGF β and Hedgehog pathways did either reduce both Gcg and Sct transcripts, or

had no significant effect on any assessed hormone (Fig. S2a). We replaced Noggin by BMP4 in this EEC differentiation cocktail ('EEC BMP^{high}' medium), generating cells immunoreactive for Sct, as well as ECs lacking Tac1 (Fig. 2a-b). Glp1⁺ cell numbers and total levels of secreted Glp1 were greatly diminished (Fig. 2a-c, S2b). We next performed bulk RNA-sequencing on duodenal and ileal organoids stimulated with EEC BMP^{high} or EEC BMP^{low} media (Fig. 2d), and validated the expression of selected genes by qPCR (Fig. 2e). EEC markers which are homogeneously distributed on crypts and villi (Chga, Tph1 (enzyme catalyzing Serotonin production), Cck and duodenal Gip) are only mildly affected by BMP activation (Fig. 2d-e). We did observe an increase in Sct and a minor upregulation of Pyy and Nts (Fig. 2d-e), which are expressed highest in the villus (Grunddal et al., 2016). Sct is enriched in the proximal part of the SI (Furness et al., 2013), but we observe that our EEC differentiation protocol generates Sct⁺ cells equally well in the proximal and distal SI organoids. Trpa1, an irritant receptor enriched in EECs of the intestinal crypt (Camacho et al., 2015), decreased with BMP activation (Fig. 2d). BMP4-mediated changes in hormone expression could be overridden by the addition of BMPRIa inhibitor LDN193189, confirming involvement of the BMPRI/2 axis (Fig. S2c-d).

To address whether BMP signalling can switch hormone expression in individual mature EECs rather than selectively depleting subtypes of EECs, we followed the fate of Gcg- or Tac1-expressing cells using cultures derived from *Gcg^{Venus}* and *Tac1^{iresCre} / Rosa26^{tdTomato}* mice (Habib et al., 2012; Harris et al., 2014). Live-cell imaging of *Gcg^{Venus}* organoids demonstrated that BMP activation induced a decrease in Venus levels, suggesting downregulation of Gcg (Fig. S2e-f). We did not observe BMP-induced apoptosis of Venus⁺ or tdTomato⁺ cells (Fig. S2g).

Changes in hormone expression in individual EECs might be caused by dynamics in transcriptional networks, and accompanied by production of other sensory receptors. To identify dynamics at a single-cell level, we performed scRNAseq of traced Tac1-, Glp1- or Gip-expressing murine cells (Habib et al., 2012). Gip⁺ K-cells exist both in crypts and villi and were isolated from organoids derived from a *Gip^{Cre} / Rosa26^{tdRFP}* mouse (Svendsen et al., 2016). Guided by their regional *in vivo* abundance, we isolated organoids from the proximal SI of the Gip-, from the distal SI of Gcg- and from the whole SI of Tac1 reporter mice. Organoids were treated with a MEK inhibitor to limit new EEC generation and either exposed to Noggin (control) or BMP4 for 24 or 96 hours (Fig. 3a). Next, EECs derived from the reporters/treatments were sorted for the reporter fluorescence and scRNAseq was performed using SORTseq (Muraro et al., 2016), an automated version of CELseq2 (Fig. 3a, S3a) (Hashimshony et al., 2016). K-medoids clustering by RaceID2 algorithm (Grün et al., 2016) showed that Tac1-, Gcg- and Gip-traced cells, classically defined as ECs, L- and K- cells, respectively, clustered accordingly to their cell-type and mostly independently of the treatment in a t-SNE space (Fig. 3b-c). We identified Alpi⁺ enterocytes and Muc2⁺ Goblet cells derived from the *Gcg^{Venus}* reporter that displayed the lowest Venus fluorescence intensity (Fig. S3b). We also detected a cluster of unknown identity with expression of the vomeronasal receptor Vmn2r55, which was identified previously (Grün et al., 2015). BMP-stimulated ECs displayed lower Sct expression compared to L- and K-cells (Fig. 3c-e). Within ECs, expression of Tph1 remained unchanged during BMP treatment, while Tac1 decreased (Fig. 3c-e). Cells clustering as classical L-cells reduced their



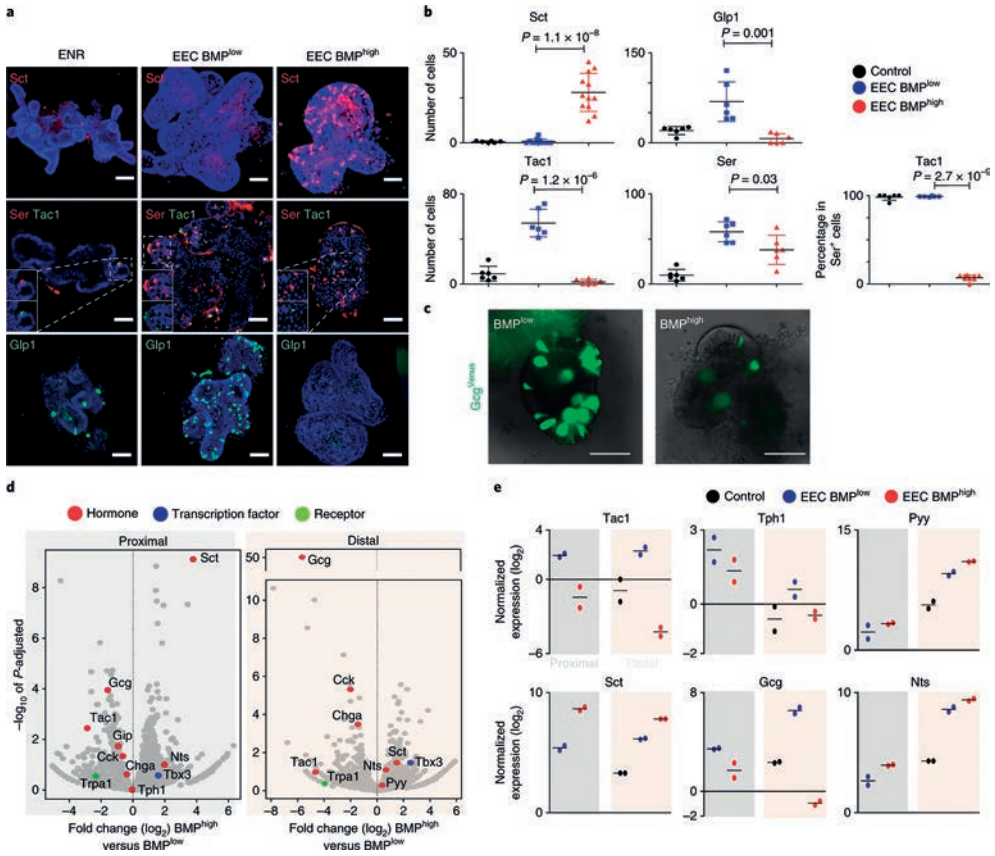


Figure 2. Activation of BMP signalling induces Villus-like hormone signature in mouse EECs. a, Organoids are differentiated for 4 days to EECs in the absence (EEC BMP^{low}) or presence of BMP4 (EEC BMP^{high}). ENR is used as a control. Activation of BMP signalling induces expression of Sct, while repressing Tac1 and Glp1. Images are presented as maximum projections, and are representative of 2 independent experiments. b, Quantification of a. The number of positive cells for each hormone were quantified and are displayed per mm of organoid epithelium. The percentage of Serotonin⁺ cells that co-express Tac1 are presented. Sample size represents 2 biologically independent experiments, in which at least 3 organoids were quantified per replicate and staining. Mean values per treatment are shown and error bars depict SD and were derived from n=12 organoids for Sct, n=6 organoids for other hormones in BMP low and high conditions. P-values were calculated from these same n-numbers using a two-sided t-test. c, Overlay of brightfield and Venus image of organoids derived from Gcg^{Venus} mice after a 4 day treatment with a BMP^{low} or BMP^{high} EEC differentiation cocktail. BMP activation represses expression of Gcg, without inducing morphological alterations. Experiment was repeated independently 10 times. d, Volcano plots showing results from RNA sequencing of organoids stimulated for 4 days with BMP low or high EEC differentiation cocktails, from proximal (left) and distal (right) SI organoids. Gene expression fold change (\log_2) of BMP^{high} versus BMP^{low} is shown on the x-axis and significance on the y-axis. Each grey dot represents a gene, and dots representing relevant genes are highlighted in different colors, according to their function. Sample size represents 2 biologically independent experiments, and p-adjusted values were calculated with a Wald test using the DESeq2 package. e, qPCR analysis of selected hormones from d. Expression levels are shown relative to control organoids in ENR medium. Experiment was performed in n=2 biologically independent experiments, and the mean expression is depicted. Scale bar is 50 μ m.

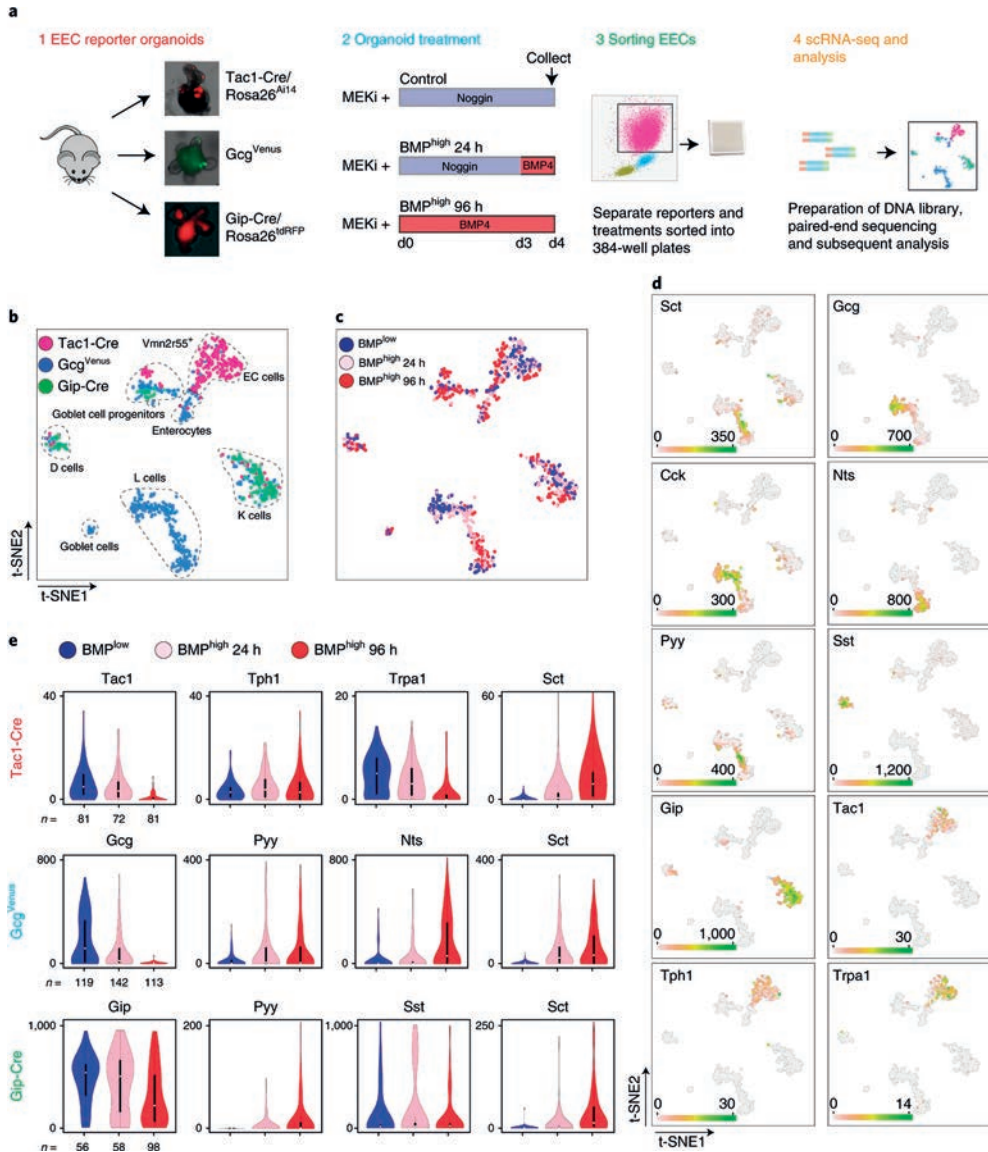


Figure 3. Single cell RNA sequencing reveals BMP regulated plasticity among different EEC subtypes. **a**, Experimental paradigm. Different EEC reporter organoids were treated with a MEK inhibitor, while receiving Noggin or BMP4. After 4 days, organoids were dissociated and traced EECs sorted and processed for single cell RNA sequencing. **b** and **c**, t-SNE map of single cell RNA sequenced EECs using the RaceID2 algorithm. Different colors, as indicated in the legend, highlight cells isolated from different reporter organoids (**b**) and treatments (**c**). **d**, Expression levels of selected hormones and receptors in the tSNE space of (**b-c**). **e**, Expression of individual hormones within different EEC reporter sorted cells are presented in violin plots, with different colors for the different treatments (as indicated in the legend). Violin plots depict median values (white dot), 50% of the values (within thick black line) and 95% of the values (within thin black line). The n number of cells per treatment and reporter is depicted. Different dynamics of hormone expression were observed over the course of BMP treatment in subtypes of EECs.

Gcg (Glp1) expression, while activating Nts and Pyy transcription following BMP treatment (Fig. 3d and S3c). Some Gcg^{Venus} -sorted cells from ileal organoids expressed Gip, combined with low levels of Gcg (Fig. 3b-d). These cells clustered together with K-cells and could not be induced to express Nts, indicating that these cells represent K-cells and not L-cells. (Fig. 3d). L-cells and to a lesser extent K-cells express Cck independent of treatment (Fig. 3d). Within Gip-traced K-cells, we observed a separate population of Sst-producing cells. BMP activation had no effect on Sst expression and caused a mild reduction in Gip expression in these clusters, while activating Sct expression only in Gip^+ but not in Sst^+ cells (Fig. 3d-e, S3c). Pyy expression could be induced in both Gip^+ and in Sst^+ cells, but to a lesser extent than in L-cells (Fig. S3c). We did observe low Cck, Gcg and no Nts expression in K-cells, indicating that these represent a separate lineage from ileal L-cells (Fig. 3d-e).

We identified uniquely expressed genes in the various clusters that corresponded to known expression or function along the crypt-to-villus axis *in vivo*. The irritant receptor *Trpa1* (proposed to be involved in serotonin release) is enriched in the crypt (Camacho et al., 2015; Nozawa et al., 2009). Concordantly, it decreased during BMP treatment within ECs (Fig. 3d-e). We found the orphan receptor *Asic5* to be expressed by Sst^+ cells (Fig. S3d). This same population also expressed the islet amyloid polypeptide (Iapp) Amylin (Fig. S3d), a peptide previously found in pancreatic β -cells with a wide range of metabolic effects (Zhang et al., 2016). The LIM homeobox factor *Lmx1a* occurs in ECs, as suggested recently (Gross et al., 2016). The homeobox protein *Hhex* - not previously observed in the gut - was expressed by Sst -producing cells (Fig. S3d). Interestingly, *Hhex* has been described as an essential factor for Sst -producing δ cells in the pancreas (Zhang et al., 2014). The T-box transcription factor *Tbx3* was produced in BMP-activated EECs (Fig. S3d), and enriched in the villus (Kaaij et al., 2013). Finally, we found specific activation of classical BMP target genes in BMP-treated cells, such as *Id1*, *Id2* and *Id3*, confirming pathway activation (Fig. S3d) (Hollnagel et al., 1999).

Transcript dynamics might not be fully predictive for changes at the peptide hormone level. Therefore, we repeated the same experimental strategy as for scRNAseq and assessed co-expression of relevant peptide hormones in the *Tac1^{iresCre} / Rosa26^{tdTomato-}* and *Gcg^{Venus-}* reporter organoids. Over the course of 4 days, BMP-inhibited $tdTomato^+$ cells remained immunoreactive for Tac1 and Serotonin, while only rarely expressing Sct (Fig S4a). Strikingly, BMP-activated $tdTomato^+$ cells lost Tac1 immunoreactivity, maintained Serotonin and gained Sct positivity (Fig S4a). Glp1 positivity was strongly correlated with Venus expression in Gcg^{Venus} organoids in BMP-untreated conditions, while this correlation is lost in BMP-treated samples (Fig. S4a). Conversely, Venus positivity was increasingly predictive for Sct expression after BMP treatment (Fig. S4a). Pyy peptide positivity remained unchanged irrespective of BMP treatment (Fig S4a), in line with the constant peptide levels between crypt and villus *in vivo* (Grunddal et al., 2016).

We performed live-cell imaging of the *Tac1^{iresCre} / Rosa26^{tdTomato-}* and *Gcg^{Venus-}* reporter organoids in BMP-untreated and -treated conditions. $tdTomato^+$ cells that existed at the beginning of the BMP treatment continued to persist over the course of 60 hours, while losing Tac1 and gaining Sct expression (Fig. S4b). Untreated cells retained Tac1 positivity (Fig. S4b). In Gcg^{Venus} - reporter organoids, we observed a similar increase in Sct peptides (Fig. S4b).

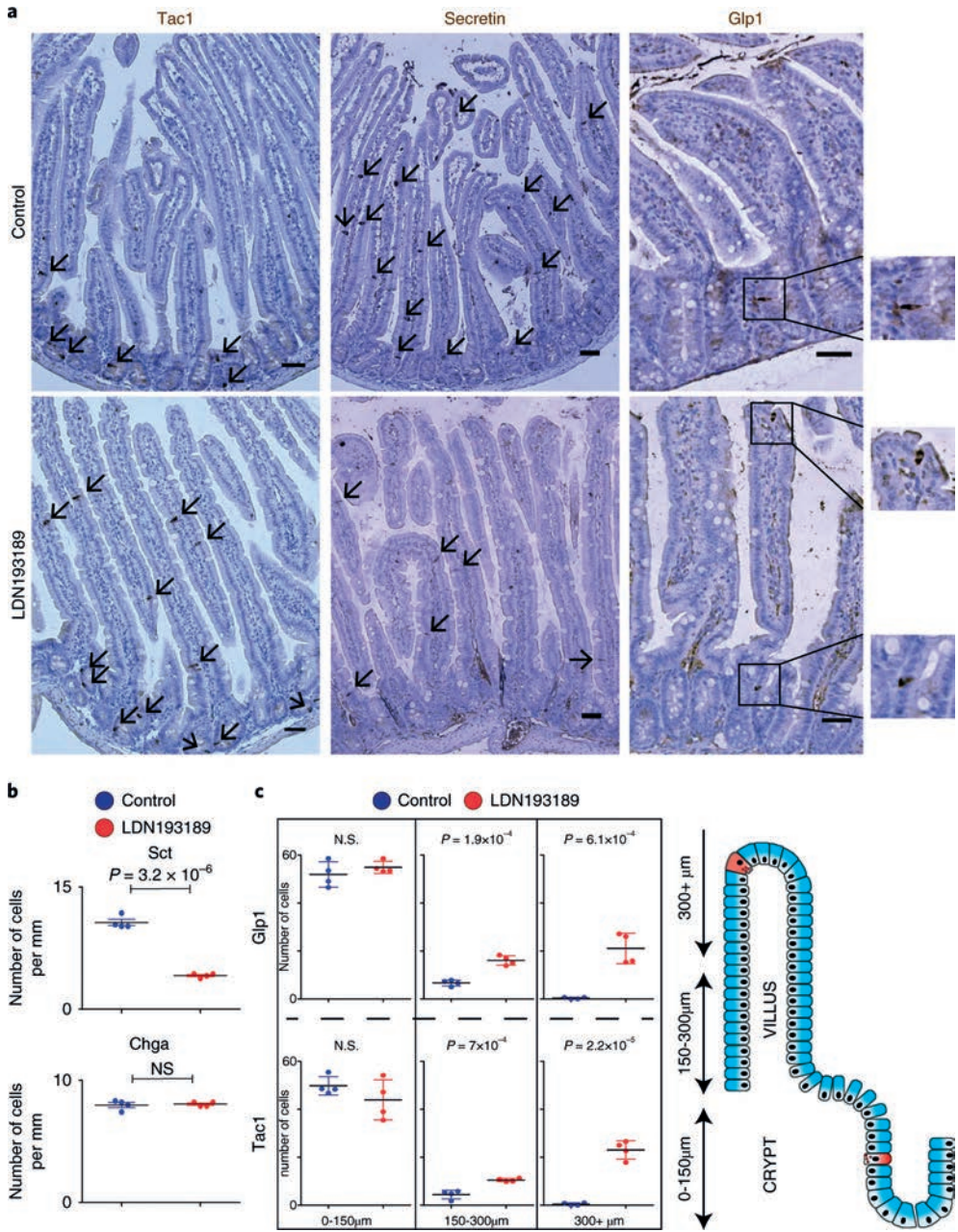


Figure 4. Manipulation of BMP gradient alters hormone expression in mice. **a**, Mice were treated for 80 hours with BMP α inhibitor LDN193189. Immunohistochemical analysis of the intestine shows a repression of Sct and induction of Glp1 and Tac1 expression upon BMP inhibition. Glp1 $^{+}$ and Tac1 $^{+}$ expressing cells are mostly restricted to the crypt in control mice, but expand into the upper villus region upon BMP inhibition. Representative image is shown from 2 separate stainings of 4 independent intestines. **b**, Quantification of **a**. Number of Chga $^{+}$ and Sct $^{+}$ positive cells per treatment. **c**, Quantification of **a**. Number of Tac1 $^{+}$ or Glp1 $^{+}$ cells are displayed for each segment of the crypt-villus axis in the different

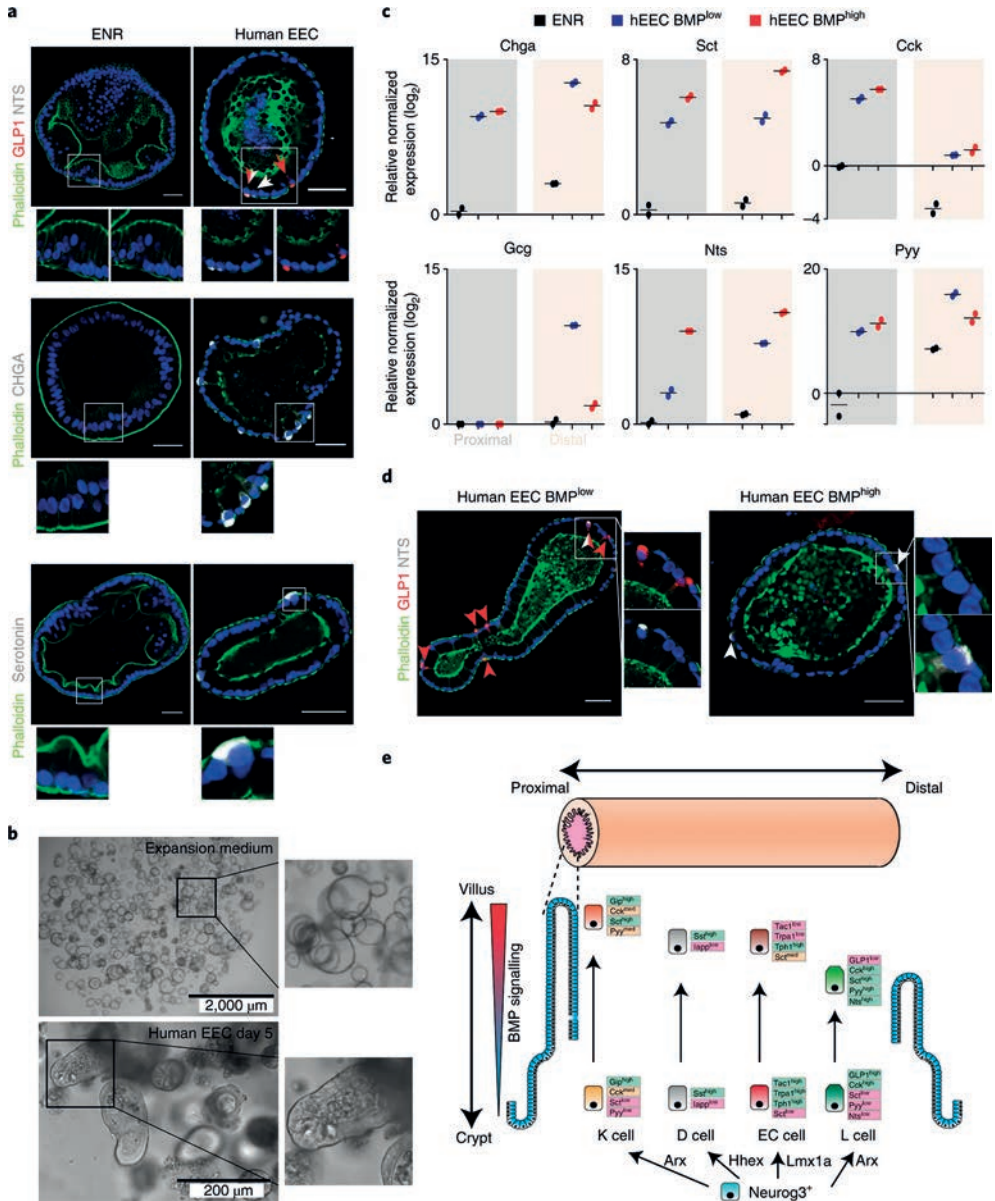
- ▶ treatments. Cells positive for Tac1 and Glp1 increase in the higher villus segments upon LDN193189 treatment. Tac1⁺ cells are counted and displayed in 10mm of the proximal small intestine. Glp1⁺ cells are counted and displayed in 30mm of the distal small intestine. Results presented are derived from n=4 mice per treatment, and statistics were calculated using a two-sided t-test. Mean values per staining and treatment are shown, and error bars present SD. Scale bar is 50 μ m.

Collectively, these data indicate that individual EECs can rewire their peptide hormone profile upon activation of BMP signalling.

The number of tdTomato⁺ and Venus⁺ EECs increased significantly over 4 days when BMP signalling was inhibited versus activated (Fig. S4a). We found that the first transcription factor expressed by and defining the EEC lineage, Neurogenin 3 (Jenny et al., 2002), was inhibited by BMP activation (Fig. S4c). To circumvent a bias that occurs at the bulk population level due to this inhibition of EEC specification, we first generated a large pool of ileal EECs using our differentiation protocol for 3 days. Next, we switched to BMP-high conditions for 24 hours (Fig. S4d). Increases in Sct, Pyy and Nts expression were more pronounced compared to a continuous BMP inhibition (Fig. 2 and Fig. S4c). These data imply that initial EEC specification requires BMP-low conditions, as exist at the bottom of the crypt.

To investigate whether villus-produced BMP controls hormone expression *in vivo*, we analyzed intestines from mice that ectopically express BMP inhibitor Noggin in the intestinal epithelium (Villin^{Noggin}) (Haramis et al., 2004). As expected, we observed an increased expression of Tac1 and Glp1 in the villi of these mice, while Sct was reduced (Fig S5a-d). We next tested the feasibility of influencing hormone expression by targeting the BMP gradient with the BMPRIa inhibitor LDN193189 (Whissell et al., 2014). An 80-hour oral treatment caused a reduction in Sct⁺ cell numbers. Overall histology of the intestine was unaffected, and the number of Chga⁺ EECs did not change significantly (Fig. 4a-b), consistent with a previous study (Qi et al., 2017). We quantified the numbers of Tac1⁺ and Glp1⁺ cells along different segments of the crypt-villus axis, assuming that BMP inhibition would not increase these in the BMP-low crypt. BMP inhibition did not cause significant changes in the lowest crypt-villus segment in the number of Tac1⁺ or Glp1⁺ EECs (Fig. 4a, 4c). However, the increase in cells immunoreactive for Tac1 or Glp1 was very pronounced higher up in the villus (Fig. 4a, 4c).

Finally, we pursued the establishment of a differentiation platform for induction of EECs in human intestinal organoids (Sato et al., 2011). Best results were obtained with dual inhibition of Notch and MEK signalling (Fig. 5a-b). This allowed us to generate all subtypes of EECs in organoids either derived from human duodenal or ileal tissue. ENR differentiated organoids did not contain EECs but mostly enterocytes, as evidenced by their extensive brush border (Fig. 5a). In our EEC differentiation protocol, BMP activation induced similar trended alterations in EEC hormone repertoires as it did in murine organoids (Fig. 5c). NTS and SCT transcripts increased upon BMP stimulation, whereas GCG transcripts were reduced (Fig. 5c). BMP activation had a neutral effect on total CHGA expression, and in contrast to the mouse, PYY was not increased upon BMP stimulation (Fig. 5c). Although cells positive for GLP1 and NTS peptides were observed in control conditions, we only observed NTS single positive cells in BMP-treated



I

II

III

IV

V

VI

VII

VIII

&

Figure 5. Human EEC differentiation protocol implies conserved BMP-controlled hormone expression. **a**, Human small intestinal organoids were induced to differentiate either for 5 days by withdrawing Wnt signals (ENR) or to EECs through additional MEK and Notch inhibition. Immunofluorescence indicates the presence of different subtypes of EECs in human organoids. White arrows indicate NTS⁺ cells, red arrows GLP1⁺ cells. Experiment has been repeated four times independently with similar results. **b**, Brightfield images of human intestinal organoids in expansion medium or after a 5 day differentiation towards EECs. Experiment was repeated independently four times. **c**, The 5-day differentiation protocol of EECs ('humanEEC') was performed in the presence and absence of BMP4. Expression levels of hormones were determined by qPCR and are shown relative to duodenal ENR control. Gcg expression is shown ▶

- ▶ relative to ileal ENR control, as it was not detected in duodenal organoids. Sample size represents $n=2$ biologically independent experiments, and the mean expression values are shown. **d**, Human EECs were produced in the absence (BMP_{low}) or presence (BMP_{high}) of BMP4. NTS overlaps with GLP1 in BMP low conditions, while only NTS single positive cells are observed in BMP_{high} conditions. Experiment was repeated independently four times. Scale bar is 50 μm . **e**, Model of EEC differentiation. K-cells are enriched in the proximal and L-cells in the distal part of the SI respectively, whereas ECs and D-cells are uniformly distributed. A crypt-to-villus BMP signalling gradient drives alterations in hormone repertoires in these EEC lineages.

conditions (Fig. 5d). This implies that BMP-control of the expressed EEC hormone repertoire is a generalizable phenomenon. In line with our observations in the murine organoid system (Basak et al., 2017), we found that human intestinal organoids maintained their regional identity in terms of representation of EEC subtypes. *GCG*, *NTS* and *PYY* were highly enriched in distal gut organoids, whereas *CCK* displayed a higher bias towards the duodenum (Fig. 5c).

Taken together, these data provide two main insights into EEC biology. First, the observations support that BMP controls hormone expression of EECs. EECs that are born in crypts from *Lgr5* stem cells encounter increasing levels of BMP signalling when migrating towards the villus tips (Clevers, 2013), and can change their hormone profile during this journey. Second, this insight in combination with the scRNAseq data proposes a simplification of EEC taxonomy (Fig. 5e). Previous high-resolution imaging and scRNAseq data suggested that almost every combination of EEC hormones can occur in individual EECs (Fothergill et al., 2017). Our current data indicate that there might be fewer unrelated differentiation pathways of EECs ('lineages') than previously anticipated and that some of the marker-hormones are not hard-wired. This implies that EECs uniquely dedicated to the production of Sct or Nts (the so called S- or N-cells) or Pyy do not exist, and that most EECs initiate expression of Sct when entering the BMP-high villus domain. Indeed, we observe that all BMP-activated EECs, except D-cells, upregulate Sct to different degrees, while L-cells (but not Sst- or Serotonin-producing cells) increase Pyy and Nts. Gip-expressing cells can be induced to express lower levels of Pyy, but not Nts. Importantly, we find that *Chga* is a marker of Serotonin-positive cells but not of other EECs, and using it as a generic marker would not allow for identifying EEC regulators such as the BMP pathway.

Pulse-chase labeling using BrdU has indicated that EECs do not necessarily follow the conveyor-belt migration pattern in which cells follow a constant flow from the bottom of the crypt to the tip of the villus (Aiken and Roth, 1992; Aiken et al., 1994). EECs can physically interact with enteric neurons through synapses, which potentially could alter cellular migration (Bellono et al., 2017; Bohorquez et al., 2015). Subpopulations of EECs can be retained in the crypt for 2 weeks while maintaining expression of *Tac1* or *Glp1*. Cells that migrate onto the villus are destined to lose *Tac1* or *Glp1* (Aiken and Roth, 1992; Aiken et al., 1994; Roth and Gordon, 1990). This ultimately suggests that controlling EEC migration along the crypt-villus axis and the Wnt/BMP gradients would be a way to influence hormone expression patterns.

METHODS

Mouse strains and experiments

Primary organoid cultures used in this culture were derived from Gcg^{Venus} , $Tac1^{iresCre}$ / $Rosa26^{tdTomato}$ and $Gip^{iresCre}$ / $Rosa26^{tdRfp}$ mice (Habib et al., 2012; Harris et al., 2014), and established as described before (Sato et al., 2009). All mice were bred on a C57BL/6 background. All animal procedures and experiments were performed in accordance with national animal welfare laws and were reviewed by the Animal Ethics Committee of the Royal Netherlands Academy of Arts and Sciences (KNAW). All mouse experiments were conducted under a project license granted by the Central Committee Animal Experimentation (CCD) of the Dutch government and approved by the Hubrecht Institute Animal Welfare Body (IvD), with project license number AVD8010020151. All rodents are housed in a barrier facility in conventional cages and are changed without using a change stations. All personnel entering the barrier must wear protective clothing (including head caps, special clogs). All animals are received directly from approved vendors (Charles River) or generated in house. Animals arriving from other sources must pass the GDL – quarantine for screening or by embryo-transfer. After screening these SPF mice are housed in micro isolator cages and are transferred to the Hubrecht laboratory.

For the BMPR inhibition experiment, LDN193189 (Selleckchem) was dissolved in citric buffer (pH3-3.1) at 2mg ml^{-1} . 12 week old mice ($n=4$) were given two oral doses of LDN193189 at 17.5 mg per kg bodyweight per day. Citric buffer was given to control mice. The total treatment was maintained for 80 hours.

Murine and human intestinal organoid culture

The basic culture medium (advanced Dulbecco's modified Eagle's medium/F12 supplemented with penicillin/streptomycin, 10 mM HEPES, Glutamax, B27 [Life Technologies, Carlsbad, CA] and 1 mM N-acetylcysteine [Sigma]) was supplemented with 50 ng/ml murine recombinant epidermal growth factor (EGF; Peprotech, Hamburg, Germany), R-spondin1 (conditioned medium, 5% final volume), and Noggin (conditioned medium, 5% final volume), called "ENR" medium. Conditioned media were produced using HEK293T cells stably transfected with HA-mouse Rspo1-Fc (gift from Calvin Kuo, Stanford University) or after transient transfection with mouse Noggin-Fc expression vector. Advanced Dulbecco's modified Eagle's medium/F12 supplemented with penicillin/streptomycin, and Glutamax was conditioned for 1 week.

Human duodenal and ileal tissues were obtained from the UMC Utrecht with informed consent of each patient. The study was approved by the UMC Utrecht (Utrecht, The Netherlands) ethical committee and was in accordance with the Declaration of Helsinki and according to Dutch law. This study is compliant with all relevant ethical regulations regarding research involving human participants. Patients were diagnosed with a small or large intestinal cancer and from the resected intestinal segments, a sample was taken from normal mucosa for this study. Human small intestinal cells were isolated, processed and cultured as described previously (Sato et al., 2011).

I

II

III

IV

V

VI

VII

VIII

&

Organoids were plated in BME (Trevigen). MEK signaling was inhibited using PD0325901 (1 μM for murine, 100nM for human organoids; Sigma Aldrich). Wnt secretion was inhibited with IWP-2 (5 μM ; Stemgent) and Notch with DAPT (10 μM , Sigma Aldrich). BMP signaling was activated by treating with human recombinant BMP4 (20ng/ml, Peprotech) and withdrawal of Noggin from the culture medium. Hedgehog signaling was inhibited with Vismodegib (10 μM , Selleckchem). TGF beta signaling was activated using recombinant mouse TGF beta-1 (3ng ml⁻¹, R&DSystems, MAB7666TGF beta-1. TGF beta type1 receptor signaling was inhibited using A83 (500nM, Tocris). All control organoids were treated with similar concentrations of the compound dissolvent, dimethyl sulfoxide (DMSO) or 0.1%BSA in PBS0. During treatments, cells were imaged using an EVOS microscope (Electron Microscopy Sciences).

For the induction of enteroendocrine differentiation in murine organoids, cells were cultured in standard culture conditions (ENR). 4-7 days after plating in BME, medium was removed and organoids were treated with different regimes. The cocktail for mouse EEC differentiation included: IWP2 (5 μM ; Stemgent), DAPT (10 μM , Sigma Aldrich) and MEK inhibitor PD0325901 (1 μM ; Sigma Aldrich), while BMP4 (20ng/ml, Peprotech) was added for activation of BMP signaling. In human organoids, differentiation was achieved by withdrawing p38 MAPK inhibitor SB202190, TGFbeta inhibitor A83, Nicotinamide and Wnt conditioned medium from the culture medium as described previously(Sato et al., 2011). Differentiation into EECs was performed by on top treating with DAPT (10 μM , Sigma Aldrich) and MEK inhibitor PD0325901 (500nM; Sigma Aldrich), BMP4 (20ng/ml, Peprotech) was added for activation of BMP signaling. A step-by-step protocol for human EEC differentiation can be found at Nature Protocol Exchange ³⁶.

Immunostainings

Whole organoids were collected by gently dissolving the BME in ice-cold medium, and subsequently fixed at RT in 4% formalin (Sigma) for at least 6 hours. Next, organoids were permeabilized and blocked in PBS containing 0,5% Triton X-100 (Sigma) and 2% normal donkey serum (Jackson ImmunoResearch) for 30 min at room temperature. Organoids were incubated for 2 hr at room temperature in blocking buffer containing primary antibodies. Primary antibodies used were goat anti-Chromogranin A (1:500; Santa Cruz), goat anti-Cholestocystokin (sc-21617,1:100; Santa Cruz), rabbit anti-Neurotensin (sc-20806,1:100; Santa Cruz), goat anti-Secretin (sc-26630,1:100; Santa Cruz), goat anti-Somatostatin (sc-7819, 1:100; Santa Cruz), goat anti-Serotonin (ab66047, 1:1000, Abcam), rabbit anti-Gastric inhibitory polypeptide (ab22624-50, 1:500;Abcam), goat anti-GLP1 (sc-7782, 1:100; Santa Cruz), rabbit anti-GLP1 (ab22625, 1:200; Abcam), rabbit anti-Peptide YY (ab22663, 1:500; Abcam) and guinea pig anti-Substance P (1:200, ab10353; Abcam). Organoids were incubated with the corresponding secondary antibodies Alexa488, 568 and 647 conjugated anti-rabbit and anti-goat (1:1000; Molecular Probes) in blocking buffer containing DAPI (1:1000, Invitrogen). Sections were embedded in Vectashield (Vector Labs) and imaged using a Sp8 confocal microscope (Leica). Image analysis was performed using ImageJ software.

For immunohistochemistry of organoids within the BME (Figure S4), medium was removed from the wells and replaced with 4% formalin for 1 hour. Next, organoids were washed with PBS, permeabilized and blocked in PBS containing 0,5% Triton X-100 (Sigma) and 2% normal donkey serum (Jackson ImmunoResearch) for 30 min at room temperature. The wells were incubated for 2 hr at room temperature in blocking buffer containing primary antibodies. After washing, secondary antibodies were added for 1 hr at room temperature in blocking buffer. Organoids were subsequently imaged within the plate using a Sp8 confocal microscope (Leica).

For immunohistochemistry of mouse intestinal tissue, intestines were first flushed with 4% formaldehyde. Next, intestines were fixed for 6 hours at RT in 4% formalin. The tissue was either embedded in paraffin or Tissue-Tek O.C.T. for cryosectioning, and stained as described previously(Farin et al., 2016; Sato et al., 2009).

Quantification of number/location of EECs on intestinal section images were performed in ImageJ software, as well as the intensity of Venus levels in the live cell imaging experiment in Figure S2e-f. Analysis of Glp1⁺ cell numbers and/or position in Figure 1a-c, Figure 4a-c and Figure S5 were performed in the ileum, and all other hormones were counted along the whole SI tract.

All quantifications were performed on the raw, unprocessed images.

RNA isolation and quantitative PCR

For qPCR analysis and bulk RNA sequencing, RNA was isolated from organoids using the RNAeasy kit (QIAGEN) as instructed in the manufacturer's protocol. PCR analysis was performed using the SYBR-Green and Bio-Rad systems as described(Muñoz et al., 2012). PCR reactions were performed in duplicate with a standard curve for every primer. Changes in expression were calculated using CFX manager software (Bio-Rad). Primers were designed using the NCBI primer design tool. Primers used in this study are presented in Supplementary Table 1.

Glp1 and Secretin secreted peptide

The supernatant from organoids was collected after 2-hour stimulation with Forskolin. GLP-1 concentration in the supernatant was measured with a GLP-1 EIA Kit (Rab0201, Sigma, detects both full length and N-terminal cleaved GLP-1) using the manufacturer's protocol. Secretin concentration was measured with a Secretin EIA kit (EK-067-04, Phoenix Pharmaceuticals) using the manufacturer's protocol.

Bulk and single cell RNA sequencing

For bulk RNA sequencing analysis, organoids stimulated with EEC BMP^{high} or EEC BMP^{low} media for 4 days were collected and dissociated in RTL buffer (RNeasy Mini kit, Quiagen). Total RNA was isolated accordingly to manufacturer's instruction (RNeasy Mini kit, Quiagen). Sequencing libraries were prepared based on a modified CELseq2 method(Hashimshony et al., 2016). Briefly, 1 ng of RNA was reverse transcribed using the Ambion kit and in vitro

I

II

III

IV

V

VI

VII

VIII

&

transcription was performed using 1 ng of cDNA as template. The aRNA was then used to prepare sequencing libraries. Samples were sequenced with sequenced paired-end at 75 bp read-length the on Illumina NextSeq.

For single cell RNA sequencing, organoids were first dissociated into single cells through mechanical disruption, after 15 min of Trypsin treatment at 37°C (TrypLE Express; Life Technologies). Next, cells were immediately sorted using a BD FACS Aria (BD Biosciences). For single cell sequencing experiment, cells were sorted as single cells into 384-well plates containing ERCC spike-ins (Agilent), RT primers and dNTP (Promega) as described before. Plates were prepared using Mosquito® HTS (TTPlabtech). Single cell RNA-sequencing libraries were prepared following the SORT-seq protocol (Muraro et al., 2016), which is based on CEL-seq2 method (Hashimshony et al., 2016). Briefly, cells were first lysed 5 min at 65°C, and RT and second strand mixes were dispensed by the Nanodrop II liquid handling platform (GC biotech). Single cell double stranded cDNAs were pooled together and in vitro transcribed for linear amplification. Illumina sequencing libraries were prepared using the TruSeq small RNA primers (Illumina) and sequenced paired-end at 75 bp read length the Illumina NextSeq.

RNA-sequencing data analysis

Paired-end reads from Illumina sequencing were aligned to the mouse transcriptome genome by BWA (Li and Durbin, 2009). For RNA-seq bulk data, normalization and differential gene expression analyses were performed using the DESeq2 package (Love et al., 2014) and visualized as volcano plots. For single cell RNA-seq data, read counts were first corrected for UMI barcode by removing duplicate reads that had identical combinations of library, cell-specific, and molecular barcodes and were mapped to the same gene. For each cell barcode the number of UMIs for every transcript was counted, and transcript counts were then adjusted to the expected number of molecules based on counts, 256 possible UMI's and poissonian counting statistics (Grün et al., 2014). Samples were then normalized by downsampling to a minimum number of 3000 transcripts/cell. Cells with fewer transcripts were excluded from the analyses. RaceID2 was used to cluster cells based on k-medoid method (Grün et al., 2016). All data analyses, quantification and data visualization were run on Rstudio. In total, we sequenced 2880 cells and, after applying a filtering criteria of 3000 expressed transcripts/cell, 820 cells were retained for further analysis.

Statistics and Reproducibility

Two sided t-tests were performed for all statistical analyses. Precise p-values are mentioned in the corresponding figures, and significance level was set at $p < 0.05$. In each figure legend, the number of biology replicates is mentioned for the corresponding experiment ($n=x$). For figures where representative images are shown, the number the experiment has been repeated is mentioned in the legend.

For immunohistochemistry, we counted the following number of cells, of organoids or length of intestine; at least 50 cells per hormone and replicate intestine (Fig. 1b-e, $n=4$ mice),

at least 150 tdTomato⁺ cells per co-staining and replicate intestine (Fig. 1f-g, n=4 mice), at least 3 organoids per hormone and replicate (Fig. 2a-b, n=2 biologically independent experiments), 10 organoids per hormone and replicate (Fig. S4a, n=2 biologically independent experiments), 10mm of the proximal small intestine for Tac1 (Fig. 4b-c, n=4 mice per treatment), 30mm of the distal small intestine for Glp1 (Fig. 4b-c, n=4 mice per treatment). mice per genotype) and at least 50 cells per hormone and replicate intestine (Fig. S5b, n=2 mice per genotype),

Data availability

Bulk and single-cell RNA-seq data that support the findings of this study have been deposited in the Gene Expression Omnibus (GEO) under accession code GSE114988.

Source data for Fig. 1c, 1e, 1g, 2b, 2e, 4a, 5b, 5c, 6b and Supplementary Fig. 1a, 2a, 2b, 2d, 3b, 4b, 4c, 5a, 5b and 6 have been provided as Supplementary Table 2. All other data supporting the findings of this study are available from the corresponding author on reasonable request.

ACKNOWLEDGEMENTS

We thank Stefan van der Elst, Reinier van der Linden and Yotam Bar-Ephraim, for their help with FACS experiments. B.A. is supported by NWO/VENI 863.15.015.

COMPETING FINANCIAL INTERESTS

The authors disclose no conflicts of interest.

AUTHOR CONTRIBUTIONS

J.B. and H.C. conceived and designed the project. J.B. designed and performed all experiments. B.A. performed analysis of RNA sequencing data. F.R. and F.G. generated the Gcg and Gip reporter mice. H.Z. generated the Tac1 reporter mouse, and T.N.N. assisted in providing the tissue. J.H.v.E supervised and performed the mouse experiments, with the help of M.v.d.B. Y.P. assisted in histology preparation. J.B., B.A. and H.C. wrote the manuscript with input from all other authors.

I
 II
 III
 IV
 V
 VI
 VII
 VIII
 &

REFERENCES

- Aiken, K.D., and Roth, K.A. (1992). Temporal differentiation and migration of substance P, serotonin, and secretin immunoreactive enteroendocrine cells in the mouse proximal small intestine. *Dev. Dyn.* 194, 303–310.
- Aiken, K.D., Kisslinger, J.A., and Roth, K.A. (1994). Immunohistochemical studies indicate multiple enteroendocrine cell differentiation pathways in the mouse proximal small intestine. *Dev. Dyn.* 201, 63–70.
- Barker, N., van Es, J.H., Kuipers, J., Kujala, P., van den Born, M., Cozijnsen, M., Haegebarth, A., Korving, J., Begthel, H., Peters, P.J., et al. (2007). Identification of stem cells in small intestine and colon by marker gene *Lgr5*. *Nature* 449, 1003–1007.
- Basak, O., Beumer, J., Wiebrands, K., Seno, H., van Oudenaarden, A., and Clevers, H. (2017). Induced Quiescence of *Lgr5+* Stem Cells in Intestinal Organoids Enables Differentiation of Hormone-Producing Enteroendocrine Cells. *Cell Stem Cell* 20, 177–190.e4.
- Bellono, N.W., Bayrer, J.R., Leitch, D.B., Castro, J., Zhang, C., O'Donnell, T.A., Brierley, S.M., Ingraham, H.A., and Julius, D. (2017). Enterochromaffin Cells Are Gut Chemosensors that Couple to Sensory Neural Pathways. *Cell* 170, 185–198.e16.
- Beumer, J., and Clevers, H. (2016). Regulation and plasticity of intestinal stem cells during homeostasis and regeneration. *Development* 143, 3639–3649.
- Bohorquez, D. V, Shahid, R.A., Erdmann, A., Kreger, A.M., Wang, Y., Calakos, N., Wang, F., and Liddle, R.A. (2015). Neuroepithelial circuit formed by innervation of sensory enteroendocrine cells. *J Clin Invest* 125, 782–786.
- Camacho, S., Michlig, S., de Senarclens-Bezençon, C., Meylan, J., Meystre, J., Pezzoli, M., Markram, H., and le Coutre, J. (2015). Anti-obesity and anti-hyperglycemic effects of cinnamaldehyde via altered ghrelin secretion and functional impact on food intake and gastric emptying. *Sci. Rep.* 5, 7919.
- Clevers, H. (2013). The intestinal crypt, a prototype stem cell compartment. *Cell* 154, 274–284.
- Connor, T.M.O., Connell, J.O., Brien, D.I.O., Goode, T., Bredin, C.P., and Shanahan, F. The Role of Substance P in Inflammatory Disease.
- Egerod, K.L., Engelstoft, M.S., Grunddal, K. V., Nøhr, M.K., Secher, A., Sakata, I., Pedersen, J., Windeløv, J.A., Füchtbauer, E.M., Olsen, J., et al. (2012). A major lineage of enteroendocrine cells coexpress CCK, secretin, GIP, GLP-1, PYY, and neurotensin but not somatostatin. *Endocrinology* 153, 5782–5795.
- Farin, H.F., Jordens, I., Mosa, M.H., Basak, O., Korving, J., Tauriello, D.V.F., de Punder, K., Angers, S., Peters, P.J., Maurice, M.M., et al. (2016). Visualization of a short-range Wnt gradient in the intestinal stem-cell niche. *Nature* 530, 340–343.
- Fothergill, L.J., Callaghan, B., Hunne, B., Bravo, D.M., and Furness, J.B. (2017). Costorage of enteroendocrine hormones evaluated at the cell and subcellular levels in male mice. *Endocrinology* 158, 2113–2123.
- Furness, J.B., Rivera, L.R., Cho, H.-J., Bravo, D.M., and Callaghan, B. (2013). The gut as a sensory organ. *Nat. Rev. Gastroenterol. Hepatol.* 1010, 729–740.
- Gross, S., Garofalo, D.C., Balderes, D.A., Mastracci, T.L., Dias, J.M., Perlmann, T., Ericson, J., and Sussel, L. (2016). The novel enterochromaffin marker *Lmx1a* regulates serotonin biosynthesis in enteroendocrine cell lineages downstream of *Nkx2.2*. *Development* 143, 2616–2628.
- Grün, D., Kester, L., and van Oudenaarden, A. (2014). Validation of noise models for single-cell transcriptomics. *Nat. Methods* 11, 637–640.

- Grün, D., Lyubimova, A., Kester, L., Wiebrands, K., Basak, O., Sasaki, N., Clevers, H., and van Oudenaarden, A. (2015). Single-cell messenger RNA sequencing reveals rare intestinal cell types. *Nature* 525, 251–255.
- Grün, D., Muraro, M.J., Boisset, J.C., Wiebrands, K., Lyubimova, A., Dharmadhikari, G., van den Born, M., van Es, J., Jansen, E., Clevers, H., et al. (2016). De Novo Prediction of Stem Cell Identity using Single-Cell Transcriptome Data. *Cell Stem Cell* 19, 266–277.
- Grunddal, K. V., Ratner, C.F., Svendsen, B., Sommer, F., Engelstoft, M.S., Madsen, A.N., Pedersen, J., Nøhr, M.K., Egerod, K.L., Nawrocki, A.R., et al. (2016). Neurotensin is coexpressed, coreleased, and acts together with GLP-1 and PYY in enteroendocrine control of metabolism. *Endocrinology* 157, 176–194.
- Haber, A.L., Biton, M., Rogel, N., Herbst, R.H., Shekhar, K., Smillie, C., Burgin, G., Delorey, T.M., Howitt, M.R., Katz, Y., et al. (2017). A single-cell survey of the small intestinal epithelium. *Nature* 551, 333–339.
- Habib, A.M., Richards, P., Cairns, L.S., Rogers, G.J., Bannon, C.A.M., Parker, H.E., Morley, T.C.E., Yeo, G.S.H., Reimann, F., and Gribble, F.M. (2012). Overlap of endocrine hormone expression in the mouse intestine revealed by transcriptional profiling and flow cytometry. *Endocrinology* 153, 3054–3065.
- Haramis, A.P.G., Begthel, H., Van Den Born, M., Van Es, J., Jonkheer, S., Offerhaus, G.J.A., and Clevers, H. (2004). De Novo Crypt Formation and Juvenile Polyposis on BMP Inhibition in Mouse Intestine. *Science* (80-.). 303, 1684–1686.
- Harris, J.A., Hirokawa, K.E., Sorensen, S.A., Gu, H., Mills, M., Ng, L.L., Bohn, P., Mortrud, M., Ouellette, B., Kidney, J., et al. (2014). Anatomical characterization of Cre driver mice for neural circuit mapping and manipulation. *Front. Neural Circuits* 8.
- Hashimshony, T., Senderovich, N., Avital, G., Klochender, A., de Leeuw, Y., Anavy, L., Gennert, D., Li, S., Livak, K.J., Rozenblatt-Rosen, O., et al. (2016). CEL-Seq2: sensitive highly-multiplexed single-cell RNA-Seq. *Genome Biol.* 17, 77.
- Hollnagel, A., Oehlmann, V., Heymer, J., Rütter, U., and Nordheim, A. (1999). Id genes are direct targets of bone morphogenetic protein induction in embryonic stem cells. *J. Biol. Chem.* 274, 19838–19845.
- Jenny, M., Uhl, C., Roche, C., Duluc, I., Guillermin, V., Guillemot, F., Jensen, J., Kedinger, M., and Gradwohl, G. (2002). Neurogenin3 is differentially required for endocrine cell fate specification in the intestinal and gastric epithelium. *EMBO J.* 21, 6338–6347.
- Kaaij, L.T., van de Wetering, M., Fang, F., Decato, B., Molaro, A., van de Werken, H.J., van Es, J.H., Schuijers, J., de Wit, E., de Laat, W., et al. (2013). DNA methylation dynamics during intestinal stem cell differentiation reveals enhancers driving gene expression in the villus. *Genome Biol.* 14, R50.
- Li, H., and Durbin, R. (2009). Fast and accurate short read alignment with Burrows-Wheeler transform. *Bioinformatics* 25, 1754–1760.
- Love, M.I., Huber, W., and Anders, S. (2014). Moderated estimation of fold change and dispersion for RNA-seq data with DESeq2. *Genome Biol.* 15, 550.
- Muñoz, J., Stange, D.E., Schepers, A.G., van de Wetering, M., Koo, B.-K., Itzkovitz, S., Volckmann, R., Kung, K.S., Koster, J., Radulescu, S., et al. (2012). The Lgr5 intestinal stem cell signature: robust expression of proposed quiescent “+4” cell markers. *EMBO J.* 31, 3079–3091.
- Muraro, M.J., Dharmadhikari, G., Grün, D., Groen, N., Dielen, T., Jansen, E., van Gorp, L., Engelse, M.A., Carlotti, F., de Koning, E.J.P., et al. (2016). A Single-Cell Transcriptome Atlas of the Human Pancreas. *Cell Syst.* 3, 385–394.

I

II

III

IV

V

VI

VII

VIII

&

Nozawa, K., Kawabata-shoda, E., Doihara, H., Kojima, R., Okada, H., Mochizuki, S., Sano, Y., Inamura, K., Matsushime, H., Koizumi, T., et al. (2009). TRPA1 regulates gastrointestinal motility through serotonin release from enterochromaffin cells. *Proc. Natl. Acad. Sci. U. S. A.* 106, 13.

Qi, Z., Li, Y., Zhao, B., Xu, C., Liu, Y., Li, H., Zhang, B., Wang, X., Yang, X., Xie, W., et al. (2017). BMP restricts stemness of intestinal Lgr5+ stem cells by directly suppressing their signature genes. *Nat. Commun.* 8, 13824.

Roth, K. a, and Gordon, J.I. (1990). Spatial differentiation of the intestinal epithelium: analysis of enteroendocrine cells containing immunoreactive serotonin, secretin, and substance P in normal and transgenic mice. *Proc. Natl. Acad. Sci. U. S. A.* 87, 6408–6412.

Sato, T., Vries, R.G., Snippert, H.J., van de Wetering, M., Barker, N., Stange, D.E., van Es, J.H., Abo, A., Kujala, P., Peters, P.J., et al. (2009). Single Lgr5 stem cells build crypt-villus structures in vitro without a mesenchymal niche. *Nature* 459, 262–265.

Sato, T., Stange, D.E., Ferrante, M., Vries, R.G.J., Van Es, J.H., Van Den Brink, S., Van Houdt, W.J., Pronk, A., Van Gorp, J., Siersema, P.D., et al. (2011). Long-term expansion of epithelial organoids from human colon, adenoma, adenocarcinoma, and Barrett's epithelium. *Gastroenterology* 141, 1762–1772.

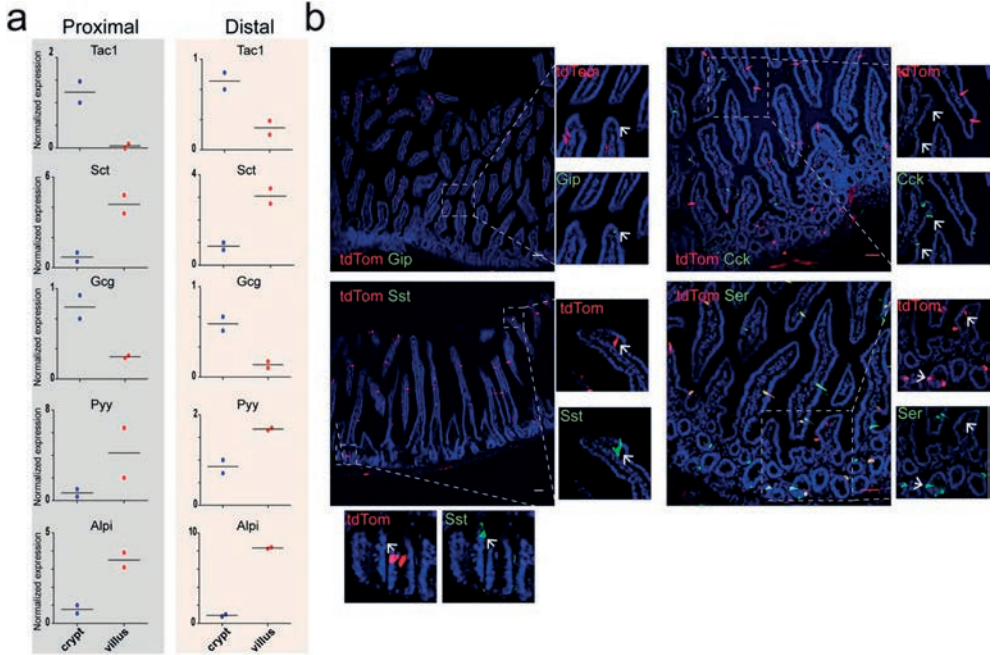
Svendsen, B., Pais, R., Engelstoft, M.S., Milev, N.B., Richards, P., Christiansen, C.B., Egerod, K.L., Jensen, S.M., Habib, A.M., Gribble, F.M., et al. (2016). GLP1- and GIP-producing cells rarely overlap and differ by bombesin receptor-2 expression and responsiveness. *J. Endocrinol.* 228, 39–48.

Whissell, G., Montagni, E., Martinelli, P., Hernando-Momblona, X., Sevillano, M., Jung, P., Cortina, C., Calon, A., Abuli, A., Castells, A., et al. (2014). The transcription factor GATA6 enables self-renewal of colon adenoma stem cells by repressing BMP gene expression. *Nat. Cell Biol.* 16, 695–707.

Zhang, J., McKenna, L.B., Bogue, C.W., and Kaestner, K.H. (2014). The diabetes gene Hhex maintains ??-cell differentiation and islet function. *Genes Dev.* 28, 829–834.

Zhang, X.-X., Pan, Y.-H., Huang, Y.-M., and Zhao, H.-L. (2016). Neuroendocrine hormone amylin in diabetes. *World J. Diabetes.*

SUPPLEMENTARY FIGURES



Supplementary Figure 1. Crypt-to-villus heterogeneity and lineage relationship of enteroendocrine cells. **a**, RNA was isolated from crypts and villi of the proximal and distal SI. qPCR analysis was performed on selected hormones. Tac1 and Gcg transcripts are enriched in the crypts of mice, while Pyy and Sct are increased in the villus. Alpi, a marker of enterocytes, confirmed enrichment of villus fractions. Sample size represents n=2 mice, and the mean values are shown. **b**, Intestine of Tac1^{iresCre} / Rosa^{Aii4} mice reveals that Tac1⁺ expressing cells give rise to Serotonin (Ser) expressing cells and are thus part of the Enterochromaffin lineage. Gip, Sst and Cck expressing EECs are rarely derived from Tac1, while the vast majority of Serotonin producing ECs are derived from Tac1. Quantification in Figure 1g (n=4 mice). Scale bar is 50 μm.

I

II

III

IV

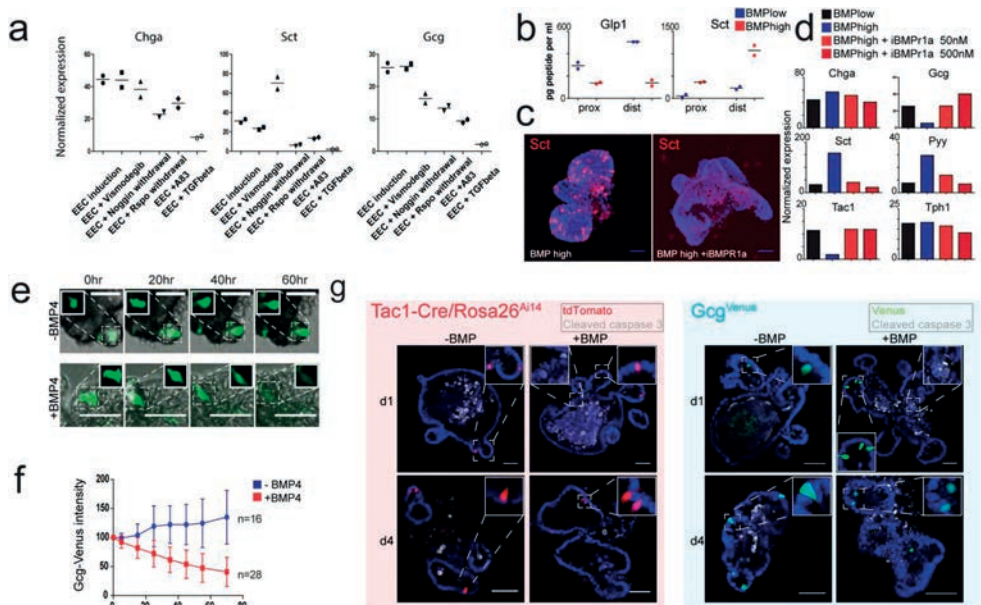
V

VI

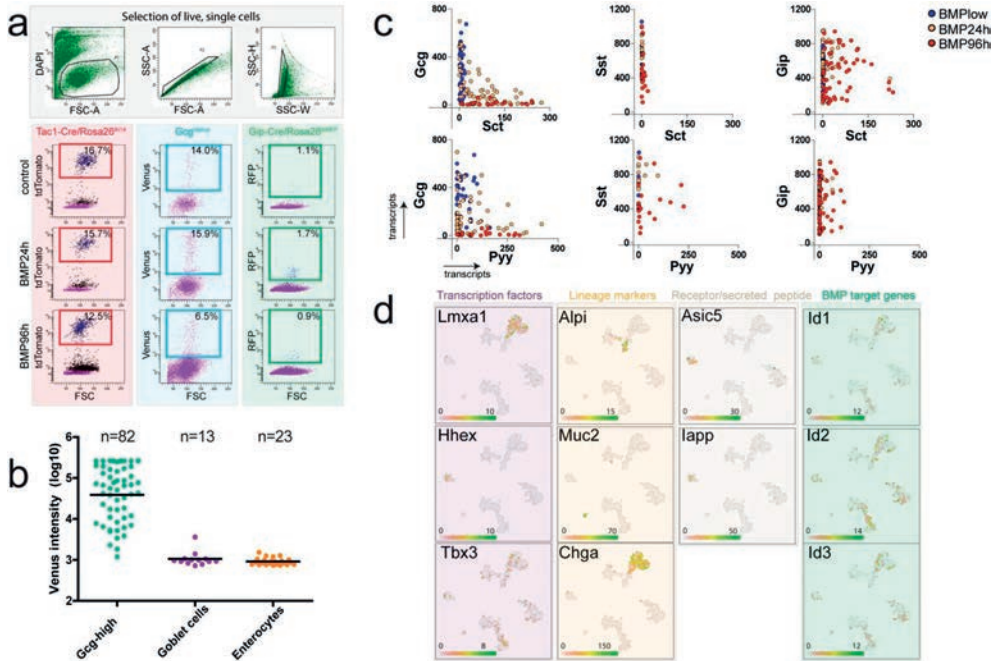
VII

VIII

&

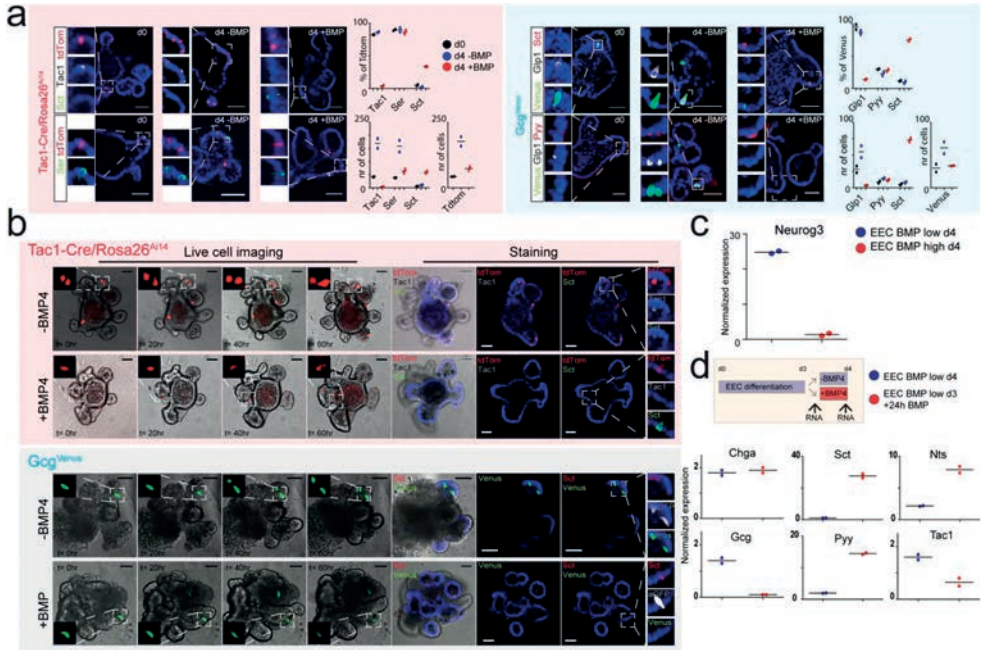


Supplementary Figure 2. Signaling through the BMP4-BMPR1a/BMPR2 axis induces hormone switching in EECs without causing apoptosis. **a**, Organoids were differentiated into enteroendocrine cells (EECs) for 4 days by the inhibition of Wnt, Notch and MEK signaling. On the background of the EEC differentiation cocktail, we inhibited Hedgehog (Vismodegib), activated BMP (Noggin withdrawal), inhibited Wnt (Rspo withdrawal), inhibited TGFbeta (A83) or activated TGFbeta (TGFβ1) signaling. qPCR analysis of selected hormones shows that activation of BMP signaling selectively induces *Sct* but represses *Gcg* expression, while having a neutral effect on *Chga*. Results are shown relative to control organoids in ENR medium. Sample size represents n=2 biologically independent experiments, and the mean values are shown. **b**, Secreted *Glp1* and *Sct* peptides after stimulation with forskolin were measured by ELISA in EEC differentiation medium with or without BMP4. Secreted *Glp1* was diminished in the background of BMP activation, while *Sct* increased. Experiment was performed in proximal and distal organoids. Sample size represents n=2 biologically independent experiments, and the mean values are shown. **c**, Addition of BMPR1a inhibitor LDN193189 to a 4-day EEC differentiation protocol containing BMP4 reverses the increase in *Sct* production, as shown by immunostaining. Image is presented as a maximum projection. Experiment was performed three times independently with similar results. Scale bar is 50 μm. **d**, qPCR analysis of selected hormones of the same experiment as in **c**. BMPR1a inhibition reverses all changes induced by BMP4 addition to the standard EEC differentiation cocktail (EEC BMP4). Sample size represents n=1 biologically independent experiment, and the average value of a technical duplicate is shown. **e**, Organoids derived from *Gcg^{Venus}* mice were imaged for 3 days in the presence and absence of BMP4. Individual L-cells shut down *Gcg* transcription when stimulated with BMP4, while control cells maintain *Gcg* positivity throughout the imaging timewindow. Imaging started 6 hours after addition of BMP4. **f**, Quantification of **e**. The number of Venus⁺ cells imaged and measured is depicted. The mean intensity of all cells at each timepoint is shown, and error bars present SD. SD was derived from n=16 cells in -BMP4 treatment and n=28 cells in +BMP4 treatment. **g**, Organoids from *Gcg^{Venus}* and *Tac1^{iresCre}/Rosa^{Ai14}* mice were differentiated to EECs in the absence or presence of BMP, and co-stained for cleaved caspase-3 to assess apoptosis. Experiment has been repeated two times with similar results. Scale bar is 50 μm.

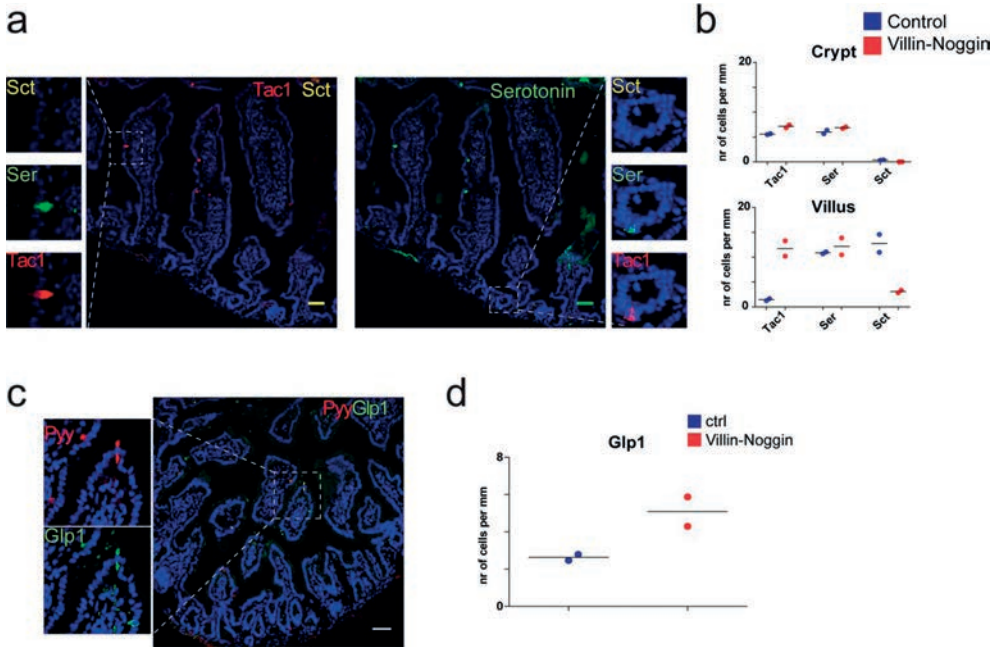


I
II
III
IV
V
VI
VII
VIII
&

Supplementary Figure 3. Single cell transcriptome analyses of EEC subtypes after BMP activation. **a**, FACS plots display the gating strategy used to sort live, single cell (DAPI-negative, right plots) subtypes of EECs from reporter organoids (left plots) in different BMP activation contexts. **b**, Venus intensity levels of Goblet cells (*Muc2⁺*), Enterocytes (*Alpi⁺*) and Gcg-high cells. Mean intensity is shown for each group, together with the number of cells in each group (n=82 Gcg-high cells, n=13 Goblet cells and n=23 enterocytes). **c**, Cells with a Venus intensity of more than 2.5×10^4 , predictive for Gcg expression (Fig. S4a, S4b), were selected from the dataset. Transcripts for Gcg, Sct and Pyy are plotted (upper plots). High Venus positivity is predictive for Gcg expression in BMP1low conditions, but not after BMP treatment. Cells with at least 100 Sst (middle plots) or Gip (lower plots) were selected from the dataset. Gip⁺ and Sst⁺ cells upregulate Pyy expression upon BMP treatment, while only cells producing Gip can co-express Sct. **d**, Expression levels of selected markers in the t-SNE space. Different transcription factors, receptors and secreted peptides were uniquely expressed by subtypes of EECs. BMP target genes associate with BMP4 treated samples.



Supplementary Figure 4. BMP signaling induces switches in peptide profile of individual EECs and blocks initial EEC specification. **a**, *Tac1^{iresCre}/Rosa^{Aii4}* and *Gcg^{Venus}* – reporter organoids were treated with a MEK inhibitor, while receiving Noggin (-BMP) or BMP4 (+BMP). The numbers of each marker positive cells are presented (in 10 organoids), and the co-localization of these hormones with tdTomato or Venus was quantified. Sample size represents n=2 biologically independent experiments, and the mean values are shown. BMP activation dampens the generation of new EECs and induces switches in the peptide profile of individual EECs. **b**, Individual EECs in *Tac1^{iresCre}/Rosa^{Aii4}* and *Gcg^{Venus}* – reporter organoids were followed using live cell imaging in the absence and presence of BMP signals. After 60 hours, organoids were fixed inside the BME and stained for different hormones, as indicated. The experiment was performed two times independently with similar results. **c**, Mouse intestinal organoids were EEC differentiated for 4 days in BMP low or high conditions. qPCR analysis reveals *Neurog3* is downregulated after BMP treatment (data is shown relative to BMP untreated sample). Sample size represents n=2 biologically independent experiments, and the mean expression values are shown. **d**, Mouse intestinal organoids were EEC differentiated for 4 days in BMP low conditions, or for 3 days in BMP low and 24 hours in BMP high conditions. qPCR analysis of selected hormones (data is shown relative to day 3 EEC differentiation). Initial EEC generation in BMP low conditions and subsequent induction of BMP signaling for 24 hours is most efficient in generating Villus-enriched hormones. Sample size represents n=2 biologically independent experiments, and the mean expression values are shown.



Supplementary Figure 5. A transgenic mouse model with a disrupted BMP gradient displays altered hormone expression. a, Immunostaining of intestines from Villin^{Noggin} mice. Tac1⁺ cells were scattered along the whole crypt-villus axis, while Sct⁺ cell numbers greatly reduced. Experiment has been repeated twice with a sample size of 2 mice per genotype. b, Quantification of a. Sample size represents n=2 mice per genotype. Mean values are depicted. c, Villin^{Noggin} mice show an increased number of Glp1⁺ L-cells in the villus. d, Quantification of c. Sample size represents n=2 mice per genotype. Mean values are depicted. Scale bar is 50 μ m.

- I
- II
- III
- IV
- V
- VI
- VII
- VIII
- &

CHAPTER
**SPECIALIZATION OF HUMAN GOBLET
CELLS AND ENTEROCYTES ALONG
THE CRYPT-VILLUS AXIS**

V

SUMMARY

The intestinal crypt is classically regarded as the site of proliferation containing few mature cells, while the villus is the functional unit where cells reach their most mature state. The hormone-producing enteroendocrine cells are an exception to this rule and undergo a BMP-regulated specialization that involves hormone switches from crypt to villus. Using human intestinal organoids, we show that expression of nutrient uptake related and ribosomal genes in enterocytes are BMP regulated. Exploiting MUC2-reporter organoids, we demonstrate a previously unrecognized heterogeneity of goblet cells along the crypt-villus axis. Lipid uptake, chylomicron production and antimicrobial compound production change accordingly in organoids. Inhibition of BMP signaling in mice blocks some zoned expression programs. These findings extend BMP regulated specialization in the human intestine to goblet cells and enterocytes.

Joep Beumer^{1,2,4}, Jens Puschhof^{1,2,4}, Fjodor Youseff Yengej^{1,2}, Adriana Martinez Silgado^{1,2}, Harry Begthel^{1,2} and Hans Clevers^{1,2*}

¹Hubrecht Institute, Royal Netherlands Academy of Arts and Sciences (KNAW), Uppsalalaan 8, 3584 CT, Utrecht the Netherlands

²Oncode Institute, Hubrecht Institute, 3584 CT Utrecht, The Netherlands.

³The Princess Maxima Center for Pediatric Oncology, 3584 CS Utrecht, The Netherlands.

⁴Co-first author

*Corresponding author

INTRODUCTION

The small intestinal epithelium is the fastest dividing tissue in humans, with an estimated turnover of about 1 week in humans. Lgr5⁺ crypt stem cells reside at the bottom of the crypts and fuel this renewal by dividing symmetrically every 24 hours (Barker et al., 2007; Beumer and Clevers, 2016). Paneth cells are derived from these same Lgr5⁺ cells and define the stem cell zone in the crypt bottom by providing essential niche factors, including Notch, Wnt and EGF signals. Enterocyte progenitors undergo multiple transit-amplifying cell divisions in the crypt before maturing in the villus. Progenitors of less numerous secretory cells tend to be non-dividing. The exodus of stem cell progeny from the crypt bottom is generally believed to be occurring in a continuous flow, hence also known as the ‘conveyor belt’ (Clevers, 2013).

The textbook view of the intestinal epithelium describes the crypt as the site of proliferation of progenitor cells that progressively differentiate and achieve their most mature state when these reach the villus. However, recent insights into differentiation trajectories of the lineages suggest a more nuanced image of context-dependent functionality, where cells are already functional in the crypt or villus bottom and can perform a different task in the villus tip. For example, enteroendocrine cells produce hormones in the crypt – the most mature hallmark of these cells – and can make different hormones in the villus (Beumer et al., 2018). This specialization is regulated by BMP signaling, a morphogen gradient increasing in strength from crypt to villus, and installed by BMP4-producing mesenchymal cells (Auclair et al., 2007; Haramis et al., 2004). A similar paradigm has been recently recognized for enterocytes, which preferentially absorb amino acids and carbohydrates in the villus bottom. Villus tip enterocytes on the contrary express genes involved in chylomicron synthesis and seemingly specialize in lipid uptake and processing (Moor et al., 2018). Here we describe the BMP signaling regulated programs in the different intestinal lineages in humans using intestinal organoids. We uncover heterogeneity of goblet cells along the crypt-villus axis and show that the specialization of goblet cells and enterocytes is regulated by BMP signaling.

METHODS

Cell culture of human intestinal organoids

Tissues from the human ileum were obtained from the UMC Utrecht with informed consent of each patient. The patients were diagnosed with small intestinal or colon adenocarcinoma that was resected. A sample from non-transformed, normal mucosa was taken for this study. The study was approved by the UMC Utrecht (Utrecht, The Netherlands) ethical committee and was in accordance with the Declaration of Helsinki and according to Dutch law. This study is compliant with all relevant ethical regulations regarding research involving human participants. Human small intestinal cells were isolated, processed and cultured as described previously (Beumer et al., 2018; Sato et al., 2011)

Organoids were differentiated as described before (Sato et al., 2011). BMP activation was achieved by withdrawing Noggin from ‘ENR’ and addition of BMP-2 (Peprotech, 50ng/ml) and

I

II

III

IV

V

VI

VII

VIII

&

BMP-4 (Peprotech, 50ng/ml). Notch signaling was inhibited by treatment with the Gamma-secretase inhibitor DAPT (Sigma, 10 μ M).

Immunostaining

Organoids and tissue were stained as described before (Beumer et al., 2018). Organoids were incubated with the corresponding secondary antibodies Alexa488-, 568- and 647-conjugated anti-rabbit and anti-goat (1:1,000; Molecular Probes) in blocking buffer containing 4',6-diamidino-2-phenylindole (DAPI; 1;1,000, Invitrogen). Sections were embedded in Vectashield (Vector Labs) and imaged using a Sp8 confocal microscope (Leica). Image analysis was performed using ImageJ software.

IHC images in Figure S1 and S2 are obtained from the human proteinatlas (Uhlen et al., 2015).

IHC in Fig. 2E was performed on the intestines of a previously performed BMP-inhibitor mouse experiment (Beumer et al., 2018).

Single cell sorting and RNA sequencing from organoids

After treatment for 5 days, organoids were dissociated through a 10-minute incubation with TrypLE (TrypLE Express; Life Technologies) supported by repeated mechanical disruption through pipetting with a narrow glass pipette until a single cell suspension was reached. Cells were sorted using a BD FACS Aria (BD Biosciences) based on fluorescence levels of DAPI for viability, Neon for goblet cells and forward and side scatter to ensure single cell collection. For single cell RNA sequencing, individual cells were collected in 384-well plates with ERCC spike-ins (Agilent), reverse transcription primers and dNTPs (both Promega). The Sort-seq method (Muraro et al., 2016) was applied for single cell sequencing. Sequencing libraries were generated with TruSeq small RNA primers (Illumina) and sequenced paired-end at 60 and 26bp read length, respectively, on the Illumina NextSeq.

For bulk RNA sequencing, two independent samples of organoids were differentiated for 5 days and collected in Eppendorf tubes containing 350 μ l RLT buffer (RNeasy kit, QIAGEN). RNA was extracted using the RNeasy mini kit (QIAGEN) following the manufacturer's instructions. Sequencing libraries were generated using a modified CELseq2 protocol (Hashimshony et al., 2016). 75 bp paired-end sequencing of libraries was performed on an Illumina NextSeq platform.

Single cell RNA sequencing analysis from organoids

Reads were mapped to the human GRCh37 genome assembly. Sort-seq read counts were filtered to exclude reads with identical library-, cell- and molecule barcodes. UMI counts were adjusted using Poisson counting statistics (Muraro et al., 2016). Cells with fewer than 1,000 or 3,000 unique transcripts were excluded from further analysis for the enterocyte and goblet cell datasets, respectively.

Subsequently, RaceID3 was used for k-medoids based clustering of cells and differential gene expression analysis between clusters using the standard settings described at <https://>

github.com/dgrun/RaceID3_StemID2_package. For pseudotemporal ordering of cells, those falling into clusters 1, 2 and 4 in the RaceID analysis were selected and grouped by media condition. The cells were aligned on a pseudotemporal trajectory using Monocle (version 2.6.4) based on differentially expressed genes between media conditions.

Bulk RNA sequencing analysis

Reads were mapped to the human GRCh37 genome assembly. The counted reads were filtered to exclude reads with identical library- and molecule barcodes. Differential gene expression analysis was performed using the DESeq2 package (Love et al., 2014).

RESULTS

Determination of a broad BMP signature in the human small intestinal epithelium using organoids

Human intestinal organoids can generate all different intestinal lineages when the factors for stem cell expansion are removed from the culture medium (Sato et al., 2011). A recent single cell RNA sequencing study recognized that enterocytes in organoids however fail to express many markers found in the intestinal villus tip, including apolipoproteins (Fujii et al., 2018). Based on our previous finding that enteroendocrine cells can adjust their hormone profile by interpreting the BMP levels, we reasoned a similar paradigm might apply to the other intestinal lineages. We therefore differentiated human small intestinal organoids using standard differentiation conditions (Sato et al., 2011), or by additional supplementation with the BMP agonists BMP2 and BMP4 combined with withdrawal of the BMP inhibitor noggin. We did not observe morphological differences between the two conditions, both containing enterocytes evidenced by their brush border (Fig. 1A). Bulk RNA sequencing reveals 912 differentially expressed genes between BMP active and inactive cells (p-adjusted $p < 0.05$, Supplementary table 1). The BMP pathway was effectively activated indicated by the target genes *ID1*, *ID2* and *ID3*, while generic enterocyte markers such as *FABP1* or *VIL1* remained largely unchanged (Fig. 1B, C). We found a broad BMP-induced downregulation of genes involved in translation, including ribosomal genes and the elongation factor *EEF1A1* (Fig. 1C). Genes involved in lipid handling and chylomicron biogenesis were among the strongest BMP target genes, including a more than 20-fold upregulation of the apolipoprotein *APOA1* (Fig. 1C). Most transporters involved in peptide, amino acid and carbohydrate uptake were readily expressed in the absence of BMP signals and were not BMP responsive. Notable exceptions were the amino acid transporter *SLC7A9* that is activated upon BMP signaling and is villus enriched (Moor et al., 2018), and the amino acid transporter *SLC1A5* that is reduced with BMP signals. Other strong BMP target genes included *PMP22*, a villus enriched transcript that is known to be produced by Schwann cells as a myelin component. Patients lacking *PMP22* display nerves that are particularly sensitive to force (Li et al., 2013), and potentially this protein plays a similar role in the villus that is known to undergo stretch stress. *DFNA5*, a protein involved in apoptosis, and the semaphorin *SEMA3G*, recently implicated in the guidance of lymph vessels, were strongly

I

II

III

IV

V

VI

VII

VIII

&

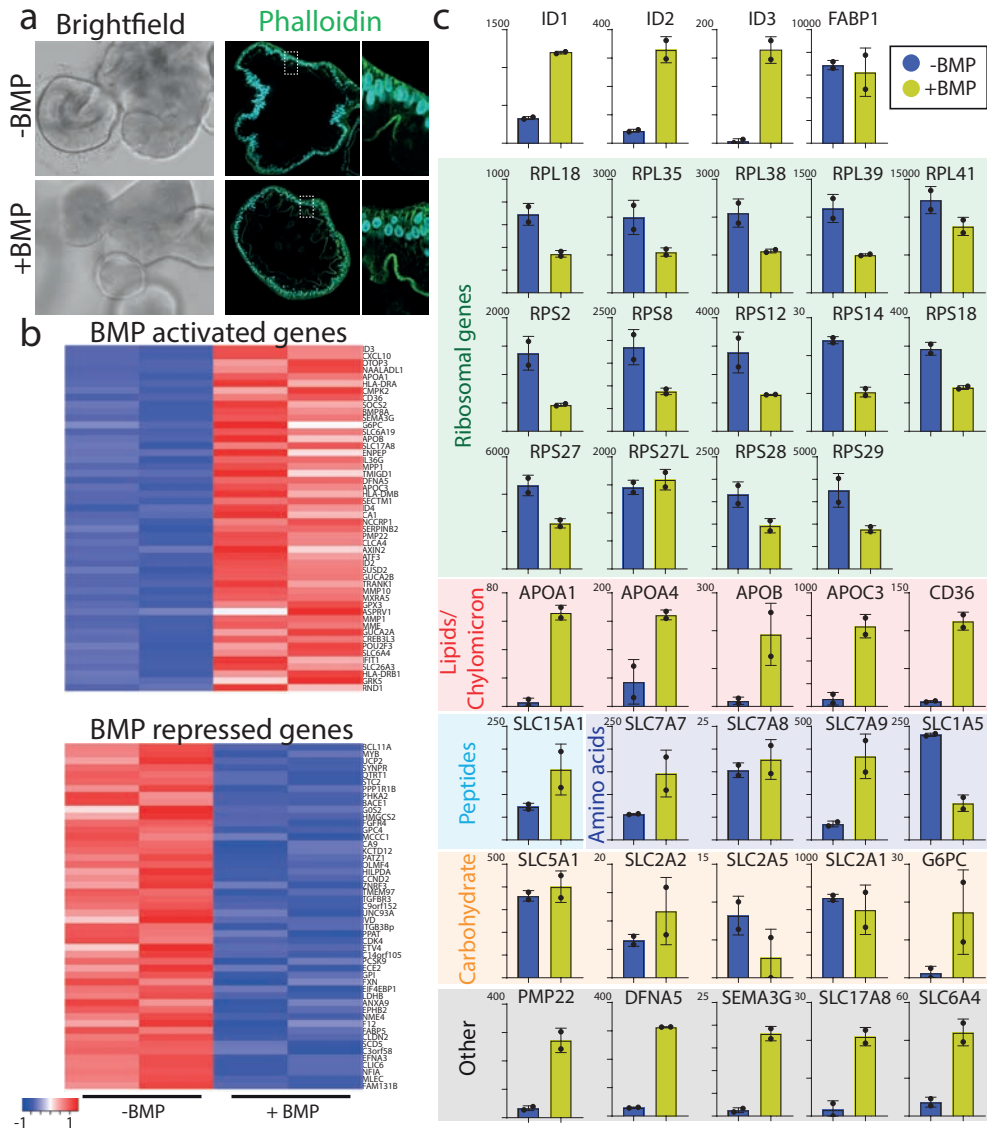


Figure 1. Broad BMP signature in human intestinal organoids. Brightfield and F-actin (Phalloidin) images of 5 day BMP-untreated and –treated organoids. Both cultures consist of differentiated organoids that contain enterocytes based on their extensive brush border. Bulk RNA sequencing was performed on –BMP and +BMP differentiated organoids. Heatmaps depict the 50 genes most significantly enriched genes in the two populations. The experiment was performed in $n=2$. Transcript levels of selected genes from the bulk RNA sequencing are shown. BMP activation causes a general repression of genes involved in translation, while promoting apolipoprotein expression.

activated by BMP signaling (Liu et al., 2016; Rogers and Alnemri, 2019). Peptidases known to play a role in final digestion of proteins, and multiple metalloproteases, were increased with BMP signals. Carbonic anhydrases (CA) are a large family of enzymes that are involved in

maintaining base-acid balance (Kivelä et al., 2005). CA1 and CA2 were BMP activated, while CA9 followed the reverse pattern. These enzymes are accordingly produced in the crypt-villus axis of humans (Fig. S1B). The BMP inhibitor Gremlin 1 and agonist BMP8a were both strong BMP2/4 target genes, and potentially act in a feedback loop regulating the BMP response. Moreover, the zebrafish homologue of BMP8a, *zbmp8a*, was found to be induced by fasting and regulate genes related to lipid metabolism (Zhong et al., 2018). Finally, we identified a broad upregulation of MHC class 2 genes, previously reported in enterocytes and of which the function in the intestine remains elusive (Fig. S1A).

Transition from bottom-villus to tip-villus enterocytes is controlled by BMP signaling

Our bulk transcriptomic data indicate that BMP activation stimulates the expression of villus tip enterocyte markers and thereby facilitate specialization along the crypt-villus axis. To establish whether these differences occur through specialization of individual enterocytes, or a global enhanced differentiation by BMP, we performed single cell RNA sequencing using SORT-seq (Fig. 2A) (Muraro et al., 2016). The transcriptome data was analyzed using RaceID3, a method that clusters cells based on k-medoids (Herman et al., 2018). We compared cells in a standard differentiation protocol that generates mostly enterocytes, in the presence and absence of BMP signals, and a stem cell culture in expansion medium. The expansion medium contained almost exclusively stem cells (cluster 1 and 6), while the differentiation condition induced rare goblet cells (cluster 3) as well as a large number of BMP-negative (cluster 4) and BMP-positive (cluster 2) enterocytes (Fig. 2A, B). These groups of enterocytes appeared equally mature based on the generic marker *FABP1* (Fig. 2B). However, the expression of apolipoproteins was exclusive to BMP-activated enterocytes, whereas genes involved in transcription, carbohydrate degradation (Sucrose isomaltase: SI) and the polymeric immunoglobulin receptor (PIGR) were enriched in BMP-inactive enterocytes (Fig. 2C). Enrichment of SI in the bottom villus over the crypt and top villus has previously been recognized in humans (Traber et al., 1992). PIGR has recently been identified as one of the most commonly silenced gene in ulcerative colitis (Kakiuchi et al., 2019; Nanki et al., 2019). Unbiased pseudotime clustering revealed a progression of stem cells through BMP-negative enterocytes towards BMP-active enterocytes (Fig. 2D). Apolipoproteins enriched towards the end of the pseudotime, while SI was produced in younger enterocytes that had not seen BMP signals (Fig. 2E). Immunofluorescent staining confirmed the reduced pIGR content in BMP-activated organoids. These findings suggest that human enterocytes can transdifferentiate by interpreting BMP-levels (Fig. 2F).

Single cell RNA sequencing of BMP active and inactive goblet cells

To study if BMP signaling could regulate a similar specialization in human goblet cells, we exploited our previously generated MUC2-NEON reporter organoids (using a NHEJ-mediated knock-in technique, see Artegiani *et al.*, 2020) and performed single cell RNA. We identified a clear cluster of goblet cells that exhibited high expression of the known markers *MUC2*, *AGR2* and *FCGBP* (Fig. 2B-D). BMP treatment divided the goblet cells in two groups (Fig. 2B, S2A).

I

II

III

IV

V

VI

VII

VIII

&

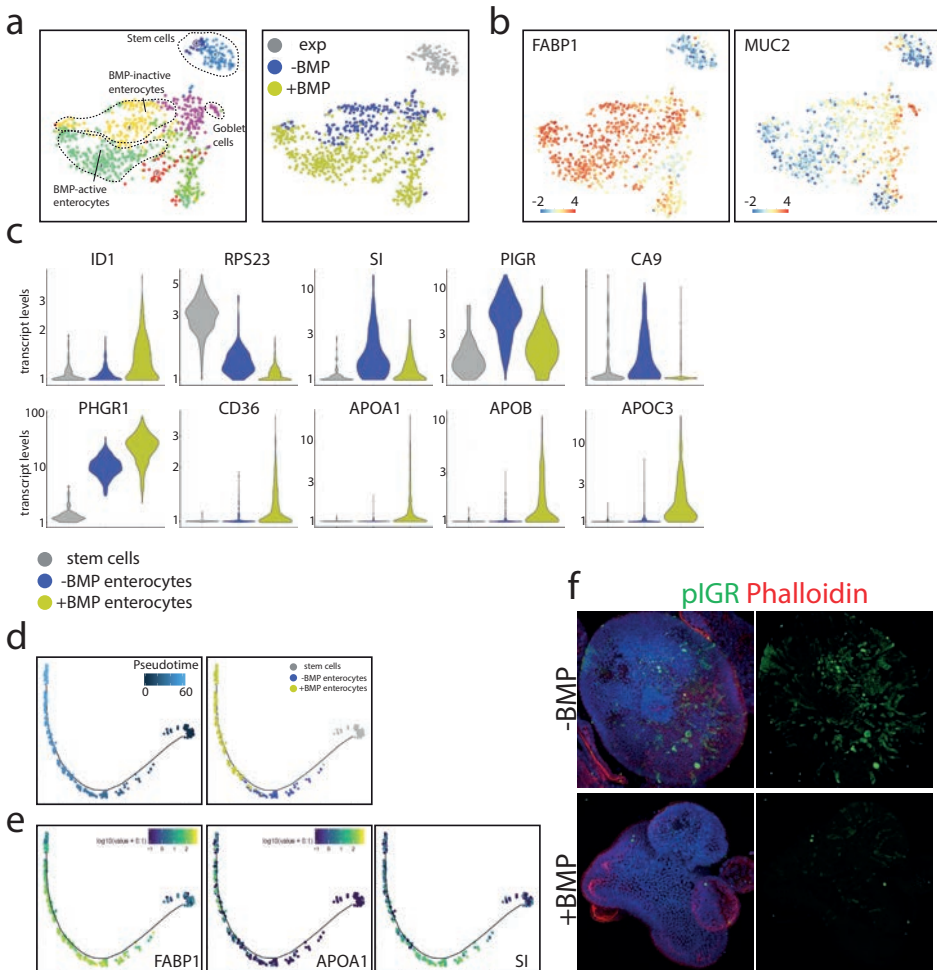


Figure 2. BMP regulated genes in human enterocytes. Single cell RNA sequencing was performed on 5 day differentiated organoids in the presence and absence of BMP, or in organoids in expansion medium. t-SNE is shown map displaying this stem cell and enterocyte-biased atlas. Different colors represent the 7 separate clusters, and BMP treated cells are highlighted. t-SNE maps displaying the expression levels of the generic enterocyte marker *FABP1* and goblet cell marker *MUC2*. Bars display color-coded unique transcript expression (logarithmic scale). Violin plots displaying the expression levels of selected genes within the stem cell cluster, BMP-inactive (cluster 4) or BMP-active enterocyte cluster (cluster 2). Unbiased pseudotime ordering of the stem cell and enterocyte clusters. Stem cells are ordered at the beginning of the pseudotime, that transit through BMP-inactive enterocytes to BMP-active enterocytes. Gene expression levels of selected genes on the pseudotime. Immunofluorescent staining of the polymeric immunoglobulin receptor (pIGR) in differentiated organoids without and with BMP. F-actin was stained using Phalloidin.

BMP-minus goblet cells exhibited unique expression of the well-known goblet markers *SPINK4*, a serine peptidase inhibitor, and *ITLN1* that act as a receptor for microbial carbohydrates (Fig. 2C,D). BMP-active goblet cells were defined by high *ZG16* levels, a lectin-like protein that

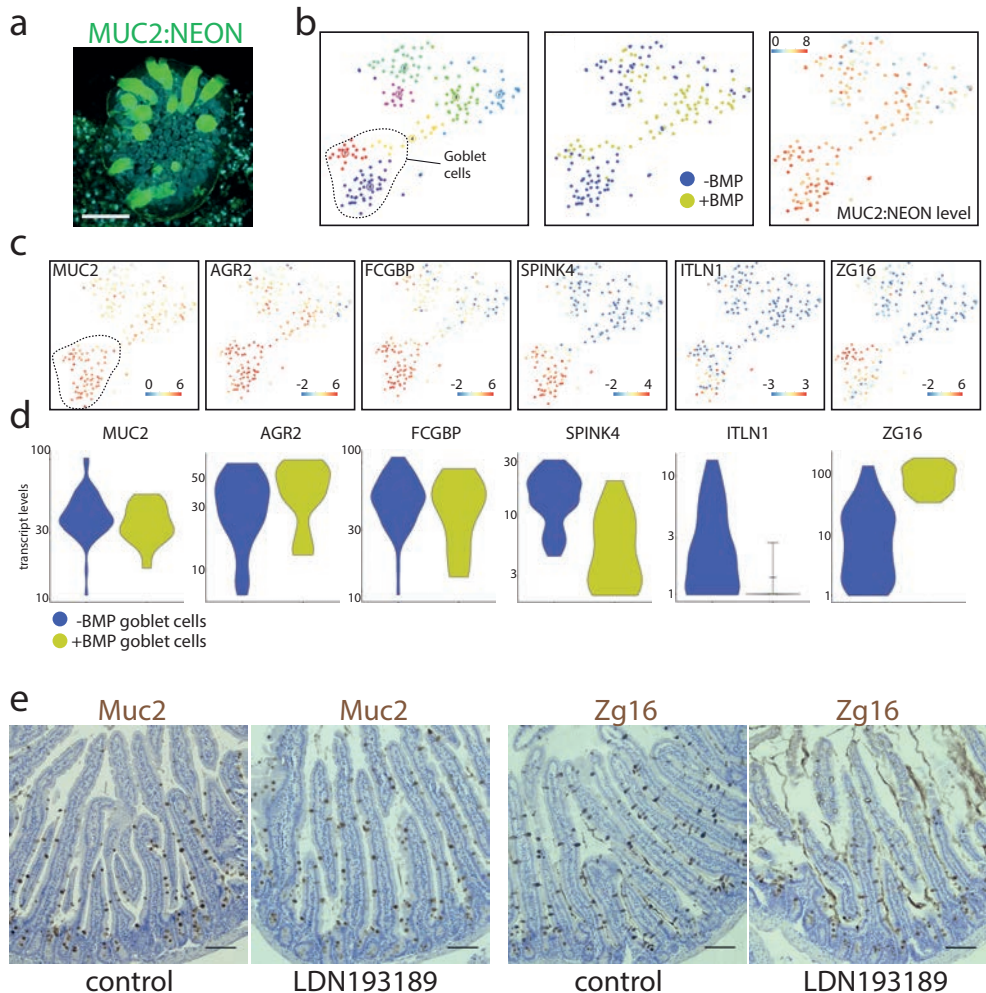


Figure 3. BMP regulated genes in human goblet cells. Confocal image of MUC2-NEON organoid, showing specific labeling of goblet cells. Single cell RNA sequencing was performed on NEON-sorted cells to enrich for goblet cells. t-SNE maps displaying the goblet cell-biased atlas. Different colors represent the 7 separate clusters, and BMP treated cells are highlighted. Fluorescent NEON-levels are plotted on the t-SNE map, showing highest level in the goblet cell clusters. t-SNE maps displaying the expression levels of the generic goblet cell marker *MUC2* and selected goblet cell markers. Bars display color-coded unique transcript expression (logarithmic scale). Violin plots displaying the expression levels of selected genes within BMP-inactive or BMP-active goblet cells. Immunohistochemical stainings of control or LDN193189-treated mice. BMP-inhibition does not affect the total number of goblet cells as evidenced by generic marker *Muc2*, but reduces the villus expression levels of *Zg16*. Scale bar is 100µm.

protects against Gram-positive bacteria by inducing their aggregation (Fig. 2C,D). The trefoil factor TFF1 was also activated by BMP in goblet cells (Fig. S2B). Consistent with the responses to BMP signals, we confirmed the divergent expression of these markers along the human crypt/villus axis (Fig. S2C). These data indicate that goblet cells produce different sets of

antimicrobial proteins in the crypt and villus in response to BMP signals. To evidence that BMP signaling controls zoned expression profiles *in vivo*, we analyzed the intestines of 80-hour BMP inhibited mice (Beumer et al., 2018). In BMP-inhibited mice, we observed a reduction in immunoreactivity of Zg16 in goblet cells, while the generic marker *Muc2* was not affected (Fig. 2E). This demonstrates that goblet cell zonation *in vivo* is regulated by a BMP gradient, similar to hormone-producing EECs.

DISCUSSION

Functional heterogeneity along the crypt-villus axis is an emerging concept. We have shown before that EECs specialize along the crypt-villus axis by interpreting BMP signals (Beumer et al., 2018). This heterogeneity was later extended to enterocytes, that show different functional programs along this axis (Moor et al., 2018). Organoids uniquely allow to study the effect of a single signaling component on individual cell types. In this study, we evidence that the villus-axis enterocyte heterogeneity in humans is regulated by BMP signals. Using goblet cell reporter organoids, we add goblet cells as a third cell type that displays dynamic functions during its lifetime.

Understanding the maturation level of the constituent cell types in organoids is important, as these cultures are widely used for functional studies. A recent single cell sequencing study in human organoids noted a lack of many enterocyte markers compared to tissue, and attributed this to potential presence of Wnt signals (Fujii et al., 2018). The presence of mature cell types is often based on expression of generic markers, such as *FABP1*, for detection of human enterocytes. While these appear both in the absence and presence of BMP signals, we now indicate functional subspecification of enterocytes which will be missed by only considering broad marker genes. Functional studies on lipid processing or chylomicron synthesis therefore would necessitate activation of BMP signaling.

Our work has therapeutic implications for multiple diseases, such as non-alcoholic steatohepatitis (NASH) or obesity. Inhibition of BMP signaling would reduce the ability for lipid uptake and chylomicron synthesis. Humans carrying mutations in *APOB* are largely resistant to atherosclerosis (Whitfield et al., 2004). Similarly, a heterozygous R19X null mutation in *APOC3* found in Pennsylvania Amish populations, is associated with cardio-protective lipid profiles. Other rare *APOC3* mutations have been shown to confer almost a complete cardioprotection (Crosby et al., 2014; Jørgensen et al., 2014; Tachmazidou et al., 2013). These cardioprotective carrierships, in which half of functional *APOB* or *APOC3* is still produced, highlight that there could wide therapeutic window for diminishing expression of these genes in the intestine. *APOC3* inhibition through RNA interference has shown favorable results in clinical trials for lowering blood triglycerides, although it is unknown whether this effect is a result of reduced liver- or intestine-derived *APOC3*, or a combination (Gaudet et al., 2015). Multiple mouse models have shown that intestinal loss of several BMP regulated genes, such as *Apob*, *Mttp* or *CD36*, leads to diminished lipid uptake, and lower serum levels of cholesterol (Farese et al., 1995; Geloan et al., 2012; Iqbal et al., 2013; Raabe et al., 1998). BMP inhibitors reduce

the development of atherosclerosis in mouse models and lower serum cholesterol, although this was reported as an intestine-independent mechanism (Derwall et al., 2012). These findings emphasize the potential of intestine-specific BMP inhibition for a wide range of diseases related to lipid uptake.

ACKNOWLEDGMENTS

We thank Anko de Graaff and the Hubrecht Imaging Centre (HIC) for microscopy assistance; Single Cell Discoveries for the provided single-cell sequencing service and support;

AUTHOR CONTRIBUTIONS

J.B., J.P. and H.C. conceptualized the project, designed the experiments, interpreted the results and wrote the manuscript. F.Y.Y. aided with functional organoid experiments. A.M.S. assisted in cell culture experiments and was supervised by J.B., J.P. and H.C.

DECLARATION OF INTERESTS

H.C. is inventor on several patents related to organoid technology; his full disclosure is given at <https://www.uu.nl/staff/JCClevers/>.

I

II

III

IV

V

VI

VII

VIII

&

REFERENCES

- Auclair, B.A., Benoit, Y.D., Rivard, N., Mishina, Y., and Perreault, N. (2007). Bone Morphogenetic Protein Signaling Is Essential for Terminal Differentiation of the Intestinal Secretory Cell Lineage. *Gastroenterology*.
- Barker, N., van Es, J.H., Kuipers, J., Kujala, P., van den Born, M., Cozijnsen, M., Haegebarth, A., Korving, J., Begthel, H., Peters, P.J., et al. (2007). Identification of stem cells in small intestine and colon by marker gene *Lgr5*. *Nature* *449*, 1003–1007.
- Beumer, J., and Clevers, H. (2016). Regulation and plasticity of intestinal stem cells during homeostasis and regeneration. *Development* *143*, 3639–3649.
- Beumer, J., Artegiani, B., Post, Y., Reimann, F., Gribble, F., Nguyen, T.N., Zeng, H., Van den Born, M., Van Es, J.H., and Clevers, H. (2018). Enteroendocrine cells switch hormone expression along the crypt-to-villus BMP signaling gradient. *Nat Cell Biol* *20*.
- Clevers, H. (2013). The intestinal crypt, a prototype stem cell compartment. *Cell* *154*, 274–284.
- Crosby, J., Peloso, G.M., Auer, P.L., Crosslin, D.R., Stitzel, N.O., Lange, L.A., Lu, Y., Tang, Z.Z., Zhang, H., Hindy, G., et al. (2014). Loss-of-function mutations in *APOC3*, triglycerides, and coronary disease. *N. Engl. J. Med.*
- Derwall, M., Malhotra, R., Lai, C.S., Beppu, Y., Aikawa, E., Seehra, J.S., Zapol, W.M., Bloch, K.D., and Yu, P.B. (2012). Inhibition of bone morphogenetic protein signaling reduces vascular calcification and atherosclerosis. *Arterioscler. Thromb. Vasc. Biol.*
- Farese, R. V., Ruland, S.L., Flynn, L.M., Stokowski, R.P., and Young, S.G. (1995). Knockout of the mouse apolipoprotein B gene results in embryonic lethality in homozygotes and protection against diet-induced hypercholesterolemia in heterozygotes. *Proc. Natl. Acad. Sci. U. S. A.*
- Fujii, M., Matano, M., Toshimitsu, K., Takano, A., Mikami, Y., Nishikori, S., Sugimoto, S., and Sato, T. (2018). Human Intestinal Organoids Maintain Self-Renewal Capacity and Cellular Diversity in Niche-Inspired Culture Condition. *Cell Stem Cell* *23*, 787–793.e6.
- Gaudet, D., Alexander, V.J., Baker, B.F., Brisson, D., Tremblay, K., Singleton, W., Geary, R.S., Hughes, S.G., Viney, N.J., Graham, M.J., et al. (2015). Antisense inhibition of apolipoprotein C-III in patients with hypertriglyceridemia. *N. Engl. J. Med.*
- Geloen, A., Helin, L., Geeraert, B., Malaud, E., Holvoet, P., and Marguerie, G. (2012). CD36 inhibitors reduce postprandial hypertriglyceridemia and protect against diabetic dyslipidemia and atherosclerosis. *PLoS One*.
- Haramis, A.P.G., Begthel, H., Van Den Born, M., Van Es, J., Jonkheer, S., Offerhaus, G.J.A., and Clevers, H. (2004). De Novo Crypt Formation and Juvenile Polyposis on BMP Inhibition in Mouse Intestine. *Science* (80-.). *303*, 1684–1686.
- Hashimshony, T., Senderovich, N., Avital, G., Klochender, A., de Leeuw, Y., Anavy, L., Gennert, D., Li, S., Livak, K.J., Rozenblatt-Rosen, O., et al. (2016). CEL-Seq2: sensitive highly-multiplexed single-cell RNA-Seq. *Genome Biol.* *17*, 77.
- Herman, J.S., Sagar, and Grün, D. (2018). FateID infers cell fate bias in multipotent progenitors from single-cell RNA-seq data. *Nat. Methods*.
- Iqbal, J., Parks, J.S., and Hussain, M.M. (2013). Lipid absorption defects in intestine-specific microsomal triglyceride transfer protein and ATP-binding cassette transporter A1-deficient mice. *J. Biol. Chem.*
- Jørgensen, A.B., Frikke-Schmidt, R., and Nordestgaard, B.G. (2014). Loss-of-Function Mutations in *APOC3* and Risk of Ischemic Vascular Disease. *J. Vasc. Surg.*

Kakiuchi, N., Yoshida, K., Uchino, M., Kihara, T., Akaki, K., Inoue, Y., Kawada, K., Nagayama, S., Yokoyama, A., Yamamoto, S., et al. (2019). Frequent mutations that converge on the NFKBIZ pathway in ulcerative colitis. *Nature*.

Kivelä, A.J., Kivelä, J., Saarnio, J., and Parkkila, S. (2005). Carbonic anhydrases in normal gastrointestinal tract and gastrointestinal tumours. *World J. Gastroenterol*.

Li, J., Parker, B., Martyn, C., Natarajan, C., and Guo, J. (2013). The PMP22 gene and its related diseases. *Mol. Neurobiol*.

Liu, X., Uemura, A., Fukushima, Y., Yoshida, Y., and Hirashima, M. (2016). Semaphorin 3G Provides a Repulsive Guidance Cue to Lymphatic Endothelial Cells via Neuropilin-2/PlexinD1. *Cell Rep*.

Love, M.I., Huber, W., and Anders, S. (2014). Moderated estimation of fold change and dispersion for RNA-seq data with DESeq2. *Genome Biol.* 15, 550.

Moor, A.E., Harnik, Y., Ben-Moshe, S., Massasa, E.E., Rozenberg, M., Eilam, R., Bahar Halpern, K., and Itzkovitz, S. (2018). Spatial Reconstruction of Single Enterocytes Uncovers Broad Zonation along the Intestinal Villus Axis. *Cell* 175, 1156–1167.e15.

Muraro, M.J., Dharmadhikari, G., Grün, D., Groen, N., Dielen, T., Jansen, E., van Gurp, L., Engelse, M.A., Carlotti, F., de Koning, E.J.P., et al. (2016). A Single-Cell Transcriptome Atlas of the Human Pancreas. *Cell Syst.* 3, 385–394.

Nanki, K., Fujii, M., Shimokawa, M., Matano, M., Nishikori, S., Date, S., Takano, A., Toshimitsu, K., Ohta, Y., Takahashi, S., et al. (2019). Somatic inflammatory gene mutations in human ulcerative colitis epithelium. *Nature*.

Raabe, M., Flynn, L.M., Zlot, C.H., Wong, J.S., Véniant, M.M., Hamilton, R.L., and Young, S.G. (1998). Knockout of the abetalipoproteinemia gene in mice: Reduced lipoprotein secretion in heterozygotes and embryonic lethality in homozygotes. *Proc. Natl. Acad. Sci. U. S. A.*

Rogers, C., and Alnemri, E.S. (2019). Gasdermins: novel mitochondrial pore-forming proteins. *Mol. Cell. Oncol*.

Sato, T., Stange, D.E., Ferrante, M., Vries, R.G.J., Van Es, J.H., Van Den Brink, S., Van Houdt, W.J., Pronk, A., Van Gorp, J., Siersema, P.D., et al. (2011). Long-term expansion of epithelial organoids from human colon, adenoma, adenocarcinoma, and Barrett's epithelium. *Gastroenterology* 141, 1762–1772.

Tachmazidou, I., Dedoussis, G., Southam, L., Farmaki, A.E., Ritchie, G.R.S., Xifara, D.K., Matchan, A., Hatzikotoulas, K., Rayner, N.W., Chen, Y., et al. (2013). A rare functional cardioprotective APOC3 variant has risen in frequency in distinct population isolates. *Nat. Commun.*

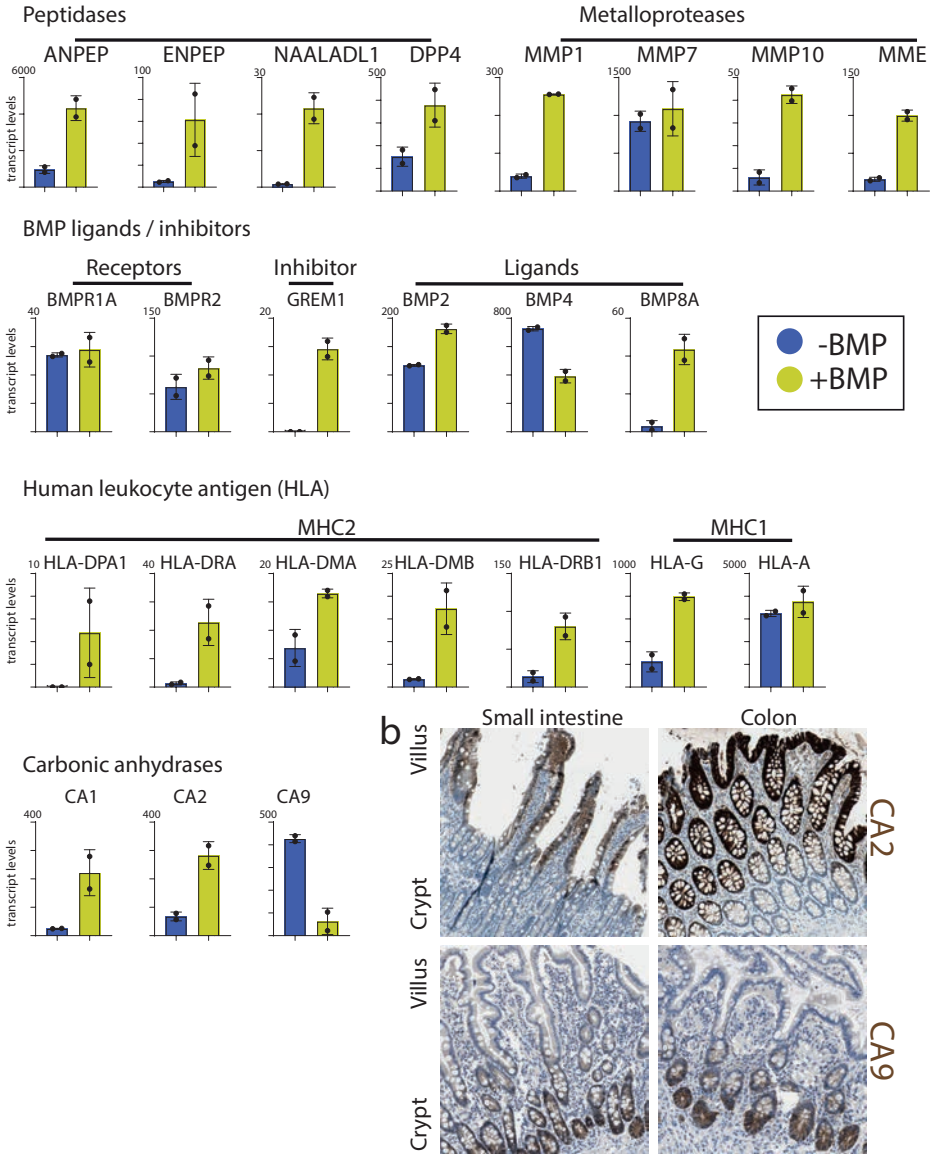
Traber, P.G., Yu, L., Wu, G.D., and Judge, T.A. (1992). Sucrase-isomaltase gene expression along crypt-villus axis of human small intestine is regulated at level of mRNA abundance. *Am. J. Physiol. - Gastrointest. Liver Physiol*.

Uhlen, M., Fagerberg, L., Hallstrom, B.M., Lindskog, C., Oksvold, P., Mardinoglu, A., Sivertsson, A., Kampf, C., Sjostedt, E., Asplund, A., et al. (2015). Tissue-based map of the human proteome, Human Protein Atlas available from www.proteinatlas.org. *Science* (80-.). 347, 1260419–1260419.

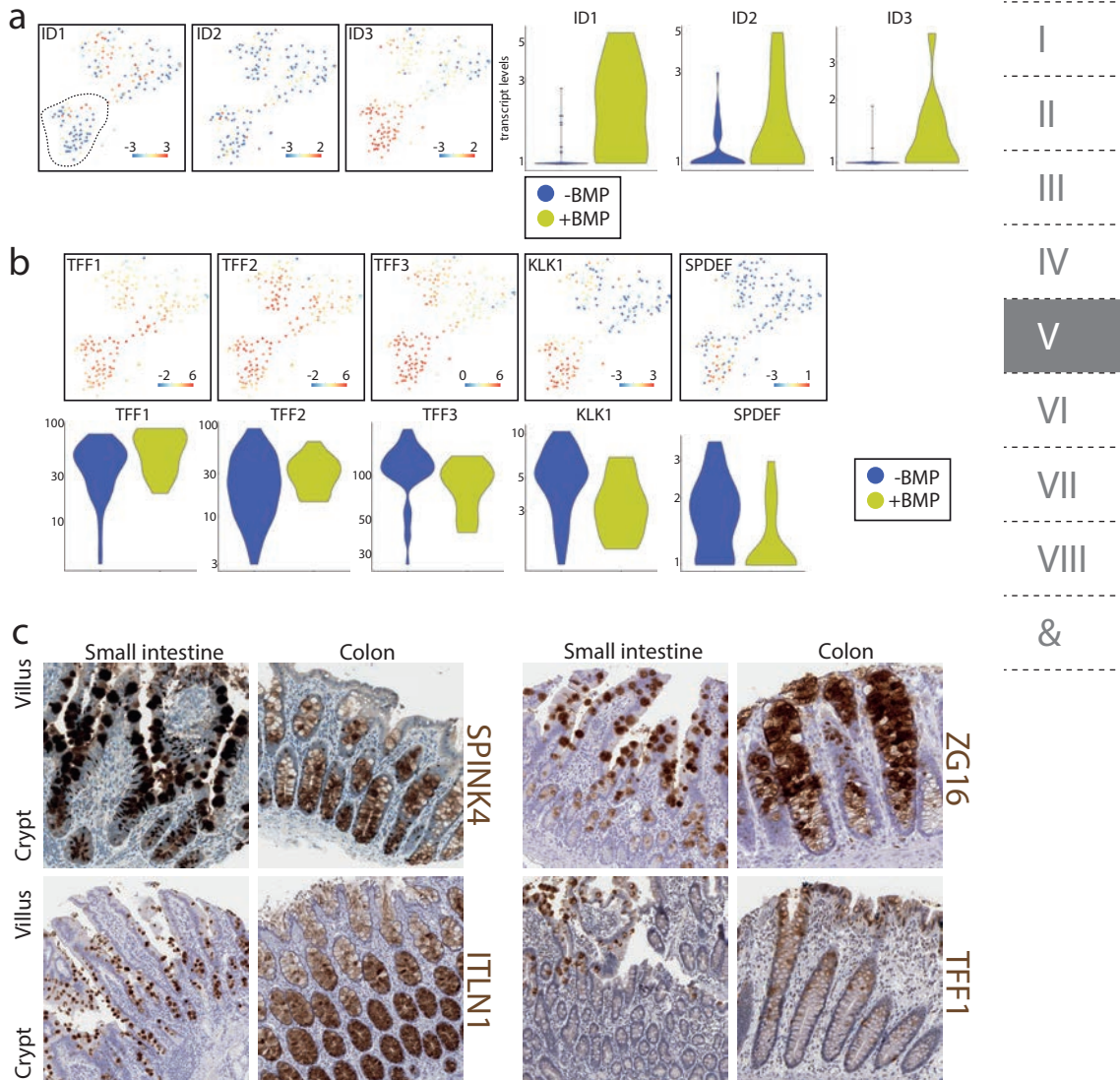
Whitfield, A.J., Barrett, P.H.R., Van Bockxmeer, F.M., and Burnett, J.R. (2004). Lipid disorders and mutations in the APOB gene. *Clin. Chem*.

Zhong, S., Wang, Y., Li, J., Wang, M., Meng, L., Ma, Z., Zhang, S., and Liu, Z. (2018). Spatial and temporal expression of *bmp8a* and its role in regulation of lipid metabolism in zebrafish *Danio rerio*. *Gene Reports*.

SUPPLEMENTARY FIGURES



Supplementary figure 1. Different classes of BMP regulated genes. Transcript levels of selected genes from the bulk RNA sequencing are shown (Figure 1). Carbonic anhydrases 2 (CA2) and 9 (CA9) display strong opposing expression gradients along the crypt-villus axis. Images were taken from the human protein atlas (Uhlen et al., 2015).



Supplementary figure 2. Heterogeneity of human goblet cells along the crypt-villus axis. t-SNE maps and violin plots displaying the expression levels of BMP target genes *ID1*, *ID2* and *ID3* from the goblet cell single cell RNA sequencing atlas (Figure 3). Bars in t-SNE maps display color-coded unique transcript expression (logarithmic scale). t-SNE maps and violin plots displaying the expression levels of selected genes from the goblet cell single cell RNA sequencing atlas (Figure 3). Bars in t-SNE maps display color-coded unique transcript expression (logarithmic scale). Immunohistochemistry confirms heterogeneous expression of goblet cell markers along the crypt-villus axis. Images were taken from the human protein atlas (Uhlen et al., 2015).

CHAPTER
**HIGH RESOLUTION MRNA AND
SECRETOME ATLAS OF HUMAN
ENTEROENDOCRINE CELLS**

VI

SUMMARY

Enteroendocrine cells (EECs) sense intestinal content and release hormones to regulate gastrointestinal activity, systemic metabolism and food intake. Little is known about the molecular make-up of human EEC subtypes and the regulated secretion of individual hormones. Here we describe an organoid-based platform for functional studies of human EECs. EEC formation is induced *in vitro* by transient expression of *NEUROG3*. A set of gut organoids was engineered in which the major hormones are fluorescently tagged. A single-cell mRNA atlas was generated for the different EEC subtypes, and their secreted products were recorded by mass-spectrometry. We note key differences to murine EECs, including hormones,

Joep Beumer^{1,2,14}, Jens Puschhof^{1,2,14}, Julia Bauzá-Martínez^{3,4,14}, Adriana Martínez-Silgado^{1,2}, Rasa Elmentaite⁵, Kylie R. James⁵, Alexander Ross^{6,7}, Delilah Hendriks^{1,2}, Benedetta Artegiani^{1,2}, Georg Busslinger^{1,2}, Bas Ponsioen⁸, Amanda Andersson-Rolf^{1,2}, Kai Kretzschmar^{1,2}, Maarten H. Geurts^{1,2}, Yotam E. Bar-Ephraim^{1,2}, Cayetano Pleguezuelos Manzano^{1,2}, Yorick Post^{1,2}, Franka van der Linden⁹, Carmen Lopez Iglesias¹⁰, Willine J. van de Wetering^{1,10}, Reinier van der Linden^{1,2}, Peter J. Peters¹⁰, Albert J.R. Heck^{3,4}, Joachim Goedhart⁹, Hugo Snippert⁸, Matthias Zilbauer⁷, Sarah A. Teichmann^{5,11,12}, Wei Wu^{3,4,#}, Hans Clevers^{1,2,13,15,*}

¹Hubrecht Institute, Royal Netherlands Academy of Arts and Sciences (KNAW) and UMC Utrecht, 3584 CT Utrecht, The Netherlands.

²Oncode Institute, Hubrecht Institute, 3584 CT Utrecht, The Netherlands.

³Biomolecular Mass Spectrometry and Proteomics, Bijvoet Center for Biomolecular Research and Utrecht Institute for Pharmaceutical Sciences, Utrecht University, Padualaan 8, 3584 CH Utrecht, The Netherlands.

⁴Netherlands Proteomics Centre, Padualaan 8, 3584 CH Utrecht, The Netherlands.

⁵Wellcome Sanger Institute, Wellcome Genome Campus, Hinxton, United Kingdom, CB10 1SA.

⁶Department of Surgery, University of Cambridge, Cambridge CB2 0QQ, UK

⁷Department of Paediatrics, University of Cambridge, Cambridge CB2 0QQ, UK

⁸Oncode Institute, Center for Molecular Medicine, University Medical Centre Utrecht, Utrecht, The Netherlands.

⁹Swammerdam Institute for Life Sciences, Section of Molecular Cytology, van Leeuwenhoek Centre for Advanced Microscopy, University of Amsterdam, Amsterdam, the Netherlands.

¹⁰The Maastricht Multimodal Molecular Imaging institute, Maastricht University, 6229 ER Maastricht, The Netherlands.

¹¹Theory of Condensed Matter, Cavendish Laboratory, Department of Physics, University of Cambridge, Cambridge, United Kingdom, CB3 0HE

¹²European Molecular Biology Laboratory, European Bioinformatics Institute (EMBL-EBI), Wellcome Genome Campus, Hinxton, United Kingdom, CB10 1SA

¹³The Princess Maxima Center for Pediatric Oncology, 3584 CS Utrecht, The Netherlands.

¹⁴Co-first author

¹⁵Lead Contact

Co-correspondence: w.wu1@uu.nl

* Correspondence: h.clevers@hubrecht.eu

sensory receptors and transcription factors. Notably, several novel hormone-like molecules were identified. Inter-EEC communication is exemplified by secretin-induced GLP-1 secretion. Indeed, individual EEC subtypes carry receptors for various EEC hormones. This study provides a rich resource to study human EEC development and function.

I

II

III

IV

V

VI

VII

VIII

&

INTRODUCTION

The principal function of the intestine is to digest food and absorb nutrients. A less studied aspect of intestinal function is its role as the largest hormone-producing organ, an activity performed by the enteroendocrine cells (EECs) (Gribble and Reimann, 2017). EECs are rare secretory cells, comprising <1% of the epithelial cells. Apical EEC receptors are believed to sense chemicals in the intestinal lumen derived from food and microbiota. These receptors are predominantly GPCRs and include olfactory receptors (Furness et al., 2013). Hormones secreted by EECs can signal to the local enteric nervous system as well as to distant organs including the pancreas and the brain, thus controlling key physiological processes related to food intake, insulin release, secretion of digestive enzymes and bowel movement. Enteric hormones have also been proposed to orchestrate mucosal immunity (Worthington et al., 2018). EECs are emerging therapeutic targets for the management of metabolic diseases (i.e. obesity and diabetes), illustrated by recently introduced type 2 diabetes drugs that stabilize the hormone Glucagon-like peptide 1 (GLP-1) or activate its receptor, leading to release of insulin from pancreatic β -cells (Sharma et al., 2018).

EECs produce some 20 different hormones. GLP-1 and Glucose-dependent insulinotropic peptide (GIP) are the so-called incretin hormones that stimulate insulin secretion. The Enterochromaffin (EC) cells of the gut produce 90% of body serotonin and regulate bowel movement (Worthington et al., 2018). Motilin (MLN) is a human EEC hormone that is a pseudogene in the mouse genome, which controls gut contractions in the inter-digestive state (Worthington et al., 2018). Cholecystokinin (CCK) regulates bile and pancreatic enzyme secretion. Multiple hormones control appetite, including the appetite-inducing (or orexigenic) Ghrelin (GHRL) and the appetite-reducing (anorexigenic) Peptide YY (PYY). Gastrin (GAST), while rare in the mouse intestine, is produced in the human duodenum and responds to luminal acid by regulating proton secretion of stomach parietal cells. Somatostatin (SST) is a peptide which inhibits secretion of most other intestinal hormones (Worthington et al., 2018).

Homeostatic renewal of the intestine is driven by Lgr5+ stem cells located at the bottom of the crypts of Lieberkuehn (Barker et al., 2007). Lgr5+ cells generate all differentiated intestinal cell types: the abundant absorptive enterocytes and the various secretory cell types. The murine EEC lineage consists of multiple subtypes, historically defined by their principle hormone product: L-cells (Glp-1, Pyy), I-cells (Cck), K-cells (Gastric inhibitory protein, Gip), N-cells (Neurotensin, Nts), S-cells (Secretin, Sct), enterochromaffin or EC-cells (Serotonin/5-HT), X-cells (Ghrl), G-cells (Gast) and D-cells (Sst) (Engelstoft et al., 2013a) (Gehart et al., 2019). While this nomenclature suggests that EEC phenotypes are hard-wired, we have recently found that the crypt-villus BMP-signaling gradient induces hormone switching in individual murine EEC lineages (Beumer et al., 2018). Of note also, the abundance of individual EEC subtypes greatly differs in a region-specific fashion along the proximal-distal gastrointestinal axis. Studies on EECs have largely focused on murine models, exploiting a variety of reporter mice for subsets of EECs to monitor their responses to nutritional or genetic challenges (Goldspink et al., 2018). We have recently described the developmental hierarchy of murine subtypes EECs

using a mouse model in which endogenous Neurogenin-3 expression, the main determinant of EEC fate, was coupled to the production of two separate fluorescent proteins with different half-lives (Gehart et al., 2019). Single cell RNA sequencing of sorted EEC progenitors allowed for construction of a time-resolved development roadmap of the mouse EEC lineage.

The human diet and microbiome and that of rodents differ greatly (Nguyen et al., 2015). It is likely that the repertoire of sensory receptors and the secretory hormone responses differ significantly between these species. The study of human EECs is challenging due to the paucity of these cells and the lack of physiologically relevant *in vitro* models, leaving many questions surrounding basic human EEC biology unanswered. Few human EEC immortalized cell lines exist, and these are known to differ substantially from their wildtype counterparts (Goldspink et al., 2018). There is currently no atlas of human EEC subtypes. Although some inducers of hormone secretion have been described in mice, there has been no experimental model to systematically assess such secretagogues for human EECs. Here, we describe an organoid-based platform to provide a detailed molecular and functional description of human EECs.

RESULTS

Production of region-specific human EECs

Previous attempts to create human EECs *in vitro* have relied on growth-factor based differentiation (Beumer et al., 2018) or overexpression of *NEUROG3*, the key transcription factor to instruct EEC fate (McCracken et al., 2014; Sinagoga et al., 2018). Both iPSC- (Zhang et al., 2019) and adult stem cell (ASC)-based (Chang-Graham et al., 2019) approaches have proven useful to understand aspects of human EEC biology, such as modeling of inherited *NEUROG3* mutations and viral infection-mediated serotonin release (Chang-Graham et al., 2019). However, imperfect differentiation and regional restriction of the donor material have limited these studies to a subset of human EECs.

To generate the full spectrum of human EECs, we established organoids from healthy adult proximal small intestine (duodenum), distal small intestine (ileum) and the ascending colon (Sato et al., 2011). These organoids were transduced with a doxycycline-inducible *NEUROG3* construct (Fig. 1A). dTomato was inserted 3' to the *NEUROG3* reading frame, separated by a self-cleavable P2A sequence to avoid creating a fusion protein. A 48-hour-pulsed expression of *NEUROG3* in the basic medium 'ENR' promoted the expression of the broad EEC marker Chromogranin A (*CHGA*) (Fig. 1B). Proximal SI hormones such as *GAST*, *CCK* and *MLN* were enriched in duodenal organoids, whereas *NTS*, *PYY* and *GCG* were predominantly observed in distal SI organoids. Of note, *GCG* encodes the preproglucagon prehormone, a protein precursor to a set of hormones including GLP-1 (see below). *SST* was comparably expressed in proximal and distal organoids, consistent with its profile in the mouse gut. A recent single cell RNA sequencing study of inflammatory bowel disease patients and healthy controls generated the profile of 83 colonic EECs, suggesting that the human colon produces a small repertoire of hormones: serotonin-producing ECs and L-cells positive for *GCG* and *PYY* (Parikh et al., 2019). Consistently, induced colon organoids only contained serotonin-producing ECs and

I

II

III

IV

V

VI

VII

VIII

&

GCG-expressing EECs. To establish the optimal window of differentiation towards EECs, we monitored hormone expression over time. We found that hormone expression peaked 5 days after initiation of *NEUROG3* expression (Fig. S1A). Therefore, we applied a 5 day-differentiation protocol in ENR throughout the remainder of this study. Under these conditions, EECs in organoids displayed a normal morphology as visualized by transmission electron microscopy. Note the typical basal concentration of hormone vesicles (Fig. 1C).

We tested hormone co-expression by immunofluorescent staining (Fig. S1B). We observed mutually exclusive expression for MLN and GAST, for GHRL and CHGA and for Serotonin and GLP-1, while a subset of GIP-positive cells co-expressed CCK. This closely resembled the co-expression patterns in mice (with the exception of MLN, a pseudogene in mice) (Haber et al., 2017) (Fig. S1B). Virtually all EECs, as identified by the broad marker CHGA, were derived from *NEUROG3*-overexpressing cells as indicated by dTomato-positivity (Fig. S1B). A definitive hallmark of a mature EEC is its ability to secrete hormones. Indeed, exposure of organoids to Forskolin, a stimulator of adenylate cyclase increasing cAMP levels and thus of general hormone secretion, greatly enhanced GLP-1 levels in the culture supernatant (Fig. 1D).

The ability to enrich for specific EEC subsets in organoids would enhance the applicability of the system. We have previously reported that BMP signaling acts on mature murine EECs in villi, but not in crypts (Beumer et al., 2018). BMP thus controls a switch in hormone repertoire of EECs during their journey from the crypt base to the villus tip. Consistent with our observations in murine EECs, we found that activation of BMP signaling enhances the expression of *NTS*, while reducing GLP-1 (Fig. S2A,B). These data indicated that human EECs generated *in vitro* are responsive to BMP. These observations were refined later in this study (see below).

Since the initial expression of *NEUROG3* occurs at random positions along the crypt axis in mice (Gehart et al., 2019), we hypothesized that exposure to other crypt differentiation signals (i.e. Notch, Wnt) prior to this expression pulse could potentially influence their eventual fate. We therefore modulated these signals prior to inducing *NEUROG3* expression, mimicking the different initiation sites along the intestinal crypt axis (Fig. S2C). As a control, we modulated the same signals after *NEUROG3* induction (Fig. S2D). Inhibition of Notch before or after expression of *NEUROG3* did not affect EEC differentiation (Fig. S2E). Inhibition of Wnt signaling before (but not after) the *NEUROG3* pulse stimulated expression of *MLN* at the expense of *GCG*, while having no effect on *SST* expression (Fig. S2E). Immunofluorescence revealed an increase in the number of *MLN*-producing cells rather than in the 'per cell'-expression levels (Fig. S2F), resulting in a strong shift in the ratio between L-cells and M-cells (Fig. S2G).

Generation of a hormone reporter biobank EEC-TAG

Mouse models in which hormone expression is coupled to a fluorescent readout have been generated for several murine EEC hormones: *Chga*, *Gcg*, *Gip*, *Cck*, *Ghrl* and *Ppy* (Engelstoft et al., 2013b, 2015; Gong et al., 2003; Parker et al., 2009; Reimann et al., 2008; Sommer and Mostoslavsky, 2014). These transgenic mouse models have been instrumental to study

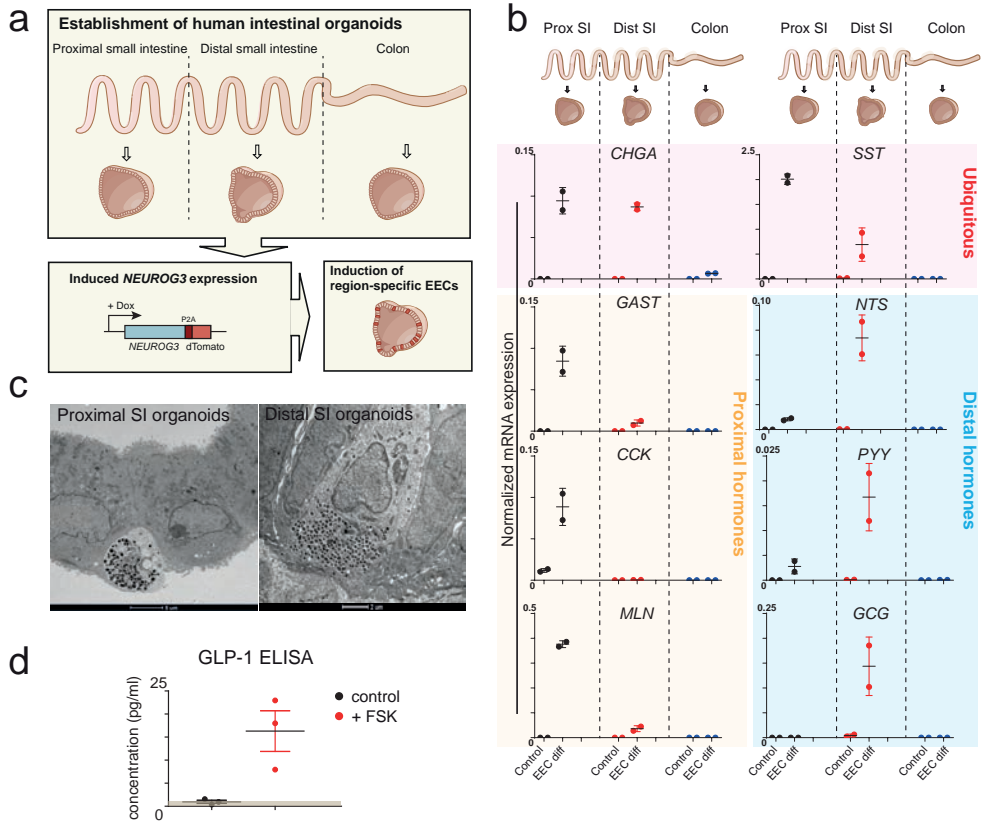


Figure 1. Production of region-specific human enteroendocrine cells in intestinal organoids. Schematic representation of the generation of region-specific enteroendocrine cells (EECs). Organoids are established from different regions of the intestinal tract of different patients, after which doxycycline (dox) – induced overexpression of Neurogenin-3 (*NEUROG3*) can drive the production of EECs. qPCR analysis showing expression of hormones, control or differentiation condition after a pulse of dox. Expression levels are normalized to GADPH. The experiment was performed in $n = 2$ independent experiments, and the mean expression and SEM are depicted. Transmission electron microscopy (TEM) of EECs in organoids showing polarized localization of hormone vesicles. Scale bar is 5 μ m (left image) and 2 μ m (right image). Concentration of supernatant GLP-1 determined by ELISA, in the absence (control) and presence of forskolin (FSK). The brown shaded area presents the detection threshold of GLP-1 (1 pg/ml). Forskolin induces secretion of GLP-1, confirming functionality of EECs. The experiment was performed in $n = 3$ independent experiments, and the mean concentration and SEM are depicted.

specific EEC subsets. CRISPR/Cas9 allows the targeting of endogenous loci. Subsequent repair through homology-directed-repair (HDR) or Non-homologous-end-joining (NHEJ) in turn allows for the introduction of exogenous genetic material (Bukhari and Müller, 2019; He et al., 2016; Schmid-Burgk et al., 2016). Enterochromaffin cells (ECs) are characterized by the production of the neurotransmitter serotonin. To mark ECs, we chose to label Tryptophan hydroxylase 1 (TPH1), the rate-limiting enzyme involved in the synthesis of serotonin. Using

HDR, we tagged TPH1 with fluorescent mClover separated by a self-cleaving P2A site, and selected targeted organoids using Blasticidin. Our lab has recently optimized a strategy for site-specific introduction of DNA into organoids using NHEJ, a technique termed CRISPR-HOT (Homology-independent Organoid Transgenesis) (manuscript under revision). We fluorescently labeled a series of secreted hormones as fusion proteins using this method (Fig. 2A). Cells were transfected 1) with a gRNA targeting the hormone locus near its stop codon, 2) a vector encoding mNeon or tdTomato and 3) a vector encoding Cas9, a constitutively produced mCherry fluorescent molecule and a gRNA linearizing the vector encoding the fluorescent molecule. Five days later, transfected cells were sorted for mCherry and plated as single cells. After two weeks, NEUROG3 was induced in the resulting clonal organoids to visualize expression of the fluorescent fusion hormones. Typically, the first fluorescent organoids appeared 2-3 days later and were then clonally expanded.

Applying these approaches to 10 different hormone loci, we generated a small biobank of hormone reporter organoids termed EEC-TAG, consisting of duodenal, ileal and colon organoids in which the major human hormones are marked (Fig. 2A). The organoid lines showed complete overlap between fluorescent reporters and the corresponding hormone product (Fig. 2B). The fluorescently tagged hormones localized to cytoplasmic vesicles.

Calcium signaling is one of the mediators of hormone secretion (Goldspink et al., 2018). To measure Ca²⁺ responses, we stably introduced a Turquoise Ca²⁺ sensor (Tq-Ca-FLITS) into NEUROG3^{tdTomato} TPH1^{mClover} reporter organoids using lentiviral transduction. The resulting genotype of the organoids is NEUROG3^{tdTomato} TPH1^{mClover} CaFLITS^{Turquoise}. We chose to stimulate the olfactory receptor OR51E2, of which the mouse homologue (*Olfir78*) is reported to be expressed in in mouse EECs (Fleischer et al., 2015; Jovancevic et al., 2017). After overexpression of OR51E2, HEK cells elicit a calcium response when stimulated with the selective agonist beta-ionone (Pietraszewska-Bogiel et al., 2019). *OR51E2* is most strongly upregulated in distal organoids (Fig. 2C). When reporter organoids were stimulated with beta-ionone, we observed calcium sparking in EECs that were TPH1-negative (Fig. 2D). This provided proof-of-concept that sensors combined with hormone reporters from EEC-TAG can aid the study of functional signaling responses in human EEC subtypes.

Single cell transcriptomics of human EEC subtypes.

Single cell transcriptomics presents a powerful technique to assess heterogeneity among cell populations and identifies genes specific to individual cell types (Haber et al., 2017; Parikh et al., 2019). Due to the paucity of EECs, studies in mice have utilized reporter mice to enrich for hormone-producing cells when performing single cell RNA sequencing. This approach cannot be used for primary human EECs, making the generation of a detailed atlas from small intestinal tissue challenging.

Murine EECs taken from primary tissue and from organoids are essentially identical (Gehart et al., 2019; Grün et al., 2015). We therefore exploited the human NEUROG3-induced organoids to perform single cell RNA sequencing and construct a human EEC atlas. NEUROG3 was induced in duodenal, ileal and colon organoids in the absence or presence of

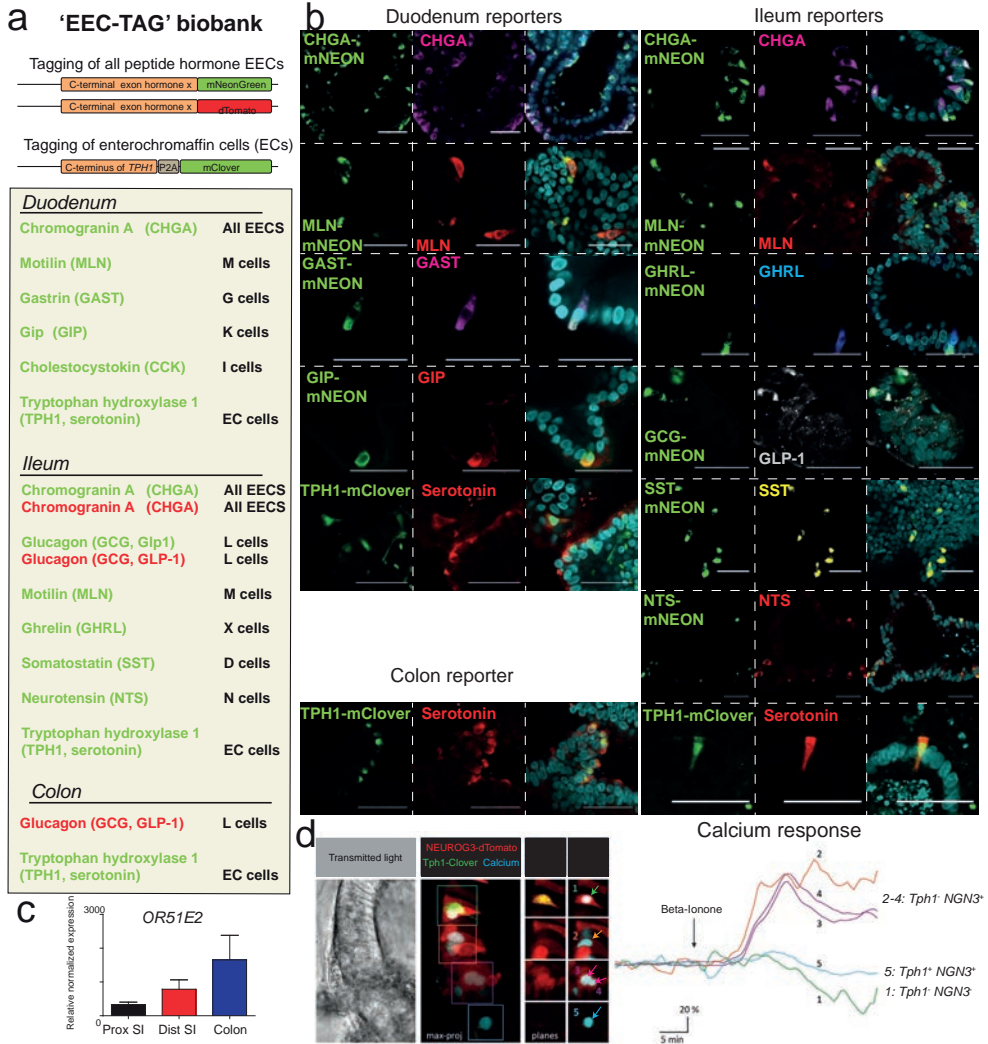


Figure 2. Generation of a human enteroendocrine cell organoid toolbox. Overview of EEC-TAG biobank comprising reporters for hormones across human duodenum, ileum and colon organoids. EECs are tagged with NHEJ (mNeon or dTomato). TPH1-positive ECs are tagged using HDR with mClover. Immunofluorescent staining confirms faithful reporter activity (knock-in left, stain middle and merge on right). Reporter expression always overlaps with the corresponding hormone. Scale bar is 50 μ m. qPCR analysis showing expression of the olfactory receptor *OR51E2* in different organoids enriched for EECs. Expressions levels are normalized to GADPH and relative to control organoids without EECs. The experiment was performed in $n=2$ independent experiments, and the mean expression and SEM are depicted. Fluorescent image of a TPH1^{mClover} NEUROG3^{dTomato} organoid that is transduced with the turquoise calcium sensor Tq-Ca-FLITS, containing a nuclear localization signal. Five examples of nuclei are highlighted of which the calcium response is followed after treatment with Beta-ionone, the agonist of OR51E2. EECs (marked in red) show increases in calcium flux ('2-4') with the exception of the TPH1⁺ cell ('1'). The non-EEC ('5') does not show calcium increases upon Beta-ionone treatment.

BMP (to generate the crypt- and villus-‘versions’ of EECs, Fig. S2). Data from a total of 8448 cells were subsequently processed by SORT-seq (Muraro et al., 2016) (Fig. S3A,B). We analyzed the transcriptome data using RaceID3, a clustering method based on k-medoids (Herman et al., 2018). After filtering (cut-off: 2000 uniquely expressed transcripts per cell), a broad intestinal cell type atlas was generated from 4281 cells (Fig. S3B). These were derived from the following sources: 1446 cells from duodenum, 2145 cells from ileum, 690 cells from colon. This atlas contained five large clusters: CHGA-positive EECs (2255), and the following well-defined ‘contaminant’ lineages: FABP1-positive enterocytes (585), OLFM4-positive stem cells (113), rare MUC2-positive goblet cells (33), LYZ/MMP7-positive Paneth cells (11), as well as several progenitor populations (Fig. S3C).

Neuropeptide W (NPW) and VGF, recently proposed as EEC hormones based on bulk RNA sequencing (Roberts et al., 2019), were broadly expressed among all EEC subtypes (Fig. S3B). While the function of VGF remains elusive, NPW is expressed in different parts of the brain. NPW increases food intake when injected in the hypothalamus (Levine et al., 2005). We confirmed protein expression of NPW by EECs in sections of human intestine by immunofluorescence (Fig. 3A).

We identified all EECs and their progenitors in the dataset by thresholding for expression of the generic EEC marker *CHGA* and thresholding against *MUC2*, *FABP1*, *LYZ* and *OLFM4*. After this, we retained 2255 cells (of which 805 cells were BMP-treated) from which we constructed an EEC atlas (Fig. 3B,C, S4A). The major clusters largely overlapped with those described in mouse, and the different EEC subtypes displayed the expected ratios related to their regional identity (Fig. S4B) (Haber et al., 2017). We contrasted our current human EEC atlas with our previously published mouse EEC atlas from tissue (Fig. S4C) (Gehart et al., 2019). Moreover, to validate the *in vitro* EEC identities, we searched for EECs in a large single cell-dataset obtained from healthy and diseased human small intestines of various ages at the Sanger Center. Of 13179 cells represented in this dataset, we derived mRNA signatures for 39 human EECs, underscoring the challenge of deriving single EEC mRNA signatures from human ileal biopsies (Fig. S4D).

The largest cluster of human EECs was formed by TPH1-expressing Enterochromaffin cells (ECs), expressing the highest levels of *CHGA* (as in mouse) and representing the most frequent EEC type *in vivo* (Fig. 3B,C). ECs occurred in three ‘flavors’: REG4^{high} and REG4^{low} cells (in cluster 4) were previously seen also in murine intestine (Haber et al., 2017). A third population of ECs, not separately observed in mice, expressed high levels of the secretogranin *SCG2* and occurred mostly in proximal SI organoid cells (cluster 9) (Fig. 3B, C). All human ECs expressed high levels of Dopa decarboxylase (*DDC*) involved in serotonin biosynthesis, as well as *SLC18A1*, involved in serotonin transport (Fig. S4E) (Lohoff et al., 2006). The prototypical EC markers *CHGB* and *GPR112* were broadly expressed by human ECs, as was the olfactory receptor *OR51E1* (mouse homologue *Olf558*), a marker of serotonin-producing neuroendocrine tumors in man (Fig. S4E) (Cui et al., 2013).

Cells producing Gastrin (*Gast*) are largely restricted to the mouse stomach, whereas in man expression continues more distally along the GI tract in EECs termed G-cells (Engelstoft et

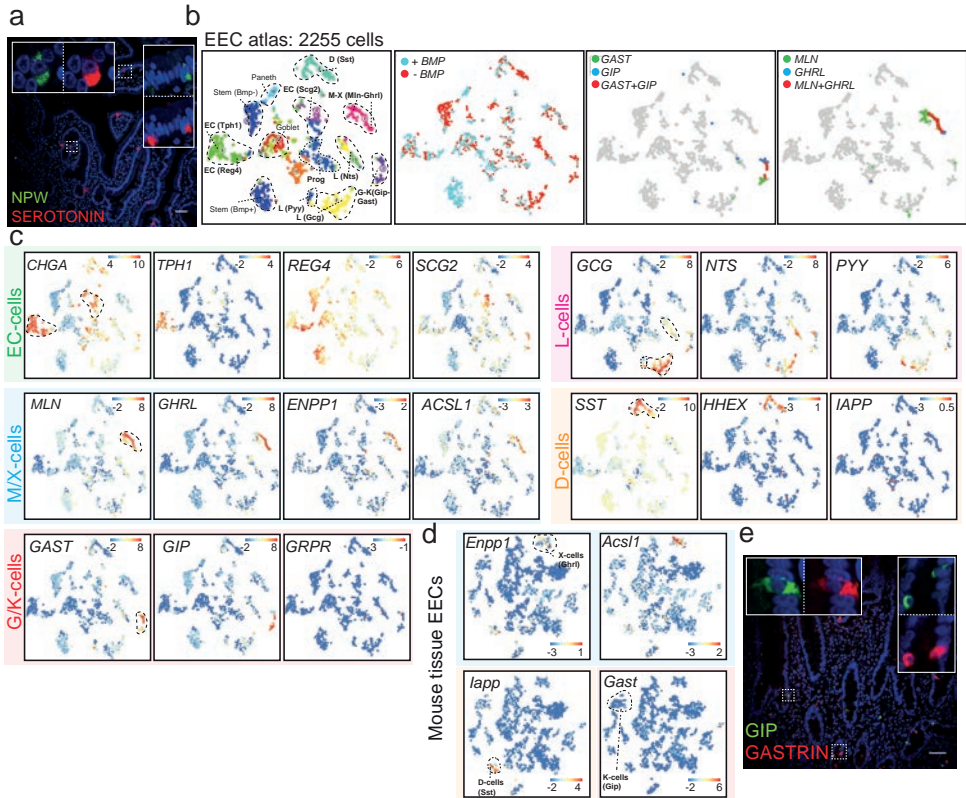


Figure 3. Single cell transcriptome atlas of human enteroendocrine cells. Immunofluorescent staining on human intestinal section (ileum) confirms EEC-specific expression of NPW. Scale bar is 50 μ m. t-SNE map displaying the human EEC atlas ($n = 2255$ cells). Different colors represent the 13 separate clusters, and BMP treated cells are highlighted. *GAST*- and *GIP*-positive cells (defined by a minimum of 25 unique transcripts per cell) show partly overlapping expression patterns (middle t-SNE map). *GHRL*- and *MLN*-positive cells (defined by a minimum of 25 unique transcripts per cell) also overlap partly (right t-SNE map). t-SNE maps displaying the expression levels of hormone and marker gene expression in the different human EEC subtypes from intestinal organoids. Bars display color-coded unique transcript expression (logarithmic scale). t-SNE maps displaying the expression levels of hormone and marker gene expression in murine tissue EECs. Bars display color-coded unique transcript expression (logarithmic scale). Immunofluorescent staining on duodenal sections confirms co-expression of *GIP* and *GASTRIN*. Scale bar is 50 μ m.

al., 2013a). Cells expressing *GAST* (cluster 3) co-expressed the receptor for Gastrin-releasing peptide, *GRPR*, a marker of G-cells in the mouse stomach (Fig. 3B,C). *GAST*-expression often overlapped with high expression of the incretin *GIP* (same cluster 3), the main hormone product of murine K-cells. We named these cells G/K-cells (Fig. 3B,C). In histological sections of the human intestine, we confirmed largely overlapping expression profiles for these two hormones (Fig. 3E). The L-cell lineage clusters 8 and 13 displayed largely overlapping expression of *GCG*, *NTS* and *PYY* (Fig. 3B, C). Cluster 2 contained *SST*-positive D-cells, also

expressing the transcription factor HHEX. HHEX has been described in murine pancreatic and intestinal Sst-producing cells (Haber et al., 2017; Zhang et al., 2014). Notably, human D-cells in tissue and organoids lacked expression of Amylin (IAPP), a peptide hormone expressed in mouse D-cells (Fig. 3B,C, S4D).

MLN+ cells do not exist in mice. We identified a clearly separated cluster of cells producing MLN and GHRL (cluster 5). A gradient from predominantly MLN- to predominantly GHRL-expressing cells can be observed in t-SNE space (Fig. 3C,D). We termed these M-X or X-M cells (based on the highest expression of either MLN or GHRL, respectively). We hypothesized that these might represent different states of the same cell type. Indeed, BMP treatment reduced levels of GHRL, while MLN levels were slightly increased (Fig. S6B)

M/X cells were further characterized by *ENPP1* expression, a known regulator of insulin responses and extracellular ATP levels (Di Paola et al., 2011), that is similarly expressed by murine X-cells (Fig. 3C,D). Ghrelin is a hormone requiring a specific acyl modification, a process shown to be dependent on the acyl-CoA synthetase *Acs1l* in mouse stomach X-cells (Bando et al., 2016). Human M/X cells and mouse intestinal X-cells both expressed high levels of this enzyme (Fig. 3C,D).

Genes uniquely expressed by human EEC subtypes.

We next searched for human EEC genes in our organoid and ileal tissue data that are not expressed by murine EECs (Fig. S4F). The heparin-binding growth factor Midkine (MDK) was broadly and highly expressed by all human EEC types, but not or lowly by other cell types such as goblet cells (Fig. 4A). While not previously seen in human EECs, it has been reported as a biomarker of human intestinal neuroendocrine tumors (Edfeldt et al., 2017). Midkine has been associated with obesity and inhibits insulin signaling in adipocytes (Fan et al., 2014). The carboxypeptidase CPB1 was produced by most EECs (highest in M/X cells), with the exception of ECs (Fig. 4A). Carboxypeptidases are typically involved in hormone processing (Sapio and Fricker, 2014). Expression of CPB1 has been observed in the rat pancreas (Yu et al., 2017). FGF14 is a human pan-EEC marker – with very limited expression in murine EECs – and belongs to a set of intracellular FGFs, that play a role in the clustering of ion channels in neurons (Fig. 4A, S4F) (Pablo and Pitta, 2017). The olfactory receptor OR51E2 was sporadically expressed by different EEC subtypes, with highest levels occurring in *PYY*⁺ cells (Fig. 4A). The mouse homologue *Olf78* on the contrary was lowly expressed in ECs only (Fig. S4F). The enzyme tryptophan 2,3-dioxygenase (*TDO2*) was found in duodenal EECs from the proximal intestine (Fig. 4A, S4A). *TDO2* can metabolize tryptophan through the kynurenine pathway and is one of the primary regulators of availability of this amino acid. Tryptophan is the precursor of serotonin and *TDO2* knockout mice experience increased serotonin levels (Too et al., 2016), suggesting that *TDO2* could be a local regulator of serotonin production in the gut. We noted the tachykinin peptide-coding *TAC3* as a broadly expressed gene in human EECs, while the mouse homologue *Tac2* is not expressed in the murine intestine (Fig. 4A). *TAC3* codes for Neurokinin B and has been described as a regulator of secretion of gonadotropin-releasing hormone in humans that is produced in the hypothalamus (Sanger, 2004). However,

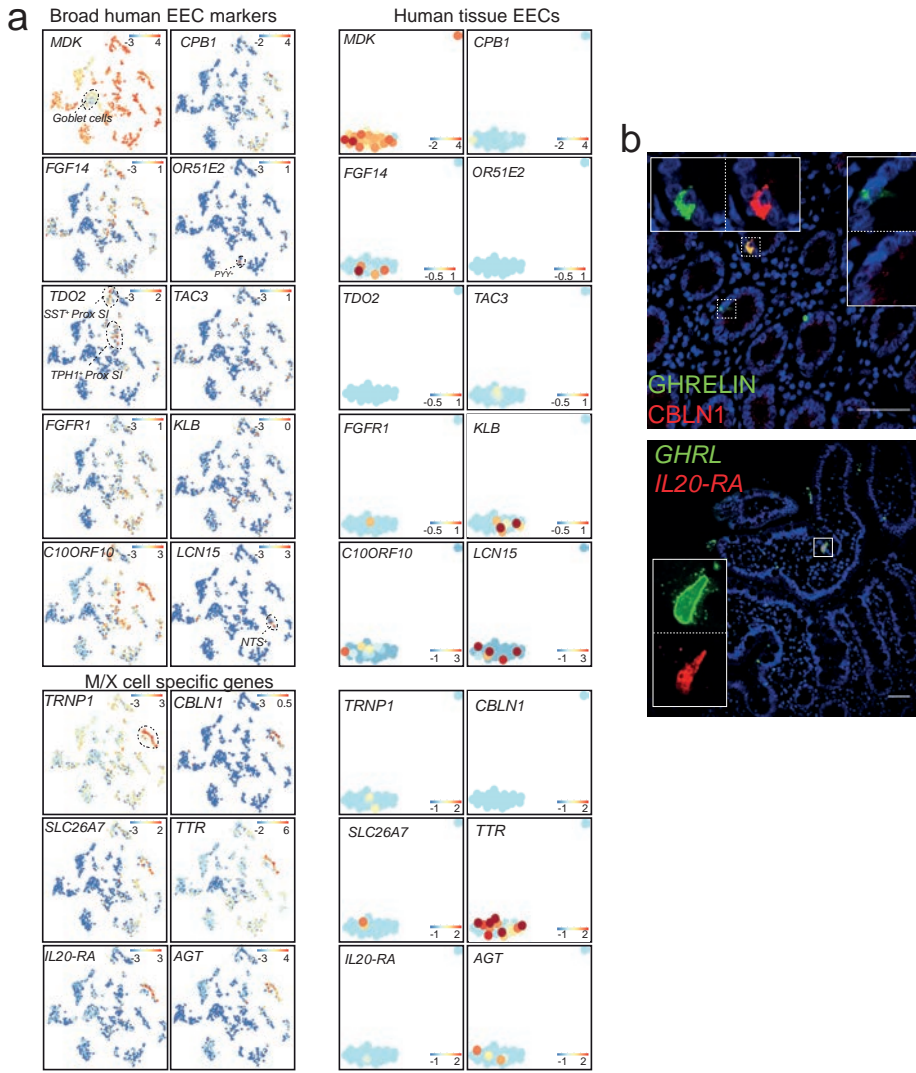


Figure 4. Novel human enteroendocrine cell markers. t-SNE maps displaying the levels of hormone and marker gene expression in the different human EEC subtypes from intestinal organoids and intestinal tissue. Bars display color-coded unique transcript expression (logarithmic scale). Immunofluorescent staining on intestinal sections confirms co-expression of GHRL and the novel EEC peptide CBLN1 (left panel). Fluorescent in situ hybridization shows that *GHRL*⁺ cells express the cytokine receptor *IL-20RA* (right panel). All sections are from the human duodenum. Scale bar is 50 μ m.

the main receptor for NKB, NK₃ (coded by *TACR3*), has been implicated in the regulation of gastrointestinal motility (Sanger, 2004). The hepatokine FGF21 has recently received much attention as a regulator of blood glucose. Several FGF21 mimetics are currently being tested for the treatment of diabetes (Kuro-o, 2019). While the receptors for FGF21 are described as a complex of FGFR1 and B-Klotho (KLB), the site of action of FGF21 is much disputed. We

observed broad expression of *FGFR1* and *KLB* by human EECs, suggesting that the *FGF21* effects could be partially mediated through the gut (Fig. 4A). *Fgfr1* is absent in murine EECs, while *Klb* is expressed at very low levels (Fig. S4F). *C10ORF10* (also known as *DEPPI*) was widely expressed by human EECs. This gene is negatively regulated by insulin in the liver and adipocyte tissue and its product controls the ratio between metabolic pathways including ketogenesis and gluconeogenesis (Li et al., 2018) (Fig. 4A). Finally, *LCN15* was produced particularly by *NTS*⁺ cells. *LCN15* is a lipocalin previously identified as one of the strongest glucose-regulated genes in Caco-2 cells (Fig. 4A) (Boztepe and Gulec, 2018). Although some lipocalins have been implicated in the development of insulin resistance, the function of *LCN15* is unknown.

Because of the absence of Motilin-expressing cells in mouse intestine, we then focused on unique genes expressed by these cells but absent in murine X-cells. *M/X* cells were positive for *TRNP1*, involved in cortical folding in the brain and the only transcription factor specific to *M/X* cells (Fig. 4A) (Stahl et al., 2013). A putative hormone, precerebellin 1 (*CBLN1*), was expressed in all *M/X* cells (Fig. 4A). *CBLN1* is known to stimulate food intake upon intracerebroventricular injection (similar to the function of Ghrelin) (Gardiner et al., 2010). We confirmed *CBLN1* expression in human *GHRL*⁺ cells *in vivo* using immunofluorescence (Fig. 4B). We noted that *M/X* cells expressed the receptor for cytokines of the IL10-family (IL20-RA), an observation confirmed *in vivo* (Fig. 4A,B). We detected high expression of the peptide hormone Angiotensin (AGT). AGT is a regulator of blood pressure, but is also described as a regulator of contraction of the musculature of human intestinal walls (similar to the gut motility-enhancing function of Motilin) (Ewert et al., 2006) (Fig. 4A). Finally, *M/X* cells displayed highest expression of all EECs of the sulfate transporter *SLC26A7* and of T₄- and Retinol-binding Transthyretin (TTR) (Fig. 4A). Although TTR is expressed by many EECs, both in mouse and human, *M/X* cells display much higher levels (Fig. 4A). We confirmed the expression of these novel EEC genes by comparison to the limited number of single cell sequenced human EECs, isolated from the ileum (Fig. 4A).

To identify heterogeneity among the different EEC subtypes, we subclustered cells sorted from organoids carrying the individual hormone reporters. Expression of the fluorescent reporters directly correlated with the levels of the pertinent hormone transcripts within the same cell (Fig. S5A). We noted that a substantial number of the cells sorted for *MLN*-reporter expression were L-cells, due to low level *MLN* expression in this population (Fig. S5A,B). Surprisingly, we identified a rare subcluster of *GCG*⁺-reporter cells that highly expressed Pancreatic Polypeptide (*PPY*) (Cox, 2007), a well-described peptide hormone from the endocrine pancreas involved in appetite regulation. This hormone has not previously been described in the context of the human or mouse small intestine, but we could confirm its expression and overlap with GLP-1 by staining on human intestinal sections (Fig. S5B,C).

Transcriptional networks in the human EEC lineages

Having established the hierarchy of human EEC subtypes and expression of novel marker genes, we analyzed expression of transcription factors known from mice to specify each of

these lineages (Fig. 5A). PAX4 specifies D/EC cells, while expression of ARX promotes all other EEC fates (Beucher et al., 2012). We accordingly detected these transcription factors in human EECs. HHEX and LMX1A defined human D and EC lineages respectively, consistent with their expression profile in mice (Fig. 5A) (Gross et al., 2016). The broad murine EEC transcription factors NKX2-2, PAX6, SOX4 and RFX6 were ubiquitously expressed in human EECs (Gehart et al., 2019). We additionally identify ASCL1 as a broad human EEC transcription factor, absent from M/X-cells and from all mouse EECs (Fig. 5A,B). *Ascl1* has been described in endocrine cells in the murine lung (Borges et al., 1997). MNX1 was highly expressed only by human ECs and is known to promote neonatal diabetes when mutated (Fig. 5A,B) (Pan et al., 2015). Together these data indicated that human EECs express key transcriptional regulators known from murine EECs, with additional expression of transcription factors described in extra-intestinal endocrine organs. *MLN*⁺ cells developmentally resembled Ghrelin-producing X-cells from mice based on their transcription factor profile.

To corroborate the role of these transcriptional networks in the generation of different human EEC subtypes, we employed CRISPR/Cas9 for loss-of-function experiments. We chose to knockout the EC-specific *LMX1A* gene and the D-cell-specific *HHEX* gene (Fig. 5A,C). Organoids were transiently transfected with a Cas9-EGFP coding plasmid that included the site-specific gRNA (Ran et al., 2013). Transfected cells were sorted and clonally expanded, after which genotyping was performed to identify homozygous loss-of-function alleles (Fig. 5D). *Lmx1a*-null mice die shortly after birth, but display intestinal loss of *Tph1* and *Chga* indicative of reduction in the enterochromaffin lineage (Gross et al., 2016). Organoids circumvent the issue of neonatal lethality for assaying gene function in adult homeostasis. Loss of *LMX1A* in human organoids led to a strong reduction in *TPH1* (Fig. 5E). Although the other EEC lineage marker genes were unaffected, we also observed a milder reduction in *SST* derived from D-cells. In contrast to mouse EECs, human *LMX1A* is expressed in D-cells as well (Fig. 5E), pointing to a potential role in their maturation or function in addition to controlling EC development.

HHEX has been linked in genome-wide association studies to the development of type 2 diabetes in humans (Scott et al., 2007). Loss of *Hhex* in mice impairs the function of Sst-producing cells in pancreatic islets, while the role in the murine intestinal tract was not investigated (Zhang et al., 2014). We found that *HHEX* gene disruption fully blocked the production of *SST*, while most other EEC lineages were increased (Fig. 5E). This could be due to progenitors differentiating towards these lineages that otherwise would have become D-cells, or because of a direct (negative) effect of *SST* on the expression of other EEC hormones. The most striking increase was observed in *GCG* expression (over 20-fold). In *Hhex*-knockout mice, pancreatic glucagon similarly increases (Zhang et al., 2014), although the products of intestinal and pancreatic Glucagon-derived peptides act oppositely on glucose homeostasis.

BMP signaling as regulator of hormone switching in human EECs

Similar to the mouse intestine, histological analysis revealed crypt-villus gradients of human hormones such as *GCG* (Fig. S6A). We interrogated BMP dependency of hormone gene expression in the single cell atlas. BMP activation induced *NTS* in L-cells at the expense of

I

II

III

IV

V

VI

VII

VIII

&

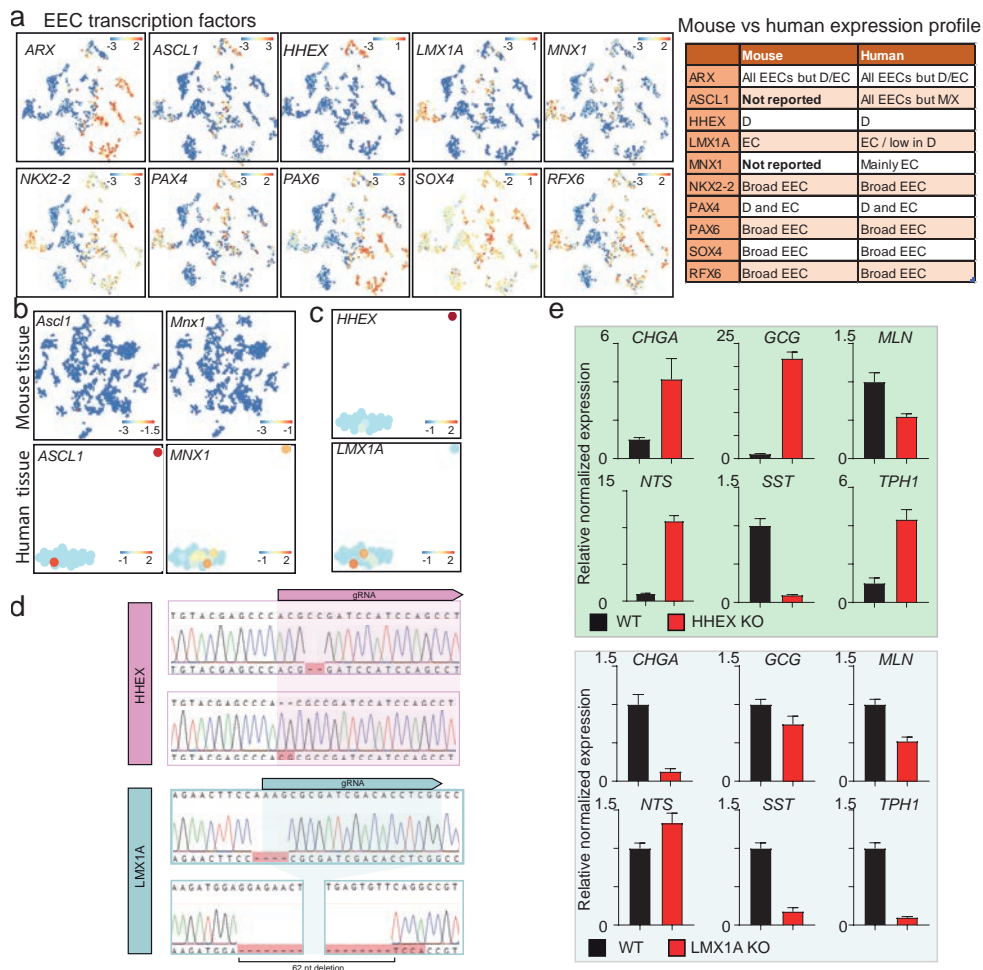


Figure 5. Transcriptional networks in human EECs. t-SNE map displaying the expression level of EEC lineage transcription factors. Bars display color-coded unique transcript expression (logarithmic scale). The murine and human patterns of expression of these genes among EEC subtypes are depicted (right table). t-SNE maps displaying the expression level of novel EEC transcription factor *ASCL1* and *MNX1* in mouse and human EECs. Bars display color-coded unique transcript expression (logarithmic scale). t-SNE maps displaying the expression level of EEC transcription factors *HHEX* and *LMX1A* in human tissue EECs. Bars display color-coded unique transcript expression (logarithmic scale). Genotyping of *LMX1A* and *HHEX* knockout organoids. qPCR analysis showing expression of hormones in wildtype organoids and *LMX1A* and *HHEX* knockout (KO) organoids. Expression is normalized to *GADPH*, and relative to wildtype. The experiment was performed as a technical duplicate, and the mean expression and SEM are depicted

GCG (Fig. S6B). Live-cell imaging of *GCG*-reporter organoids confirmed that BMP activation decreased reporter expression in individual L-cells (without causing cell death) (Fig. S6C). Additionally, we observed BMP-mediated repression of *GHRL* in M/X cells, which was

accompanied by a mild increase in *MLN* expression (Fig. S6B). In murine intestine, we have temporally resolved the differentiation process of EEC subtypes and found that expression of Ghrelin diminishes with migration of the X-cell along the crypt-villus axis (Gehart et al., 2019). This expression was not replaced by a second hormone; as said, Motilin does not exist as a coding gene in the mouse genome. Thus, human *MLN*/*GHRL*-producing EECs appeared to undergo a BMP-controlled switch in hormone expression as previously described in mouse.

High-definition transcriptomic profiling of EECs.

We next utilized our reporter organoid platform to construct ‘deep’ profiles of the EEC subtype transcriptome and proteome, as well as of their secreted products (Fig. S7A). With current technologies, transcriptomics of pooled cells has a superior sensitivity compared to single cell RNA sequencing. We exploited our reporter organoids to generate a deep transcriptomic signature of EC-, L- and M-cells. In addition, *CHGA*-mNeon⁺ cells were sorted to generate a broad EEC signature, while *CHGA*⁻ cells served as non-EEC control. We identified the top 20 uniquely expressed markers from the RNA sequencing dataset for the different EEC populations (Fig. S7B). Due to the higher sensitivity and cell number of bulk RNA sequencing compared to single cell analysis, we uncovered multiple EEC subtype features that went unnoticed in our single cell atlas. For example, the transcription factor *IRX3*, member of the Iroquois homeobox family, was one of the most defining markers of *TPH1*⁺ cells, yet has not been described in murine EECs (Haber et al., 2017) (Fig. S7B). *IRX3* has gained attention recently as a neuronal regulator of energy balance, and genetic variants in *IRX3* associate with obesity in humans (Schneeberger, 2019).

Sensory receptors of EECs, which are typically GPCRs, tend to be lowly expressed. We analyzed our bulk transcriptomic datasets for receptors enriched in subpopulations of EECs. We noted conserved expression of receptors known from mouse EECs, including *FFAR2* (broad EEC), *GPBAR1* (L-cell), *SSTR5* (L-cell), *OR51E1* (mouse homologue Olfr558; EC), *ADGRG4* (*Gpr112*; EC) and the extracellular calcium sensor *CASR* (broad EEC) (Furness et al., 2013) (Fig. S7C). Newly uncovered receptors included the following: Human EECs expressed multiple orphan receptors, such as *GPR162* (L-cells), not found in mice (Fig. S7C) and reported to be expressed in parts of the brain regulating food intake, while genetic variants in *GPR162* are linked to impairments in glucose homeostasis (Caruso et al., 2016). *GPR68* is an orphan GPCR uniquely produced by ECs (Fig. S7C). A recent study found that the orphan peptide CART (cocaine-and amphetamine-regulated protein) can activate *GPR68* (Foster et al., 2019). Multiple sources are suggested for CART, including the brain and EECs, and the peptide has a role in the regulation of anxiety, reward and feeding behaviors (Shcherbina et al., 2018). GABA-A receptors have been reported in some murine EECs, but we find expression of the subunit of the GABA-B receptor *GABBR2* broadly among EECs, potentially allowing these cells to respond to GABA (Fig. S7C) (Hyland and Cryan, 2010). We identified production of multiple hormone receptors in EECs, including the melanocortin receptor *MC1R* (Fig. S7C). *MC4R* has been described in murine L-cells as a regulator of hormone secretion that can

I

II

III

IV

V

VI

VII

VIII

&

be exploited by enriching the microbiome with MSH-like producing bacteria (Panaro et al., 2014). ECs selectively expressed the receptor for the thyroid-stimulating-hormone, *TSHR*, not observed before (Fig. S7C). Serotonin is known to regulate the levels of circulating thyroid hormones (Sullo et al., 2011), and expression of *TSHR* in ECs suggests that this regulation could work bidirectionally. ECs also expressed the receptor for the L-cell hormone PYY, *NPY1R* (Fig. S7C), reported in murine enterocytes as a regulator of electrolyte transport (Goldspink et al., 2018). We did not confirm expression of *NPY1R* in the CHGA-mNeon⁺ population, enriched for human non-EECs which includes enterocytes. L-cells highly expressed the Secretin receptor *SCTR* that we also observed in our single cell atlas, but was not seen in mice (Fig. S7C, S8A). Fluorescent in-situ-hybridization (FISH) confirmed the expression of *SCTR* in EECs *in vivo* by overlap with *CHGA* (Fig. S8B). Since we observed the highest expression of *SCTR* in L-cells, we measured GLP-1 secretion upon a 24-hour secretin treatment in organoids. Indeed, secretin induced GLP-1 secretion at levels comparable to forskolin as measured by ELISA, or as observed by the loss of intracellular fluorescence of GCG-neon (Fig. S8C-E).

Proteomic profiling of EECs

We next isolated intracellular proteins and performed mass-spectrometry to establish EEC subtype-specific proteomes (Fig. S7A). PCA-analysis revealed a clear separation of the different reporter populations on the proteome level. Of note, MLN and GCG displayed considerable overlap due to low *MLN* expression in GCG⁺ cells (as discussed above) (Fig. S9A). The analysis confirmed many of the novel markers for EEC populations at the protein level, including the L-cell hormone PYY, the broad EEC marker MIDKINE and the M-cell produced peptidase CPB1 (Fig. S9B). A highly expressed marker identified at RNA level but completely lacking in the proteome was *CRYBA2*, a structural lens protein and member of the crystallin family (Fig. S9C). *CRYBA2* recently gained attention as a novel marker of human endocrine cells (not of mouse) in the pancreas and colon (Muraro et al., 2016; Parikh et al., 2019). We could also not identify *CRYBA2* on human intestinal sections using IHC (Fig. S9D). In the human genome, *CRYBA2* is located adjacent to another important EEC marker gene that is well-established, *FEV* (Haber et al., 2017). *CRYBA2* and *FEV* RNAs were expressed in a virtually identical pattern in our single cell atlas (Fig. S9C). We speculate that *CRYBA2* mRNA expression is a consequence of open chromatin related to transcriptional activity of *FEV*.

The human EEC secretome

The human EEC organoid cultures uniquely allow proteomic analysis of secreted products. EEC hormones are secreted basolaterally, i.e. towards the outside of the organoids. We isolated supernatants of EEC organoids stimulated with Forskolin. Supernatants were separated in a fraction larger than 10kDa (representing among others unprocessed hormones) and a fraction smaller than 10kDa (representing processed endogenous hormones). The latter was directly analyzed using LC-MS, whereas the former was subjected to tryptic digestion prior to LC-MS analysis. Analyses were performed on the secretomes of both proximal and distal small intestinal organoids, representing the most prominent peptide hormone producers.

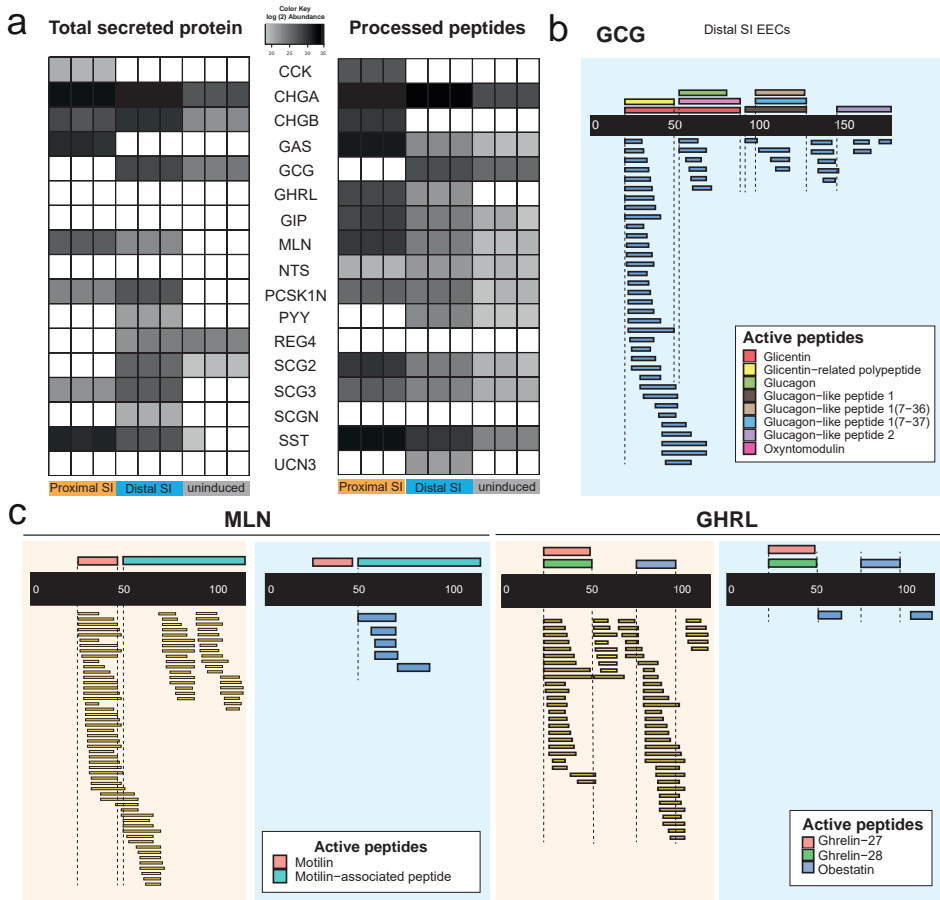


Figure 6. Processing of known region-specific human EEC secreted products. Overview of abundances of peptides in the secretome of proximal SI and distal SI organoids enriched for EECs, or uninduced distal organoids lacking EECs. Abundances of the total secreted proteins (>10kDa, left table) or the processed peptides (<10 kDa, right table) are shown. Measured peptides (<10 kDa) in the supernatant of distal SI organoids mapping to the preproglucagon hormone are shown below the black bar. Known bioactive peptides are shown above the black bar. Measured peptides (<10 kDa) in the supernatant mapping to different secreted prehormones (MLN and GHRL) are shown below the black bar. Data from proximal (yellow background) and distal SI organoid (blue background) supernatants are displayed. Known bioactive peptides are shown above the black bar.

We observed secretion of all known hormones, with a bias for the regional hormones in the supernatants of region-corresponding organoids (Fig. 6A, S10). Notably, endogenously processed peptides were mostly found for those hormones that are known to generate biologically active sequences upon proteolytic processing (e.g., REG4, for which the full-length product is biologically active, was only found in the fraction larger than 10kDa). Intracellular EEC markers with highest abundance in the whole cell-proteome datasets, such as the enzyme TPH1 or highly abundant proteins like histones or actin, were not observed in the supernatant,

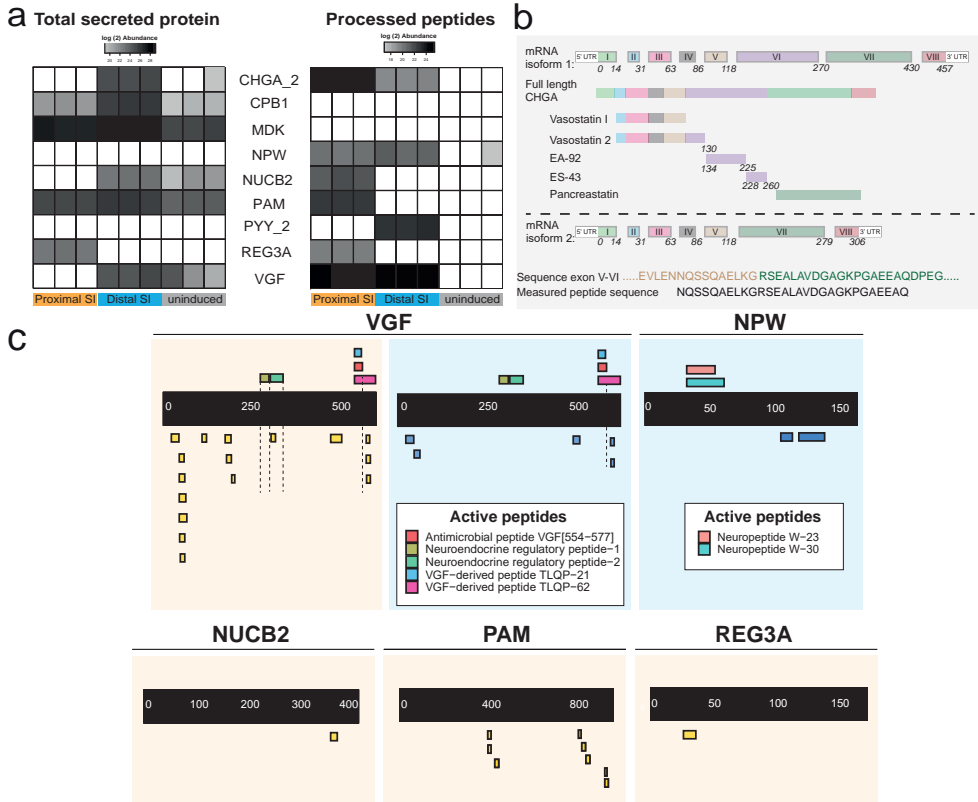


Figure 7. Novel secreted products from human EECs. Overview of abundances of novel intestinal peptides in the secretome of proximal SI and distal SI organoids enriched for EECs, or uninduced distal organoids lacking EECs. Abundances of the total secreted proteins (>10kDa, left table) or the processed peptides (<10 kDa, right table) are shown. Overview of processing of the known isoform 1 of CHROMOGRANIN A (CHGA). Isoform 2 of CHGA (lower panel) lacks exon VI. Peptides in the supernatant are measured that contain both sequences from exon V and VII, indicating isoform 2 is produced in human EECs. Measured peptides (<10 kDa) in the secretome mapping to different hormones or secreted factors are shown below the black bar. Data from proximal (yellow background) and distal SI organoid (blue background) supernatants are displayed. Known bioactive peptides are shown above the black bar.

confirming specific detection of secreted proteins. CHGA was the highest expressed protein in the proteome dataset, and accordingly was the most abundant peptide in both proximal and distal EEC organoid supernatants. Processed peptides smaller than <10kDa generally displayed C-terminal trimming, likely due to the endogenous activity of carboxypeptidases (Fig. 6B,C S10). We observed all known fragments of the proglucagon pro-hormone (Fig. 6B). Individual fragments rarely spanned more than a single biologically active peptide (e.g. a fragment containing both GLP1- and GLP-2), implying that endogenous processing occurred efficiently. Neuronostatin, a recently discovered fragment of the pro-somatostatin hormone, was also found abundantly in the EEC secretome (Fig. S10) (Vainio et al., 2012).

The supernatant peptides were biased towards bioactive fragments of multiple hormones and enzymes, including for PCSK1N and GHRL (Fig. 6C,S10). The signal peptide (20-25 N-terminal amino acids of the prohormones) was consistently cleaved from all hormones (Fig. 6B,C, S10). Apart from quantitative differences, we also detected region-specific biases in the ratio between bioactive peptides and those with no known activity. For example, in duodenal organoids we found an overrepresentation for the bioactive peptides of GHRL and MLN (proximal-enriched hormones).

Next, we looked for secreted peptides not attributed to EECs before. CHGA codes for a 457-amino acid preproprotein that is cleaved into many different bioactive products. A shorter second isoform is predicted that would lack exon 6 and multiple peptide products (Vasostatin 2, EA-92, and ES-43) but has not been shown to be coding (Loh et al., 2012). We now find abundant peptides spanning terminal sequences of exon 5 and exon 7, suggesting this isoform is translated in human EECs (Fig. 7A, B). Intriguingly, we also detected secretion of a range of other previously unknown EEC products consistent with the observed RNA expression (Fig. 4A, S7). These include NPW, MIDKINE, VGF, and the peptidase CPB1, providing further evidence that these could act as hormones or affect hormone processing (Fig. 7A, C). Mouse EECs express REG4; we found expression and secretion of the antimicrobial peptide REG3A from human EECs (Fig. 7A,C, S7) (Grün et al., 2015). We further identified EEC-specific secretion of the enzyme PAM (Peptidyl-glycine alpha-amidating monooxygenase), known to modify endocrine peptides by C-terminal amidation, important for their activation (Fig. 7A, C). Coding variants of PAM have been associated with type 2 diabetes risk and can affect insulin secretion (Thomsen et al., 2018). We detected the Nucleobindin-2 (NUC2B) precursor, that is processed to the neuropeptides Nesfatin-1, 2 and 3 (Ramesh et al., 2015). Nesfatin-1 has recently gained attention as an anorexigenic and insulinotropic peptide, produced in the hypothalamus and pancreas. Nesfatin-1 has been shown to regulate GLP-1 and GIP secretion *in vitro* (Ramesh et al., 2015).

DISCUSSION

Human EECs are rare and have been largely inaccessible for *in vitro* studies. Yet, they hold great promise as central players in the treatment of metabolic diseases. Our study provides an organoid-based toolbox to address a diversity of questions on human EEC biology. We have generated a high-resolution transcriptomic and proteomic profile of human EECs from three locations along the gastrointestinal tract, including a first assessment of their secreted products. This dataset yields new hormones, transcription factors and receptors, and can be mined for novel therapeutic targets. The expression atlas highlights key differences with murine counterparts, stressing the importance of performing studies on EEC function in a human model system. Since fusions of hormones and fluorescent proteins retain the ability to be secreted, we envision EEC-TAG organoids to be used in studies aimed at identifying specific inducers of hormone secretion, or of controlling differentiation of individual EEC subtypes.

I

II

III

IV

V

VI

VII

VIII

&

The transcriptional networks generating the different EEC subtypes have been well worked out in mice (Beucher et al., 2012; Gehart et al., 2019; Gross et al., 2016; Piccand et al., 2019). These networks could result from a stochastically acting system that generates fixed ratios of different EECs. This would explain why organoids generate rather conserved ratios of individual subtypes when compared to their tissue of origin, even in the absence of mesenchymal and luminal factors (Beumer et al., 2018). We have shown previously that BMP signaling regulates differential hormone expression within the same EEC subtype, an observation that is extended here for the hormone pair Ghrelin/Motilin (Figure S6). Inhibition of Wnt signaling before the induced expression of *NEUROG3* caused a dramatic shift in EEC distribution from *GLP1⁺* L-cells to *MLN⁺* M-X-cells (Figure S1), demonstrating that the ratio of EEC subtypes can be influenced by stem cell niche factors. It remains unknown why L-cells would preferentially be specified within the *Wnt^{high}* stem cell zone; evidence suggest that their secreted GLP-2 is involved in the regulation of intestinal proliferation and crypt fission (Drucker et al., 1996).

A recent study has surveyed broad human EEC population using antibody-based sorting approaches and bulk RNA sequencing on human patient material (Roberts et al., 2019). This study identified some novel EEC features, such as the expression of Neuropeptide W, confirmed by the current human EEC atlas built from organoids.

We present the first transcriptomic and proteomic profiling of Motilin-producing cells. Motilin is a regulator of gut motility that displayed intriguing evolutionary dynamics, being inactivated independently in lineages leading to the mouse and rat, and guinea pigs (He et al., 2010). The Motilin receptor underwent a similar fate (He et al., 2010). This raises questions as to how the cell type (the X-cell) that produces Motilin diverged from that point. For example, the production of a certain hormone is likely to be accompanied by the expression of receptors that are sensing stimuli associated with this product. We found many similarities between mouse X-cells and the human counterparts, that we termed M-X cells. The developmental transcription factors are similar to mice (Fig. 5A), while the expression of genes required for Ghrelin modifications such as *Acs11* are conserved (Fig. 3C-D). We noted important differences also; among these the expression of putative hormones including *CBLN1* and *AGT*. The latter has been proposed – apart from controlling blood pressure - as motility regulator similar to Motilin (Fig. 4). We also identify a cytokine receptor in M-X cells, *IL-20RA*, which could link a sensory mechanism for pathogens to a motility response expelling such infection. Of note, irritable bowel syndrome (IBS), characterized by alterations in gut motility, is associated with a reduction in the *IL20RA*-ligand *IL-10*, potentially mediated through M-X cells (Gonsalkorale et al., 2003).

While transthyretin (*TTR*) has been identified in multiple EEC populations, we identify very high levels in M/X cells (Fig. 4A). A *TTR* mutation underlies the most common form of amyloidosis, characterized by cardiomyopathy and cardiac failure, but also destruction of enteric neurons and associated problems in gastrointestinal motility (Ueda and Ando, 2014). Of interest, gastrointestinal motility problems are partly relieved by Motilin agonists. Although the liver is suspected as the principle source of amyloid *TTR*, our results indicate that local, M/X-cell produced *TTR* may play a role in pathogenesis.

The expression of receptors for some EEC hormones by EECs has been reported in mouse, particularly for Somatostatin (e.g. *Sstr5* in L-cells) (Chisholm and Greenberg, 2002). We now find that human EECs can also sense extracellular PYY (NPY1R) and Secretin (SCTR). The PYY-receptor *Npy1r* has been suggested as an enterocyte marker in mouse, a finding we do not confirm (Goldspink et al., 2018).. Rather, we observe exclusive expression in human Serotonin-producing ECs. *SCTR* expression is low in ECs and enriched in EECs producing *GCG* and *GAST/GIP*. We show that Secretin can stimulate L-cells to secrete GLP-1. Importantly, a Secretin stimulation test is commonly used in diagnostics of Zollinger-Ellison syndrome patients that suffer from gastrin-producing tumors (Berna et al., 2006). Secretin normally represses blood gastrin by inhibiting the secretion of gastrin from the stomach G-cells (the major site of Gastrin production), likely through modulating the luminal pH. Patients suffering from small intestinal gastrinoma however show sharp increases in serum gastrin upon secretin administration. Our data suggest this to occur through the broad SCTR-expression among small intestinal gastrin-producing G-cells. More broadly, our data indicate that human EECs have an extensive capacity to cross-communicate through their hormone products. Taken together, the EEC atlas and EEC-TAG biobank represent rich resources to identify regulators of human EEC development and function.

METHODS

Cell culture of human intestinal organoids

Tissues from the human duodenum, ileum and colon were obtained from the UMC Utrecht with informed consent of each patient. The patients were diagnosed with small intestinal or colon adenocarcinoma that was resected. A sample from non-transformed, normal mucosa was taken for this study. The study was approved by the UMC Utrecht (Utrecht, The Netherlands) ethical committee and was in accordance with the Declaration of Helsinki and according to Dutch law. This study is compliant with all relevant ethical regulations regarding research involving human participants. Human small intestinal cells were isolated, processed and cultured as described previously (Beumer et al., 2018; Sato et al., 2011)

For differentiation towards EECs, organoids were treated with 1 µg/ml doxycycline (Sigma) in 'ENR' medium (Sato et al., 2009). Secretin (Tocris) was used at a concentration of 10 µg/ml. Beta-ionone (Sigma) was used at 100 mg/ml. BMP activation was achieved by withdrawing Noggin from 'ENR' and addition of BMP-2 (Peprotech, 50ng/ml) and BMP-4 (Peprotech, 50ng/ml). Notch signaling was inhibited by treatment with the Gamma-secretase inhibitor DAPT (Sigma, 10µM). Wnt inhibition was performed by treatment with the Porcupine inhibitor IWP-2 (Stemgent, 5µM)

Constructs for EEC-TAG reporter and knockout generation

The *NEUROG3* was cloned in a two insert Gibson reaction into BSKS II vector. Of note, two PCR reactions were done: first, *NEUROG3* was amplified from human genomic DNA, since the entire coding region lies in one exon. Second, the BSKS vector was amplified. The forward

I

II

III

IV

V

VI

VII

VIII

&

and reverse primers for Gly linker, FLAG, HA and P2A sequence were annealing to each other (Supplementary Table 1). All three DNA fragments were then combined in BSKS-NEUROG3-Flag-HA-P2A. In the next step, NEUROG3-P2A sequence was excised using EcoRI enzyme and cloned into previously published pLX-NS2 vector (Sachs et al., 2019). Organoids were lentivirally transduced as described before (Koo et al., 2012).

For generation of the reporter organoid lines using CRISPR-HOT, we utilized a method described in (Artegiani, Hendriks et al., under revision). Briefly, we used a targeting plasmid containing a fluorescent protein (mNEON or tdTomato) which can be linearized at a defined base position by a specific sgRNA and Cas9 provided from a second plasmid, which also encodes mCherry (Schmid-Burgk et al., 2016). These two plasmids are co-electroporated with a plasmid encoding the sgRNA for the respective locus (Supplementary table 1).

The HDR donor plasmid allows C-terminal knock-in of the fluorescent reporter mClover3 in the *TPH1* locus and was generated using pUC118 as a backbone. First, the endogenous SapI site in pUC118 was inactivated. Then, a selection cassette (PGK promoter driven expression of blasticidin) flanked by LoxP and two SapI sites was cloned into the SapI-inactivated pUC118 using infusion cloning (638910, Takara). Subsequently, a P2A sequence and the fluorescent protein mClover3 was PCR amplified (Phusion High fidelity DNA polymerase, M0530S, NEB) from the Addgene plasmid #74252 and cloned upstream of the selection cassette using infusion cloning (638910, Takara) and NotI (R0189S, NEB) digestion of the pUC118 selection-cassette containing plasmid. Next, homology arms corresponding to the genomic regions, approximately 1000bp, upstream and downstream of the *TPH1* stop codon were PCR amplified (Phusion High fidelity DNA polymerase, M0530S, NEB) from genomic DNA (extracted and purified from human small intestinal organoid DNA). The PCR primers contained overhangs allowing subsequent Golden Gate cloning (Supplementary Table 1).

The PCR amplified homology arms were purified (QIAquick PCR Purification Kit, 28104, Qiagen) and finally, the targeting vector was generated by SapI (R0569S, NEB) mediated Golden Gate insertion of the homology arms into the pUC118 selection-cassette containing plasmid.

The sgRNA was selected based on the WTSI website (<https://www.sanger.ac.uk/htgt/wge/>) and chosen as close to the *TPH1* stop codon as possible. The gRNA sequence overlapped with the stop codon, so that the homology vector was not cut. The target sequence was ordered as two complementary oligos (IDT) and cloned in the Cas9-EGFP vector (addgene plasmid #48138) following the protocol described before (Ran et al., 2013).

For the generation of *HHEX* and *LMX1A* knockout organoids, gRNAs were selected using the WTSI website and cloned in the Cas9-EGFP vector (addgene plasmid #48138) following the protocol described before (Ran et al., 2013). gRNAs used in this story are presented in Supplementary Table 1.

Human intestinal organoids were transiently transfected using a NEPA21 electroporator and a previously developed protocol (Fujii et al., 2015). 3-7 days after electroporation, either mCherry (for generation of NHEJ-mediated reporter organoids) or EGFP (for generation of *HHEX* and *LMX1A* knockout lines) positive cells were sorted using a FACS-ARIA (BD Biosciences). Wnt-surrogate (0.15 nM, U-Protein Expression) and Rho kinase inhibitor (10 μ M,

Calbiochem) were added to the culture medium up to 1 week after sorting to enhance single cell outgrowth. All reporter organoids were generated in organoid lines also transduced with *NEUROG3*-overexpression (with or without dTomato) vector.

To confirm correct integration of mNeon/dTomato reporter into the hormone locus, organoids grown from mCherry-positive cells were differentiated towards EECs using overexpression of *NEUROG3*. Organoids where fluorescent cells appeared during EEC differentiation were picked, digested using TrypLE (TrypLE Express; Life Technologies) and clonally expanded to establish stable knock-in organoid lines.

Organoids grown from Cas9-EGFP transfected cells were genotyped for *HHEX* and *LMX1A* to confirm homozygous frameshift mutation (primers in Supplementary Table 1).

Calcium sensor

A red calcium probe (pTorPE-R-GECO1, addgene plasmid #32465) was used as a template to engineer a cyan genetically encoded calcium probe. The cpApple was replaced with a circular permuted mTurquoise. The resulting probe was dubbed Tq-Ca-FLITS (Turquoise Calcium Fluorescence Lifetime Indicator for Truthful Sensing). A triple nuclear localization signal (3xnlS) was added to the N-terminus of the calcium probe to simplify analysis. Details of the engineering and characterization will be described elsewhere (Van der Linden et al., in preparation).

PCRs were performed on Tq-Ca-FLITS (Fw AAACAAGCGGGAGACGTGGAGGAAAAC CCTGGACCTCTCGAGatgggatcagatccaaaaagaagag, Rev ATGGCACTAGGCTAGTTCTAG AcCTACTTCGCTGTCATCATTTGGAC) as well as H2B-mMaroon (Fw TCGGCGCGC CACGCGT, Rev CGTCTCCCGCTTGTTCAGTAGACTAAAATTCGTCGCGCCAGATCCGC TAGCattaagttgtgcccc) and the two PCRs were cloned into a lentiviral vector using InPhusion Cloning (Takara), to produce H2B-mMaroon-P2A-Tq-Ca-FLITS, two simultaneously expressed cistrons separated by a de-optimized P2A (Lo et al., 2015).

Live cell imaging of calcium reporter organoids

H2B-mMaroon-P2A-Tq-Ca-FLITS organoids were imaged on a Leica SP8 confocal laser scanning microscope, equipped with Argon laser and White Light Laser, the latter allowing spectral flexibility for optimal visualization of all fluorophores. For cell type identification, cells were first imaged in 5 channels (Tq-Ca-FLITS-mTurquoise2, Clover, TdTomato, H2B-Maroon and transmitted light) and subsequently Tq-Ca-FLITS and H2B-mMaroon were time lapse imaged during administration of beta-ionone in XYZT-mode. Post-acquisitional analysis was done with custom-made Fiji-script.

Transmission electron microscopy

Organoids were fixed with 1.5% glutaraldehyde in 0.1M cacodylate buffer. They were kept in the fixative for 24 h at 4°C. Then, they were washed with 0.1M cacodylate buffer and postfixated with 1% osmium tetroxide in the same buffer containing 1.5% potassium ferricyanide for 1

I

II

III

IV

V

VI

VII

VIII

&

hour (dark) at 4°C. Then the samples were dehydrated in ethanol, infiltrated with Epon resin for 2 days, embedded in the same resin and polymerised at 60°C for 48 hours. Ultrathin sections were obtained using a Leica Ultracut UCT ultramicrotome (Leica Microsystems, Vienna) and mounted on Formvar-coated copper grids. They were stained with 2% uranyl acetate in water and lead citrate. Then, sections were observed in a Tecnai T12 electron microscope equipped with an Eagle 4kx4k CCD camera (Thermo Fisher Scientific, The Netherlands).

Alternatively, organoids were chemically fixed at 4 °C with a mixture of 2% paraformaldehyde and 0.2% glutaraldehyde in PB buffer. After washing with PB containing 50 mM glycine, cells were embedding in 12% gelatine and infused in 2.3 M sucrose. Mounted gelatine blocks were frozen in liquid nitrogen. Thin sections were prepared in an ultracryomicrotome (Leica EM Ultracut UC6/FC6, Leica Microsystems, Vienna, Austria). Ultrathin cryosections were collected with 2% methylcellulose in 2.3 M sucrose. The observations were performed in an Electron Microscope Tecnai T12 as mentioned.

Immunostaining

Organoids were stained as described before (Beumer et al., 2018). Primary antibodies used were goat anti-chromogranin A (1:500; Santa Cruz), goat anti-cholecystokinin (sc-21617, 1:100; Santa Cruz), rabbit anti-neurotensin (sc-20806, 1:100; Santa Cruz), goat anti-somatostatin (sc-7819, 1:100; Santa Cruz), goat anti-serotonin (ab66047, 1:1,000, Abcam), rabbit anti-gastric inhibitory polypeptide (ab22624-50, 1:500; Abcam), goat anti-GLP1 (sc-7782, 1:100; Santa Cruz), rabbit anti-GLP1 (ab22625, 1:200; Abcam), rabbit anti-MLN (HPA069392, 1:200, Atlas antibodies), mouse anti-Gastrin (60346, 1:200, Proteintech), mouse anti beta-Catenin (610154, 1:100; BD transduction laboratories), goat anti-Ghrelin (sc-10368, 1:200; Santa Cruz), rabbit anti-Neuropeptide W (NBP2-57337, 1:100; Novus), rabbit anti-Precerebellin (ABN304, 1:100; Sigma) and rabbit anti-PPY (HPA032122, 1:200; Atlas antibodies). Organoids were incubated with the corresponding secondary antibodies Alexa488-, 568- and 647-conjugated anti-rabbit and anti-goat (1:1,000; Molecular Probes) in blocking buffer containing 4',6-diamidino-2-phenylindole (DAPI; 1;1,000, Invitrogen). Sections were embedded in Vectashield (Vector Labs) and imaged using a Sp8 confocal microscope (Leica). Image analysis was performed using ImageJ software.

Fluorescent in situ hybridization

FISH was performed using the RNAScope® Multiplex Fluorescent Reagent Kit v2 (Advanced Cell Diagnostics) according to the manufacturer's protocol (Wang et al., 2012). In brief, paraffin embedded ileal surgical sections were deparaffinized, treated with hydrogen peroxide for 10 minutes and boiled in target retrieval buffer for 15 minutes before a 30-minute protease treatment. Probes directed against *CHGA/SCTR*, *CHGA/GCG* and *GHRL/ IL20RA* were multiplexed, respectively, amplified and detected using fluorescent probes based on opal dyes. Slides were counterstained with DAPI for 30 seconds, mounted using ProLong™ Gold Antifade Mountant (Thermo Fisher scientific) and images were obtained using a SP8 confocal fluorescent microscope (Leica).

ELISA

The supernatant from organoids either cultured in ENR for 5 days or differentiated towards EECs were collected after a 24-hour stimulation with 10 μ M Forskolin (Tocris). GLP-1 concentration was measured using a GLP-1 EIA kit (Rab0201 from Sigma that detects both full-length and N-terminal cleaved GLP-1) following the manufacturer's protocol,

RNA isolation and quantitative PCR

Organoid RNA was isolated using a RNeasy kit (QIAGEN), following the manufacturer's protocol. Quantitative PCR (qPCR) analysis was performed using biological and technical duplicates as described described before (Muñoz et al., 2012). Primers were designed using the NCBI primer design tool, tested using a standard curve, and are presented in Supplementary Table 1.

Processing human intestinal tissue for single cell RNA sequencing

Human intestinal mucosal biopsies were obtained from patients undergoing colonoscopy at Addenbrooke's Hospital, Cambridge, UK. All patients gave informed consent for extra biopsy samples to be taken for research use when undergoing elective colonoscopy (REC 17/EE/0265). Only those patients with a macroscopically normal mucosa and subsequent histological confirmation of a normal mucosa with no intestinal pathology were included in this study.

Once acquired, biopsies were immediately placed into Hanks Buffered Saline Solution (HBSS) and washed three times in fresh HBSS. Biopsies were then placed into an HBSS solution containing 1.07 Wunsch units/ml Liberase DH (Roche) and 70 U/ml hyaluronidase (Merck) and incubated at 37°C for 15 minutes whilst on a plate shaker at 750 rpm. The samples were then mechanically disrupted by pipetting the solution up and down using a p1000 pipette, and then incubated at 37°C for a further 15 minutes on a plate-shaker at 750rpm. The samples were then washed three times by pelleting the cells using centrifugation at 400g for 4 minutes, removal of the supernatant and resuspending in DMEM/F12 (Thermofisher). On the third wash the cells were left in suspension, and a 10 μ L aliquot was placed into a Countess[®] Automated Cell Counter to estimate the cellular concentration.

3,000 cells suspended in DMEM/F12 (Thermofisher) were loaded into a individual channels of a 10x single cell chip as per the manufacturer's protocol (version 2, 3') and run in standard conditions by the chromium controller (10X genomics). cDNA libraries were prepared according to the manufacturer's protocol and sequenced on an Illumina Hi-seq 4000 (2x50bp paired-end reads).

For aligning the reads, cellrangerV2 and transcriptome GRCh38-1.2.0 were used. Scanpy v1.4 was used for clustering. Cells from the whole dataset (13179 cells) with less than 200 genes and genes in less than 3 cells were excluded. EECs were identified based on the expression of at least 10 CHGA counts per cell.

I

II

III

IV

V

VI

VII

VIII

&

Single cell sorting for RNA sequencing from organoids

Organoids were dissociated to single cells using a 10-minute incubation with TrypLE (TrypLE Express; Life Technologies) and repeated mechanical disruption through pipetting. Cells were sorted using a BD FACS Aria (BD Biosciences) based on fluorescence levels. For single cell RNA sequencing, individual cells were collected in 384-well plates with ERCC spike-ins (Agilent), reverse transcription primers and dNTPs (both Promega). Single cell sequencing was performed according to the Sort-seq method (Muraro et al., 2016). Sequencing libraries were generated with TruSeq small RNA primers (Illumina) and sequenced paired-end at 60 and 26 bp read length, respectively, on the Illumina NextSeq.

For bulk RNA sequencing, cells were sorted into Eppendorf tubes containing RLT buffer (RNeasy kit, QIAGEN). 5,000 – 30,000 cells were sorted per reporter in duplicates (and triplicates for tdTomato negative cells). RNA was extracted using the RNeasy mini kit (QIAGEN) following the manufacturer's instructions. Sequencing libraries were generated using a modified CELseq2 protocol (Hashimshony et al., 2016). 75 bp paired-end sequencing of libraries was performed on an Illumina NextSeq platform.

Single cell RNA sequencing analysis from organoids

Reads were mapped to the human GRCh37 genome assembly. Sort-seq read counts were filtered to exclude reads with identical library-, cell- and molecule barcodes. UMI counts were adjusted using Poisson counting statistics (Muraro et al., 2016). Cells with fewer than 2,000 unique transcripts were excluded from further analysis.

Subsequently, RaceID3 was used for k-medoids based clustering ($knn = 10$) of cells and differential gene expression analysis between clusters using the standard settings described at https://github.com/dgrun/RaceID3_StemID2_package.

The dataset was then subsetted to require expression of EEC markers and exclude cells based on expression of markers of other cell types with the following transcript count cutoffs: CHGA > 5; MUC2 < 5; FABP1 < 15; LYZ < 15; OLFM4 < 10. The resulting set of EECs was again subjected to clustering ($knn = 5$) and differential gene expression as described above.

For reporter analyses, cells sorted by fluorescent reporter positivity were analyzed as one dataset per reporter to gain more detailed insights into single EEC subpopulations. The following deviations from standard settings were made per reporter: GCG: $knn = 5$; outlg = 1; probthr = 0.00001; perplexity = 10; MLN: $knn = 10$; probthr = 0.0000001; SST: $knn = 10$; perplexity = 20

For mouse validation, the tissue-derived single cell count tables from Gehart et al. (2019) were reanalyzed using the procedure and settings described above. No subsetting for EECs was performed.

Bulk RNA sequencing analysis

Reads were mapped to the human GRCh37 genome assembly. The counted reads were filtered to exclude reads with identical library- and molecule barcodes. Differential gene expression analysis was performed using the DESeq2 package (Love et al., 2014). For display in heatmaps,

genes were ranked by fold change compared against tdTomato negative cells. After filtering for an adjusted p-value < 0.05, the row z-score for the top 20 genes was calculated.

Preparation of secreted peptides and proteins for LC-MS

Organoids differentiated for 5 days to EECs were washed extensively in PBS and stimulated with 10 μ M Forskolin (Tocris). Conditioned media was collected for 24 hours and supplemented with 1x cOmplete Protease Inhibitor Cocktail on harvest (Roche). Potential cell debris was removed by centrifugation at 10,000 x g, for 5 min at 4°C. Conditioned media supernatant was denatured in final 4M Urea, 50mM ammonium bicarbonate and fractionated by molecular weight with a 10 kDa Vivaspin centrifugal device (Sartorius, Göttingen, Germany), at 12,000 x g, for 10 min at 4°C. (i) Endogenously processed peptides recovered from the filtrate were acidified to 5% formic acid, desalted by reversed phase C18 1cc columns (Waters Corporation, Milford, USA), further purified by home-made strong cation exchange STAGE tip, and dried by vacuum centrifugation. (ii) Longer secreted proteins in the 10 kDa retentate were recovered and diluted to final 2 M Urea, 50 mM ammonium bicarbonate, for reduction with dithiothreitol, alkylation with iodoacetamide, and overnight digestion with trypsin (Promega, Madison, USA) at 37°C. Digested peptides were similarly acidified to 5% formic acid, desalted by reversed phase C18 1cc columns (Waters), and dried by vacuum centrifugation.

Preparation of FACS-sorted EECs for proteome analyses

FACS sorted enteroendocrine cells were lysed in 8M Urea, 50 mM Ammonium bicarbonate, 0.5 % Sodium deoxycholate, 1x cOmplete protease inhibitor, 50 μ g/mL DNase I, and sonicated with the Biorupter (3 cycles, 20 s on, 20 s off at 4°C) (Diagenode, Liege, Belgium). Cell debris was pelleted by centrifugation at 14,000 x g for 1 hour at 15°C, and supernatant containing extracted proteins were reduced, alkylated, diluted 4 times with 50mM ammonium bicarbonate, and digested sequentially with Lys-C (Wako) and trypsin (Promega). Peptide digests were quenched to 5% formic acid, and sodium deoxycholate was precipitated and removed by centrifugation at 14,000 x g, 4°C for 10 minutes. Peptides in the supernatant were diluted to final 20% acetonitrile and purified by SCX STAGE tips. Eluted peptides were dried by vacuum centrifugation.

LC-MS

Peptides were reconstituted in 2% FA for LC-MS injection. Data was acquired using an UHPLC 1290 system (Agilent, California, USA) coupled to an Orbitrap HF-X mass spectrometer (Thermo Scientific, Massachusetts, USA). Peptides were first trapped in a 2 cm \times 100 μ M Reprosil C18 trap column (Dr Maisch, Ammerbuch, Germany) of 3 μ M pore size for 5 min in solvent A (0.1% formic acid in water). After trapping, samples separated in an analytical column (Agilent Poroshell, EC-C18, 2.7 μ m, 50 cm \times 75 μ m) using a gradient of 0.1% formic acid in 80% acetonitrile (solvent B). Depending on total peptide input, species complexity, and elution profiles, different LC gradient lengths were used for FACS-sorted whole proteomes (35min, 13-40% solvent B), secreted proteins (65min, 13-40% solvent B) and endogenously processed peptides (95min, 13-44% solvent B). MS acquisition was performed in data-dependent mode.

I

II

III

IV

V

VI

VII

VIII

&

Full scans (MS1) were acquired from 375 to 1600 m/z at resolution 60,000, with 20 ms injection time and 3×10^6 AGC target value. The TOP 15 most intense precursor ions were selected for fragmentation using 1.4 m/z isolation window. Isolated precursors were fragmented using high energy C-trap dissociation (HCD) at normalized collision energy (NCE) of 27%. MS2 scans were acquired at resolution 30,000, with 50 ms injection time and an AGC target value of 1×10^5 . Exclusion times were set to 8, 12 or 16 seconds for proteomics, digested retentates and endogenously processed peptides respectively.

Proteomics data analysis

Collected spectral data was processed using Proteome Discoverer 2.3 (Thermo Scientific, Massachusetts, USA), and searched using Sequest HT search engine, against UniProt *Homo sapiens* database (173235 entries, downloaded in August 2019, including common contaminants). Precursor and fragment mass tolerance were set to 10 ppm and 0.02 Da respectively. Protein N-terminal Acetylation and methionine oxidation were set as variable modifications. For the endogenously processed peptides, peptides of length 6 - 50 amino acids were generated from the database upon unspecific cleavage. For digested retentates and analyses of the FACS-sorted EECs proteomes, cysteine carbamidomethylation was set as fixed modification and up to 2 missed trypsin cleavages were allowed. Identified peptides were filtered to 1% FDR using the Percolator algorithm.

In proteome analyses, intensities of proteins detected in 2 out of 3 replicates in at least one group were $\log(2)$ transformed and missing values were imputed from the normal distribution independently for each sample using Perseus software (v_1.6.2.2). Processed data was assessed for statistical significance among the groups using One-way ANOVA or Student's T-test, and resulting *p*-values were corrected for type I error using Benjamini-Hochberg approach (*q*-value). Tukey Honest Significant Difference test was performed to assess difference between the groups when required. Hormone processing plots were generated from peptides identified at high confidence (1 % FDR) in at least 2 out of 3 replicates. For novel secreted products, peptides identified in 3 out of 3 replicates and not observed in the secretome of control organoids were used. Peptide sequences identified based on retention time alignment (not supported by spectral evidence) were not used in hormone processing plots. Statistical analysis and plots were generated using *in-house* built R scripts (R version 3.6.0).

ACKNOWLEDGMENTS

We thank Anko de Graaff and the Hubrecht Imaging Centre (HIC) for microscopy assistance; Single Cell Discoveries for the provided single-cell sequencing service and support; Harry Beghtel and Jeroen Korving for support with immunohistochemistry. We are grateful to Folkert Morsink and Johan Offerhaus of the University Medical Center Utrecht for providing sections of human intestinal biopsies. J.B.M., A.J.R.H. and W.W. acknowledge financial support from the Horizon 2020 program INFRAIA project Epic-XS (Project 823839) and the NWO funded Netherlands Proteomics Centre through the National Road Map for Large-scale Infrastructures program X-Omics (Project 184.034.019)

AUTHOR CONTRIBUTIONS

J.B., J.P. and H.C. conceptualized the project, designed the experiments, interpreted the results and wrote the manuscript. J.B.M., W.W. and A.J.R.H. performed the proteomic and secretomic experiments and analysis. A.M.S. assisted in cell culture experiments and was supervised by J.B., J.P. and H.C. J.B. and J.P. generated and analyzed the organoid-derived EEC single cell atlas. R.E., K.J., A.R., M.Z. and S.T. generated and analyzed the primary human EEC single cell dataset. G.B. generated and provided the Neurogenin-3 overexpression vector. D.H. and B.A. generated and provided the targeting vectors for CRISPR-HOT-mediated reporter organoids. A.A.R., and M.H.G provided different constructs. Y.P. and C.P.M. contributed to functional EEC assays. F.V.D.L and J.G. provided the Tq-Ca-FLITS reporter. B.P. and H.S. performed imaging and quantification of calcium responses. Y.E.B.E. and R.V.D.L assisted with FACS experiments. K.K. provided organoid lines. C.L.I., W.J.V.D.W. and P.J.P. performed transmission electron microscopy.

DECLARATION OF INTERESTS

H.C. is inventor on several patents related to organoid technology; his full disclosure is given at <https://www.uu.nl/staff/JCClevers/>.

I

II

III

IV

V

VI

VII

VIII

&

REFERENCES

- Bando, M., Iwakura, H., Koyama, H., Hosoda, H., Shigematsu, Y., Ariyasu, H., Akamizu, T., Kangawa, K., and Nakao, K. (2016). High incorporation of long-chain fatty acids contributes to the efficient production of acylated ghrelin in ghrelin-producing cells. *FEBS Lett.* 590, 992–1001.
- Barker, N., van Es, J.H., Kuipers, J., Kujala, P., van den Born, M., Cozijnsen, M., Haegebarth, A., Korving, J., Begthel, H., Peters, P.J., et al. (2007). Identification of stem cells in small intestine and colon by marker gene *Lgr5*. *Nature* 449, 1003–1007.
- Berna, M.J., Hoffmann, K.M., Long, S.H., Serrano, J., Gibril, F., and Jensen, R.T. (2006). Serum gastrin in Zollinger-Ellison syndrome: II. Prospective study of gastrin provocative testing in 293 patients from the national institutes of health and comparison with 537 cases from the literature. Evaluation of diagnostic criteria, proposal of new . *Medicine (Baltimore)*. 85, 331–364.
- Beucher, A., Gjernes, E., Collin, C., Courtney, M., Meunier, A., Collombat, P., and Gradwohl, G. (2012). The homeodomain-containing transcription factors *Arx* and *Pax4* control enteroendocrine subtype specification in mice. *PLoS One*.
- Beumer, J., Artegiani, B., Post, Y., Reimann, F., Gribble, F., Nguyen, T.N., Zeng, H., Van den Born, M., Van Es, J.H., and Clevers, H. (2018). Enteroendocrine cells switch hormone expression along the crypt-to-villus BMP signaling gradient. *Nat Cell Biol* 20.
- Borges, M., Linnoila, R.I., Van De Velde, H.J.K., Chen, H., Nelkin, B.D., Mabry, M., Baylin, S.B., and Ball, D.W. (1997). An achaete-scute homologue essential for neuroendocrine differentiation in the lung. *Nature*.
- Boztepe, T., and Gulec, S. (2018). Investigation of the influence of high glucose on molecular and genetic responses: An in vitro study using a human intestine model. *Genes Nutr.* 13.
- Bukhari, H., and Müller, T. (2019). Endogenous Fluorescence Tagging by CRISPR. *Trends Cell Biol*.
- Caruso, V., Sreedharan, S., Carlini, V.P., Jacobsson, J.A., Haitina, T., Hammer, J., Stephansson, O., Crona, F., Sommer, W.H., Risérus, U., et al. (2016). mRNA GPR162 changes are associated with decreased food intake in rat, and its human genetic variants with impairments in glucose homeostasis in two Swedish cohorts. *Gene* 581, 139–145.
- Chang-Graham, A.L., Danhof, H.A., Engevik, M.A., Tomaro-Duchesneau, C., Karandikar, U.C., Estes, M.K., Versalovic, J., Britton, R.A., and Hyser, J.M. (2019). Human Intestinal Enteroids With Inducible Neurogenin-3 Expression as a Novel Model of Gut Hormone Secretion. *Cell. Mol. Gastroenterol. Hepatol*.
- Chisholm, C., and Greenberg, G.R. (2002). Somatostatin-28 regulates GLP-1 secretion via somatostatin receptor subtype 5 in rat intestinal cultures. *Am. J. Physiol. - Endocrinol. Metab.* 283.
- Couzens, M., Liu, M., Tüchler, C., Kofler, B., Nessler-Menardi, C., Parker, R.M.C., Klocker, H., and Herzog, H. (2000). Peptide YY-2 (PYY2) and pancreatic polypeptide-2 (PPY2): Species- specific evolution of novel members of the neuropeptide Y gene family. *Genomics* 64, 318–323.
- Cox, H.M. (2007). Neuropeptide Y receptors; antisecretory control of intestinal epithelial function. *Auton. Neurosci. Basic Clin.* 133, 76–85.
- Cui, T., Tsolakis, A. V., Li, S.C., Cunningham, J.L., Lind, T., Öberg, K., and Giandomenico, V. (2013). Olfactory receptor 51E1 protein as a potential novel tissue biomarker for small intestine neuroendocrine carcinomas. *Eur. J. Endocrinol*.
- Drucker, D.J., Ehrlich, P., Asa, S.L., and Brubaker, P.L. (1996). Induction of intestinal epithelial proliferation by glucagon-like peptide 2. *Proc. Natl. Acad. Sci. U. S. A.* 93, 7911–7916.

- Edfeldt, K., Daskalakis, K., Bäcklin, C., Norlén, O., Tiensuu Janson, E., Westin, G., Hellman, P., and Stålberg, P. (2017). DcR3, TFF3, and Midkine Are Novel Serum Biomarkers in Small Intestinal Neuroendocrine Tumors. *Neuroendocrinology*.
- Engelstoft, M.S., Egerod, K.L., Lund, M.L., and Schwartz, T.W. (2013a). Enteroendocrine cell types revisited. *Curr. Opin. Pharmacol.*
- Engelstoft, M.S., Park, W. mee, Sakata, I., Kristensen, L. V., Husted, A.S., Osborne-Lawrence, S., Piper, P.K., Walker, A.K., Pedersen, M.H., Nøhr, M.K., et al. (2013b). Seven transmembrane G protein-coupled receptor repertoire of gastric ghrelin cells. *Mol. Metab.*
- Engelstoft, M.S., Lund, M.L., Grunddal, K. V., Egerod, K.L., Osborne-Lawrence, S., Poulsen, S.S., Zigman, J.M., and Schwartz, T.W. (2015). Research Resource: A Chromogranin A Reporter for Serotonin and Histamine Secreting Enteroendocrine Cells. *Mol. Endocrinol.* 29, 1658–1671.
- Ewert, S., Spak, E., Olbers, T., Johnsson, E., Edebo, A., and Fändriks, L. (2006). Angiotensin II induced contraction of rat and human small intestinal wall musculature in vitro. *Acta Physiol.*
- Fan, N., Sun, H., Wang, Y., Zhang, L., Xia, Z., Peng, L., Hou, Y., Shen, W., Liu, R., and Peng, Y. (2014). Midkine, a potential link between obesity and insulin resistance. *PLoS ONE*. 9.
- Fleischer, J., Bumbalo, R., Bautze, V., Strotmann, J., and Breer, H. (2015). Expression of odorant receptor Olfr78 in enteroendocrine cells of the colon. *Cell Tissue Res.* 361, 697–710.
- Foster, S.R., Hauser, A.S., Vedel, L., Strachan, R.T., Huang, X.P., Gavin, A.C., Shah, S.D., Nayak, A.P., Haugaard-Kedström, L.M., Penn, R.B., et al. (2019). Discovery of Human Signaling Systems: Pairing Peptides to G Protein-Coupled Receptors. *Cell* 179, 895–908.e21.
- Fujii, M., Matano, M., Nanki, K., and Sato, T. (2015). Efficient genetic engineering of human intestinal organoids using electroporation. *Nat. Protoc.* 10, 1474–1485.
- Furness, J.B., Rivera, L.R., Cho, H.-J., Bravo, D.M., and Callaghan, B. (2013). The gut as a sensory organ. *Nat. Rev. Gastroenterol. Hepatol.* 1010, 729–740.
- Gardiner, J. V., Beale, K.E., Roy, D., Boughton, C.K., Bataveljic, A., Campbell, D.C., Bewick, G.A., Patel, N.A., Patterson, M., Leavy, E.M., et al. (2010). Cerebellin1 is a novel orexigenic peptide. *Diabetes, Obes. Metab.*
- Gehart, H., van Es, J.H., Hamer, K., Beumer, J., Kretschmar, K., Dekkers, J.F., Rios, A., and Clevers, H. (2019). Identification of Enteroendocrine Regulators by Real-Time Single-Cell Differentiation Mapping. *Cell*.
- Goldspink, D.A., Reimann, F., and Gribble, F.M. (2018). Models and Tools for Studying Enteroendocrine Cells. *Endocrinology*.
- Gong, S., Zheng, C., Doughty, M.L., Losos, K., Didkovsky, N., Schambra, U.B., Nowak, N.J., Joyner, A., Leblanc, G., Hatten, M.E., et al. (2003). A gene expression atlas of the central nervous system based on bacterial artificial chromosomes. *Nature*.
- Gonsalkorale, W.M., Perrey, C., Pravica, V., Whorwell, P.J., and Hutchinson, I. V. (2003). Interleukin 10 genotypes in irritable bowel syndrome: Evidence for an inflammatory component? *Gut* 52, 91–93.
- Gribble, F.M., and Reimann, F. (2017). Signalling in the gut endocrine axis. *Physiol. Behav.*
- Gross, S., Garofalo, D.C., Balderes, D.A., Mastracci, T.L., Dias, J.M., Perlmann, T., Ericson, J., and Sussel, L. (2016). The novel enterochromaffin marker *Lmx1a* regulates serotonin biosynthesis in enteroendocrine cell lineages downstream of *Nkx2.2*. *Development* 143, 2616–2628.
- Grün, D., Lyubimova, A., Kester, L., Wiebrands, K., Basak, O., Sasaki, N., Clevers, H., and van Oudenaarden, A. (2015). Single-cell messenger RNA sequencing reveals rare intestinal cell types. *Nature* 525, 251–255.

- Haber, A.L., Biton, M., Rogel, N., Herbst, R.H., Shekhar, K., Smillie, C., Burgin, G., Delorey, T.M., Howitt, M.R., Katz, Y., et al. (2017). A single-cell survey of the small intestinal epithelium. *Nature* 551, 333–339.
- Hashimshony, T., Senderovich, N., Avital, G., Klochendler, A., de Leeuw, Y., Anavy, L., Gennert, D., Li, S., Livak, K.J., Rozenblatt-Rosen, O., et al. (2016). CEL-Seq2: sensitive highly-multiplexed single-cell RNA-Seq. *Genome Biol.* 17, 77.
- He, J., Irwin, D.M., Chen, R., and Zhang, Y.P. (2010). Stepwise loss of motilin and its specific receptor genes in rodents. *J. Mol. Endocrinol.* 44, 37–44.
- He, X., Tan, C., Wang, F., Wang, Y., Zhou, R., Cui, D., You, W., Zhao, H., Ren, J., and Feng, B. (2016). Knock-in of large reporter genes in human cells via CRISPR/Cas9-induced homology-dependent and independent DNA repair. *Nucleic Acids Res.*
- Herman, J.S., Sagar, and Grün, D. (2018). FateID infers cell fate bias in multipotent progenitors from single-cell RNA-seq data. *Nat. Methods.*
- Hyland, N.P., and Cryan, J.F. (2010). A gut feeling about GABA: Focus on GABAB receptors. *Front. Pharmacol.* OCT.
- Jovancevic, N., Khalifaoui, S., Weinrich, M., Weidinger, D., Simon, A., Kalbe, B., Kernt, M., Kampik, A., Gisselmann, G., Gelis, L., et al. (2017). Odorant receptor 51E2 agonist β -ionone regulates RPE cell migration and proliferation. *Front. Physiol.* 8.
- Koo, B.K., Stange, D.E., Sato, T., Karthaus, W., Farin, H.F., Huch, M., Van Es, J.H., and Clevers, H. (2012). Controlled gene expression in primary Lgr5 organoid cultures. *Nat. Methods* 9, 81–83.
- Kuro-o, M. (2019). The Klotho proteins in health and disease. *Nat. Rev. Nephrol.*
- Levine, A.S., Winsky-Sommerer, R., Huitron-Resendiz, S., Grace, M.K., and De Lecea, L. (2005). Injection of neuropeptide W into paraventricular nucleus of hypothalamus increases food intake. *Am. J. Physiol. - Regul. Integr. Comp. Physiol.*
- Li, W., Ji, M., Lin, Y., Miao, Y., Chen, S., and Li, H. (2018). DEPP/DEPP1/C10ORF10 regulates hepatic glucose and fat metabolism partly via ROS-induced FGF21. *FASEB J.* 32, 5459–5469.
- Lo, C.A., Kays, I., Emran, F., Lin, T.J., Cvetkovska, V., and Chen, B.E. (2015). Quantification of Protein Levels in Single Living Cells. *Cell Rep.* 13, 2634–2644.
- Loh, Y.P., Cheng, Y., Mahata, S.K., Corti, A., and Tota, B. (2012). Chromogranin A and derived peptides in health and disease. In *Journal of Molecular Neuroscience*, pp. 347–356.
- Lohoff, F.W., Dahl, J.P., Ferraro, T.N., Arnold, S.E., Gallinat, J., Sander, T., and Berrettini, W.H. (2006). Variations in the vesicular monoamine transporter 1 gene (VMAT1/SLC18A1) are associated with bipolar I disorder. *Neuropsychopharmacology.*
- Love, M.I., Huber, W., and Anders, S. (2014). Moderated estimation of fold change and dispersion for RNA-seq data with DESeq2. *Genome Biol.* 15, 550.
- McCracken, K.W., Catá, E.M., Crawford, C.M., Sinagoga, K.L., Schumacher, M., Rockich, B.E., Tsai, Y.H., Mayhew, C.N., Spence, J.R., Zavros, Y., et al. (2014). Modelling human development and disease in pluripotent stem-cell-derived gastric organoids. *Nature.*
- Muñoz, J., Stange, D.E., Schepers, A.G., van de Wetering, M., Koo, B.-K., Itzkovitz, S., Volckmann, R., Kung, K.S., Koster, J., Radulescu, S., et al. (2012). The Lgr5 intestinal stem cell signature: robust expression of proposed quiescent “+4” cell markers. *EMBO J.* 31, 3079–3091.

- Muraro, M.J., Dharmadhikari, G., Grün, D., Groen, N., Dielen, T., Jansen, E., van Gorp, L., Engelse, M.A., Carlotti, F., de Koning, E.J.P., et al. (2016). A Single-Cell Transcriptome Atlas of the Human Pancreas. *Cell Syst.* 3, 385–394. I
- Nguyen, T.L.A., Vieira-Silva, S., Liston, A., and Raes, J. (2015). How informative is the mouse for human gut microbiota research? *DMM Dis. Model. Mech.* II
- Pablo, J.L., and Pitta, G.S. (2017). FGF14 is a regulator of KCNQ2/3 channels. *Proc. Natl. Acad. Sci. U. S. A.* III
- Pan, F.C., Brissova, M., Powers, A.C., Pfaff, S., and Wright, C.V.E. (2015). Inactivating the permanent neonatal diabetes gene *Mnx1* switches insulin-producing β -cells to a δ -like fate and reveals a facultative proliferative capacity in aged β -cells. *Dev.* IV
- Panaro, B.L., Tough, I.R., Engelstoft, M.S., Matthews, R.T., Digby, G.J., Møller, C.L., Svendsen, B., Gribble, F., Reimann, F., Holst, J.J., et al. (2014). The melanocortin-4 receptor is expressed in enteroendocrine I cells and regulates the release of peptide YY and glucagon-like peptide 1 in vivo. *Cell Metab.* 20, 1018–1029. V
- Di Paola, R., Caporarello, N., Marucci, A., Dimatteo, C., Iadicicco, C., Del Guerra, S., Prudente, S., Sudano, D., Miele, C., Parrino, C., et al. (2011). ENPP1 affects insulin action and secretion: Evidences from in vitro studies. *PLoS One.* VI
- Parikh, K., Antanaviciute, A., Fawcner-Corbett, D., Jagielowicz, M., Aulicino, A., Lagerholm, C., Davis, S., Kinchen, J., Chen, H.H., Alham, N.K., et al. (2019). Colonic epithelial cell diversity in health and inflammatory bowel disease. *Nature.* VII
- Parker, H.E., Habib, A.M., Rogers, G.J., Gribble, F.M., and Reimann, F. (2009). Nutrient-dependent secretion of glucose-dependent insulinotropic polypeptide from primary murine K cells. *Diabetologia.* VIII
- Piccand, J., Vagne, C., Blot, F., Meunier, A., Beucher, A., Strasser, P., Lund, M.L., Ghimire, S., Nivlet, L., Lapp, C., et al. (2019). Rfx6 promotes the differentiation of peptide-secreting enteroendocrine cells while repressing genetic programs controlling serotonin production. *Mol. Metab.* 29, 24–39. &
- Pietraszewska-Bogiel, A., van Weeren, L., and Goedhart, J. (2019). Seeing cells smell: Dynamic optical measurements of Ca^{2+} and cAMP signaling from Olfactory Receptors transiently expressed in HEK293TN cells. *bioRxiv* 771261.
- Ramesh, N., Mortazavi, S., and Unniappan, S. (2015). Nesfatin-1 stimulates glucagon-like peptide-1 and glucose-dependent insulinotropic polypeptide secretion from STC-1 cells in vitro. *Biochem. Biophys. Res. Commun.* 462, 124–130.
- Ran, F.A., Hsu, P.D., Wright, J., Agarwala, V., Scott, D.A., and Zhang, F. (2013). Genome engineering using the CRISPR-Cas9 system. *Nat Protoc.* 8.
- Reimann, F., Habib, A.M., Tolhurst, G., Parker, H.E., Rogers, G.J., and Gribble, F.M. (2008). Glucose Sensing in L Cells: A Primary Cell Study. *Cell Metab.*
- Roberts, G.P., Larraufie, P., Richards, P., Kay, R.G., Galvin, S.G., Miedzybrodzka, E.L., Leiter, A., Li, H.J., Glass, L.L., Ma, M.K.L., et al. (2019). Comparison of human and murine enteroendocrine cells by transcriptomic and peptidomic profiling. In *Diabetes*, p.
- Sachs, N., Pappaspyropoulos, A., Zomer-van Ommen, D.D., Heo, I., Böttinger, L., Klay, D., Weeber, F., Huelsz-Prince, G., Iakobachvili, N., Amatngalim, G.D., et al. (2019). Long-term expanding human airway organoids for disease modeling. *EMBO J.* 38.
- Sanger, G.J. (2004). Neurokinin NK 1 and NK 3 receptors as targets for drugs to treat gastrointestinal motility disorders and pain. *Br. J. Pharmacol.* 141, 1303–1312.

- Sapio, M.R., and Fricker, L.D. (2014). Carboxypeptidases in disease: Insights from peptidomic studies. *Proteomics - Clin. Appl.* 8, 327–337.
- Sato, T., Vries, R.G., Snippert, H.J., van de Wetering, M., Barker, N., Stange, D.E., van Es, J.H., Abo, A., Kujala, P., Peters, P.J., et al. (2009). Single Lgr5 stem cells build crypt-villus structures in vitro without a mesenchymal niche. *Nature* 459, 262–265.
- Sato, T., Stange, D.E., Ferrante, M., Vries, R.G.J., Van Es, J.H., Van Den Brink, S., Van Houdt, W.J., Pronk, A., Van Gorp, J., Siersema, P.D., et al. (2011). Long-term expansion of epithelial organoids from human colon, adenoma, adenocarcinoma, and Barrett's epithelium. *Gastroenterology* 141, 1762–1772.
- Schmid-Burgk, J.L., Höning, K., Ebert, T.S., and Hornung, V. (2016). CRISPaint allows modular base-specific gene tagging using a ligase-4-dependent mechanism. *Nat. Commun.*
- Schneeberger, M. (2019). Irx3, a new leader on obesity genetics. *EBioMedicine* 39, 19–20.
- Scott, L.J., Mohlke, K.L., Bonnycastle, L.L., Willer, C.J., Li, Y., Duren, W.L., Erdos, M.R., Stringham, H.M., Chines, P.S., Jackson, A.U., et al. (2007). A genome-wide association study of type 2 diabetes in finns detects multiple susceptibility variants. *Science* (80-.). 316, 1341–1345.
- Sharma, D., Verma, S., Vaidya, S., Kalia, K., and Tiwari, V. (2018). Recent updates on GLP-1 agonists: Current advancements & challenges. *Biomed. Pharmacother.*
- Shcherbina, L., Lindqvist, A., Thorén Fischer, A.H., Ahlqvist, E., Zhang, E., Falkmer, S.E., Renström, E., Koffert, J., Honka, H., and Wierup, N. (2018). Intestinal CART is a regulator of GIP and GLP-1 secretion and expression. *Mol. Cell. Endocrinol.* 476, 8–16.
- Sinagoga, K.L., McCauley, H.A., Múnera, J.O., Reynolds, N.A., Enriquez, J.R., Watson, C., Yang, H.C., Helmraath, M.A., and Wells, J.M. (2018). Deriving functional human enteroendocrine cells from pluripotent stem cells. *Development.*
- Sommer, C.A., and Mostoslavsky, G. (2014). Rna-seq analysis of enteroendocrine cells reveals a role for fabp5 in the control of gip secretion. *Mol. Endocrinol.*
- Stahl, R., Walcher, T., De Juan Romero, C., Pilz, G.A., Cappello, S., Irmeler, M., Sanz-Aquela, J.M., Beckers, J., Blum, R., Borrell, V., et al. (2013). Trnp1 regulates expansion and folding of the mammalian cerebral cortex by control of radial glial fate. *Cell.*
- Sullo, A., Brizzi, G., and Maffulli, N. (2011). Chronic peripheral administration of serotonin inhibits thyroid function in the rat. *Muscles. Ligaments Tendons J.* 1, 48–50.
- Thomsen, S.K., Raimondo, A., Hastoy, B., Sengupta, S., Dai, X.Q., Bautista, A., Censin, J., Payne, A.J., Umaphysivam, M.M., Spigelman, A.F., et al. (2018). Type 2 diabetes risk alleles in PAM impact insulin release from human pancreatic β -cells. *Nat. Genet.* 50, 1122–1131.
- Too, L.K., Li, K.M., Suarna, C., Maghzal, G.J., Stocker, R., McGregor, I.S., and Hunt, N.H. (2016). Deletion of TDO2, IDO-1 and IDO-2 differentially affects mouse behavior and cognitive function. *Behav. Brain Res.* 312, 102–117.
- Ueda, M., and Ando, Y. (2014). Recent advances in transthyretin amyloidosis therapy. *Transl. Neurodegener.*
- Vainio, L., Perjes, A., Ryti, N., Magga, J., Alakoski, T., Serpi, R., Kaikkonen, L., Piuholta, J., Szokodi, I., Ruskoaho, H., et al. (2012). Neuronostatin, a novel peptide encoded by somatostatin gene, regulates cardiac contractile function and cardiomyocyte survival. *J. Biol. Chem.* 287, 4572–4580.
- Wang, F., Flanagan, J., Su, N., Wang, L.C., Bui, S., Nielson, A., Wu, X., Vo, H.T., Ma, X.J., and Luo, Y. (2012). RNAscope: A novel in situ RNA analysis platform for formalin-fixed, paraffin-embedded tissues. *J. Mol. Diagnostics* 14, 22–29.

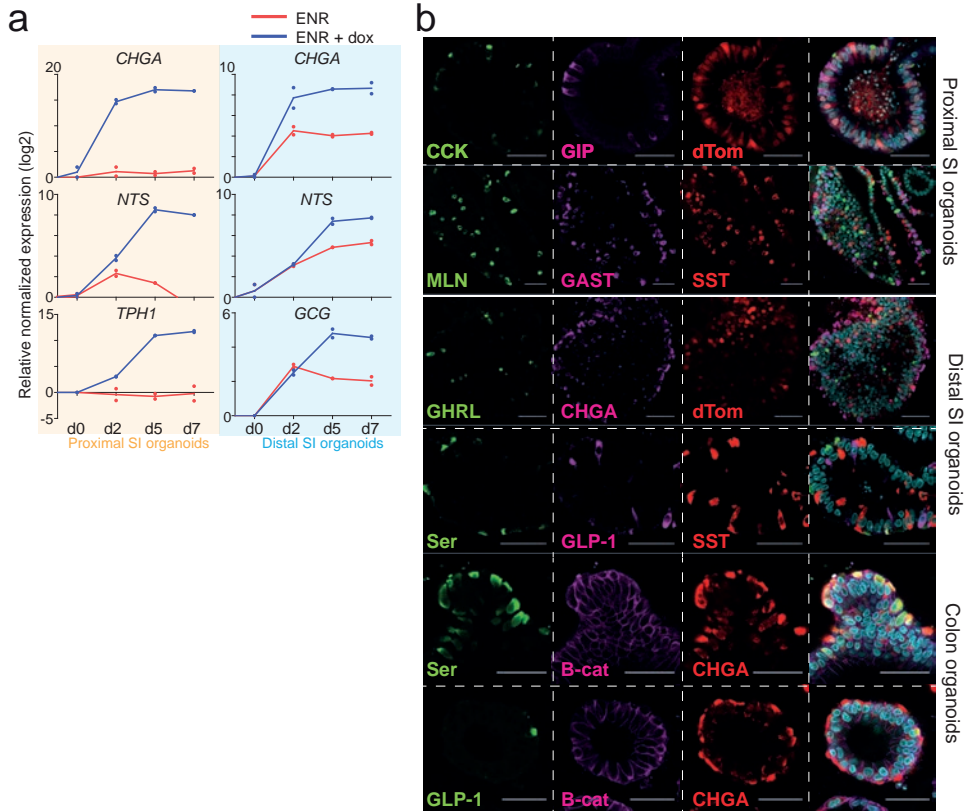
Worthington, J.J., Reimann, F., and Gribble, F.M. (2018). Enteroendocrine cells-sensory sentinels of the intestinal environment and orchestrators of mucosal immunity. *Mucosal Immunol.*

Yu, S.L., Han, S., Kim, H.R., Park, J.W., Jin, D. Il, and Kang, J. (2017). Phosphorylation of carboxypeptidase B1 protein regulates β -cell proliferation. *Int. J. Mol. Med.*

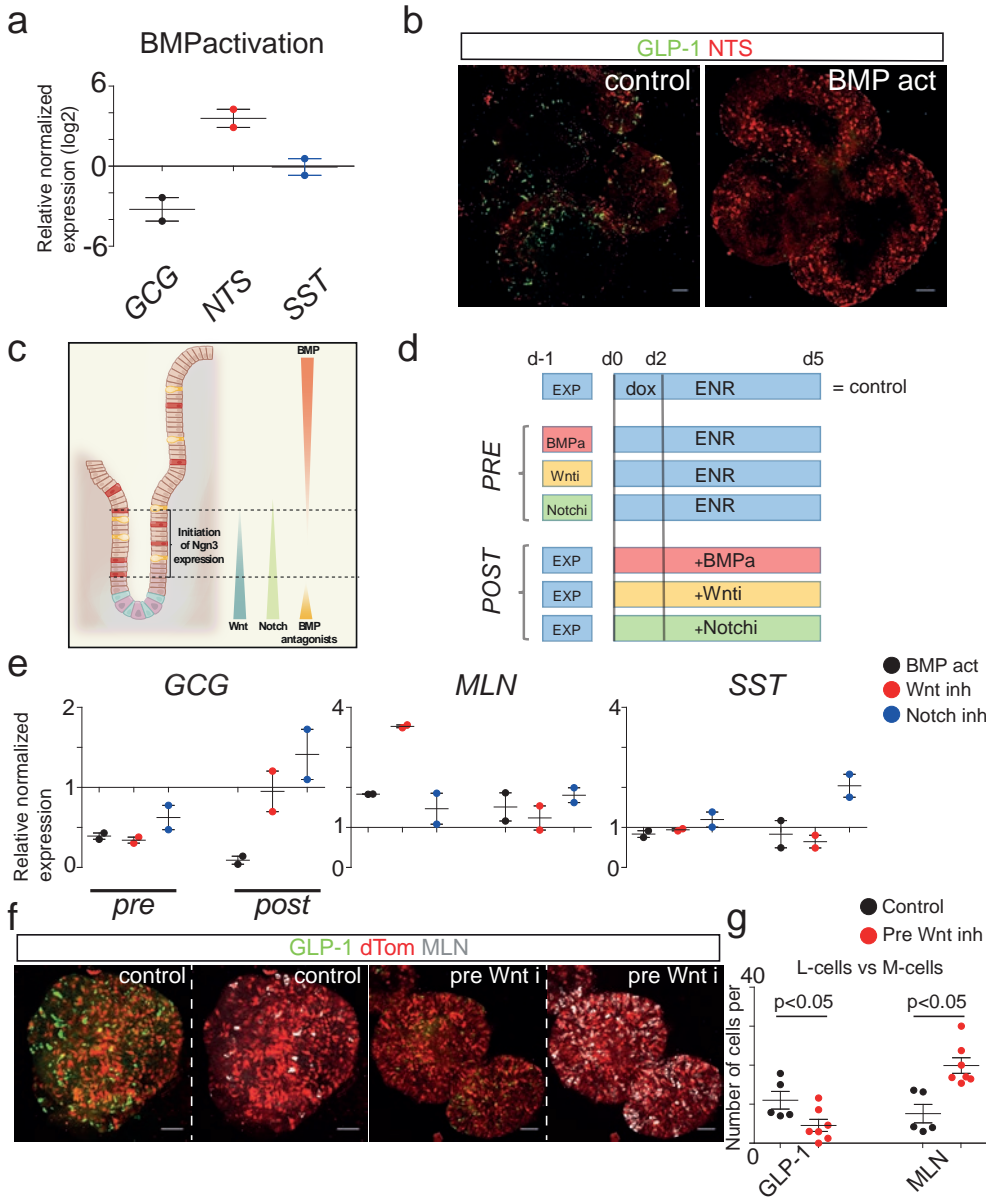
Zhang, J., McKenna, L.B., Bogue, C.W., and Kaestner, K.H. (2014). The diabetes gene Hhex maintains β -cell differentiation and islet function. *Genes Dev.* 28, 829–834.

Zhang, X., McGrath, P.S., Salomone, J., Rahal, M., McCauley, H.A., Schweitzer, J., Kovall, R., Gebelein, B., and Wells, J.M. (2019). A Comprehensive Structure-Function Study of Neurogenin3 Disease-Causing Alleles during Human Pancreas and Intestinal Organoid Development. *Dev. Cell.*

SUPPLEMENTARY FIGURES



Supplementary figure 1. Enteroendocrine cells in human intestinal organoids display normal coexpression profiles. qPCR analysis showing expression of hormones over the course of EEC differentiation. Expressions levels are normalized to GADPH and relative to day 0. The experiment was performed in $n = 2$ independent experiments, and the individual datapoints are depicted. Immunofluorescent staining of EEC-enriched organoids. Multiple hormones are expressed mutually exclusive. Scale bar is 50 μ m.

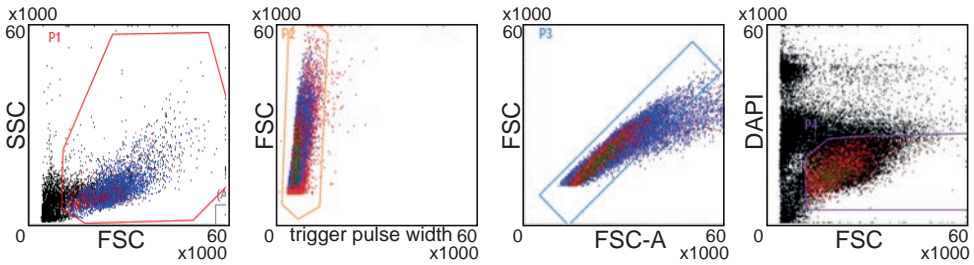


Supplementary figure 2. Manipulation of Wnt and BMP signaling allows controlling sub-specification of EECs. qPCR analysis showing expression of hormones after BMP treatment. Expression levels are normalized to GADPH, and relative to a non-treated control. The experiment was performed in $n=2$ independent experiments, and the mean expression and SEM are depicted. Immunofluorescent staining of BMP treated organoids. Scale bar is 50 μm . Schematic representation of morphogen gradients in the intestinal crypt related to sites of initiation of Neurogenin-3 (Ngn3) expression. Experimental paradigm. Different signalling pathways were modulated (BMP activation; BMPa, Wnt inhibition; Wnti, Notch inhibition; Notchi) either 24 hours before (pre) or at the start (post) of *NEUROG3* expression mediated by doxycycline (dox) treatment. Control organoids were kept in standard expansion conditions (EXP) ▶

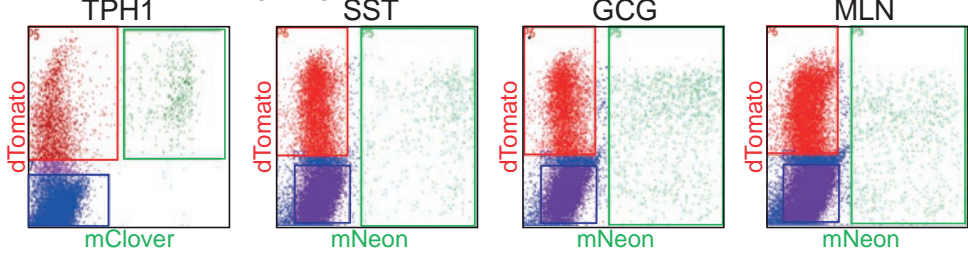
- ▶ before dox treatment, and in standard differentiation conditions (ENR) after initiation of dox treatment. qPCR analysis showing expression of hormones after different treatments shown in. Expression levels are normalized to GADPH, and relative to a non-treated control. The experiment was performed in $n=2$ independent experiments, and the mean expression and SEM are depicted. Immunofluorescent staining of organoids differentiated towards EECs after a 24 hour inhibition of Wnt (pre Wnt i). Scale bar is 50 μm . Quantification of (F). Pre-inhibition of Wnt signalling caused a shift of L-cell to M-cell differentiation.

I
II
III
IV
V
VI
VII
VIII
&

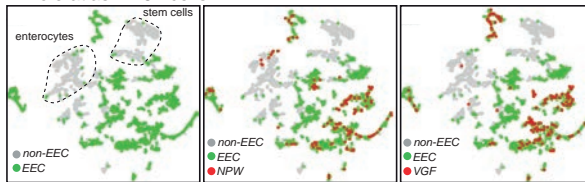
a Live and single cell gating



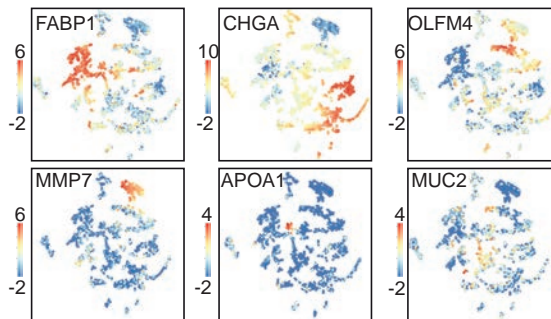
Reporter-specific gating



b Whole atlas: 4281 cells

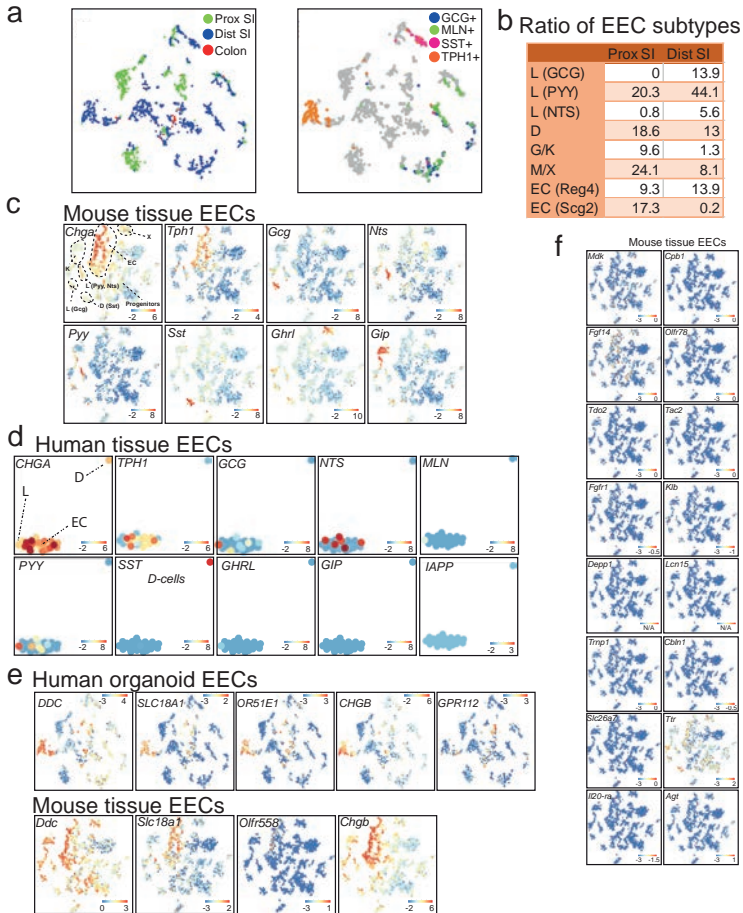


c

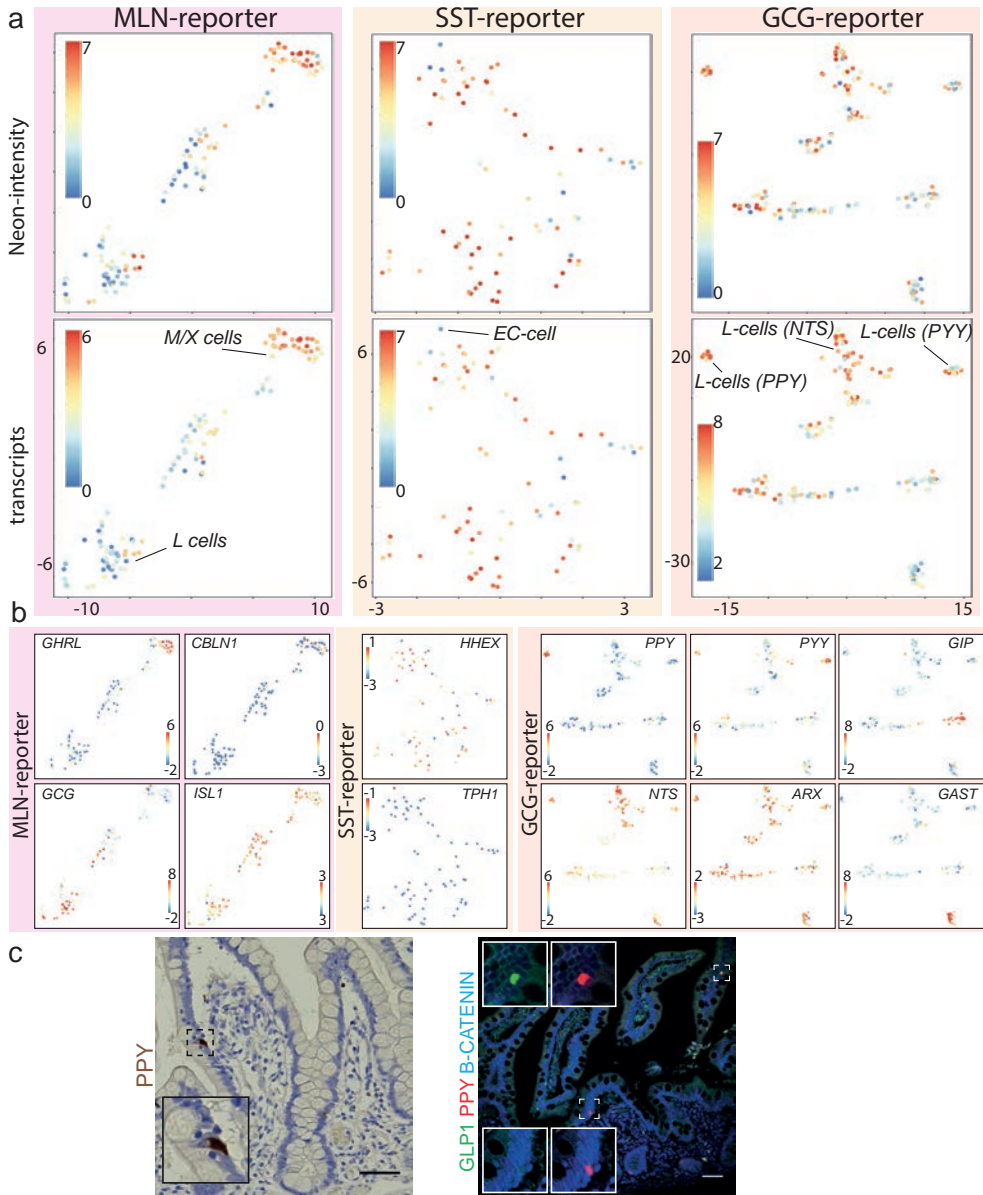


Supplementary figure 3. Generation of a human single cell RNA sequencing atlas of the intestinal tract using organoids. Fluorescence-activated cell sorting (FACS) gating parameters for sorting of different EEC subtypes from reporter organoids. A broad human intestinal organoid atlas ($n=4281$ cells) generated by ▶

- ▶ single cell RNA sequencing and displayed using a *t*-distributed stochastic neighbor-embedding (*t*-SNE) map. Cells defined as EECs (see methods) are shown in green. Cells expressing NPW or VGF (>1 transcripts, respectively) are highlighted in red and are found exclusively in EEC clusters. *t*-SNE maps displaying lineage markers in the whole human intestinal organoid cell atlas (n= 8448 cells). Bars display color-coded unique transcript expression (logarithmic scale).



Supplementary figure 4. Single cell RNA sequencing of human EECs from organoids and tissue and mouse EECs from tissue. *t*-SNE maps displaying the origin (left, tissue; right, reporter organoid) of cells from the the human EEC atlas (n= 2255 cells). The percentages of EECs corresponding to the different subtypes in proximal and distal SI organoids. *t*-SNE maps displaying the expression levels of hormones in the different murine EEC subtypes from intestinal tissue. Bars display color-coded unique transcript expression (logarithmic scale). *t*-SNE maps displaying the expression levels of hormones in the different human EEC subtypes from intestinal tissue. Bars display color-coded unique transcript expression (logarithmic scale). *t*-SNE maps displaying conserved expression of different EC markers in human and mouse EECs. Bars display color-coded unique transcript expression (logarithmic scale). *t*-SNE maps displaying the levels of hormone and marker gene expression of human M/X cells in the different murine EEC subtypes from intestinal tissue. Bars display color-coded unique transcript expression (logarithmic scale).



I

II

III

IV

V

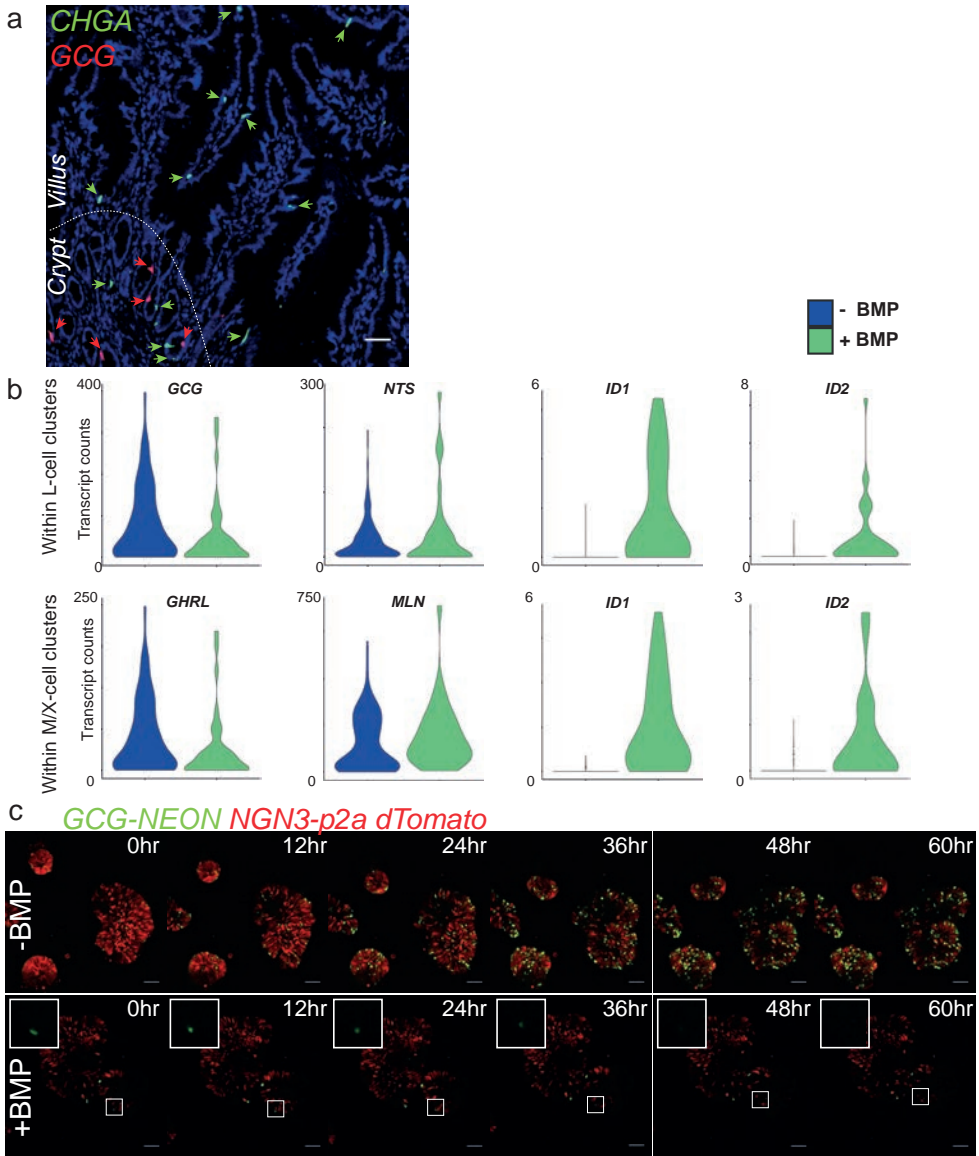
VI

VII

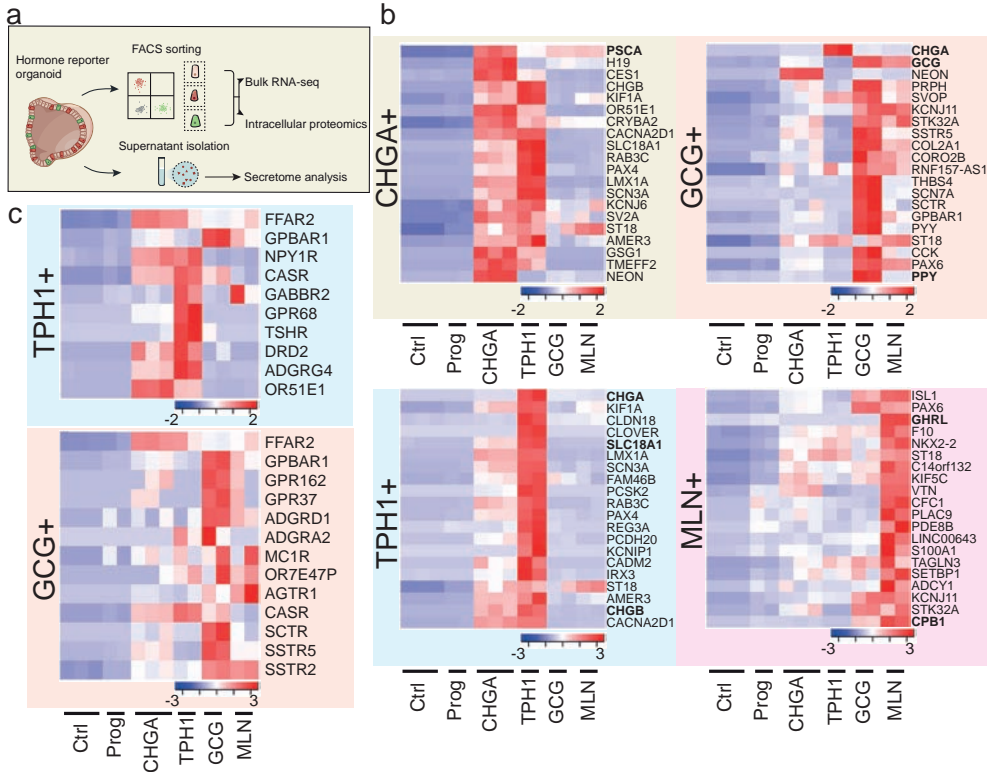
VIII

&

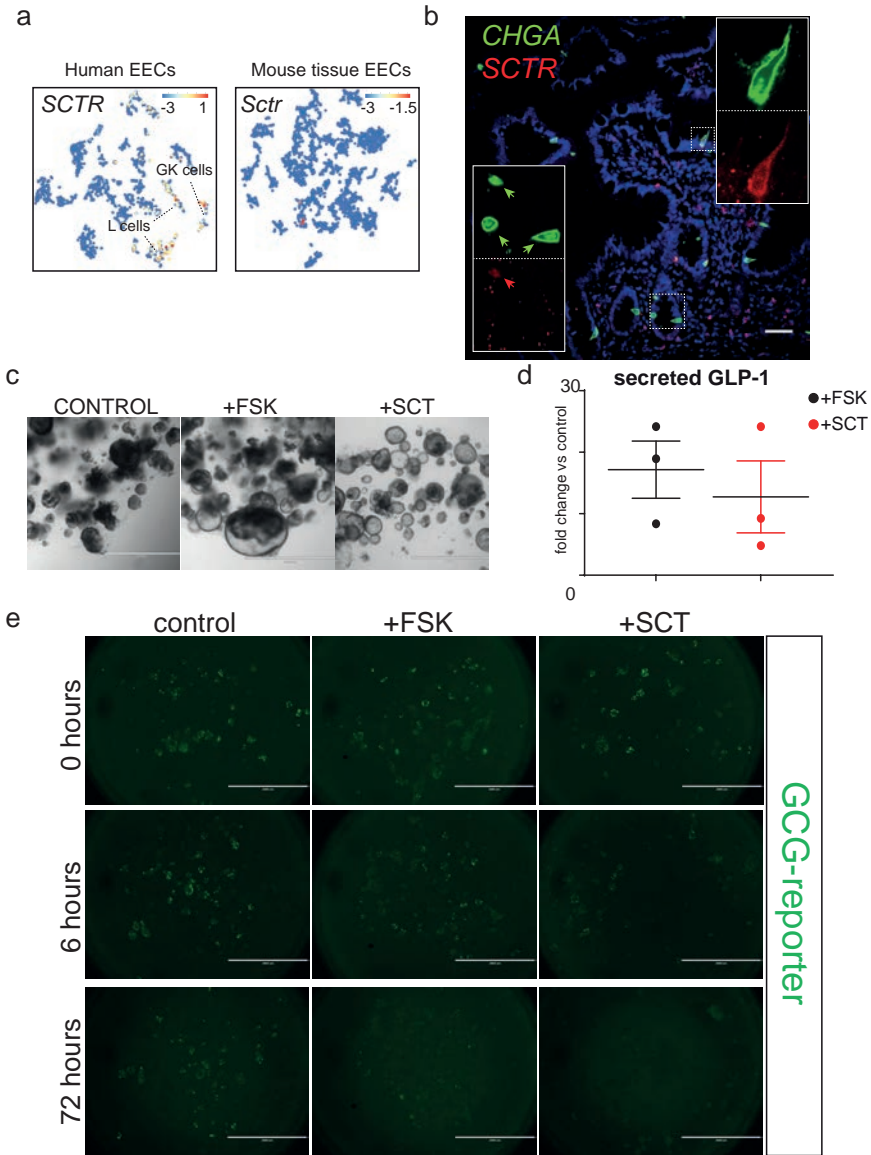
Supplementary figure 5. Subclustering of human EEC subtypes reveals heterogeneity including rare expression of PPY in L-cells. Subclustering was performed on EECs sorted from different reporter organoids. t-SNE maps displaying the correlation between transcript levels and reporter intensity. t-SNE maps displaying different hormones in EECs from the different reporter organoids. PPY-expressing cell form a distinct cluster of GCG⁺ - cells. Immunohistochemistry of human ileal sections confirms PPY expression *in vivo*. Scale bar is 50 μ m.



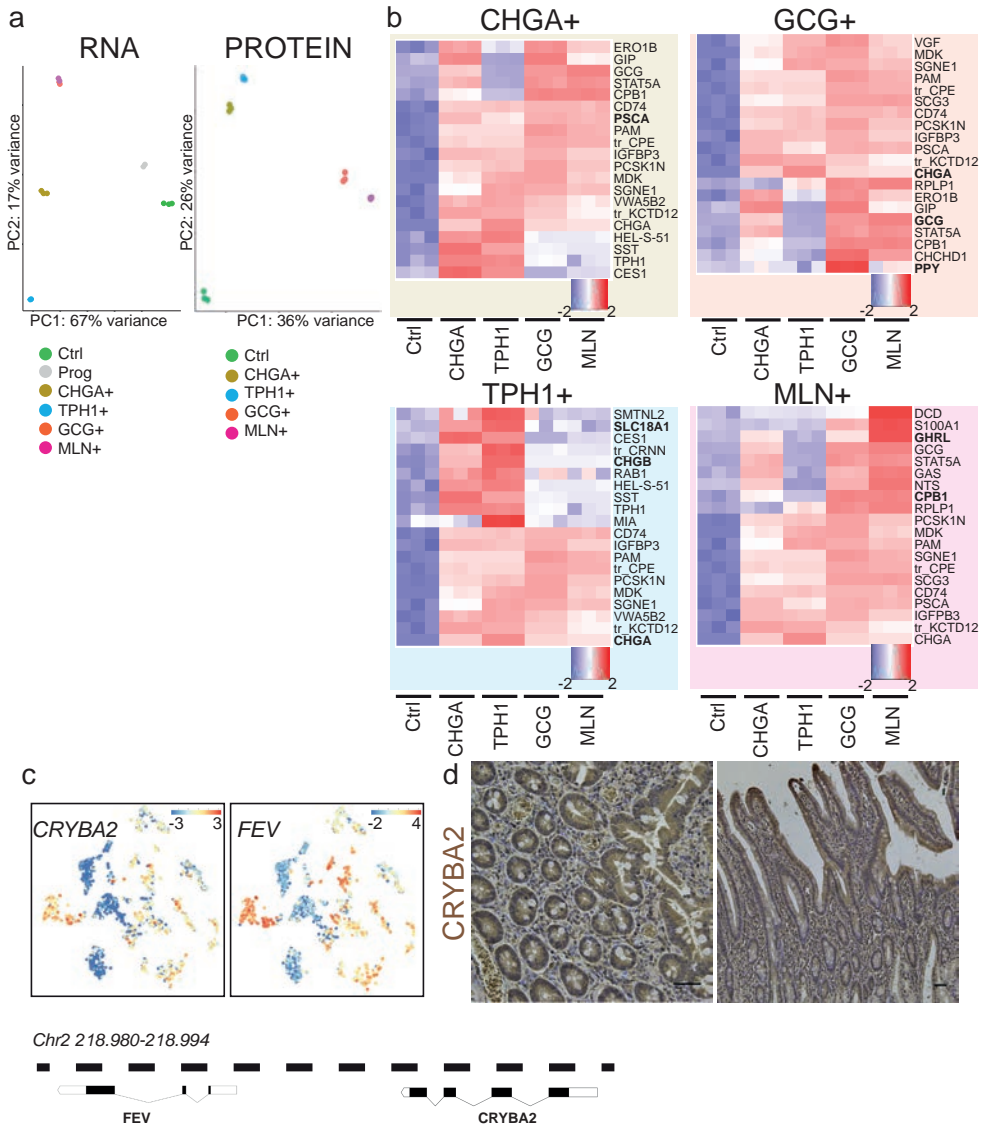
Supplementary figure 6. BMP signaling regulates expression of hormones in individual enteroendocrine cells. Fluorescent in situ hybridization on human ileal section shows crypt-restricted expression of *GCG* (red arrowheads), whereas *CHGA* expression (green arrowheads) is expressed also in the villus. Scale bar is 50 μm . Violin plots depict the expression levels of selected hormones in single BMP-treated cells versus untreated cells in the EEC single cell RNA sequencing atlas. *ID1* and *ID2* are BMP target genes that confirm specific pathway activation of BMP agonist-treated cells. Snapshots are shown of *GCG-neon* reporter organoids that were treated with BMP after 2 days of dox treatment to induce *NEUROG3-dTomato* expression (= 0hr timepoint). BMP treatment blocks the appearance of *GCG*-positive cells, while pre-existing L-cells downregulate *GCG* expression. No cell death is observed. Scale bar is 50 μm .



Supplementary figure 7. Bulk transcriptomic profiling of sorted enteroendocrine cell subtypes. Experimental paradigm. Hormone reporter organoids are differentiated, after which subpopulations of EECs are sorted using FACS and processed for bulk RNA-sequencing or intracellular proteomics. In a separate experiment, the supernatant of organoids is collected after 24 hour forskolin stimulation and processed for proteomic analyses to determine the EEC secretome. Heatmaps showing the 20 most significant RNA markers enriched in purified reporter populations. In bold genes are highlighted that are also among the 20 most significant markers on protein level. Colored bars represent Z-scores. Heatmaps showing receptor expression most unique to TPH1⁺ or GCG⁺ cells. The receptor for EEC hormone Secretin (SCTR) is expressed highly in L-cells but not ECs, while ECs display unique expression of the PYY receptor (NPY1R).

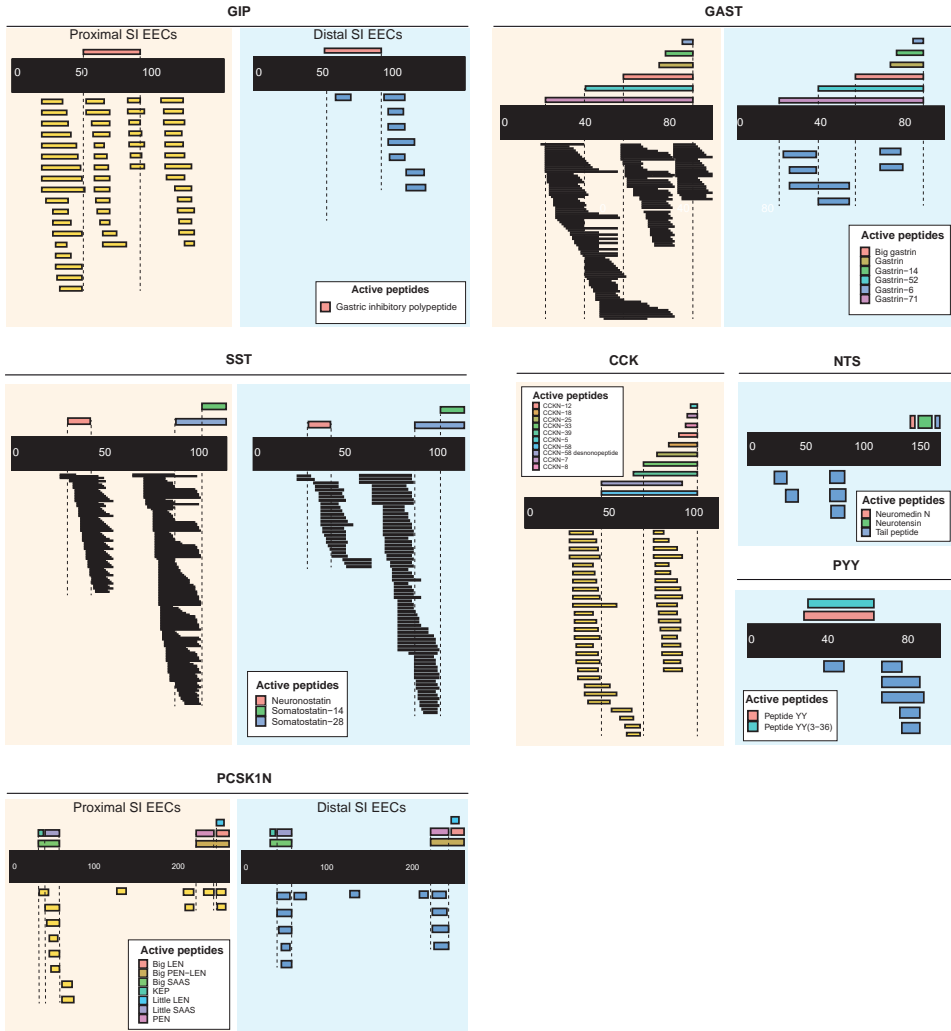


Supplementary figure 8. Secretin regulates release of GLP-1 from L-cells. t-SNE map displaying the expression level of the Secretin receptor (*SCTR*) in the EEC single cell sequencing atlas. Bars display color-coded unique transcript expression (logarithmic scale). Fluorescent in situ hybridization on human ileal sections shows rare *SCTR*-expressing cells (red arrowhead) that sometimes co-express *CHGA* (green arrowhead). Scale bar is 50 μ m. Representative bright-field images of EEC-differentiated organoids after 24 hours Forskolin (FSK) or Secretin (SCT) treatment. Both FSK and SCT treatment causes swelling of organoids, indicative of cAMP activation. Scale bar is 1mm. ELISA showing the fold increase in GLP-1 concentrations of EEC-enriched organoids after treatment with FSK or SCT. The experiment was performed in $n=3$ independent experiments, and the mean fold change and SEM are depicted. GCG-reporter organoids were differentiated towards EECs and treated with FSK or SCT. Intracellular levels of GCG-neon reduce over the course of FSK and SCT treatment. Scale bar is 2mm.



I
II
III
IV
V
VI
VII
VIII
&

Supplementary figure 9. Proteomic profiling of EECs. Principle component analysis (PCA) of RNA and protein data from different EEC populations. CHGA⁺ cells were used as control. CHGA⁺ cells that were positive for dTomato (induced NEUROG3-expression) were defined as EEC progenitors (Prog.). Heatmaps showing the 20 most significant markers on protein level defining each EEC populations. Colored bars represent Z-scores. In bold genes are highlighted that are also among the 20 most significant markers on RNA level. t-SNE maps displaying the expressions level of *CRYBA2* and *FEV* in the EEC single cell sequencing atlas, illustrating a high degree of overlap in expression. Bars display color-coded unique transcript expression (logarithmic scale). The location of the *CRYBA2* and *FEV* genes on Chromosome 2 are depicted below. Immunohistochemistry on human duodenal sections shows a lack of *CRYBA2* expression *in vivo*. Scale bar is 50 μm.



Supplementary figure 10. Processing of EEC hormones in proximal and distal SI organoids. Measured peptides (<10 kDa) in the secretome mapping to different secreted prehormones are shown below the black bar. Data from proximal (yellow background) and distal SI organoid (blue background) supernatants are displayed.

CHAPTER
SNAKE VENOM GLAND ORGANIDS

VII

SUMMARY

Wnt dependency and Lgr5 expression define multiple mammalian epithelial stem cell types. Under defined growth factor conditions, such Adult Stem Cells (ASCs) grow as 3D organoids that recapitulate essential features of the pertinent epithelium. Here, we establish long-term expanding venom gland organoids from several snake species. The newly assembled transcriptome of the Cape coral snake reveals that organoids express high levels of toxin transcripts. Single cell RNA sequencing of both organoids and primary tissue identifies distinct venom-expressing cell types as well as proliferative cells expressing homologs of known mammalian stem cell markers. A hard-wired regional heterogeneity in the expression of individual venom components is maintained in organoid cultures. Harvested venom peptides

Yorick Post^{1,13}, Jens Puschhof^{1,2,13}, Joep Beumer^{1,13}, Harald M. Kerkkamp³, Merijn A.G. de Bakker³, Julien Slagboom⁴, Buys de Barbanson^{1,2}, Nienke R. Wevers⁵, Xandor M. Spijkers^{5,6}, Thomas Olivier⁵, Taline D. Kazandijan⁷, Stuart Ainsworth⁷, Carmen Lopez Iglesias⁸, Willine J. van de Wetering^{1,8}, Maria C. Heinz^{2,9}, Ravian L van Ineveld^{2,10}, Regina G.D.M. van Kleef¹, Harry Begthel¹, Jeroen Korving¹, Yotam E. Bar-Ephraim^{1,2}, Walter Getreuer¹², Anne C. Rios^{2,10}, Remco H. S. Westerink¹¹, Hugo J. G. Snippert^{2,9}, Alexander van Oudenaarden^{1,2}, Peter J. Peters⁸, Freek J. Vonk³, Jeroen Kool⁴, Michael K. Richardson³, Nicholas R. Casewell⁷ and Hans Clevers^{1,2,10,14,*}

¹ Hubrecht Institute, Royal Netherlands Academy of Arts and Sciences (KNAW) and UMC Utrecht, 3584 CT Utrecht, The Netherlands.

² Oncode Institute, Hubrecht Institute, 3584 CT Utrecht, The Netherlands.

³ Institute of Biology Leiden, Department of Animal Science and Health, 2333 BE Leiden, The Netherlands.

⁴ Division of BioAnalytical Chemistry, Department of Chemistry and Pharmaceutical Sciences, Vrije Universiteit Amsterdam, 1081 LA Amsterdam, The Netherlands.

⁵ Mimetas BV, Organ-on-a-chip Company, 2333 CH Leiden, The Netherlands.

⁶ Department of Translational Neuroscience, Utrecht University Medical Center, 3584 CG, Utrecht, The Netherlands.

⁷ Centre for Snakebite Research & Interventions, Parasitology Department, Liverpool School of Tropical Medicine, Liverpool, L3 5QA, UK.

⁸ The Maastricht Multimodal Molecular Imaging institute, Maastricht University, 6229 ER Maastricht, The Netherlands.

⁹ Molecular Cancer Research, Center for Molecular Medicine, University Medical Center Utrecht, Utrecht University, 3584 CX Utrecht, The Netherlands.

¹⁰ The Princess Maxima Center for Pediatric Oncology, 3584 CS Utrecht, The Netherlands.

¹¹ Neurotoxicology Research Group, Division of Toxicology, Institute for Risk Assessment Sciences (IRAS), Utrecht University, 3584 CL Utrecht, The Netherlands.

¹² Serpo, 2288 ED Rijswijk, The Netherlands.

¹³ Co-first author

¹⁴ Lead Contact

* Correspondence: h.clevers@hubrecht.eu

reflect crude venom composition and display biological activity. This study extends organoid technology to reptilian tissues and describes an experimentally tractable model system representing the snake venom gland.

I

II

III

IV

V

VI

VII

VIII

&

INTRODUCTION

Snakebite envenoming is a neglected tropical disease estimated to be responsible for >100,000 deaths worldwide each year (Gutierrez et al., 2017). Upon injection through specialized fangs, venomous snakes primarily use their venom to immobilize prey. For numerous snake species, the venom delivered by a single bite is enough to kill prey that is many times larger than the snake. During vertebrate evolution, the snake venom gland has been adapted from the salivary gland (Kochva 1987). Secretory columnar cells in the gland epithelium secrete a complex mixture of peptides and proteins, stored in the lumen and channeled to the fangs through connecting ducts. Venom toxins are classified into distinct protein families with diverse modes-of-action (Fry et al., 2009), which makes them a rich source for drugs targeting human proteins (Clark et al., 2019). Snake venoms differ greatly in toxin composition and the architecture of the machinery involved in its production and release. Venom from viperid snakes (such as the rattlesnake) mainly consists of hemotoxic enzymes (Ainsworth et al., 2018), whereas elapids (such as the king cobra) typically produce smaller peptides with neurotoxic effects (Vonk et al., 2013). Three-finger toxins (3FTx) constitute a diverse and highly expressed class of toxins that mainly exert a neurotoxic effect through interaction with acetylcholine receptors (Tsetlin 2015). Kunitz-type

inhibitors (KUN) also exert neurotoxic activities, though some are anticoagulant (Harvey 2001; Millers et al., 2009). Phospholipase A2 (PLA2) proteins can act as myotoxins or neurotoxins and display antiplatelet activities (Gutiérrez and Lomonte 2013), whereas cysteine-rich secretory proteins (CRISP) block smooth muscle contraction (Yamazaki and Morita 2004). Finally, snake venom metalloproteinases (SVMP), L-amino acid oxidases (LAAO) and C-type lectins (CTL) mostly disrupt blood coagulation (Slagboom et al., 2017; Izidoro et al., 2014). Much still needs to be learned about toxin production- and release-cycles, heterogeneity of venom-producing cells and factors influencing venom composition.

Organoids are defined as self-organizing 3D structures that can be grown from stem cells and that recapitulate essential features of the tissue under study (Clevers 2016). We originally showed that a serum-free medium containing R-spondin, EGF and Noggin suffices to support the growth of mouse *Lgr5+* intestinal ASCs into ever-expanding epithelial organoids. These 'mini-guts' contain all known cell types of the gut lining (Sato et al., 2009), observations that were extended through single cell RNA sequencing (Grün et al., 2015; Beumer et al., 2018, Gehart et al., 2019). Subsequently, similar R- spondin-based protocols have been reported for a wide diversity of healthy and diseased mammalian epithelia (Artegiani and Clevers 2018). Of interest to the current study, Coppes and colleagues have demonstrated the feasibility of growing mammalian salivary gland organoids (Maimets et al., 2016).

Little is known about the biology of adult stem cells in reptiles. Different short-term culture systems have been described for snake venom glands (Sells et al., 1989; Carneiro et al., 2006), yet long-term cultures capturing structural and functional properties of the snake venom gland have not been developed. Here, we aim to establish long-term culture conditions for functional snake venom gland epithelium using R- spondin-based organoid technology.

RESULTS

Epithelial organoid cultures derived from snake venom glands

Venom glands from nine different snake species, representing members of both the Elapidae (*Naja pallida*, *Naja annulifera*, *Naja nivea*, *Naja atra* and *Aspidelaps lubricus cowlesi*) and Viperidae (*Echis ocellatus*, *Deinagkistrodon acutus*, *Crotalus atrox* and *Bitis arietans*) families, were dissociated and embedded in basement membrane extract (BME) at 32°C (Figure 1A). Supplying a medium containing a ‘generic’ mammalian organoid cocktail (see below) resulted in initial expansion of organoids for all

species (Figure 1B and S1A) (some were subsequently lost due to bacterial contamination, insensitive to the antibiotics used). Passaging yielded expanding organoids that histologically resembled the original gland epithelium (Figure 1C). The venom gland organoids could be expanded optimally using R-spondin (the Wnt signal-amplifying ligand of Lgr5 (de Lau et al., 2011)), the BMP inhibitor Noggin, EGF, the small molecule TGF beta inhibitor A83-01, PGE2 and FGF10 (Figure 1D and S1B). This ‘expansion medium’ controls the same cellular signaling pathways that are required for mammalian epithelial organoids (Fatehullah et al., 2016). Reptilian organoid expansion was only successful at lower temperatures (Figure S1C), consistent with the average body temperature of poikilotherm species such as snakes. When cultured at 37°C, a heat shock response (*HSPA8*) was observed within two hours, that is described to preclude cell division and consequently prohibited organoid growth (Richter et al., 2010) (Figure S1D). The proliferating cells self-organized into cystic spheres lined by a simple polarized epithelium (Figure 1E and Video S1), while budding of organoids was occasionally observed. Under these conditions, organoids expanded exponentially for > 20 passages without significant changes in growth kinetics or morphology (Figure 1B). As demonstrated previously for mammalian organoids (Bolhaqueiro et al., 2018), a lentiviral construct encoding histone 2B coupled to a fluorescent protein (H2B-RFP) allowed visualization of the organoid chromatin (Figure S1E).

Newly assembled transcriptome reveals high toxin expression in organoids

Simultaneous withdrawal of all growth factors (with the exception of PGE2 to maintain cystic organoids) for 7 days resulted in less-proliferative organoids (Figure 2A). These organoids contained highly polarized cells with secretory vesicles, described previously as the main producers of venom in the snake venom gland (Mackessy 1991) (Figure 2B). Furthermore, ciliated cells could occasionally be observed by electron-microscopy (Figure S2A). High-speed imaging captured functionally beating cilia in a subset of organoids (Video S2). Based on these features of apparently mature and functional cell types, we defined this cultured condition as our ‘differentiation’ cocktail.

Snake venom contains dozens to hundreds of different bioactive compounds (Fox and Serrano 2008). No annotated genome exists for *A. l. cowlesi*. To gain deeper insight into the expression of individual toxin-encoding genes, we assembled a *de novo* transcriptome of *A. l. cowlesi* using Trinity (Haas et al., 2013) (Figure 2C). Libraries of contigs (311,948) generated

I

II

III

IV

V

VI

VII

VIII

&

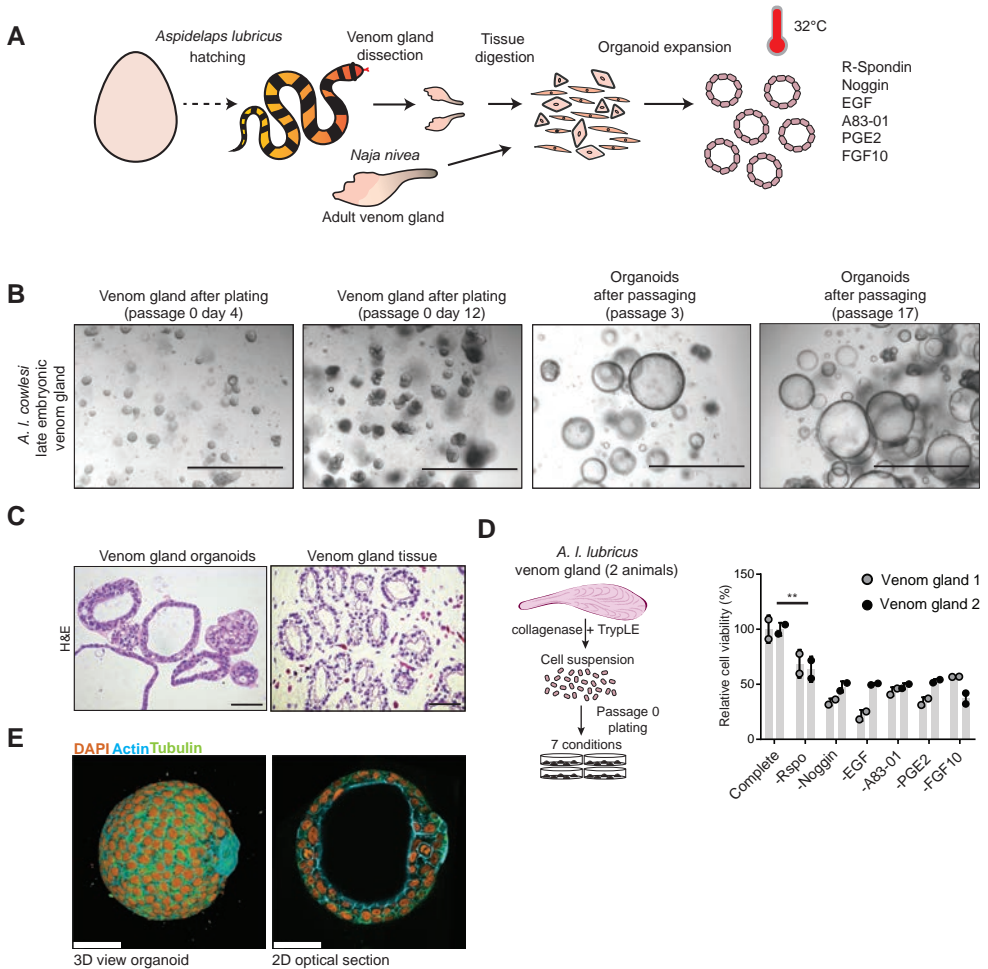


Figure 1. Establishment of organoid culture conditions for snake venom gland, see also Figure S1. Schematic representation of the derivation of venom gland organoids from late embryonic (~7–2 days before hatching) *A. l. cowlesi* (n=7) (See also Figure S1A). Time course of organoid expansion after seeding of cells from a single *A. l. cowlesi* venom gland in BME (passage 0) until passage 17. Scale bars, 1000 μ m. Haematoxylin and eosin (H&E) stain of late embryonic *A. l. cowlesi* venom gland and organoids. Scale bars, 50 μ m. Schematic representation of medium component dropout screen on primary tissue outgrowth. Quantification of relative cell viability per condition after 14 days, normalized to complete expansion medium (See also Figure S1B). Immunofluorescent staining of organoid for DNA (DAPI), Tubulin (green) and Actin (blue). Scale bars, 50 μ m.

from late-embryonic liver, pancreas and venom gland as well as from venom gland organoids were used to determine gene-expression levels for each of the three tissues as well as the venom gland organoids. The organoid transcriptome showed toxins to represent the dominant class of expressed genes, while homologs of established markers of mammalian liver and pancreas were restricted to their corresponding organ (Figure 2D). Toxin expression in venom gland tissue

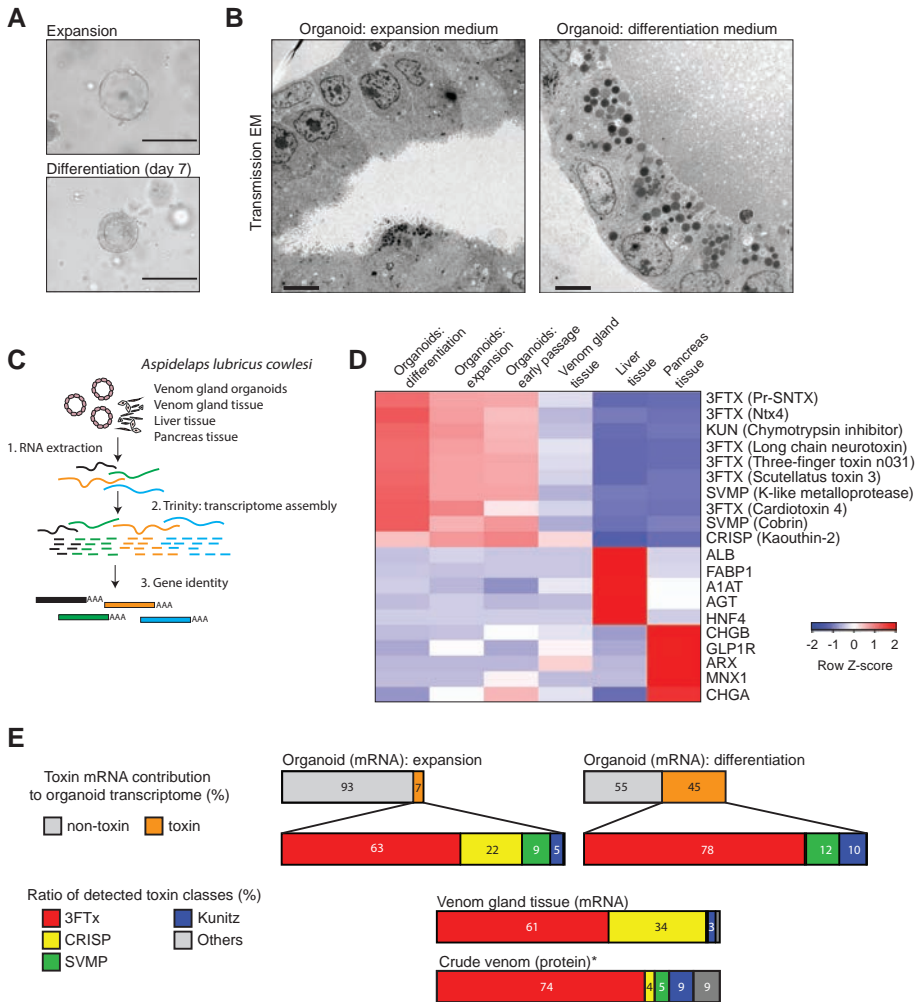


Figure 2. Venom gland organoids express a near-normal spectrum of toxins. Representative bright-field images of organoids after seven days expansion medium or differentiation medium. Scale bars, 200 μ m. Transmission electron microscopy (TEM) of organoids in expansion and differentiation medium shows simple epithelial cells and polarized exocrine cells with secretory vesicles oriented towards the lumen. Scale bars, 5 μ m. Schematic representation of *de novo* transcriptome assembly using Trinity. Input contained late embryonic *A. l. cowlesi* RNA isolated from venom gland tissue, pancreas tissue, liver tissue and three venom gland organoid samples (early passage expansion, late passage expansion, late passage differentiation). Heatmap of organoid and tissue gene expression determined by mRNA sequencing mapped on *de novo* transcriptome. Highlighted are highly expressed toxin classes (3FTX, KUN, SVMP, CRISP), as well as liver and pancreas markers. Contribution of toxin-encoding genes (orange) and non-toxin genes (grey) to the transcriptome per sample, and the contribution of toxin classes in expansion medium and differentiation medium compared to venom gland tissue mRNA and venom proteome (*dataset from Whiteley and Casewell et al., 2019) (3FTx = three-finger toxin, CRISP = cysteine-rich secretory protein, SVMP = snake venom metalloproteinase, Kunitz = Kunitz trypsin inhibitor, others include cobra venom factor (CVF), L-amino acid oxidase (LAOO) and phosphodiesterases (PDE)) (See also Figure S2B).

was markedly lower compared to organoids, most likely due to presence of non-epithelial cells in gland tissue. Amongst the toxins, three-finger toxins (3FTx) were most abundant (Figure 2E). We also detected expression of cysteine-rich secretory proteins (CRISP), snake venom metalloproteinases (SVMP) and kunitz type protease inhibitors (KUN) (Figure 2E and S2B). The relative abundance of these toxin classes matched the venom gland tissue at transcriptome level, and the crude venom composition at protein level (Whiteley et al., 2019) (Figure 2E). Of note, the seven-day differentiation protocol increased overall toxin gene expression but reduced the expression of CRISP (Figure 2D and E). We concluded that *A. l. cowlesi* organoids produced a near-normal spectrum of venom factors.

Adult *Naja nivea* venom gland-derived organoids

To further demonstrate the long-term propagation capacity of adult venom gland derived cells using our protocol, we expanded organoids from *Naja nivea*, the Cape cobra. Venom glands from a euthanized adult individual (>1-year-old) were dissociated and cultured using the same conditions as used above (Figure 3A). Organoids recapitulated the epithelial phenotype and were expanded for over 18 passages (Figure 3A and B). While cells were viable and proliferating in ‘expansion medium’, we noticed reduced swelling (smaller lumen) in *N. nivea* organoids making it more difficult to mechanically split these cultures. Upon additional activation of cyclic AMP using forskolin (FSK), organoids exhibited improved swelling allowing easier splitting (Figure 3C). For further passaging (after passage 5) of *N. nivea* organoids, we supplemented expansion medium with FSK. Forskolin-induced swelling is well known in primary human intestinal organoids, where it is used to monitor the ability to transport chloride ions (Dekkers et al., 2013).

Exposure to ‘differentiation medium’, including the withdrawal of FSK resulted in the expected phenotype of less proliferative organoids (Figure 3D) accompanied by increased expression of 3FTx and KUN by qPCR (Figure 3E). To establish a ‘deep’ gene expression profile, we performed bulk mRNA sequencing of *N. nivea* organoids in differentiation medium. PolyA enriched reads could be mapped to the *de novo* *A. l. cowlesi* transcriptome (Figure 2C). We thus identified a number of putative toxins enriched in organoids from *N. nivea*, such as beta-bungarotoxin-like, kappa-bungarotoxin-like and sarafotoxin-like (Figure 3F). Three-finger toxins are the main venom components of elapid snakes. Utilizing the high sequence conservation of 3FTX, we were able to PCR-amplify the coding sequence of several variants starting from *A. l. cowlesi* and *N. nivea* organoid cDNA (Figure 3G). When translating these 3FTX coding sequences *in silico* we detected peptide sequences that have not been described before in the NCBI database and are specific to the individual species (Figure 3H).

As our access to *A. l. cowlesi* venom gland material was more regular (one clutch a year), we focused our further characterization on organoid lines derived from *A. l. cowlesi*.

Organoids display cellular heterogeneity in toxin expression

The cellular heterogeneity of the venom gland epithelium has largely been described morphologically. We have recently demonstrated the usefulness of organoids for the detailed

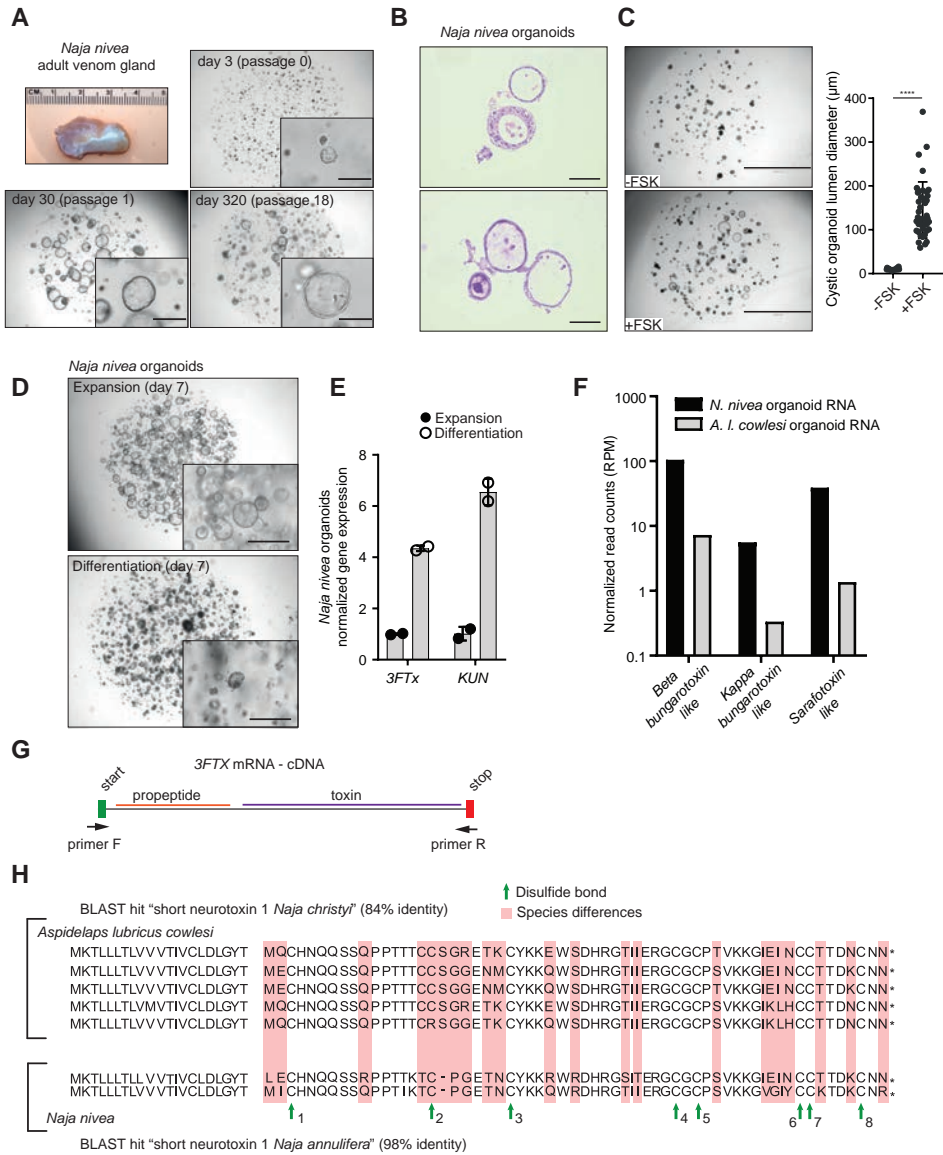


Figure 3. *Naja nivea* organoids derived from adult venom gland reveal species-specific toxins. Adult *Naja nivea* venom gland (n=2) and organoid outgrowth after seeding of primary cells (passage0) until passage 18 (Related to Figure S1A). Scale bars, 200 µm. HE and PAS staining of *Naja nivea* organoids derived from an adult venom gland. Scale bars, 50 µm. Brightfield images and quantification of *Naja nivea* organoids grown in complete expansion medium with or without supplementation of forskolin (FSK) and matching quantification. Scale bars, 2000 µm. Brightfield images of *Naja nivea* organoids after 7 day expansion or differentiation protocol. Scale bars, 200 µm. Gene expression of toxins (*3FTX* and *KUN*) in *N. nivea* organoids upon exposure to expansion or differentiation medium (7 days). Determined by qPCR, normalized to *ACTB* and relative to expansion medium. Plot of normalized read count of three selected toxins for *N. nivea* and *A. l. cowlesi* organoid bulk mRNA sequencing after 7 days of differentiation. *N. nivea* data generated from bulk RNA sequencing mapped on *de novo* *A. l. cowlesi* transcriptome (n=1). *A. l.*

- *cowlesi* read count from differentiation data Figure 3 (n=1). Schematic representation of PCR amplification of *3FTX* coding sequence from cDNA obtained from organoids. Location of forward (F) and reverse (R) primer. Peptide sequence of *in silico* translated *3FTX* coding sequences of *A. l. cowlesi* and *N. nivea*. Highlighted in red species differences, green arrow conserved disulfide sites. BLASTP hit for best match with proteins in the NCBI database.

delineation of cell lineages in the enteroendocrine compartment of the gut (Beumer et al., 2018). Using a similar strategy, we performed single cell RNA sequencing of organoids in expansion and differentiation medium and compared it to their primary tissue counterparts obtained from *A. l. cowlesi* late embryonic venom gland. From organoids, a total of 1,536 cells were sorted, processed using the SORT-seq method (Muraro et al., 2016) and analyzed using the RaceID3 package (Herman et al., 2018). Reads were mapped to the *de novo* assembled *A. l. cowlesi* transcriptome, processed using a newly generated pipeline and filtered for >2,000 transcripts per cell. The 1,092 cells which passed the thresholds displayed a median expression of 10,480 transcript counts per cell (Figure S3A and S3B). K-medoids-based clustering compartmentalized the cells into 12 different cell clusters, as visualized by *t*-distributed stochastic neighbor embedding (t-SNE) (Figure 4A). Cells derived from expansion and differentiation medium clustered mostly separately (Figure 4B). Expression of one of the most abundant three-finger toxins (*Pr-SNTX*) (Figure S2B) revealed the presence of at least 4 cell clusters producing venom factors (Figure 4C). In line with the bulk transcriptome data, the vast majority of venom-producing cells were derived from differentiated organoids.

Single cell RNA sequencing of freshly isolated venom gland tissue (using the same pipeline as for the organoid cells) yielded 1,255 cells which passed the same threshold (Figure 4D). Based on their transcriptomic profile, these cells fell into 20 different cell clusters (Figure 4D). Using mammalian markers of cell types expected to be present in glandular organs, we determined the following composition of our dataset: 53% epithelial cells (*EPCAM*, *KRT8*) (Figure 4E and S3C), 27% stromal cells (*COL3A1*), 8% hematopoietic cells (*HEMGN*, *LYZ*), 7% smooth muscle cells (*ACTA2*) and 4% endothelium (*CDH5*) (Figure S3C). Expression of three-finger toxin *Pr-SNTX* was highest in two of the cell clusters of epithelial origin (Figure 4F). We also detected strong co-expression of protein disulfide isomerase (*PDI*) with 3FTx variants (*Scutellatus toxin 3*) in the organoids (Figure 4G) as well as in the primary tissue cells (Figure 4H). This enzyme is a key factor to ensure correct disulfide bond folding (Wang and Tsou 1993), conceivably supporting the disulfide bond-rich structure of three finger toxins. A more detailed analysis of toxin-related gene expression per cluster uncovered that individual venom factors were strongly enriched in separate organoid clusters, suggesting the presence of specialized cells for some of the toxin families (Figure S3D).

We extracted all 670 epithelial cells from the dataset and performed reclustering (Figure S3E). This resulted in 10 different epithelial subclusters, each enriched for different venom factors. Comparing the heterogeneity in the expression of different toxin classes (*3FTx*, *CRISP*, *KUN*, *SVMP* and *CTL*) we concluded that organoids successfully recapitulate the cellular complexity of venom producing cells *in vivo* (Figure S3F).

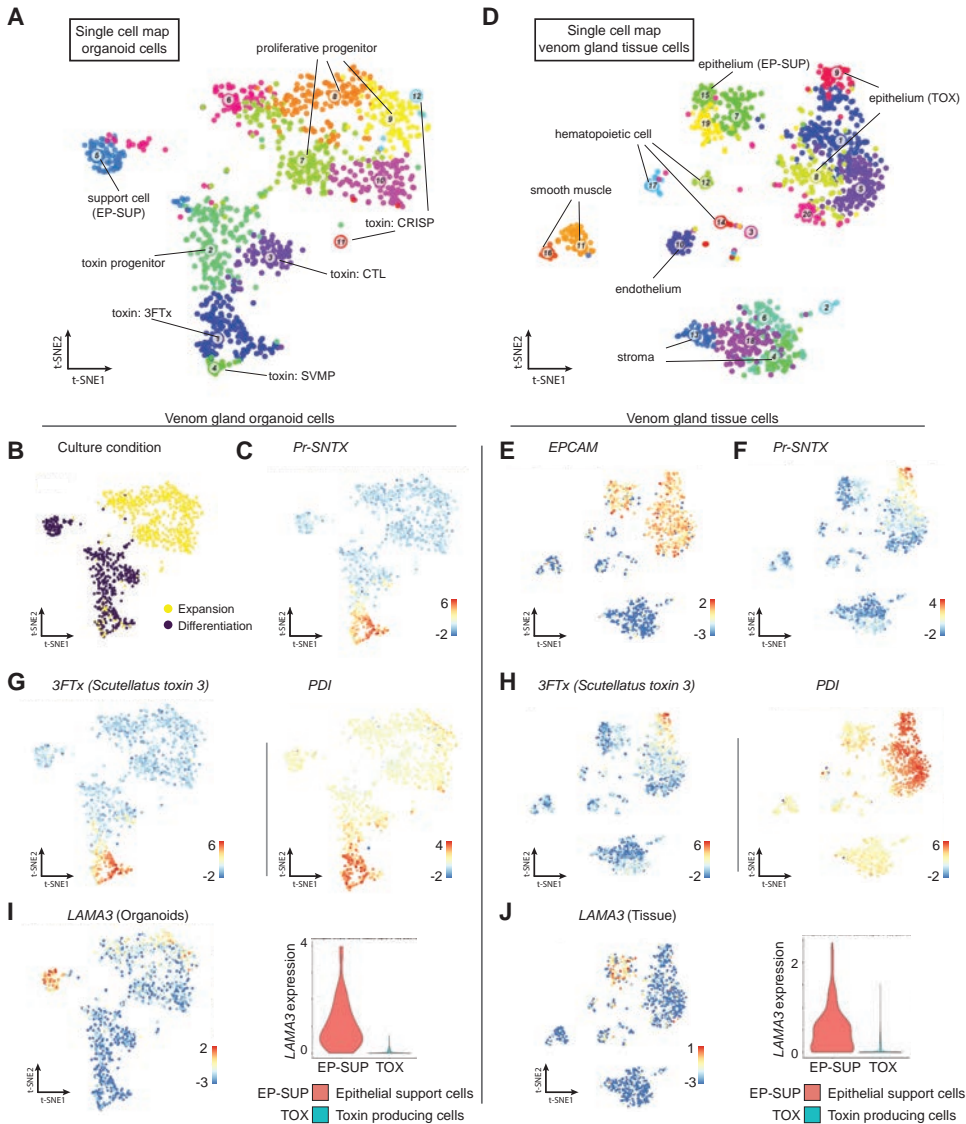


Figure 4. Single cell transcriptome analysis of organoids and primary tissue reveals distinct venom gland cell types, see also Figure S3, S4, S5 and S6. Single cell RNA sequencing: clustering of *A. l. cowlesii* venom gland organoid cells (n=1092) visualized by *t*-distributed stochastic neighbor-embedding (*t*-SNE) map. Colors highlight different clusters (n=12). *t*-SNE map indicating exposure to expansion medium (yellow) or differentiation medium (purple) for seven days. Expression level of three-finger toxin *Pr-SNTX* in *t*-SNE map (color coded logarithmic scale of transcript expression). Clustering of primary *A. l. cowlesii* venom gland tissue cells (n=1255) visualized by *t*-distributed stochastic neighbor-embedding (*t*-SNE) map. Colors highlight different clusters (n=20). Expression level of epithelial cell marker *EPCAM* in *t*-SNE map (color coded logarithmic scale of transcript expression). Expression level of three-finger toxin *Pr-SNTX* in *t*-SNE map (color coded logarithmic scale of transcript expression). (G-H) Expression levels of selected genes in *t*-SNE map (color coded logarithmic scale of transcript expression). Left is venom gland organoids cells and right is primary venom gland tissue cells. (I-J) Expression levels of *LAMA3* in *t*-SNE map (color coded ▶

- ▶ logarithmic scale of transcript expression) and violin plots visualizing expression levels of cluster-enriched toxins. For both organoid cells (I) and venom gland tissue cells (J) color coded EP-SUP cells (red) and TOX cells (green).

Cluster 1 in organoids and cluster 6 in primary tissue comprised cells enriched for transcripts of *3FTX* genes (Figure S4A), a subset of these cells additionally expressed Kunitz variants (*KUN*) (Figure S4B). The cells in cluster 4 (organoids) and cluster 6 and 8 (tissue) were positive for *SVMP* (Figure S4C). Organoid cells expressing CRISP genes were enriched in cluster 11 and 12; in the tissue these genes were found to be expressed in a larger number of cells enriched in cluster 3 (Figure S4D). Organoid cluster 3 consisted of cells co-expressing C-type lectin (CTL) and Waprin-related toxins (Figure S4E) (Torres et al., 2003; Ogawa et al., 2005). CTLs have not previously been detected in the *Aspidelaps lubricus* venom proteome and did not form an independent cluster in the tissue dataset (Whiteley et al., 2019).

Cluster 5, containing cells exclusively derived from differentiated organoids, was devoid of any known toxin expression. Comparing this cluster with venom producing clusters 1, 2, 3 and 4, we found these cells to be enriched in extracellular matrix component transcripts such as laminin (*LAMA3*) (Figure 4I). This transcriptomic separation is indicative of two different cellular lineages captured by the organoids, an “epithelial supportive cell” fate (EP-SUP) and a “toxin producing cell” fate (TOX) (Figure S5A). In the complete dataset of venom gland tissue cells, we found cluster 7, 15 and 19 to be enriched in *LAMA3* expression, while these cells expressed much fewer toxin transcripts compared to the other epithelial cells (Figure 4J and S5B). In organoids as well as tissue, the EP-SUP lineage additionally expressed *CTGF*, *COL7A1* and *FRZB* (Figure S5C-E). Based on our single cell sequencing of the venom gland tissue, all epithelial lineage/cell types were represented in the organoids. Importantly, marker expression analysis of each of the 12 cell clusters in early and late passage organoids supported the notion that cellular composition of organoids was stable over time in culture (Figure S5F).

Characterization of the Wnt-activated proliferative cells

Having identified the distribution of toxin expression in differentiated cells, we next focused on the expression patterns specific to cell clusters observed under expansion conditions. While some cells in expansion medium clustered together with toxin-expressing cells in cluster 1, 4, 11 and 12, the vast majority fell within the expansion medium-specific clusters 6–10 (Figure 4A and B). Cluster 10 was distinct in displaying high expression of phospholipase A2 inhibitor (*PLI*) (Figure S6A), previously described in other snake species as a self-protective mechanism against venom PLA2 toxins (Lima et al., 2011). Expression of *PLI* was also found in epithelial cells from primary tissue (Figure S6B).

Cells in organoid clusters 7, 8 and 9 expressed the proliferation marker Ki-67 (*MKI67*) (Figure 5A). Transcripts for the snake homologs of the mammalian stem cell markers *RNF43* (Koo et al., 2012), *ASCL2* (van der Flier et al., 2009) and *LGR5* (Barker et al., 2007) were enriched in these clusters and were specifically observed under expansion conditions, while being rare

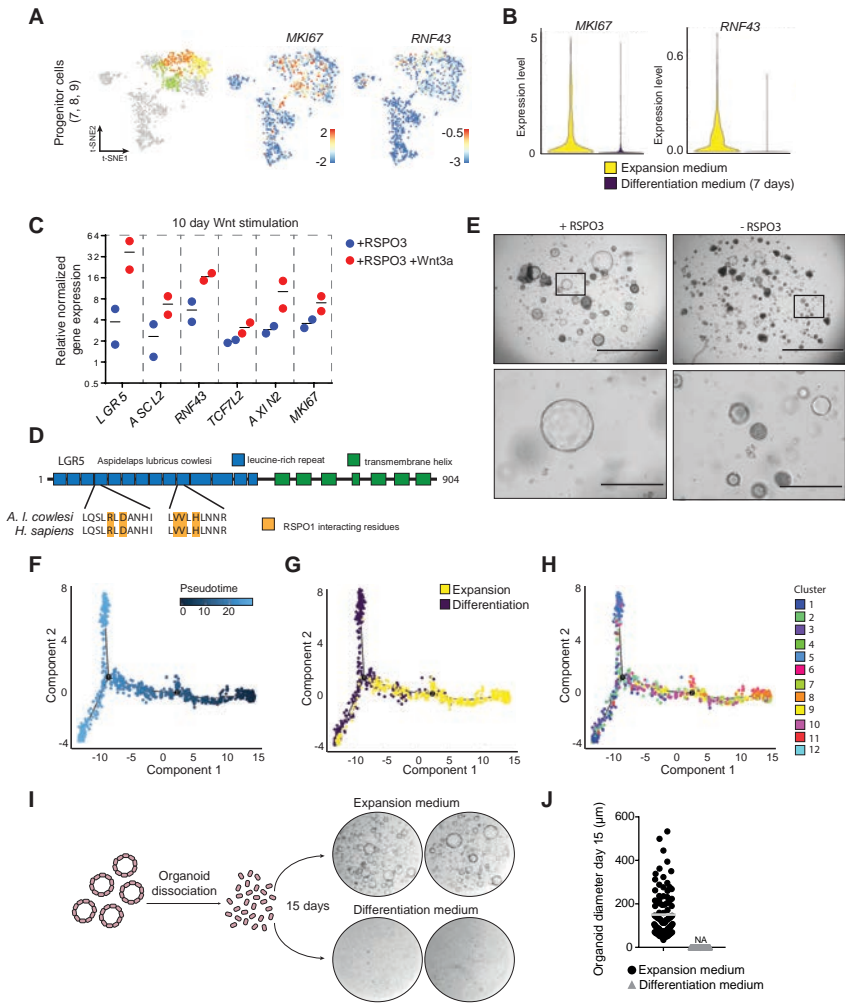


Figure 5. Non-venomous organoid cells include Wnt-active proliferating cells, see also Figure S6. Expression levels of *MKI67* and *RNF43* in *t*-SNE map (color coded logarithmic scale of transcript expression). Violin plot of *MKI67* and *RNF43* expression levels in cells from expansion medium (yellow) or differentiation medium (purple). Changes in organoid gene expression levels after 10 day Wnt activation (addition of RSPO and RSPO plus exogenous Wnt3a). Expression levels were determined by qPCR and shown relative to ‘no RSPO and no Wnt3a exposure’, normalized to *ACTB*. Schematic overview of *A. I. cowlesi* LGR5 protein and alignment of R-spondin-interacting residues with the human amino acid sequence. Representative brightfield images of organoids grown for 14 days with (+RSPO3) or without (- RSPO3) R-spondin in culture medium. Scalebars, 2000 μ m (upper panels) and 400 μ m (lower panels). Ordering of cells from single cell sequencing data along a pseudotemporal trajectory using Monocle. Position of cells exposed to expansion medium (yellow) or differentiation medium (purple) for seven days along the pseudotemporal trajectory. Position of cells belonging to the 12 different clusters along the pseudotemporal trajectory. (I-J) Schematic overview of experimental setup and representative brightfield images of organoid outgrowth in expansion medium and differentiation medium starting from a near-single cell state. Circular images represent 20 μ L BME droplets containing cells/organoids. J is quantification of I.

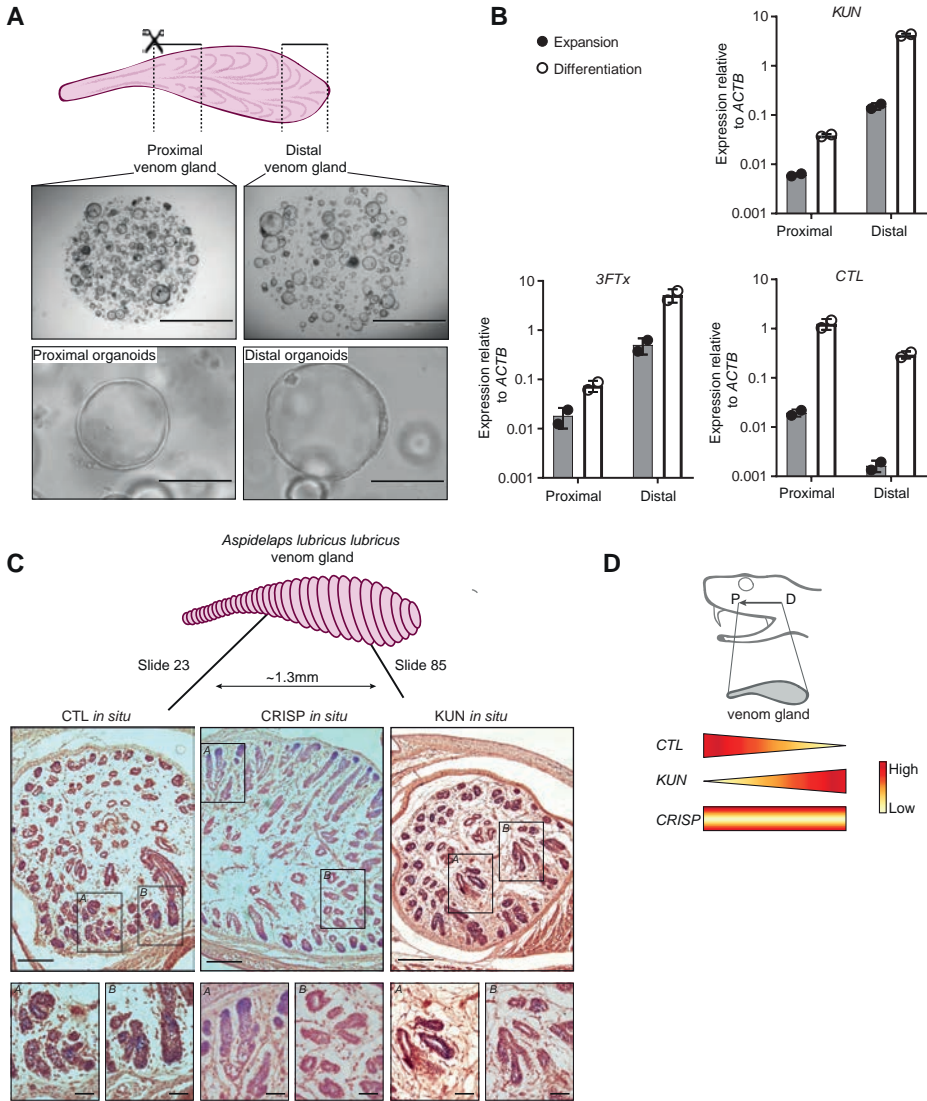


Figure 6. Hard-wired regional heterogeneity in toxin expression is maintained in organoids from proximal and distal venom gland, see also Figure S7. Schematic representation and brightfield images of organoids derived from the proximal and distal region of the *A. l. cowlesi* venom gland. Scale bars, upper panels 2000 μm , lower panels 200 μm . Gene expression of toxins (*KUN*, *3FTX* and *CTL*) in proximal and distal organoid lines (passage 4) exposed to expansion medium or differentiation medium (7 days). Expression levels were determined by qPCR shown relative to *ACTB*. Schematic representation of venom gland sections from proximal to distal. And BM-purple stain of in situ hybridization for CTL (slide 23), CRISP and KUN (slide 85) in *A. l. cowlesi* venom gland tissue. Scale bars, upper panels 200 μm , lower panels 50 μm . Schematic overview of regional heterogeneity in venom gland toxin expression: CTL expression proximal, KUN expression distal and CRISP expression along the proximal-distal axis on the basal side.

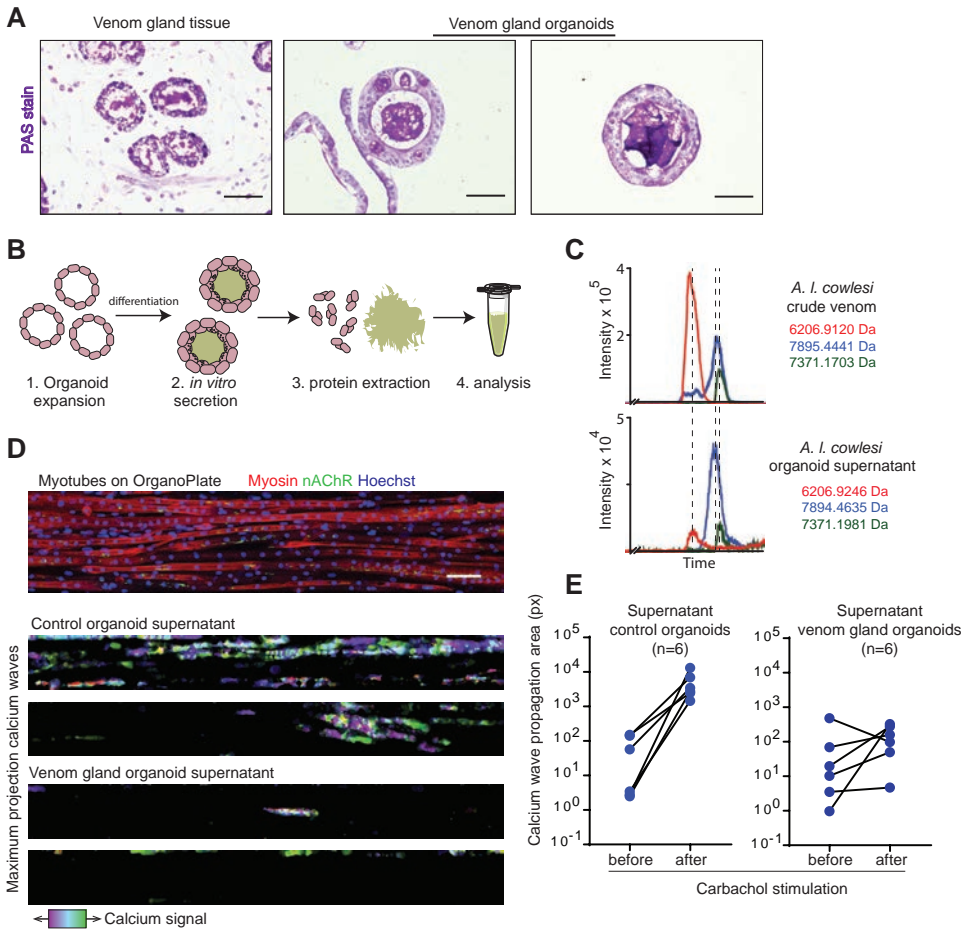


Figure 7. Organoids produce biologically active toxins, related to Figure S8. Luminal accumulation of secreted proteins was determined using periodic acid-Schiff (PAS) staining in late embryonic venom gland tissue and organoids. Scale bars, 50 μm . Schematic representation of organoid extraction. Organoids were expanded for four days and then subjected to a seven-day differentiation protocol. In PBS, the lumen was opened using mechanical shearing and cells disrupted using sonication. Cellular debris was pelleted by centrifugation and supernatant collected for analysis. Direct comparison of *A. l. cowlesi* crude venom (upper panel) with organoid extract (lower panel) using liquid chromatography–mass spectrometry (LC-MS) identifies three overlapping products. Ion- chromatogram displays signal intensity (y-axis) over retention time in minutes (x-axis) with indicated mass per trace. Immunofluorescence staining of C2C12 myotubes in OrganoPlate, myosin (red), nAChR (green) and Hoechst (blue) (upper panel). Scale bar, 100 μm . The calcium wave propagation was imaged before and after exposure to different supernatants in chips. Maximum projected images depict the total calcium signal over all image frames after carbachol stimulation, in which purple reflects activity to the left and green to the right (lower panels). Quantification of (D). The total calcium signal was calculated before and after carbachol stimulation based on total fluorescent signal. The venom gland organoid supernatant blunts the induction of calcium sparks.

in primary tissue (Figure 5A, 5B and S6B - F). This implied these clusters to represent reptilian adult stem/progenitor cells.

Addition of R-spondin 3 enhanced expression of the stem cell markers *LGR5*, *ASCL2* and *RNF43* together with the well-established Wnt targets *TCF7L2* and *AXIN2*. Supplementation of exogenous Wnt3a further increased expression of these marker genes. As expected, stimulation of the Wnt pathway also induced the proliferation marker *MKI67* (Figure 5C). *A. l. cowlesi* LGR5 shares the same leucine-rich repeats and transmembrane helices with high conservation in the R-spondin interacting residues (R144, D146, V213, V214 and H216) compared to the human protein (Figure 5D) (Chen et al., 2013). Indeed, human R-spondin 3 was found to be essential for organoid expansion (Figure 5E, 1D and S1B).

The non-epithelial niche is replaced in organoid culture by the addition of defined exogenous growth factors. Using the single cell sequencing dataset of venom gland tissue, we searched for expression of such secreted factors. We detected the EP-SUP cluster as an epithelial source of *WTN10A* expression (Figure S6G). Stromal cells (cluster 4, 6, 13 and 18) specifically expressed *WNT9A*, *FGF7* and the BMP-antagonists *CHRD* (Piccolo et al., 1996) and *FSTLI* (Sylva et al., 2011) (Figure S6H - K). As expected, transcripts for these proteins with a stromal source *in vivo* were not detected in the organoids. Pseudotemporal ordering of venom gland organoid cells grown in expansion- and differentiation medium using Monocle (Trapnell et al., 2014) was then applied to shed light on the venom gland stem cell hierarchy. Cells from the proliferative progenitor clusters 7, 8 and 9 were placed at the start of the pseudotime axis, in agreement with their stem/progenitor state. A bifurcation was formed by the EP- SUP cells of cluster 5 and toxin-producing (TOX) cells from clusters 1, 2, 3 and 4 (Figure 5F - H). To confirm the lack of proliferative and stem cell capacity in the mature clusters (cluster 1 - 5, Figure 4A and B), we differentiated organoids using the growth factor depletion described above. This caused a dramatic reduction in outgrowth and proliferative capacity compared to expansion conditions (Figure 5I and J).

Regional heterogeneity in toxin production in the venom gland is maintained in organoid culture

Secretory cells of other mammalian organs, such as the intestine, display regional variation in the types of secreted products. For instance, organoids derived from different regions of the mouse small intestine produce a region-specific repertoire of hormones that is maintained indefinitely *in vitro* (Beumer et al., 2018). We investigated regional heterogeneity in toxin production in the snake venom gland using our organoid culture system. The venom gland of embryonic *A. l. cowlesi* was dissected into a proximal (located near the duct) and a distal part and established region-specific organoids (Figure 6A). After culturing organoids for 1 month (4 passages), we analyzed toxin expression in expansion and differentiation medium by qPCR. We found *CTL* expression to be strongly enriched in 'proximal' organoids, whereas 'distal' organoids cells predominantly produced *3FTX* and *KUN* toxins (Figure 6B). Next, we utilized RNA *in situ* hybridization to visualize the expression of these toxins in venom gland tissue. We found a strong enrichment of *CTL* transcripts in the proximal part of the gland,

whereas *KUN* was predominantly expressed in the distal tissue, confirming our findings in organoids (Figure 6C, S7A and B). This is in line with a previous report of *CTL* expression in the proximally located accessory gland in the king cobra (Vonk et al., 2013). *CRISP* expression was homogenous along the proximal- distal axis of the gland, while displaying a bias towards basal over luminal cells (Figure 6C). These data highlighted regional heterogeneity in toxin expression in the snake venom gland (Figure 6D). Long-term maintenance of this phenotype in organoid culture showed this not to be determined by extrinsic (non-epithelial) growth factors.

Venom gland organoids secrete functionally active toxins

To investigate whether the stem cell-based organoids produced functionally active venom components, we analyzed organoid protein extracts after 7 days of differentiation. The presence of secretory vesicles and the apparent accumulation of proteins in the lumen of organoids suggested significant production of secretory proteins (Figure 7A and 3B). To validate functional translation and secretion of toxins, we generated a fluorescent three-finger toxin reporter organoid line. Using CRISPR-HOT (Artegiani et al., under review, Nature Cell Biol), we tagged one of the endogenous three-finger toxins (*NTX4*) with a fluorescent protein (mNeon-Green) (Figure S8B). We detected the green fluorescent fusion protein inside the cells of the organoids and accumulating in the lumen (Figure S8B).

We also directly compared organoid extract (Figure 7B) with *A. l. cowlesi* crude venom using liquid chromatography-mass spectrometry (LC-MS). This revealed three main peaks between 6-8 kDa of near identical mass between the two samples (Figure 7C). Tryptic digest analysis of these peptides yielded patterns compatible with several venom-related proteins such as 3FTx and CRISP (Figure S8A).

Snake venom neurotoxins are described to act primarily on acetylcholine receptors (nAChR and mAChR) (Nirthanan et al., 2004; Karlsson et al., 2000). As an initial assessment of the biological activity of organoid-secreted venom peptides, we exposed murine muscle cultures (endogenously expressing the nAChR) to the organoid supernatant and recorded signal propagation using calcium imaging in an OrganoPlate (Trietsch et al., 2013) (Figure 7D, S8C - F). This organ-on-a-chip platform allows live cell imaging during venom exposure in 96 independent mature muscle cultures per plate. The venom peptides derived from differentiated organoids abolished the stimulatory effect of the acetylcholine receptor agonist carbachol on muscle cells, as did the positive control alpha-bungarotoxin (α -BTX). Supernatant from non-venom producing (human) organoids did not inhibit calcium wave propagation after addition of carbachol (Figure 7E, S8G - I).

In a similar set-up, we exposed rat cortical neurons grown on microelectrode array (MEA) plates to organoid supernatant and recorded neuronal activity (Figure S9A). Upon acute exposure, we noticed a marked increase in neuronal activity, following a similar trend observed with recombinant alpha- bungarotoxin (Figure S9B - D). This occurred most likely through an antagonistic effect on inhibitory GABA_A-receptors (McCann et al., 2006), without affecting neuronal cell viability (Figure S9E - G).

I

II

III

IV

V

VI

VII

VIII

&

DISCUSSION

We report the establishment of reptilian adult stem cell-based organoids. Using a mammalian niche growth factor cocktail, these cells can be expanded seemingly indefinitely. The ability to culture venom gland epithelial cells over long periods of time represents a platform for a comprehensive understanding of the biology of the venom gland and the various venom constituents. Short-term cultures of different Viperidae snakes have previously been reported, such as explants of *Bothrops jararaca* (Carneiro et al., 2006; Yamanouye et al., 2006), suspension cultures of *Bitis gabonica* (Sells et al., 1989) and unpolarized two-dimensional cell lines of *Crotalus durissus terrificus* (Duarte et al., 1999). The venom gland organoid cultures provides advantages in structural conservation (Figure 1C), cellular heterogeneity (Figure 4), regional heterogeneity (Figure 6), long-term expansion (Figure 1B and 3A), genetic modifiability (Figure S1E and S8B) and broad applicability across snake species (Figure S1A). With a *de novo*-generated transcriptome of *A. l. cowlesi*, we demonstrate that the venom gland organoid cells produce a diverse spectrum of venom factors over many passages (Figure 2).

Previous mammalian organoid cultures have highlighted the importance of Wnt-driven stem cell maintenance *in vitro* (Clevers 2016). Indeed, we identify a proliferative population of cells in the venom gland organoids that is defined by the expression of the snake homologs of established Wnt-driven stem cell genes of mammalian epithelia: *LGR5* (Barker et al., 2007), *ASCL2* (van der Flier et al., 2009) and *RNF43* (Koo et al., 2012). The importance of R-spondin in reptilian cell proliferation highlights the critical role and a high level of conservation of the Wnt pathway in ASC biology. We believe that the culture conditions used here may be widely applicable to vertebrate species.

While a divergent composition of snake venoms between species, and even between and within individuals, is well-established (Casewell et al., 2014; Augusto-de-Oliveira et al., 2016; Zancolli et al., 2019), the cellular heterogeneity underlying the production of individual toxins is not well described. Initial attempts at characterizing the cell types of the snake venom gland through electron microscopy has resulted in the morphological identification of at least 4 cell types, of which columnar epithelial cells containing granules have been suggested to be the main source of venom production and secretion (Mackessy 1991). The amount and type of venom detectable in individual cells is influenced by the secretory cycle, referring to temporal dynamics in venom production and secretion (Taylor et al., 1986; Shaham and Kochva 1969). A previous study identified heterogeneity in the binding of single-component antibodies to secretory granules and attributed this mainly to the secretory cycle-dependent production of toxins rather than cellular heterogeneity of the venom gland (Taylor et al., 1986).

Our data describe cellular heterogeneity in the venom gland epithelium at the level of transcription. Gene expression profiling at single cell resolution of both organoids and primary tissue uncovers the coincident expression of characteristic groups of toxins by individual cell types. Future studies may use venom gland organoids to dissect the stimuli and timing of venom production and secretion. The ability to indefinitely expand these organoids and repeatedly harvest venom supernatants in a highly defined environment may help overcome hurdles posed by the significant variation in snake venom composition.

Finally, the current study opens new avenues for bioprospecting of snake venom components and may be developed into a production platform for (modified) snake venom, allowing novel therapeutic strategies to tackle snakebite.

ACKNOWLEDGMENTS

We thank Reinier van der Linden for flow cytometry assistance; Benedetta Artegiani and Delilah Hendriks for generation of CRISPR-HOT technology and assistance in applying it to snake venom gland organoids; Anko de Graaff and the Hubrecht Imaging Centre (HIC) for microscopy assistance; BaseClear B.V. for bulk mRNA sequencing and *de-novo* transcriptome assembly; Bas Ponsioen for providing the lentiviral H2B-RFP construct; Single Cell Discoveries for the provided single-cell sequencing service and support; local snake breeders for donating venom gland material to this study, and Sebastiaan Voskuil, Edwin Boel, Marc Bonten and Frank Driehuis for advice regarding antibiotic treatments. X.M.S. was supported by ALS foundation Netherlands. N.R.C. was supported by a Sir Henry Dale Fellowship (200517/Z/16/Z) jointly funded by the Wellcome Trust and the Royal Society.

AUTHOR CONTRIBUTIONS

Y.P., J.P., J.B. and H.C. conceptualized the project, designed the experiments, interpreted the results and wrote the manuscript. H.B. and J.K. performed immunohistochemistry experiments. J.P., B.D.B., A.V.O., M.C.H. and H.J.G.S. performed bulk and single cell mRNA sequencing analysis on *de novo* transcriptome. Y.E.B.E. assisted with FACS experiments. C.L.I., W.J.V.D.W. and P.J.P. performed transmission electron microscopy. M.A.G.D.B. performed *in situ* hybridization experiments. R.L.V.I. and A.C.R. generated immunofluorescent images. J.S. and J.K. performed mass spectrometry analysis. S.A., T.D.K. and N.R.C. performed toxin gene expression analysis on bulk RNA sequencing data. N.R.W., X.M.S. and T.O. performed and analyzed toxicity tests on Mimetas OrganoPlate. H.M.H., F.J.V. and M.K.R. assisted in initializing the project and provided access to venom gland tissue. R.H.S.W. and R.G.D.M.K. provided helpful insight in functional venom characterization. W.G. and N.R.C. provided venom gland tissue.

DECLARATION OF INTERESTS

H.C. is inventor on several patents related to organoid technology; his full disclosure is given at <https://www.uu.nl/staff/JCClevers/>. N.R.W. and T.O. are employees of MIMETAS BV, the Netherlands, which is marketing the OrganoPlate. OrganoPlate is a registered trademark of MIMETAS.

I

II

III

IV

V

VI

VII

VIII

&

STAR METHODS

Lead Contact and Materials Availability

Further information and requests for resources and reagents should be directed to the Lead Contact, Hans Clevers (h.clevers@hubrecht.eu).

Unique/stable reagents generated in this study are available and can be requested from the Lead Contact, a completed Materials Transfer Agreement may be required.

EXPERIMENTAL MODEL AND SUBJECT DETAILS

Snakes

All animal procedures complied with local ethical guidelines. Adult *Crotalus atrox* (n = 2) venom glands were purchased from Natural Toxins Research Center in Texas, USA. Adult *Echis ocellatus* (n = 1) and *Deinagkistrodon acutus* (n = 1) venom glands were obtained from snakes maintained at the Liverpool School of Tropical Medicine, UK. Adult *Naja pallida* (n = 1), *Naja nivea* (n = 1) and *Bitis arietans* (n = 2) venom glands were obtained from residual post-mortem material from Serpo, Rijswijk, the Netherlands. Embryonic *Naja atra* (n = 2), *Naja annulifera* (n = 3) and *Aspidelaps lubricus cowlesi* (n = 7, two different nests) from eggs were obtained from local breeders in the Netherlands. All snakes were captive bred and maintained in individual cages within a temperature, humidity and light-controlled environment according to local protocols for husbandry of venomous snakes. Sex of the animals was not determined as it was presumed to have no biological impact on the experimental procedure or conclusion of the study. Non-invasive venom extraction ('milking') was performed with adult *Echis ocellatus*, *Deinagkistrodon acutus*, *Naja pallida*, *Naja nivea* and *Bitis arietans* during lifetime prior to euthanizing and venom gland isolation for organoid culture.

Venom gland organoid cultures

Cells from a single gland were plated in approximately 100 μ L Cultrex Pathclear Reduced Growth Factor Basement Membrane Extract (BME) (3533-001, Amsbio). After BME solidification, culture medium was added. Expansion culture medium was based on AddMEM/F12 (GIBCO) supplemented with B27, Glutamax, HEPES, 100 U/mL Penicillin-Streptomycin (all Thermo-Fisher), 100 mg/mL Primocin (Invivogen), 1.25mM N-acetylcysteine, 10 mM Nicotinamide (both Sigma-Aldrich) and the following growth factors: 2% Noggin conditioned medium (U-Protein Express), 2% Rspo3 conditioned medium (U-Protein Express), 50 ng/mL EGF (Peprotech), 0.5 μ M A83-01 (Tocris), 1 μ M PGE2 (Tocris), 100 ng/mL FGF10 (Peprotech), 100 nM Gastrin (Tocris). *Naja nivea* organoid cultures were supplemented with 1 μ M FSK (Tocris). For the first seven days after seeding, the expansion medium was supplemented with 10 μ M Y-27632 (Abmole). In case of bacterial contaminations following antibiotics were added: 50 mg/mL Gentamicin (Sigma), 2.5 μ g/ml Ciprofloxacin (Sigma-Aldrich), 20 μ M Erythromycin (Sigma-Aldrich) and 100 nM Azithromycin (Sigma-Aldrich). Ten days after seeding organoids were removed from the BME, mechanically dissociated into small fragments using a Pasteur

pipette and re-seeded in fresh BME. Passage was performed in 1:3 – 1:5 split ratio once every ten days for at least 6 months.

C2C12 cell line

The C2C12 mouse myoblast cell line was purchased from Sigma-Aldrich (91031101). Sigma is partnered with the European Collection of Authenticated Cell Cultures (ECACC) repository. Cells were cultured in T75 flasks (734-2705, Corning) in DMEM (11965092, Thermo Fisher Scientific) supplemented with 10% fetal bovine serum (FBS, 16140-071, Thermo Fisher Scientific), 2 mM glutamine (G7513, Sigma-Aldrich) and 1% penicillin/streptomycin (P4333, Sigma-Aldrich) at 37°C. C2C12 cells were routinely tested for mycoplasma contamination and were found negative.

Primary rat cortical neurons

Primary rat cortical cells were isolated from postnatal day 0-1 pups of timed pregnant Wistar rat dams (Envigo) as described previously (Dingemans et al., 2016). Briefly, pups were decapitated and cortices were rapidly dissected on ice and kept in dissection medium (Neurobasal®-A supplemented with 25 g/L sucrose, 450 µM L-glutamine, 30 µM glutamate, 1% penicillin/streptomycin and 10% FBS, pH 7.4) during the entire procedure. Cortices were dissociated to a single-cell suspension by mincing with scissors, trituration and filtering through a 100 µm mesh (EASYstrainer, Greiner). The cell suspension was diluted to a 2 × 10⁶ cells/mL solution. Droplets of 50 µL were placed on the electrode fields in wells of 48-wells MEA plates (Axion BioSystems) pre-coated with 0.1% PEI solution diluted in borate buffer (24 mM sodium borate/50 mM boric acid in Milli-Q, pH adjusted to 8.4). Cells were left to adhere for 2 hours before adding 450 µL dissection medium. Primary rat cortical cultures were kept at 37°C in a humidified 5% CO₂ incubator. At day in vitro (DIV) 2, 90% of the dissection medium was replaced with glutamate medium (Neurobasal®-A supplemented with 25 g/L sucrose, 450 µM L-glutamine, 30 µM glutamate, 1% penicillin/streptomycin and 2% B27 supplement, pH 7.4) to prevent glial overgrowth. At DIV4, 90% of the glutamate medium was replaced with FBS medium (Neurobasal®-A supplemented with 25 g/L sucrose, 450 µM L-glutamine, 1% penicillin/streptomycin and 10% FBS, pH 7.4).

METHOD DETAILS

Venom gland isolation.

All animal procedures complied with local ethical guidelines. Adult *Crotalus atrox* (n=2) venom glands were purchased from Natural Toxins Research Center in Texas, USA. Adult *Echis ocellatus* (n=1) and *Deinagkistrodon acutus* (n=1) venom glands were obtained from snakes maintained at the Liverpool School of Tropical Medicine, UK. Adult *Naja pallida* (n=1), *Naja nivea* (n=1) and *Bitis arietans* (n=2) venom glands were obtained from residual post-mortem material from Serpo, Rijswijk, The Netherlands. *Naja atra* (n=2), *Naja annulifera* (n=3) and *Aspidelaps lubricus cowlesi* (n=7, two different nests) eggs were obtained from local breeders.

I

II

III

IV

V

VI

VII

VIII

&

In the last week of development (~day 53– 58), snakes were removed from the egg by an incision in the shell. To avoid bacterial contamination, eggs were briefly rinsed with bleach and 70% ethanol prior to opening in a laminar flow cabinet. Animals were directly euthanized by decapitation. The venom glands were surgically removed under an overhead microscope and stored on ice in AdDMEM/F12 (Gibco) supplemented with penicillin/streptomycin.

Venom gland organoid cultures, reagents.

Isolated venom glands were chopped into small pieces of approximately 1 mm using a scalpel. Muscle and connective tissue were removed and discarded as much as possible. Epithelial tissue pieces were enzymatically digested in 5 mL collagenase (Sigma- Aldrich, C9407, 1 mg/mL) with 10 μ M ROCK inhibitor Y-27632 (Abmole, M1817) in AdDMEM/F12 (Gibco) for about 30 minutes while shaking (120 RPM) at 32 °C. The homogenous cell suspension was pelleted and washed twice with AdDMEM/F12 prior to plating. Cells from a single gland were plated in approximately 100 μ L Cultrex Pathclear Reduced Growth Factor Basement Membrane Extract (BME) (3533-001, Amsbio). After BME solidification, culture medium was added. Expansion culture medium was based on AdDMEM/F12 (Gibco) supplemented with B27, Glutamax, HEPES, 100 U/mL Penicillin- Streptomycin (all Thermo-Fisher), 100 mg/mL Primocin (Invivogen), 1.25mM N-acetylcysteine, 10 mM Nicotinamide (both Sigma-Aldrich) and the following growth factors: 2% Noggin conditioned medium (U-Protein Express), 2% Rspo3 conditioned medium (U-Protein Express), 50 ng/mL EGF (Peprotech),

0.5 μ M A83-01 (Tocris), 1 μ M PGE2 (Tocris), 100 ng/mL FGF10 (Peprotech), 100 nM Gastrin (Tocris). *Naja nivea* organoid cultures were supplemented with 1 μ M FSK (Tocris). For the first seven days after seeding, the expansion medium was supplemented with 10 μ M Y-27632 (Abmole). In case of bacterial contaminations following antibiotics were added: 50 mg/mL Gentamicin (Sigma), 2.5 μ g/ml Ciprofloxacin (Sigma-Aldrich), 20 μ M Erythromycin (Sigma-Aldrich) and 100 nM Azithromycin (Sigma- Aldrich). Ten days after seeding organoids were removed from the BME, mechanically dissociated into small fragments using a Pasteur pipette and re-seeded in fresh BME. Passage was performed in 1:3 – 1:5 split ratio once every ten days for at least 6 months.

For differentiation experiments, established organoids were passaged and grown in expansion medium for four days. After four days, the medium was removed and residual medium washed away two times with PBS, after which differentiation medium was added containing; a base of AdDMEM/F12 (Gibco) supplemented with GlutaMAX, HEPES, 100 U/mL Penicillin-Streptomycin (all Thermo-Fisher), 100 μ g/mL Primocin (InvivoGen), 1.25mM N-acetylcysteine, 10 mM Nicotinamide (both Sigma-Aldrich) and 1 μ M PGE2 (Tocris) applied for seven days.

Quantification of cell viability/outgrowth efficiency was performed using CellTiter-Glo® according to the manufacturer's protocol.

Wnt-conditioned medium was produced as previously described, and used at 50% of the medium volume (Sato et al., 2011).

Images of organoid cultures were taken on EVOS FL Cell Imaging System (Thermo Fisher). Video of beating cilia in organoid was captured (20 frames/second, 20x objective) on EVOS FL Auto 2 (Thermo Fisher).

pLV lentiviral vector containing a CMV promoter driving the expression of TagRFP and Puro resistance gene (via IRES) was transduced in venom gland organoids.

Immunohistochemistry and imaging.

Organoids were harvested in cell recovery solution (354253, Corning) and fixed in 4% formaldehyde solution (Sigma-Aldrich) for at least 2 hours at room temperature. Venom glands used for immunohistochemistry were directly embedded in 4% paraformaldehyde upon dissection and fixed for at least 2 hours. Samples were washed and dehydrated by an increasing ethanol gradient before embedding in paraffin. Sections were cut and hydrated before staining. Hematoxylin and eosin (H&E) and periodic acid–Schiff (PAS) staining on organoids and tissue was performed as previously described (Sato et al., 2009). Slides were imaged using a Leica DM4000 microscope.

3D imaging of organoids was performed as described previously (Dekkers et al, 2019). In short, organoids were harvested using ice cold PBS and fixed in 4% paraformaldehyde at 4°C for 45 min. Organoids were then washed with PBT (PBS, 0.1% Tween) and incubated overnight with primary antibodies, B-catenin (H-102, Santa Cruz) and b-tubulin (H-235 Santa Cruz). The next day, organoids were washed with PBT (PBS, 0.1% Tween) and incubated overnight at 4°C with secondary antibodies, Alexa-fluor-647 Phalloidin (both from Thermo Fisher Scientific) and DAPI (Invitrogen). Dense organoids were optically cleared overnight in a glycerol-fructose clearing solution prior to imaging. Cystic organoids were not optically cleared to prevent these from collapsing. Organoid imaging was performed on a Zeiss LSM 880 using a 10x dry and 25x oil immersion objective. Imaris imaging software was used for 3D rendering of images.

For immunofluorescence in the OrganoPlate, cultures were fixed and stained as previously described (Wevers et al., 2018). The following antibodies were used: anti-myosin (A4.1025, DSHB), anti-desmin (ab8470, Abcam), anti-dystrophin (ab15277, Abcam), goat anti-mouse AlexaFluor 555 (A21422, Thermo Fisher Scientific), goat anti-mouse AlexaFluor 647 (A21236, Thermo Fisher Scientific), goat anti-rabbit AlexaFluor 555 (A32732, Thermo Fisher Scientific) and donkey anti-rabbit 647 (SAB4600177, Sigma-Aldrich). The nicotinic acetylcholine receptor was visualized using α -bungarotoxin AlexaFluor 488 (B13422, Thermo Fisher Scientific). Nuclei were stained using Hoechst (H3570, Thermo Fisher Scientific). All steps were performed at room temperature (RT). Cells were imaged using the Micro XLS-C HCI System (Molecular Devices). A 3D reconstruction of a myotube culture was made using Fiji.

In situ hybridization

Late embryonic *A. l. cowlesi* heads were fixed in 4% PFA overnight at 4°C. Fixed heads were divided in two through the midline of the body, separating the left and right venom gland. Material was dehydrated using sequential methanol steps (25, 50, 75, 100%), washed with

I

II

III

IV

V

VI

VII

VIII

&

three times for one hour 100% ethanol and embedded in paraffin. Sections of 10 μm were deparaffinized (nucleoclear, ethanol, Milli-Q) and pretreated (PBST, ProtK 10 min, PBS and 4% PFA). For hybridization, slides were covered with hybridization mix for one hour at 60°C (2% blocking powder, 50% formamide, 5x SSC, 1mg/mL tRNA, 50 $\mu\text{g}/\text{mL}$ heparin, 0,1% Triton X-100, 0,1% CHAPS and 5mM EDTA) prior to overnight incubation with probe mix (800 - 1000 ng/mL) at 60°C. On the next day, the slides were washed (2x SSC, 0,1% CHAPS, 50% Formamide) for 30 minutes three times prior to overnight anti-Dig-AP (in 10% sheep serum) incubation at 4°C. Signal was visualized using BM-purple and counterstained with 0,1% neutral red. Images were taken on a Leica DM4000 microscope.

Following primers were used for probe generation:

<i>CRISP</i>	F_TGCTGCAACAGTCTTCTGGAAC	R_ATATAGTTTGCATGAAGGGCATCA
<i>CTL</i>	F_TCTGGGGATTCTGCCTCTTG	R_ACTTGCAGATGAAGGGCAGG
<i>KUN</i>	F_CCCTGCTTAACCTCCCCAA	R_GGCAGGGTCTCCAGGAAGG

Electron microscopic analysis

Organoids were harvested in cell recovery solution (354253, Corning) to remove BME and fixed by chemical fixation using 3% glutaraldehyde in cacodylate buffer. The fixation was followed by 1% osmium tetroxide plus 1.5% potassium ferrocyanide postfixation. Then, the organoids were dehydrated in series of ethanol and gradually embedded in Epon resin. Ultrathin sections were observed in a Tecnai Spirit T12 Electron Microscope equipped with an Eagle CCD camera (Thermo Fisher Scientific).

Organoid protein extraction

Organoids were grown and differentiated as described above. For LC- MS analysis, a minimum of 500 μL of organoid containing BME (~25 droplets) was harvested for protein extraction. In short, differentiation medium was removed and any residual liquid removed with PBS washes, organoids were collected and mechanically dissociated in 500 μL PBS using a glass Pasteur pipette in a 1.5 mL eppendorf tube. Tubes were sonicated for 15 cycles (30 sec on, 30 sec off) using the Bioruptor Plus (Diagnode). Any leftover debris was spun down at 12,000 rpm, the supernatant collected, snap frozen on dry ice and stored at -80 °C.

For functional toxicity readout, a minimum of 500 μL of organoid containing BME was washed in the tissue culture plate with PBS and supplemented with C2C12 differentiation medium for two days prior to collection of supernatants. The same procedure was applied to harvest supernatant from human colon control organoid cultures as a negative control (Sato et al., 2011).

Liquid chromatography–mass spectrometry and Mascot database search

For comparison of *A. l. cowlesi* crude venom and organoid extracts, liquid chromatographic separation was performed with parallel at-line nanofractionation and mass spectrometry analysis. MS data of venom and organoid samples was analyzed for identical masses found in the samples to confirm production of venom toxins by organoids.

LC separation was performed using a Shimadzu UPLC system (‘s Hertogenbosch, The Netherlands), and a 250×4.6 mm Waters Xbridge Peptide BEH300 C18 analytical column with a 3,5- μm particle size combined with a 300- \AA pore size. Separations were performed in a Shimadzu CTD-30A column oven at 30°C. Mobile phase A comprised of 98% H₂O, 2% ACN and 0.1% FA, and mobile phase B comprised of 98% ACN, 2% H₂O and 0.1% FA. A linear increase of mobile phase B from 0% to 50% in 20 min was followed by a linear increase from 50% to 90% B in 4 min and a 5 min isocratic separation at 90% B. The starting conditions were reached again in 1 min and the column was then equilibrated for 10 min at 0% B. A post-column flow split in 1:9 ratio directed the larger fraction to a FractioMate™ FRM100 nanofraction collector (SPARK-Holland & VU, Netherlands, Emmen & Amsterdam) or a modified Gilson 235P autosampler. To further confirm that venom toxins were present in the organoid extracts, crude organoid extracts were subjected to tryptic digestion after which these were analyzed with nanoLC- MS/MS. For this, 20 μL of each organoid sample was transferred to an Eppendorf tube containing 15 μL of digestion buffer (25 mM NH₄HCO₃, pH 8.2). Subsequently, 1.5 μL of reducing agent (0.5% β - mercaptoethanol) was added to each tube followed by a 10-min incubation step at 95°C. Post incubation, the samples were cooled to room temperature and centrifuged at 150 RCF for 10 seconds in a Himac CT 15RE centrifuge. Next, 3 μL of alkylating agent (55 mM iodoacetamide) was added to the tubes before incubation in the dark at room temperature for 30 min. Next, 3 μL of 0.1 $\mu\text{g}/\mu\text{L}$ trypsin was added before incubation at 37°C for 3 h, and then an additional 3 μL of trypsin was added to the tubes and the samples were incubated overnight. Subsequently, 1 μL of 5% FA was added to quench the digestion, followed by brief centrifugation to remove any particulate matter. Finally, the samples were centrifuged for 10 s at 150 RCF and the supernatants were transferred to autosampler vials with glass inserts and analyzed with nanoLC-MS/MS. The data files obtained were run through the Mascot search engine (MASCOT; Matrix Science, London, United Kingdom) against the Swiss-Prot, NCBIInr database.

Myotube cultures

The C2C12 mouse myoblast cell line (91031101, Sigma-Aldrich) was cultured in T75 flasks (734-2705, Corning) in DMEM (11965092, Thermo Fisher Scientific) supplemented with 10% fetal bovine serum (FBS, 16140-071, Thermo Fisher Scientific), 2 mM glutamine (G7513, Sigma-Aldrich), and 1% penicillin/streptomycin (P4333, Sigma-Aldrich). C2C12 cells were routinely tested for mycoplasma contamination and were found negative. Cells were harvested and resuspended to obtain a cell suspension of 5,000 cells/ μL in cold medium supplemented with 1:25 Matrigel-GFR (356231, Corning). The C2C12 cell suspension was seeded in the perfusion channel of an OrganoPlate 2-lane (9603- 400B, Mimetas) against a collagen-I ECM gel as previously described (Wevers et al., 2018). The plate was incubated on a flat surface for 3 hours to allow cell attachment, after which medium perfusion was started with C2C12 differentiation medium composed of DMEM supplemented with 2% horse serum (26050-088, Thermo Fisher Scientific), 1 μM insulin (I9278, Sigma-Aldrich), 2 mM glutamine, and 1%

penicillin/streptomycin. From day 2-5, the differentiation medium was supplemented with 10 μM cytarabine (C1768, Sigma-Aldrich) to inhibit cell proliferation.

For cell viability assay, C2C12 cells were exposed for 30 minutes to supernatant from venom gland organoids, supernatant from human colon organoids, recombinant alpha bungarotoxin and a killing control. After that exposure was terminated and fresh medium added for 24h and 48h. WST8 assay was used according to the manufacturer's protocol to quantify cell viability.

Calcium imaging

Calcium imaging assays were performed at day 8 after plating. C2C12 myotubes in the OrganoPlate were incubated with 20 μM Cal-520 (ab171868, Abcam), 0.04% Pluronic-127 (P6866, Thermo Fisher Scientific) in C2C12 differentiation medium without serum for 60 minutes at 37°C, followed by 30 more minutes at RT. Next, cultures were exposed to C2C12 differentiation medium (negative control), human colon organoid supernatant (negative control), snake venom gland organoid supernatant or 10 μM α -bungarotoxin (positive control) for 30 minutes. Calcium imaging recordings were made using an ImageXpress Micro XLS-C Confocal High-Content Imaging System (Molecular Devices, wide field mode, 4x magnification, 2 Hz). An individual chip was imaged for 90 seconds to record baseline calcium activity. Myotubes in the chip were then exposed to 500 μM carbachol or vehicle (0.5% water) and immediately placed back in the microscope for another 90 seconds of calcium imaging to record the response to carbachol or vehicle. This pipeline was repeated for each chip.

The calcium imaging recordings were processed using scripts developed in Fiji (Schindelin et al., 2012). Recordings were corrected for camera-induced noise via Kalman Filtering and corrected for bleaching.

Movement of fluorescent signal was quantified via Gaussian Window MSE resulting in RGB-encoded videos showing movement of fluorescent signal to the left and right side in purple and green, respectively. The colored areas were measured per timeframe and averaged over time. All videos were processed to correct for flow-induced artefacts caused by movement of fluorescent cell debris. In the case of calcium wave propagation, movement was detected to a similar extent in both the left and right direction (<2 fold difference) and the average area of the two directions was determined. In the case of flow of fluorescent debris, the movement detected in one direction is dominant over the other (≥ 2 fold difference) and movement in the dominant direction was excluded.

MEA recordings rat cortical neurons

Primary rat cortical cells were isolated from postnatal day 0-1 pups of timed pregnant Wistar rat dams (Envigo) as described previously (Dingemans et al., 2016). Briefly, pups were decapitated and cortices were rapidly dissected on ice and kept in dissection medium (Neurobasal®-A supplemented with 25 g/L sucrose, 450 μM L-glutamine, 30 μM glutamate, 1% penicillin/streptomycin and 10% FBS, pH 7.4) during the entire procedure. Cortices were dissociated to a single-cell suspension by mincing with scissors, trituration and filtering

through a 100 μm mesh (EASYstrainer, Greiner). The cell suspension was diluted to a 2×10^6 cells/mL solution. Droplets of 50 μL were placed on the electrode fields in wells of 48-wells MEA plates (Axion BioSystems) pre-coated with 0.1% PEI solution diluted in borate buffer (24 mM sodium borate/50 mM boric acid in Milli-Q, pH adjusted to 8.4). Cells were left to adhere for ~ 2 hr before adding 450 μL dissection medium. Primary rat cortical cultures were kept at 37°C in a humidified 5% CO_2 incubator. At day *in vitro* (DIV) 2, 90% of the dissection medium was replaced with glutamate medium (Neurobasal[®]-A supplemented with 25 g/L sucrose, 450 μM L-glutamine, 30 μM glutamate, 1% penicillin/streptomycin and 2% B27 supplement, pH 7.4) to prevent glial overgrowth. At DIV4, 90% of the glutamate medium was replaced with FBS medium (Neurobasal[®]-A supplemented with 25 g/L sucrose, 450 μM L-glutamine, 1% penicillin/streptomycin and 10% FBS, pH 7.4).

Spontaneous electrical activity was recorded on the day of exposure (DIV9-11) as described previously (Nicolas et al., 2014; Tukker et al., 2018). In short, signals were recorded using a Maestro 768-channel amplifier with integrated heating system and temperature controller and a data acquisition interface (Axion BioSystems). Data acquisition was managed with Axion's Integrated Studio (AxIS 2.4.2.13) and recorded as .RAW files. All channels were sampled at the same time with a gain of 1200x and a sampling frequency of 12.5kHz/channel with a 200-500 Hz band-pass filter. Prior to the recording, MEA plates were allowed to equilibrate for ~ 10 min in the Maestro.

Spontaneous neuronal activity was recorded prior to exposure to generate a baseline recording. Immediately following this recording, cells were exposed to the test compounds (α -bungarotoxin, organoid supernatant and vehicle control) and activity was recorded for another 30 min. Each well was exposed to only one single concentration of one compound in order to prevent receptor (de)sensitization.

To determine (modulation of) spontaneous activity, .RAW data files were re-recorded to obtain Alpha Map files. In this re-recording, spikes were detected with the AxIS spike detector (Adaptive threshold crossing, Ada BandFit v2) and a variable threshold spike detector set at 7x standard deviation (SD) of internal noise level (rms) on each electrode. Post/pre-spike duration was set to 3.6/2.4 ms respectively. For further data analysis, spike files were loaded in NeuralMetric Tool (version 2.2.4, Axion BioSystems) and only active electrodes ($\text{MSR} \geq 0.1$ spikes/s) in active wells (≥ 1 active electrode) were included in data analysis. The effects of test compounds on spontaneous activity were determined by comparing the baseline activity with activity following exposure. A custom-made MS Excel macro was used to calculate treatment ratios (TR) per well for the mean spike rate, which were normalized to appropriate vehicle control.

For cell viability, rat cortical cells were cultured at a density of 3.0×10^4 cells/well. At DIV9-10, cells were exposed for 24 h to the test compounds, after which cell viability was assessed using a combined CFDA-AM / neutral red / alamar blue assay. In short, cells were incubated for 30 minutes with 12.5 mM alamar blue and 4 mM CFDA-AM in FBS at 37°C . Resorufin was measured spectrophotometrically at 540/590 nm (Infinite M200 microplate; Tecan), whereas hydrolyzed CFDA was measured spectrophotometrically at 493/541 nm.

I

II

III

IV

V

VI

VII

VIII

&

The aB/CFDA solution was then replaced by 200 mL neutral red solution (175 mM in PBS, Invitrogen) for 1 h at 37 °C. Next, cells were incubated for 30 min with 200 mL extraction solution (1% glacial acetic acid, 50% ethanol, and 49% H₂O) during gentle shaking at room temperature. After 30 min extraction, fluorescence was measured spectrophotometrically at 530/645 nm.

RNA extraction and de-novo transcriptome assembly

RNA isolations of organoids and tissues for *de-novo* transcriptome assembly and bulk RNA sequencing were performed using TRIzol (Invitrogen) following the manufacturer's instructions. Organoid RNA isolations for quantitative PCR were performed with RNeasy Mini Kit (Qiagen) following the manufacturer's instructions. Quantitative PCR analysis was performed using the SYBR Green and Bio-Rad systems. Changes in expression were calculated using CFX manager software (Bio-Rad). Primers were designed using NCBI primer design tool with the coding sequence of annotated scaffolds of interest as input. Primers used in this study are;

ACTB, F_CTGGCCTAGGACACAGTACG, R_GCTCAGACTCCATTGCAACA
LGR5, F_GTTCCCTTCCTGCATGTCT, R_ACCAACTAGCATCTTTTGCTT
ASCL2, F_CACTCGGCTTATTCGTCCGA, R_CTCCCGAACCAACTGGTGAA
AXIN2, F_GATAGAAGCTGAGGCAGCCC, R_CCCCTTCGCATGTCCTCTAC
RNF43, F_TTCCCATGAGTTCATCGGC, R_GGCGGTACCTGATGTTGACT
TCF7L2, F_GCTATCACCGGGCACTGTAG, R_GGTCCTCACGAGATTGCCTG
MKI67, F_CAGGTGCATGAATCTGGTATTGAA, R_ATTTAGCGCTGCTTCTGTGACC
3FTX, F_GTGGTGGTGACAATCGTGTG, R_GGTTGCGATGACTGTTGGTT
KUN, F_GTCCAGGACTCTGTGAACTGC, R_GCATTGTTTTGCAGCCAGGTT
CTL, F_TACACCCAGGAACCCTTCT, R_TATTGGTGACGGAGACGCAC
HSPA8, F_AGCAGTACAAAGCGGAGGAC, R_TCTGCCGTGCTCTTCATGTT

Sequencing and de-novo transcriptome assembly was performed by BaseClear B.V. as follows: PolyA enriched RNA from liver tissue, pancreas tissue, venom gland tissue, organoids early passage, organoids late passage expansion and organoids late passage differentiation was sequenced. Paired- end sequence reads were generated using the Illumina HiSeq2500 system. FASTQ sequence files were generated using bcl2fastq2 version 2.18. Initial quality assessment was based on data passing the Illumina Chastity filtering. Subsequently, reads containing PhiX control signal were removed using an in-house filtering protocol. The second quality assessment was based on the remaining reads using the FASTQC quality control tool version 0.11.5. The transcriptome assembly was performed with Trinity (version 2.4.0, Haas et al., 2013), using the combined data of all six samples. The resulting consensus assembly was filtered to remove all sequences shorter than 500bp, resulting in 311,948 remaining scaffolds. These were aligned with BLASTN (version 2.6.0) against a local copy of the NCBI-NT database (built in February 2018). Toxin-encoding contigs were validated by manual sequence analysis

(e.g. ORF identification) of those exhibiting annotations consistent with known snake venom toxin proteins.

Bulk and single cell RNA sequencing.

Bulk RNA sequencing of *N. nivea* was performed by the Utrecht Sequencing Facility (uSeq) as follows: Libraries were prepared based on polyA enrichment. Paired-end sequence reads were generated using the NextSeq500 system.

For organoid single cell RNA sequencing, *A. l. cowlesi* organoids were grown and differentiated as described above. BME was removed by washing in ice-cold DMEM (Gibco). For tissue sequencing, embryonic *A. l. cowlesi* venom glands were dissociated with collagenase I as described above and subsequently processed in the same way as organoids. Organoids or tissue fragments were resuspended in TrypLE Express (Gibco) pre-heated to 32°C and dissociated under repeated pipetting. Upon reaching single cell state, samples were pelleted, washed, resuspended in FACS buffer (advanced DMEM, 10 mM Y-27632 and DAPI) and strained (35 µm). Cells were immediately sorted into 384-well plates containing ERCC spike-ins (Agilent), RT primers and dNTP (Promega) using a BD FACSJazz (BD Biosciences). Plates were prepared using Mosquito HTS (TTPlabtech). scRNA-seq libraries were prepared following the SORT-seq protocol (Muraro et al., 2016), which is based on the CEL-seq2 method (Hashimshony et al., 2016). Briefly, cells were first lysed for 5 min at 65 °C, and RT and second-strand mixes were dispensed by the Nanodrop II liquid handling platform (GC Biotech). Single-cell double-stranded cDNAs were pooled together and *in vitro* transcribed for linear amplification. Illumina sequencing libraries were prepared using the TruSeq small RNA primers (Illumina) and these DNA libraries were sequenced paired-end at 60 and 26 bp read length, respectively, on the Illumina NextSeq.

Bulk and single cell RNA sequencing analysis.

Bulk paired-end reads of *A. l. cowlesi* and *N. nivea* tissue and organoids were mapped to the *de novo* assembled *A. l. cowlesi* transcriptome using STAR. When a read mapped to multiple scaffolds, a fractional count of 1/x was recorded, where x is the number of scaffolds the read maps to. To reduce the complexity of the count table, scaffolds with identical blast hits were merged by summation of their transcript counts. All scripts used for read counting are deposited at <https://github.com/BuysDB/reptilianOrganoids>. For single cell analysis, paired-end reads were demultiplexed on the cell barcode and UMI and adapters trimmed using Cutadapt 2. Next, the reads were mapped and counted as described for the bulk samples, additionally we removed amplification duplicates by UMI-scaffold combinations. Scaffold annotations were filtered to exclude the terms (“mitochondrial”, “mitochondrion”, “ribosomal”, “rRNA”, “ribosomal”, “microsatellite”, “transposon”, “SINE”, “LINE repeat”, “noBlast”) and requiring them to be detected in at least 2 cells, resulting in 42,507 unique annotations. Subsequently, cells were filtered by requiring at least 2000 counts and at least 100 different genes to be expressed, leaving 1,092 cells (1,255 for tissue) to be included for dimensionality reduction and k-medoids-based

I

II

III

IV

V

VI

VII

VIII

&

clustering using RaceID3 according to the vignette (Herman et al., 2018), starting with an expected cluster number of 10 (organoid) and 20 (tissue). Violin plots were generated using Seurat functions (Butler et al. 2018) (version 3.0.0.9000) on the dataset analyzed by RaceID3. Single cell trajectories were analyzed using Monocle (version 2.6.4) (Trapnell et al., 2014). In short, genes were selected as input features based on differential expression between expansion and differentiation medium and dimensionality was reduced for display using reverse graph embedding.

QUANTIFICATION AND STATISTICAL ANALYSIS

No statistical methods were used to predetermine sample size. The experiments were not randomized and the investigators were not blinded to the sample allocation during experiments and outcome assessment. All data are presented as mean \pm standard error of the mean (SEM), unless stated otherwise. Value of n is always displayed in the figure as individual data points, more information can be found in the figure legends. Statistical tests included unpaired two-tailed t test for Figures 1D, S1C, S6I, and S7E–S7G and paired two-tailed t test for Figures S7B–S7D using GraphPad Prism. ns $p > 0.05$, * $p \leq 0.05$, ** $p \leq 0.01$, *** $p \leq 0.001$, **** $p \leq 0.0001$.

DATA AND CODE AVAILABILITY

All bulk and single cell RNA sequencing data of this study have been deposited in the Gene Expression Omnibus (GEO) under accession code GSE129581.

REFERENCES

- Ainsworth, S., J. Slagboom, N. Alomran, D. Pla, Y. Alhamdi, S. I. King, F. M. S. Bolton, J. M. Gutierrez, F. J. Vonk, C. H. Toh, J. J. Calvete, J. Kool, R. A. Harrison and N. R. Casewell (2018). "The paraspecific neutralisation of snake venom induced coagulopathy by antivenoms." *Commun Biol* 1: 34.
- Artegiani, B. and H. Clevers (2018). "Use and application of 3D-organoid technology." *Hum Mol Genet* 27(R2): R99-R107.
- Augusto-de-Oliveira, C., D. R. Stuginski, E. S. Kitano, D. Andrade-Silva, T. Liberato, I. Fukushima, S. M. Serrano and A. Zelanis (2016). "Dynamic Rearrangement in Snake Venom Gland Proteome: Insights into Bothrops jararaca Intraspecific Venom Variation." *J Proteome Res* 15(10): 3752-3762.
- Barker, N., J. H. van Es, J. Kuipers, P. Kujala, M. van den Born, M. Cozijnsen, A. Haegebarth, J. Korving, H. Begthel, P. J. Peters and H. Clevers (2007). "Identification of stem cells in small intestine and colon by marker gene *Lgr5*." *Nature* 449(7165): 1003-1007.
- Beumer, J., B. Artigiani, Y. Post, F. Reimann, F. Gribble, T. N. Nguyen, H. Zeng, M. Van den Born, J. H. Van Es and H. Clevers (2018). "Enteroendocrine cells switch hormone expression along the crypt-to-villus BMP signalling gradient." *Nat Cell Biol* 20(8): 909-916.
- Bolhaqueiro, A. C. F., R. H. van Jaarsveld, B. Ponsioen, R. M. Overmeer, H. J. Snippert and G. Kops (2018). "Live imaging of cell division in 3D stem-cell organoid cultures." *Methods Cell Biol* 145: 91- 106.
- Butler, A., P. Hoffman, P. Smibert, E. Papalexis and R. Satija (2018). "Integrating single-cell transcriptomic data across different conditions, technologies, and species." *Nat Biotechnol* 36(5): 411- 420.
- Carneiro, S. M., M. B. Zablich, C. M. Kerchove, A. M. Moura-da-Silva, D. O. Quissell, R. P. Markus and N. Yamanouye (2006). "Venom production in long-term primary culture of secretory cells of the *Bothrops jararaca* venom gland." *Toxicon* 47(1): 87-94.
- Casewell, N. R., S. C. Wagstaff, W. Wuster, D. A. Cook, F. M. Bolton, S. I. King, D. Pla, L. Sanz, J. J. Calvete and R. A. Harrison (2014). "Medically important differences in snake venom composition are dictated by distinct postgenomic mechanisms." *Proc Natl Acad Sci U S A* 111(25): 9205-9210.
- Chen, P. H., X. Chen, Z. Lin, D. Fang and X. He (2013). "The structural basis of R-spondin recognition by LGR5 and RNF43." *Genes Dev* 27(12): 1345-1350.
- Clark, G. C., N. R. Casewell, C. T. Elliott, A. L. Harvey, A. G. Jamieson, P. N. Strong and A. D. Turner (2019). "Friends or Foes? Emerging Impacts of Biological Toxins." *Trends Biochem Sci*.
- Clevers, H. (2016). "Modeling Development and Disease with Organoids." *Cell* 165(7): 1586-1597.
- de Lau, W., N. Barker, T. Y. Low, B. K. Koo, V. S. Li, H. Teunissen, P. Kujala, A. Haegebarth, P. J. Peters, M. van de Wetering, D. E. Stange, J. E. van Es, D. Guardavaccaro, R. B. Schasfoort, Y. Mohri, K. Nishimori, S. Mohammed, A. J. Heck and H. Clevers (2011). "*Lgr5* homologues associate with Wnt receptors and mediate R-spondin signalling." *Nature* 476(7360): 293-297.
- Dekkers, J. F., M. Alieva, L. M. Wellens, H. C. R. Ariese, P. R. Jamieson, A. M. Vonk, G. D. Amatngalim, H. Hu, K. C. Oost, H. J. G. Snippert, J. M. Beekman, E. J. Wehrens, J. E. Visvader, H. Clevers and A. C. Rios (2019). "High-resolution 3D imaging of fixed and cleared organoids." *Nat Protoc* 14(6): 1756-1771.
- Dekkers, J. F., C. L. Wiegerinck, H. R. de Jonge, I. Bronsveld, H. M. Janssens, K. M. de Winter-de Groot, A. M. Brandsma, N. W. de Jong, M. J. Bijvelds, B. J. Scholte, E. E. Nieuwenhuis, S. van den Brink, H. Clevers, C. K. van der Ent, S. Middendorp and J. M. Beekman (2013). "A functional CFTR assay using primary cystic fibrosis intestinal organoids." *Nat Med* 19(7): 939-945.

I

II

III

IV

V

VI

VII

VIII

&

- Dingemans, M. M., M. G. Schutte, D. M. Wiersma, A. de Groot, R. G. van Kleef, F. M. Wijnolts and R. H. Westerink (2016). "Chronic 14-day exposure to insecticides or methylmercury modulates neuronal activity in primary rat cortical cultures." *Neurotoxicology* 57: 194-202.
- Duarte, M. M., H. Montes de Oca, C. R. Diniz and C. L. Fortes-Dias (1999). "Primary culture of venom gland cells from the South American rattlesnake (*Crotalus durissus terrificus*)." *Toxicon* 37(12): 1673- 1682.
- Fatehullah, A., S. H. Tan and N. Barker (2016). "Organoids as an in vitro model of human development and disease." *Nat Cell Biol* 18(3): 246-254.
- Fox, J. W. and S. M. Serrano (2008). "Exploring snake venom proteomes: multifaceted analyses for complex toxin mixtures." *Proteomics* 8(4): 909-920.
- Fry, B. G., N. Vidal, L. van der Weerd, E. Kochva and C. Renjifo (2009). "Evolution and diversification of the Toxicofera reptile venom system." *J Proteomics* 72(2): 127-136.
- Gehart, H., J. H. van Es, K. Hamer, J. Beumer, K. Kretzschmar, J. F. Dekkers, A. Rios and H. Clevers (2019). "Identification of Enteroendocrine Regulators by Real-Time Single-Cell Differentiation Mapping." *Cell* 176(5): 1158-1173 e1116.
- Grun, D., A. Lyubimova, L. Kester, K. Wiebrands, O. Basak, N. Sasaki, H. Clevers and A. van Oudenaarden (2015). "Single-cell messenger RNA sequencing reveals rare intestinal cell types." *Nature* 525(7568): 251-255.
- Gutierrez, J. M., J. J. Calvete, A. G. Habib, R. A. Harrison, D. J. Williams and D. A. Warrell (2017). "Snakebite envenoming." *Nat Rev Dis Primers* 3: 17063.
- Gutierrez, J. M. and B. Lomonte (2013). "Phospholipases A2: unveiling the secrets of a functionally versatile group of snake venom toxins." *Toxicon* 62: 27-39.
- Haas, B. J., A. Papanicolaou, M. Yassour, M. Grabherr, P. D. Blood, J. Bowden, M. B. Couger, D. Eccles, B. Li, M. Lieber, M. D. MacManes, M. Ott, J. Orvis, N. Pochet, F. Strozzi, N. Weeks, R. Westerman, T. William, C. N. Dewey, R. Henschel, R. D. LeDuc, N. Friedman and A. Regev (2013). "De novo transcript sequence reconstruction from RNA-seq using the Trinity platform for reference generation and analysis." *Nat Protoc* 8(8): 1494-1512.
- Harvey, A. L. (2001). "Twenty years of dendrotoxins." *Toxicon* 39(1): 15-26.
- Hashimshony, T., N. Senderovich, G. Avital, A. Klochendler, Y. de Leeuw, L. Anavy, D. Gennert, S. Li, K. J. Livak, O. Rozenblatt-Rosen, Y. Dor, A. Regev and I. Yanai (2016). "CEL-Seq2: sensitive highly-multiplexed single-cell RNA-Seq." *Genome Biol* 17: 77.
- Herman, J. S., Sagar and D. Grun (2018). "FateID infers cell fate bias in multipotent progenitors from single-cell RNA-seq data." *Nat Methods* 15(5): 379-386.
- Izidoro, L. F., J. C. Sobrinho, M. M. Mendes, T. R. Costa, A. N. Grabner, V. M. Rodrigues, S. L. da Silva, F. B. Zanchi, J. P. Zuliani, C. F. Fernandes, L. A. Calderon, R. G. Stabeli and A. M. Soares (2014). "Snake venom L-amino acid oxidases: trends in pharmacology and biochemistry." *Biomed Res Int* 2014: 196754.
- Karlsson, E., M. Jolkkonen, E. Mulugeta, P. Onali and A. Adem (2000). "Snake toxins with high selectivity for subtypes of muscarinic acetylcholine receptors." *Biochimie* 82(9-10): 793-806.
- Kochva, E. (1987). "The origin of snakes and evolution of the venom apparatus." *Toxicon* 25(1): 65- 106.
- Koo, B. K., M. Spit, I. Jordens, T. Y. Low, D. E. Stange, M. van de Wetering, J. H. van Es, S. Mohammed, A. J. Heck, M. M. Maurice and H. Clevers (2012). "Tumour suppressor RNF43 is a stem- cell E3 ligase that induces endocytosis of Wnt receptors." *Nature* 488(7413): 665-669.

- Lima, R. M., M. I. Esteveao-Costa, I. L. Junqueira-de-Azevedo, P. L. Ho, M. R. Diniz and C. L. Fortes-Dias (2011). "Phospholipase A2 inhibitors (betaPLIs) are encoded in the venom glands of *Lachesis muta* (Crotalinae, Viperidae) snakes." *Toxicon* 57(1): 172-175.
- Mackessy, S. P. (1991). "Morphology and ultrastructure of the venom glands of the northern pacific rattlesnake *Crotalus viridis oreganus*." *J Morphol* 208(1): 109-128.
- Maimets, M., C. Rocchi, R. Bron, S. Pringle, J. Kuipers, B. N. Giepmans, R. G. Vries, H. Clevers, G. de Haan, R. van Os and R. P. Coppes (2016). "Long-Term In Vitro Expansion of Salivary Gland Stem Cells Driven by Wnt Signals." *Stem Cell Reports* 6(1): 150-162.
- McCann, C. M., J. Bracamontes, J. H. Steinbach and J. R. Sanes (2006). "The cholinergic antagonist alpha-bungarotoxin also binds and blocks a subset of GABA receptors." *Proc Natl Acad Sci U S A* 103(13): 5149-5154.
- Millers, E. K., M. Trabi, P. P. Masci, M. F. Lavin, J. de Jersey and L. W. Guddat (2009). "Crystal structure of textilinin-1, a Kunitz-type serine protease inhibitor from the venom of the Australian common brown snake (*Pseudonaja textilis*)." *FEBS J* 276(11): 3163-3175.
- Muraro, M. J., G. Dharmadhikari, D. Grun, N. Groen, T. Dielen, E. Jansen, L. van Gorp, M. A. Engelse, F. Carlotti, E. J. de Koning and A. van Oudenaarden (2016). "A Single-Cell Transcriptome Atlas of the Human Pancreas." *Cell Syst* 3(4): 385-394 e383.
- Nicolas, J., P. J. Hendriksen, R. G. van Kleef, A. de Groot, T. F. Bovee, I. M. Rietjens and R. H. Westerink (2014). "Detection of marine neurotoxins in food safety testing using a multielectrode array." *Mol Nutr Food Res* 58(12): 2369-2378.
- Nirthanan, S. and M. C. Gwee (2004). "Three-finger alpha-neurotoxins and the nicotinic acetylcholine receptor, forty years on." *J Pharmacol Sci* 94(1): 1-17.
- Ogawa, T., T. Chijiwa, N. Oda-Ueda and M. Ohno (2005). "Molecular diversity and accelerated evolution of C-type lectin-like proteins from snake venom." *Toxicon* 45(1): 1-14.
- Piccolo, S., Y. Sasai, B. Lu and E. M. De Robertis (1996). "Dorsoventral patterning in *Xenopus*: inhibition of ventral signals by direct binding of chordin to BMP-4." *Cell* 86(4): 589-598.
- Richter, K., M. Haslbeck and J. Buchner (2010). "The heat shock response: life on the verge of death." *Mol Cell* 40(2): 253-266.
- Sato, T., D. E. Stange, M. Ferrante, R. G. Vries, J. H. Van Es, S. Van den Brink, W. J. Van Houdt, A. Pronk, J. Van Gorp, P. D. Siersema and H. Clevers (2011). "Long-term expansion of epithelial organoids from human colon, adenoma, adenocarcinoma, and Barrett's epithelium." *Gastroenterology* 141(5): 1762-1772.
- Sato, T., R. G. Vries, H. J. Snippert, M. van de Wetering, N. Barker, D. E. Stange, J. H. van Es, A. Abo, P. Kujala, P. J. Peters and H. Clevers (2009). "Single *Lgr5* stem cells build crypt-villus structures in vitro without a mesenchymal niche." *Nature* 459(7244): 262-265.
- Schindelin, J., I. Arganda-Carreras, E. Frise, V. Kaynig, M. Longair, T. Pietzsch, S. Preibisch, C. Rueden, S. Saalfeld, B. Schmid, J. Y. Tinevez, D. J. White, V. Hartenstein, K. Eliceiri, P. Tomancak and A. Cardona (2012). "Fiji: an open-source platform for biological-image analysis." *Nat Methods* 9(7): 676-682.
- Sells, P. G., M. Hommel and R. D. Theakston (1989). "Venom production in snake venom gland cells cultured in vitro." *Toxicon* 27(11): 1245-1249.
- Shaham, N. and E. Kochva (1969). "Localization of venom antigens in the venom gland of *Vipera plaestinae* using a fluorescent-antibody technique." *Toxicon* 6(4): 263-268.

I

II

III

IV

V

VI

VII

VIII

&

- Slagboom, J., J. Kool, R. A. Harrison and N. R. Casewell (2017). "Haemotoxic snake venoms: their functional activity, impact on snakebite victims and pharmaceutical promise." *Br J Haematol* 177(6): 947-959.
- Sylva, M., V. S. Li, A. A. Buffing, J. H. van Es, M. van den Born, S. van der Velden, Q. Gunst, J. H. Koolstra, A. F. Moorman, H. Clevers and M. J. van den Hoff (2011). "The BMP antagonist follistatin-like 1 is required for skeletal and lung organogenesis." *PLoS One* 6(8): e22616.
- Taylor, D., D. Iddon, P. Sells, S. Semoff and R. D. Theakston (1986). "An investigation of venom secretion by the venom gland cells of the carpet viper (*Echis carinatus*)." *Toxicon* 24(7): 651-659.
- Torres, A. M., H. Y. Wong, M. Desai, S. Mochhala, P. W. Kuchel and R. M. Kini (2003). "Identification of a novel family of proteins in snake venoms. Purification and structural characterization of nawaprin from *Naja nigricollis* snake venom." *J Biol Chem* 278(41): 40097-40104.
- Trapnell, C., D. Cacchiarelli, J. Grimsby, P. Pokharel, S. Li, M. Morse, N. J. Lennon, K. J. Livak, T. S. Mikkelsen and J. L. Rinn (2014). "The dynamics and regulators of cell fate decisions are revealed by pseudotemporal ordering of single cells." *Nat Biotechnol* 32(4): 381-386.
- Trietsch, S. J., E. Naumovska, D. Kurek, M. C. Setyawati, M. K. Vormann, K. J. Wilschut, H. L. Lanz, A. Nicolas, C. P. Ng, J. Joore, S. Kustermann, A. Roth, T. Hankemeier, A. Moisan and P. Vulto (2017). "Membrane-free culture and real-time barrier integrity assessment of perfused intestinal epithelium tubes." *Nat Commun* 8(1): 262.
- Tsetlin, V. I. (2015). "Three-finger snake neurotoxins and Ly6 proteins targeting nicotinic acetylcholine receptors: pharmacological tools and endogenous modulators." *Trends Pharmacol Sci* 36(2): 109-123.
- Tukker, A. M., F. M. J. Wijnolts, A. de Groot and R. H. S. Westerink (2018). "Human iPSC-derived neuronal models for in vitro neurotoxicity assessment." *Neurotoxicology* 67: 215-225.
- van der Flier, L. G., M. E. van Gijn, P. Hatzis, P. Kujala, A. Haegebarth, D. E. Stange, H. Begthel, M. van den Born, V. Guryev, I. Oving, J. H. van Es, N. Barker, P. J. Peters, M. van de Wetering and H. Clevers (2009). "Transcription factor achaete scute-like 2 controls intestinal stem cell fate." *Cell* 136(5): 903-912.
- Vonk, F. J., N. R. Casewell, C. V. Henkel, A. M. Heimberg, H. J. Jansen, R. J. McCleary, H. M. Kerckamp, R. A. Vos, I. Guerreiro, J. J. Calvete, W. Wuster, A. E. Woods, J. M. Logan, R. A. Harrison, T. A. Castoe, A. P. de Koning, D. D. Pollock, M. Yandell, D. Calderon, C. Renjifo, R. B. Currier, D. Salgado, D. Pla, L. Sanz, A. S. Hyder, J. M. Ribeiro, J. W. Arntzen, G. E. van den Thillart,
- M. Boetzer, W. Pirovano, R. P. Dirks, H. P. Spaink, D. Duboule, E. McGlenn, R. M. Kini and M. K. Richardson (2013). "The king cobra genome reveals dynamic gene evolution and adaptation in the snake venom system." *Proc Natl Acad Sci U S A* 110(51): 20651-20656.
- Wang, C. C. and C. L. Tsou (1993). "Protein disulfide isomerase is both an enzyme and a chaperone." *FASEB J* 7(15): 1515-1517.
- Wevers, N. R., D. G. Kasi, T. Gray, K. J. Wilschut, B. Smith, R. van Vught, F. Shimizu, Y. Sano, T. Kanda, G. Marsh, S. J. Trietsch, P. Vulto, H. L. Lanz and B. Obermeier (2018). "A perfused human blood-brain barrier on-a-chip for high-throughput assessment of barrier function and antibody transport." *Fluids Barriers CNS* 15(1): 23.
- Whiteley, G., N. R. Casewell, D. Pla, S. Quesada-Bernat, R. A. E. Logan, F. M. S. Bolton, S. C. Wagstaff, J. M. Gutierrez, J. J. Calvete and R. A. Harrison (2019). "Defining the pathogenic threat of envenoming by South African shield-nosed and coral snakes (genus *Aspidelaps*), and revealing the likely efficacy of available antivenom." *J Proteomics* 198: 186-198.

Yamanouye, N., C. M. Kerchove, A. M. Moura-da-Silva, S. M. Carneiro and R. P. Markus (2006). “Long-term primary culture of secretory cells of *Bothrops jararaca* venom gland for venom production in vitro.” *Nat Protoc* 1(6): 2763-2766.

Yamazaki, Y. and T. Morita (2004). “Structure and function of snake venom cysteine-rich secretory proteins.” *Toxicon* 44(3): 227-231.

Zancolli, G., J. J. Calvete, M. D. Cardwell, H. W. Greene, W. K. Hayes, M. J. Hegarty, H. W. Herrmann, A. T. Holycross, D. I. Lannutti, J. F. Mulley, L. Sanz, Z. D. Travis, J. R. Whorley, C. E. Wuster and W. Wuster (2019). “When one phenotype is not enough: divergent evolutionary trajectories govern venom variation in a widespread rattlesnake species.” *Proc Biol Sci* 286(1898): 20182735.

SUPPLEMENTAL VIDEOS

Supplementary video 1. Three-dimensional imaging of *Aspidelaps lubricus cowlesi* organoids. Part 1; DAPI (orange), Beta-catenin (yellow), Tubulin (red) and Actin (blue). Part 2; DAPI (orange), Beta-catenin (red), Tubulin (green) and Actin (blue).

Supplementary video 2. Functionally beating cilia in VGO (20x objective, 20 frames/second).

I

II

III

IV

V

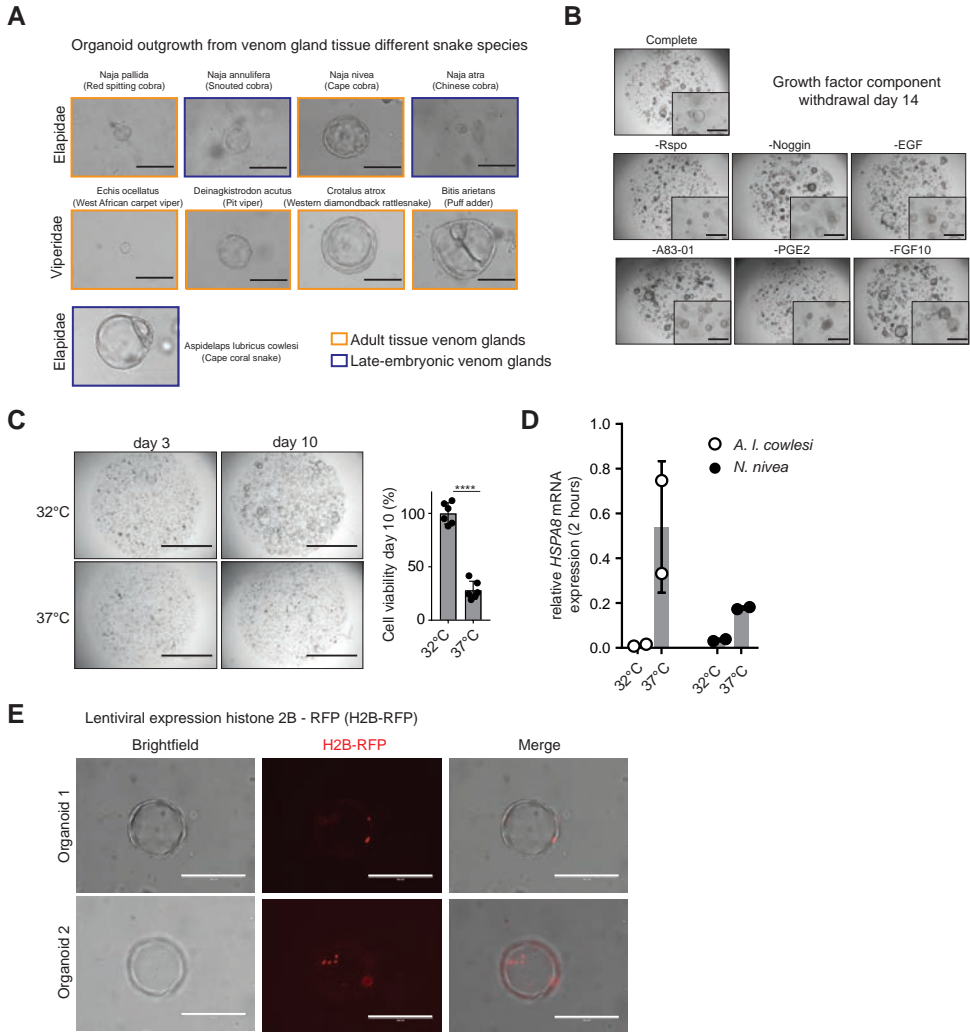
VI

VII

VIII

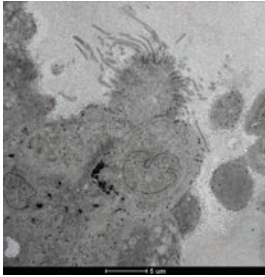
&

SUPPLEMENTARY FIGURES



Supplementary figure 1. Culture characteristics of venom gland organoids in mammalian growth factor medium, related to Figure 1. Organoid outgrowth from venom gland tissue of different Elapidae ($n=5$) and Viperidae ($n=4$) snake species. Origin of tissue was from either adult venom glands (orange) or late embryonic venom glands (blue). Scale bars, 200 μm . Representative images of organoid outgrowth in complete medium or medium without one of the indicated components for 14 days. This dropout screen was performed on established organoids (passage 3). Scale bars, 400 μm . Brightfield images and quantification of *A. l. cowlesi* organoids grown in complete expansion medium at 32°C or 37°C from the moment of splitting into a near single cell suspension to day 3 and day 10 after plating. Viability determined at day 10 using CellTiter-Glo, normalized to cells at 32°C. Scale bars, 2000 μm . Relative *HSPA8* expression normalized to *ACTB* determined by qPCR. For *A. l. cowlesi* and *N. nivea* organoids at 32°C and 37°C for 2 hours. Images of successful lentiviral transduction of venom gland organoids. Detection of histone 2B-RFP (H2B-RFP) stable construct integration and nuclear expression in red. Scale bars, 200 μm .

A Ciliated cell in venom gland organoid
A. l. cowlesi



B

Name	Toxin class
Oxyuranus scutellatus scutellatus toxin 3 mRNA, complete cds	3FTX
Naja sputatrix post synaptic alpha neurotoxin precursor (ntx) gene, ntx-4 allele	3FTX
Pseudechis rosignolii Pr-SNTX mRNA for three-finger toxin, complete cds	3FTX
Naja atra gene encoding cardiotoxin 4	3FTX
Laticauda laticaudata LIL gene for long chain neurotoxin, partial cds	3FTX
Ophiophagus hannah isolate OH-35 short chain alpha neurotoxin precursor	3FTX
Laticauda semifasciata (sea snake) gene for erabutoxin c	3FTX
Bungarus flaviceps muscarinic toxin-like protein mRNA, complete cds	3FTX
Naja atra clone n031_7f_1 three-finger toxin precursor, gene, partial cds	3FTX
Bungarus flaviceps non-conventional three finger toxin isoform 6 mRNA	3FTX
Pseudechis rosignolii Pr-LNTX mRNA for three-finger toxin, complete cds	3FTX
Naja kaouthia kaouthin-2 precursor, mRNA, complete cds	CRISP
Ophiophagus hannah opharin precursor, mRNA, complete cds	CRISP
Laticauda semifasciata latisemin mRNA, complete cds	CRISP
Bungarus multicinctus clone B218_4L_2 three-finger toxin precursor, genes,	Kunitz
Austrelaps labialis putative Kunitz-type proteinase inhibitor mRNA	Kunitz
Naja atra aci gene for chymotrypsin inhibitor precursor, exons 1-3	Kunitz
Naja atra mRNA for chymotrypsin inhibitor (aci gene)	Kunitz
Bungarus fasciatus L-amino acid oxidase mRNA, complete cds	LAEO
Macropisthodon rudis isolate PDE-1 phosphodiesterase gene, partial cds	PDE
Naja atra K-like metalloprotease precursor, mRNA, partial cds	SVMP
Naja naja cobrin precursor, mRNA, complete cds	SVMP
Naja atra metalloproteinase atrase A mRNA, complete cds	SVMP
Naja atra metalloproteinase atrase B mRNA, complete cds	SVMP
Drysdalia coronoides MTP4 mRNA, complete cds	SVMP
Naja atra atragin precursor, mRNA, partial cds	SVMP
Micrurus corallinus MCOR0067C C-type lectin precursor, mRNA	CTL
Demansia vestigiata vestiginin-2 precursor, mRNA, complete cds	Waprin

Supplementary figure 2. Venom gland organoids are heterogeneous in cellular composition and express different toxin classes, related to Figure 2. Transmission electron microscopy image of ciliated cell present in *A. l. cowlesi* organoid. Scale bar, 5 μ m. Highest expressed toxin genes in *A. l. cowlesi* venom gland organoids. Table of *de novo* scaffold BLASTN hit and toxin class.

I

II

III

IV

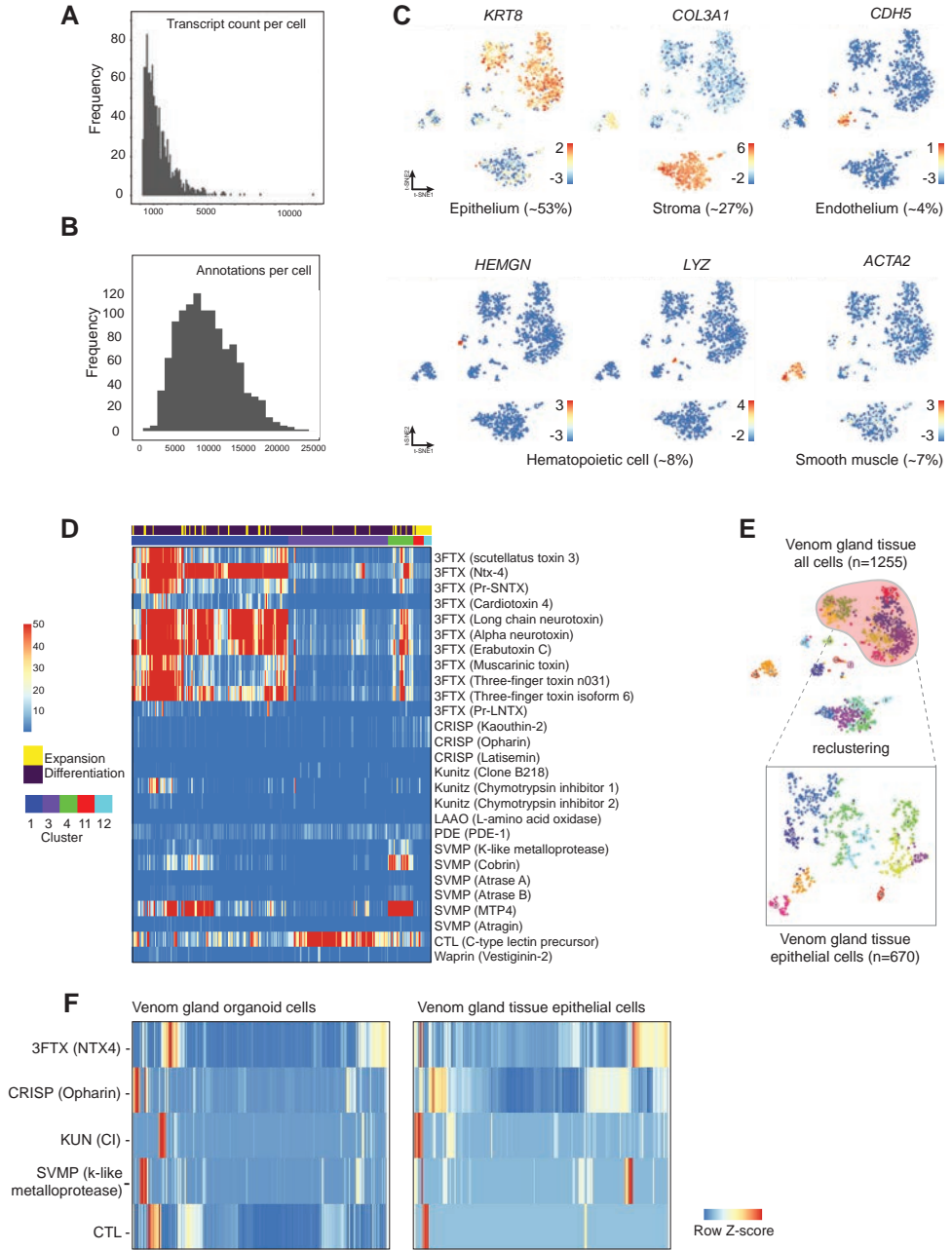
V

VI

VII

VIII

&



I

II

III

IV

V

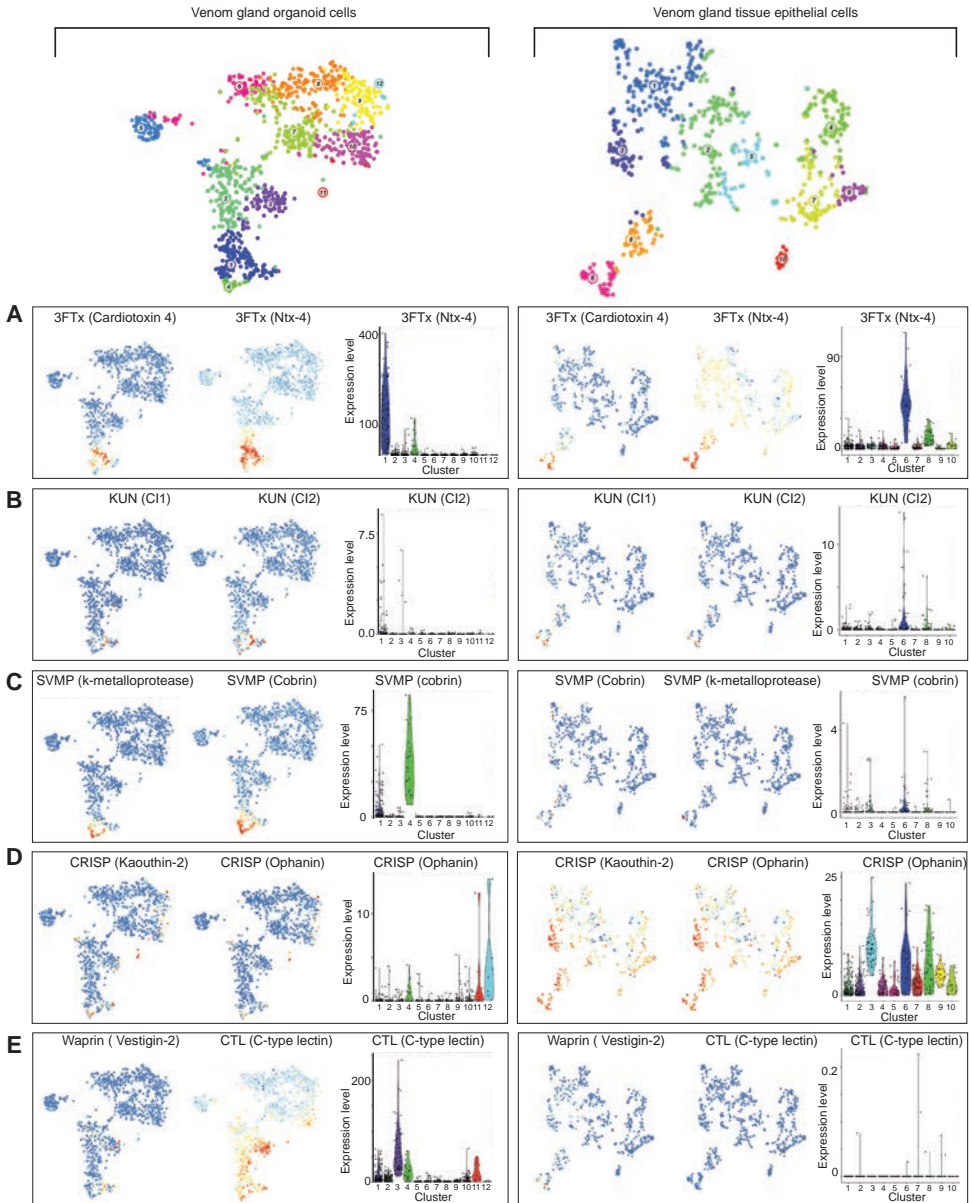
VI

VII

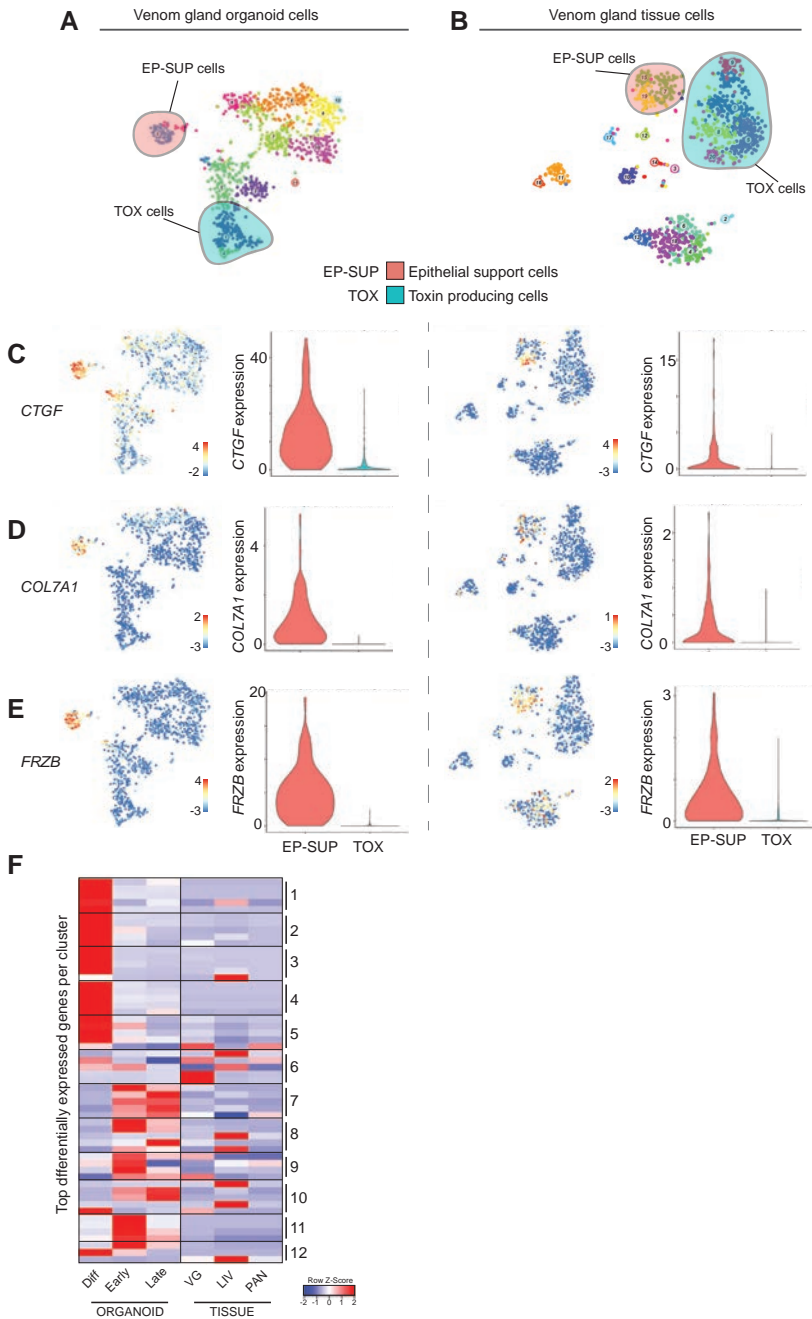
VIII

&

- ◀ **Supplementary figure 3. Single cell transcriptome analysis of venom gland primary tissue and organoid cells, related to Figure 4.** Details on single cell sequencing analysis; transcript count per cell. Details on single cell sequencing analysis; annotations per cell. Single cell RNA sequencing: clustering of *A. l. cowlesi* primary venom gland tissue cells (n=1255) visualized by *t*-distributed stochastic neighbor-embedding (*t*-SNE) map. Expression level of cell type marker genes in *t*-SNE map (color coded logarithmic scale of transcript expression): epithelial cells, *KRT8* (n=670); stromal cells, *COL3A1* (n=342); hematopoietic cells, *HEMGN*, *LYZ* (n=103); smooth muscle cells, *ACTA2* (n=90); endothelial cells, *CDH5* (n=50). Heatmap of toxin gene (y-axis) expression per individual cell (x-axis). All cells from toxin-expressing clusters 1, 3, 4, 11 and 12 are displayed for expression of most abundant toxin genes, see Figure S2B. Color coded expansion medium, differentiation medium and cluster numbers. Schematic representation of reclustering epithelial cells (10 clusters, n=670) from total venom gland tissue dataset (20 clusters, n=1255). Visualized by *t*-distributed stochastic neighbor-embedding (*t*-SNE) map. Heatmap of expression per toxin class (3FTx, CRISP, KUN, SVMP and CTL) of highest expressed genes (*NTX4*, *Opharin*, *Chymotrypsin inhibitor*, *K-like metalloprotease* and *CTL*) (y-axis) per cell (x-axis) for both organoids and epithelial tissue cells.



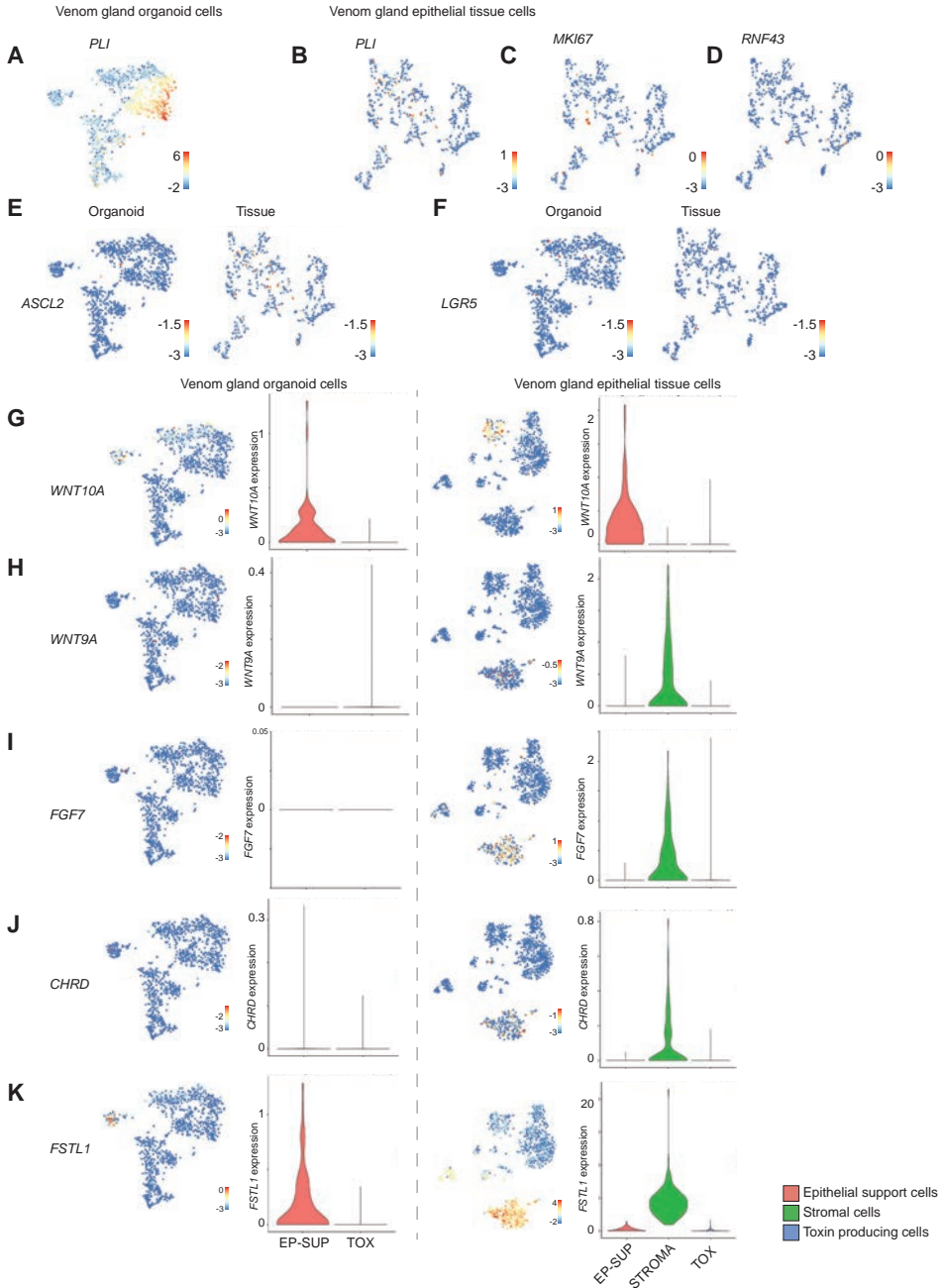
Supplementary figure 4. Dedicated venom gland epithelial cells express different classes of toxins, related to Figure 4. (A-E) Expression levels of selected toxin genes in *t*-SNE map (color coded logarithmic scale of transcript expression) and violin plots visualizing expression levels of cluster-enriched toxins. Left panels are venom gland organoid cells and right panels are venom gland tissue epithelial cells, both from *A. I. cowlesi*.



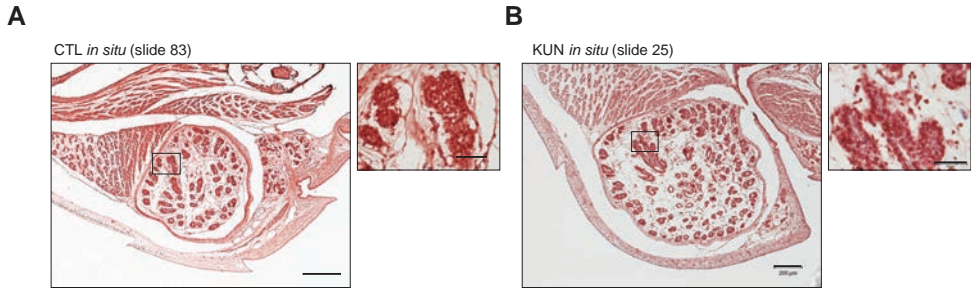
I
II
III
IV
V
VI
VII
VIII
&

Supplementary figure 5. Two different lineages of epithelial cells captured in organoids and primary tissue, related to Figure 4. *t*-SNE map of organoid dataset, highlighted are the clusters that account for the EP-SUP and TOX lineage. *t*-SNE map of tissue dataset, highlighted are the clusters that account for the EP-SUP and TOX lineage. (C-E) Expression levels of selected EP-SUP genes in *t*-SNE map (color coded logarithmic scale of transcript expression) and violin plots visualizing expression levels in the two distinct

▶ lineages. Left panels are organoid cells and right panels are tissue cells. (F) Heatmap of marker expression (12 clusters (3 to 5 genes per cluster) from organoid single cell sequencing dataset (Figure 4)) in bulk mRNA samples from venom gland organoids in differentiation (Diff) and expansion medium early (Early) and late (Late) and venom gland (VG), liver (LIV) and pancreas (PAN) tissue. Expression levels visualized as color coded Row Z-score.



- Supplementary figure 6. Non-venomous cells express stem cell markers and niche factors, related to Figure 4 and 5. (A-F) Expression levels of selected genes in *t*-SNE map (color coded logarithmic scale of transcript expression). Left panels are organoid cells and right panels are tissue cells. (G-K) Expression levels of selected niche signal genes in *t*-SNE map (color coded logarithmic scale of transcript expression) and violin plots visualizing expression levels in the distinct lineages. Left panels are organoid cells and right panels are tissue cells.



Supplementary figure 7. Regional heterogeneity in toxin expression validated *in vivo*, related to Figure 6 (A-B) Schematic representation of venom gland proximal and distal sections. BM-purple stain of *in situ* hybridization. Lack of detectable CTL (slide 83, distal) and KUN (slide 25, proximal) signal in *A. l. cowlesi* venom gland tissue. Scale bars, 200 μ m, close up panels 50 μ m.

I

II

III

IV

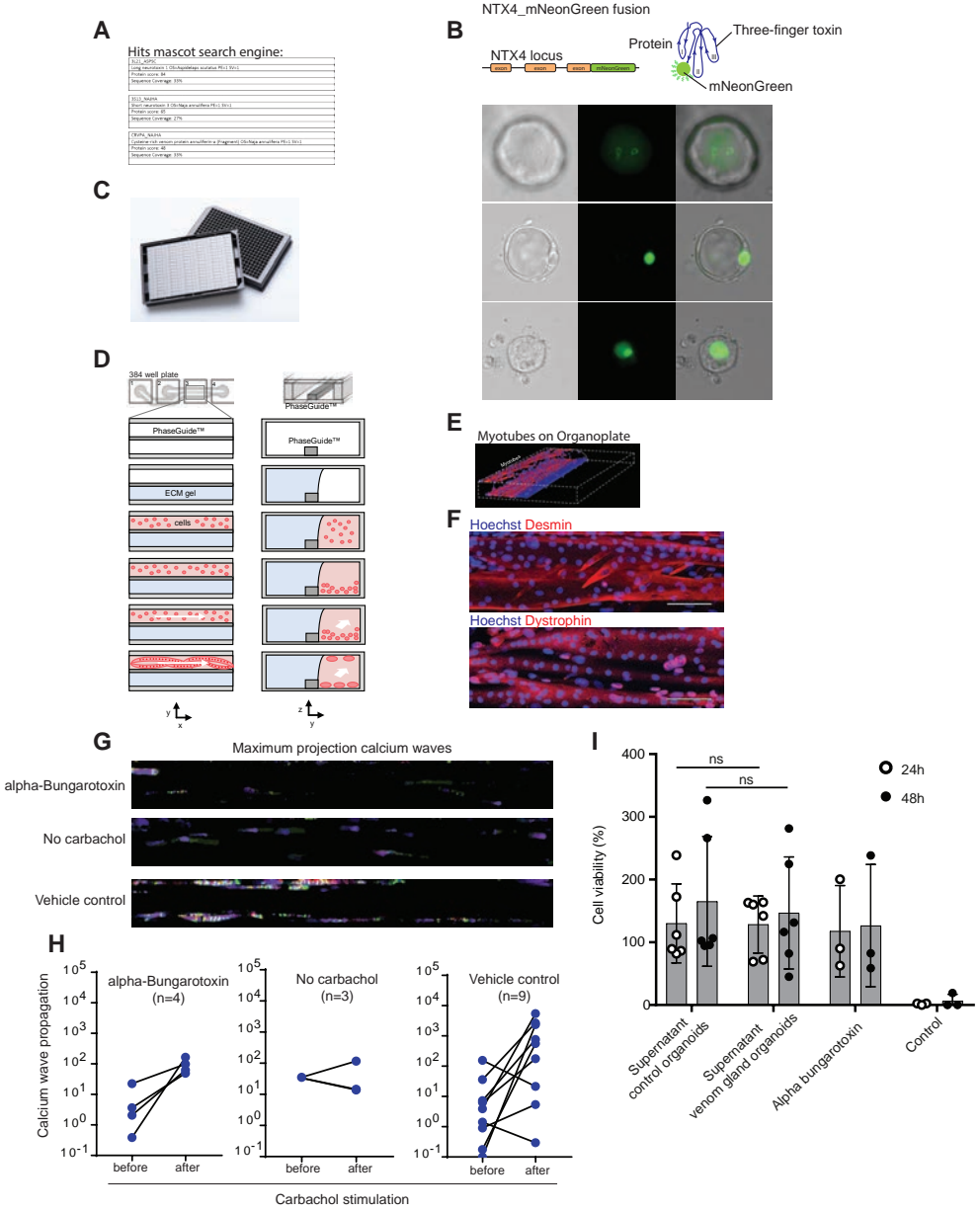
V

VI

VII

VIII

&



I

II

III

IV

V

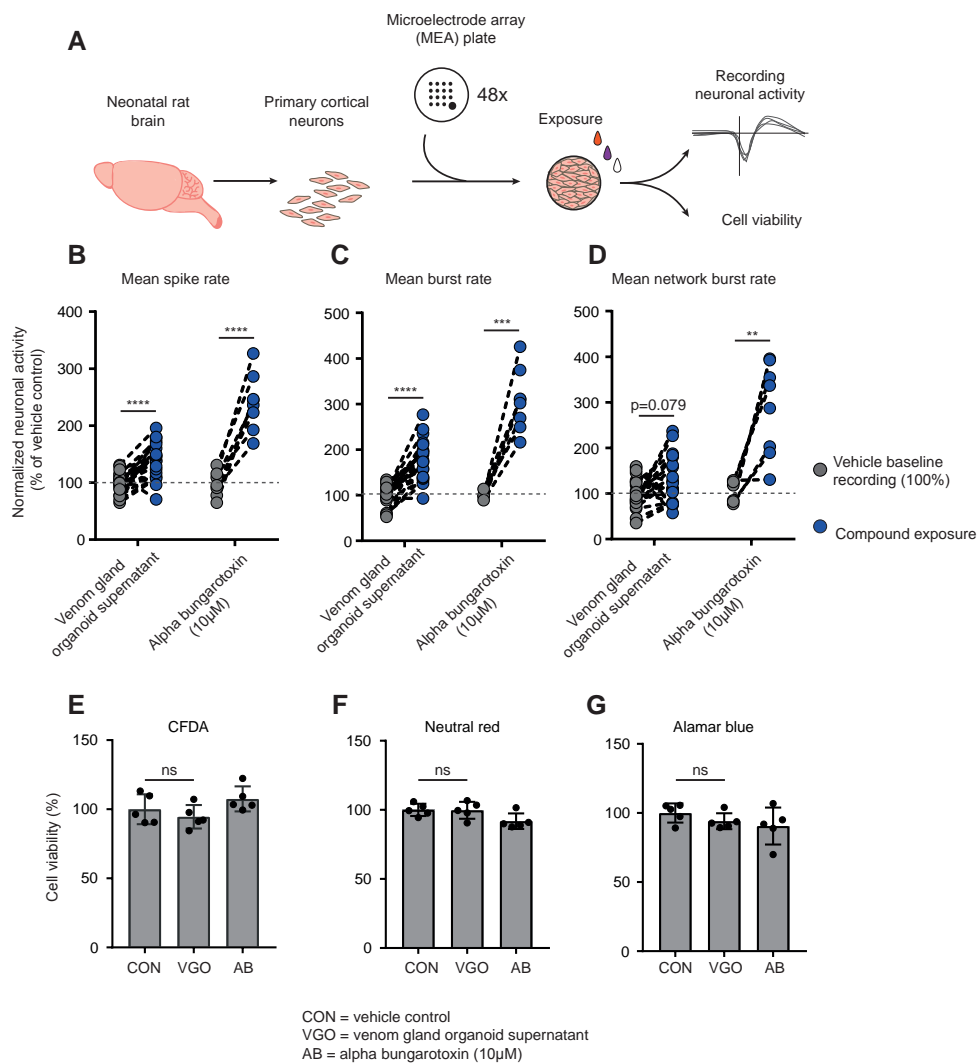
VI

VII

VIII

&

- ◀ **Supplementary figure 8. Venom gland organoids functionally secrete proteins that block calcium signals in muscle cells on OrganoPlate, Related to Figure 7.** Example of protein hits obtained with a Mascot search of the spectra measured from LC-MS analysis. Based on tryptic digest of an organoid supernatant. Generation of an endogenous fluorescent tag of three-finger toxin *NTX4* using CRISPR-HOT in *A. l. cowlesi* organoids MIMETAS 2-lane OrganoPlate® Schematic overview of OrganoPlate microfluidic network covering four wells of the 384-well-plate. Representative immunofluorescent 3D reconstruction of myotubes forming a perfusable tube structure. Staining for Hoechst (blue) and Myosin (red). Confocal image of mature myotubes stained for Desmin, Dystrophin (red) and Hoechst (blue). Cultures were exposed to different supernatants in chips, after which calcium wave propagation was imaged before and after carbachol stimulation. Maximum projected images depict calcium wave propagation over all image frames after carbachol exposure, in which purple reflects activity to the left and green to the right. Quantification of (F). The total calcium wave movement was calculated before and after carbachol stimulation based on total fluorescent signal. Cell viability assay (WST8) of C2C12 murine muscle cultures 24h and 48h after a 30-minute exposure to supernatants.



Supplementary figure 9. Venom gland organoid proteins increase neuronal activity in rat cortical neurons, related to Figure 7. (A) Schematic representation of experimental setup. Culture of neonatal rat cortical neurons on MEA plates. Exposure to organoid proteins and control is followed by recording of neuronal activity and cell viability assessment. (B-D) Quantification of neuronal activity measured as ‘mean spike rate’ (B), ‘mean burst rate’ (C) and ‘mean network burst rate’ (D) normalized to culture well-matched vehicle control. Exposure to venom gland organoid supernatant and recombinant alpha bungarotoxin. Paired t-test: **** $p < 0.0001$, *** $p = 0.0002$, ** $p = 0.005$. (E-G) Cell viability assessment using CFDA, Neutral red and Alamar blue. Normalized to vehicle control (100%). Differences are not significant (n.s.).

CHAPTER
SUMMARIZING DISCUSSION

VIII

Joep Beumer

Hubrecht Institute, Royal Netherlands Academy of Arts and Sciences (KNAW) and UMC Utrecht,
3584 CT Utrecht, The Netherlands.

INTRODUCTION

The intestinal epithelium is among the fastest dividing organs in mammals and therefore the prototype organ to study adult stem cells (Clevers, 2013). Many niche signals that control the cell division and differentiation behavior of intestinal stem cells were already established when the work in this thesis was commenced. These are reviewed in Chapter 1. An exception to this were the rare hormone-producing enteroendocrine cells (described in Chapter 2), of which the differentiation remained poorly understood. We used organoid technology to study the role of different signaling pathways in their ability to shape the intestinal epithelium. EGFR signaling and cell division activity were identified as key regulators of enteroendocrine cell (EEC) differentiation (Chapter 3). We further uncovered a role of the BMP signaling pathway in controlling hormone expression along the crypt-villus axis, inducing apparent transdifferentiation of enteroendocrine cells (Chapter 4). This finding was later extended to enterocytes and goblet cells, that similarly specialize along this axis (Chapter 5). Human intestinal organoids were employed to generate a transcriptomic and secretomic atlas of enteroendocrine cells, that uncovered key differences with their murine counterparts (Chapter 6). In the final chapter, organoid technology was extended to a reptile for the first time, which allowed for the expansion of snake venom glands (Chapter 7). In the following sections, we will summarize the key findings of these studies, together with their implications for therapies and follow-up work.

GENERATION OF THE ENTEROENDOCRINE CELL

Lgr5⁺ intestinal stem cells divide every 24 hours, and generate all the differentiated cell types of the epithelium. These cells exist in a Wnt-high niche that supports their stem cell potential. Wnt ligands derive both from the mesenchyme and epithelium (Beumer and Clevers, 2016). Stem cell daughter cells that exit the Wnt-high niche differentiate into different cell types. These include enterocytes that absorb nutrients, secretory Paneth cells (antimicrobials, niche factors), Goblet cells (mucus) and EECs (hormones). Stem cells and enterocytes depend on active Notch signaling, while progenitors losing this signal are destined towards secretory cell types (VanDussen et al., 2012). All secretory progenitors that have lost the Notch signal present Notch ligands to neighboring enterocytes enforcing lateral inhibition (van Es et al., 2012). Hence, the enterocyte fate is determined by stem cell daughter cells losing Wnt signals while maintaining an active Notch pathway. Before maturing towards enterocytes, these progenitors undergo multiple transit-amplifying divisions to increase their numbers. The Paneth cell is the only secretory cell type remaining in the crypt bottom, located between Lgr5⁺ stem cells. Next to loss of Notch signaling, Wnt activation is important for the specification of Paneth cells. Goblet cells and EECs both require loss of Notch, and are specified independent of Wnt.

Many groups have proposed the existence of non-dividing stem cells that act as a reserve population next to the dividing Lgr5⁺ stem cells (Montgomery et al., 2011; Sangiorgi and Capecchi, 2008; Takeda et al., 2011). This work has partly been based on the proposition that stem cells should be quiescent to protect their genome from cell cycle division associated

I

II

III

IV

V

VI

VII

VIII

&

damage. Genetic markers used for this population were however co-expressed by other cell types including Lgr5⁺ stem cells, hampering definite conclusions from lineage tracing (Muñoz et al., 2012). In 2016, the lab of Doug Winton exploited an innovative tracing technique in the intestine and followed the fate of all non-dividing cells *in vivo*. This work found that these cells are not multipotent but are destined towards Paneth cells and EECs. These cells retain stem cell potential that can be activated upon damage (Buczacki et al., 2013).

While studying the cell cycle control of intestinal stem cells in organoids, we found that loss of EGF signals induces a quiescent state of Lgr5⁺ stem cells in organoids that can be maintained for at least a week. This was the first evidence that EGF-controlled cell proliferation is uncoupled from Wnt/Notch-controlled multipotency: stem cells that exit the cell cycle do not differentiate automatically. The important distinction between our work in organoids with the Winton study is that *in vivo* these quiescent cells would be constantly displaced from the crypt bottom by proliferating cells, and therefore are always destined to differentiate due to loss of Wnt and Notch signals.

Although we found that EGFR-inhibited stem cells retain Lgr5 expression and are multipotent, these cells do display a bias towards generating secretory cells, and in particular EECs, when EGF was re-supplemented. This is in line with the quiescent cells that the Winton lab identified, that display a bias towards EECs and never generate goblet cells. This implies cell cycle exit of progenitor cells as an important distinction between EECs and goblet cells. Goblet cells are much more numerous than EECs, and potentially require additional cell divisions at the progenitor level. Recent work has suggested that cyclin-dependent kinases can phosphorylate and destabilize Neurogenin-3, the pro-EEC transcription factor (Azzarelli et al., 2017; Krentz et al., 2017). This could provide the mechanistic link between cell cycle exit and a bias towards EEC fate. This work led to our most efficient differentiation protocol towards EECs, which involved combined Notch inhibition (induction of secretory cells), Wnt inhibition (blocking Paneth cell fate) and EGFR inhibition (blocking Goblet cell fate).

BMP SIGNALING INSTRUCTS A DIVISION OF LABOR ALONG THE CRYPT-VILLUS AXIS

EECs produce a plethora of hormones, and more than 20 different neurotransmitters and peptides have been reported (Worthington et al., 2018). When the work in this thesis was commenced, there were no signals established that decide which hormones EECs produce. We used intestinal organoids to screen signaling pathways in their ability to control hormone expression. In these screens, we found that BMP molecules could induce a set of hormones, while repressing others (Beumer et al., 2018). The BMP signaling pathway forms a morphogen gradient in the intestinal epithelium: low in the crypt, and highest in the villus tips. BMP signaling is known to repress the stem cell signature, and thereby restricts the stem cell zone to the bottom of the crypt (Haramis et al., 2004; Qi et al., 2017). Its role in differentiation of the different epithelial cell types has not been studied.

In the 90s, multiple studies reported on the differential expression of EEC hormones along the crypt-villus axis (Aiken and Roth, 1992; Grunddal et al., 2016; Roth and Gordon, 1990).

The set of hormones repressed with BMP activation in our study corresponded to classical crypt hormones, while those induced are villus-enriched hormones. Blocking the BMP gradient *in vivo* expands the crypt-hormones in the villus area, while blocking the expression of villus hormones. Using lineage tracing, we could evidence that crypt and villus hormones can be produced by the same EEC, that undergoes switches in its hormone repertoire during the lifetime. With the demonstration of this BMP-regulated plasticity of EECs, we effectively reduced the number of EEC subtypes: we show that multiple hormone-producing cells that were before regarded as separate entities (S-cells that make secretin, N-cells that make neurotensin), are BMP-induced, villus states of other EEC subtypes.

While we performed modulations of BMP signaling in intestinal organoids, we noted that apart from hormones that were severely affected, expression of enterocyte and goblet cell markers also changed. The lab of Shalev Itzkovitz recently reported RNA sequencing data in segments of the crypt-villus axis (Moor et al., 2018). This work, which focused on enterocytes, shows that enterocytes specialize along this axis, and produce different functional markers during their lifetime. While enterocytes at the bottom of the villus mainly produce carbohydrate transporters, lipid uptake and chylomicron synthesis genes predominate at the villus tip (Moor et al., 2018). We exploited human intestinal organoids differentiated towards enterocytes or goblet cells, and performed transcriptomic analysis in the presence and absence of BMP signals. These experiments show that although mature enterocytes and goblet cells arise both without and with BMP signals, the gene expression profiles are significantly different. Generic enterocyte and goblet cell markers do not change, in line with an intestinal knockout of the BMP-receptor *BMPRIa* that does not influence the total number of these differentiated cells (Auclair et al., 2007). However, other functional markers of enterocytes, not investigated in these mouse models, change significantly. Enterocytes exclusively produce apolipoproteins in the presence of BMP, and express genes that allow digestion and uptake of carbohydrates in the absence of BMP. We additionally describe specialization of goblet cells based on BMP signals that change their antimicrobial repertoire along the crypt-villus axis.

It is currently unknown why intestinal cell types specialize so extensively along the epithelium, although it is likely that interactions with microbiota and oxygen concentration could play a role. It remains unclear if and how the exposure to BMP signals could be modulated: if this does not occur, the transdifferentiation or specialization of intestinal cell types inevitably occurs. One potential mechanism to influence this exposure to BMPs is alternative migration through the conveyor belt. It has been shown that EECs can stay at the bottom of the crypt for longer times, thereby escaping their hormone switching (Aiken et al., 1994). BMP signals also derive from the serum, and these could as well be regulated. For example, cholesterol synthase inhibitors called statins are known inducers of BMP production in multiple tissues, including the bone and intestine (Chen et al., 2010; Kodach et al., 2007). Such feedback loops could on a whole-body level could regulate cholesterol uptake through signaling different levels of BMP to the intestinal epithelium.

I

II

III

IV

V

VI

VII

VIII

&

AN ATLAS OF HUMAN ENTEROENDOCRINE CELLS

Most EEC studies have focused on mice. Mouse models in which EEC hormones were knocked out, or reporters where individual EECs could be isolated, have generated many insights into the functioning and expression profiles of murine EECs. *In vitro* models widely used include multiple cell lines established from neuroendocrine tumors. These tumor cells however are not ideal EEC models, since often only a single hormone is produced, and some sensory receptors are not expressed (Goldspink et al., 2018). Moreover, EEC functioning is at part influenced by other cell types that are not captured in such a system. Another limitation of these mouse-based studies are the large differences between mouse EECs and human EECs, which have only been partly explored. These include for example the expression of different hormones.

To address these challenges, we used intestinal organoids to build models to study the functioning of human EECs in a more native environment, and derived a transcriptomic and proteomic description of the gut hormone producing cells in humans. We exploited a pulse of *Neurog3*-overexpression in organoids derived from different regions of the gut to generate the full spectrum of human EECs. Using novel Cas9-and non-homologous end joining-based knock-in strategies, we labeled almost every hormone fluorescently in these organoids. Combining transcriptomic and proteomic analyses, we constructed a high-definition atlas of human EECs and their secreted products. We find multiple novel secreted products not known before in the gut, but which are described in other endocrine systems such as the pancreas. Additionally, we identify multiple new sensory receptors in EECs. Multiple of these factors have been associated with regulation of feeding behavior before. Finally, we identify extensive expression of hormone receptors among EEC subpopulations, allowing these to sense hormones from other EEC subtypes. This has been described for Somatostatin in mice, but we now extend this observation to Pyy and Secretin receptors. Secretin receptors are expressed in L-cells that secrete Glp-1 upon Secretin stimulation. We also identify the Secretin receptor in Gastrin-producing EECs. Interestingly, a secretin-stimulation test is one of the definitive diagnosis criteria from Zollinger-Ellison syndrome, but the receptor for secretin has never been shown to be expressed in wildtype gastrin-producing cells.

SNAKE VENOM GLAND ORGANOIDS

Snakes have fascinated humankind for millennia. The ancient Greek deity Asclepius, who is associated with healing and medicine, carries as his symbol a rod with a snake. The Greeks used snake venom in many healing practices. In modern day, multiple drugs have been derived from these toxins, and include blood pressure lowering drugs. Yet, many snakes are close to extinction, or are difficult to breed, rendering a thorough analysis and therapeutic exploitation of their venom impossible. The other 'bad' side of snakes is much better known. Snakebite kills over 100.000 humans every year, particularly in developed countries. This is often caused by a lack of effectivity of anti-venom. Due to huge variation in venom composition, up to the level of an individual snake over time, anti-venom production that protects against every bite remains challenging (Gómez-Betancur et al., 2019).

Similarly to the gut EECs, accessing the secretory cells of the snake venom gland is hard. A model system that would allow studying the functioning of the venom gland without needing to milk snakes could greatly accelerate unlocking the therapeutic potential, as well as better protecting humans against the lethal side of these animals. We therefore set out to establish an organoid system from snake venom glands. We describe culture conditions for long-term expansion of the cape coral snake, *Aspidelaps lubricus*, and the cape cobra, *Naja nivea*. These cultures produce functional toxins. We also identify extensive heterogeneity in venom producing cells, that we confirmed *in vivo*. Snake venom is a complex mixture of molecules, and it was unknown whether these derive from a single cell type. We show that different cells make different parts of this mixture. We believe the organoid culture system can be used to identify regulators of venom production (such as diet factors), and isolating venomous molecules to study their function. We already show in this study that two different culture media can generate a completely different spectrum of toxins. Moreover, toxins require multiple modifications that cannot be made in other cellular systems such as bacteria, and for that reason our organoids could be used as a production platform for toxins from other species. We demonstrate that the venom gland organoids can be genetically modified with Cas9 or lentiviruses. Finally, this is the first organoid system from reptiles, and proves that reptilian stem cells use similar developmental principles as their mammalian counterparts.

I
II
III
IV
V
VI
VII
VIII
&

CONCLUDING REMARKS

In this thesis, we have described organoids as a model to study developmental cues underpinning homeostatic turnover, with a focus on the intestine and its hormone-producing EECs. I believe this work highlights the utility of organoids to identify such cues. Organoids allow for a reductionist approach, in which the role of individual signaling components acting on the epithelium in the absence of mesenchyme can be studied. It also stresses the importance of understanding the maturation level of the cell types in organoids. These cultures are widely used to study the functioning of cell types, for example lipid uptake in the intestine. A lack of BMP exposure in this scenario would severely hamper definite conclusions, as enterocytes in such cultures would lack expression of essential players in lipid handling.

We secondly demonstrated organoids as a model to study the functioning of hard-to-study cell types, in particular the intestinal EECs. These enigmatic cells regulate crucial physiological processes such as insulin release and appetite, and are attractive therapeutic targets. We describe the human EEC repertoire, including novel secreted products, and sensory receptors that were not known before. These could be targeted by small molecules to stimulate secretion of the corresponding hormone.

I believe the intestinal epithelium is a largely unexplored tissue for treatment of metabolic diseases. This is paradoxical as it is the site where food is for the first time sensed and absorbed. Therapies targeting the intestinal epithelium do not require to enter the blood stream, preventing potential off-target effects. BMP inhibitors for example could limit the intestinal lipid uptake, and enhance GLP-1 expression, that could be attractive for NASH or obesity. We currently

still do not fully understand how the EEC subtypes are specified. Moreover, although we describe many GPCRs in EECs, we might miss more due to their low expression, and a number of these are orphan. Unbiased high throughput screens for developmental and secretion regulators exploiting our human EEC platform could aid unlocking the therapeutic potential of gut hormones.

REFERENCES

- Aiken, K.D., and Roth, K.A. (1992). Temporal differentiation and migration of substance P, serotonin, and secretin immunoreactive enteroendocrine cells in the mouse proximal small intestine. *Dev. Dyn.* 194, 303–310.
- Aiken, K.D., Kisslinger, J.A., and Roth, K.A. (1994). Immunohistochemical studies indicate multiple enteroendocrine cell differentiation pathways in the mouse proximal small intestine. *Dev. Dyn.* 201, 63–70.
- Auclair, B.A., Benoit, Y.D., Rivard, N., Mishina, Y., and Perreault, N. (2007). Bone Morphogenetic Protein Signaling Is Essential for Terminal Differentiation of the Intestinal Secretory Cell Lineage. *Gastroenterology*.
- Azzarelli, R., Hurley, C., Sznurkowska, M.K., Rulands, S., Hardwick, L., Gamper, I., Ali, F., McCracken, L., Hindley, C., McDuff, F., et al. (2017). Multi-site Neurogenin3 Phosphorylation Controls Pancreatic Endocrine Differentiation. *Dev. Cell* 41, 274–286.e5.
- Beumer, J., and Clevers, H. (2016). Regulation and plasticity of intestinal stem cells during homeostasis and regeneration. *Development*.
- Beumer, J., Artegiani, B., Post, Y., Reimann, F., Gribble, F., Nguyen, T.N., Zeng, H., Van den Born, M., Van Es, J.H., and Clevers, H. (2018). Enteroendocrine cells switch hormone expression along the crypt-to-villus BMP signalling gradient. *Nat. Cell Biol.*
- Buczacki, S.J. a, Zecchini, H.I., Nicholson, A.M., Russell, R., Vermeulen, L., Kemp, R., and Winton, D.J. (2013). Intestinal label-retaining cells are secretory precursors expressing Lgr5. *Nature* 495, 65–69.
- Chen, P.Y., Sun, J.S., Tsuang, Y.H., Chen, M.H., Weng, P.W., and Lin, F.H. (2010). Simvastatin promotes osteoblast viability and differentiation via Ras/Smad/Erk/BMP-2 signaling pathway. *Nutr. Res.*
- Clevers, H. (2013). The intestinal crypt, a prototype stem cell compartment. *Cell* 154, 274–284.
- van Es, J.H., Sato, T., van de Wetering, M., Lyubimova, A., Yee Nee, A.N., Gregorieff, A., Sasaki, N., Zeinstra, L., van den Born, M., Korving, J., et al. (2012). Dll1+ secretory progenitor cells revert to stem cells upon crypt damage. *Nat. Cell Biol.* 14, 1099–1104.
- Goldspink, D.A., Reimann, F., and Gribble, F.M. (2018). Models and Tools for Studying Enteroendocrine Cells. *Endocrinology*.
- Gómez-Betancur, I., Gogineni, V., Salazar-Ospina, A., and León, F. (2019). Perspective on the therapeutics of anti-snake venom. *Molecules*.
- Grunddal, K. V., Ratner, C.F., Svendsen, B., Sommer, F., Engelstoft, M.S., Madsen, A.N., Pedersen, J., Nøhr, M.K., Egerod, K.L., Nawrocki, A.R., et al. (2016). Neurotensin is coexpressed, coreleased, and acts together with GLP-1 and PYY in enteroendocrine control of metabolism. *Endocrinology* 157, 176–194.
- Haramis, A.P.G., Begthel, H., Van Den Born, M., Van Es, J., Jonkheer, S., Offerhaus, G.J.A., and Clevers, H. (2004). De Novo Crypt Formation and Juvenile Polyposis on BMP Inhibition in Mouse Intestine. *Science* (80-.). 303, 1684–1686.
- Kodach, L.L., Bleuming, S.A., Peppelenbosch, M.P., Hommes, D.W., van den Brink, G.R., and Hardwick, J.C.H. (2007). The Effect of Statins in Colorectal Cancer Is Mediated Through the Bone Morphogenetic Protein Pathway. *Gastroenterology*.
- Krentz, N.A.J., van Hoof, D., Li, Z., Watanabe, A., Tang, M., Nian, C., German, M.S., and Lynn, F.C. (2017). Phosphorylation of NEUROG3 Links Endocrine Differentiation to the Cell Cycle in Pancreatic Progenitors. *Dev. Cell* 41, 129–142.e6.

I

II

III

IV

V

VI

VII

VIII

&

- Montgomery, R.K., Carlone, D.L., Richmond, C. a, Farilla, L., Kranendonk, M.E.G., Henderson, D.E., Baffour-Awuah, N.Y., Ambruzs, D.M., Fogli, L.K., Algra, S., et al. (2011). Mouse telomerase reverse transcriptase (mTert) expression marks slowly cycling intestinal stem cells. *Proc. Natl. Acad. Sci. U. S. A.* *108*, 179–184.
- Moor, A.E., Harnik, Y., Ben-Moshe, S., Massasa, E.E., Rozenberg, M., Eilam, R., Bahar Halpern, K., and Itzkovitz, S. (2018). Spatial Reconstruction of Single Enterocytes Uncovers Broad Zonation along the Intestinal Villus Axis. *Cell* *175*, 1156–1167.e15.
- Muñoz, J., Stange, D.E., Schepers, A.G., van de Wetering, M., Koo, B.-K., Itzkovitz, S., Volckmann, R., Kung, K.S., Koster, J., Radulescu, S., et al. (2012). The Lgr5 intestinal stem cell signature: robust expression of proposed quiescent “+4” cell markers. *EMBO J.* *31*, 3079–3091.
- Qi, Z., Li, Y., Zhao, B., Xu, C., Liu, Y., Li, H., Zhang, B., Wang, X., Yang, X., Xie, W., et al. (2017). BMP restricts stemness of intestinal Lgr5+ stem cells by directly suppressing their signature genes. *Nat. Commun.* *8*, 13824.
- Roth, K. a, and Gordon, J.I. (1990). Spatial differentiation of the intestinal epithelium: analysis of enteroendocrine cells containing immunoreactive serotonin, secretin, and substance P in normal and transgenic mice. *Proc. Natl. Acad. Sci. U. S. A.* *87*, 6408–6412.
- Sangiorgi, E., and Capecchi, M.R. (2008). *Bmi1* is expressed in vivo in intestinal stem cells. *Nat. Genet.* *40*, 915–920.
- Takeda, N., Jain, R., LeBoeuf, M.R., Wang, Q., Lu, M.M., and Epstein, J.A. (2011). Interconversion between intestinal stem cell populations in distinct niches. *Science* *334*, 1420–1424.
- VanDussen, K.L., Carulli, a. J., Keeley, T.M., Patel, S.R., Puthoff, B.J., Magness, S.T., Tran, I.T., Maillard, I., Siebel, C., Kolterud, a., et al. (2012). Notch signaling modulates proliferation and differentiation of intestinal crypt base columnar stem cells. *Development* *139*, 488–497.
- Worthington, J.J., Reimann, F., and Gribble, F.M. (2018). Enteroendocrine cells-sensory sentinels of the intestinal environment and orchestrators of mucosal immunity. *Mucosal Immunol.*

APPENDIX

NEDERLANDSE SAMENVATTING

LIST OF PUBLICATIONS

DANKWOORD

CURRICULUM VITAE



NEDERLANDSE SAMENVATTING

Alle organen slijten continu en verliezen gedurende dit proces cellen. Een zichtbaar voorbeeld hiervan is haaruitval. Het verlies van deze cellen wordt gecompenseerd door zogenaamde stamcellen. Deze cellen kunnen zichzelf vernieuwen door celdeling, en maken daarnaast alle gespecialiseerde cellen van een orgaan. Stamcellen in een volwassen stadium van een dier maken louter de cellen van het corresponderende orgaan, en heten ook wel adulte stamcellen. Het zijn alleen de embryonale stamcellen, vroeg na de bevruchting van een eicel, die alle cellen van een complex organisme kunnen maken.

De studie van adulte stamcellen is zeer complex, voornamelijk omdat tot een decennium geleden niet precies bekend was welke cellen in verschillende organen de functionele stamcellen zijn. De progressie van de muizengenetica en analyses van genexpressies leidden ongeveer 10 jaar geleden tot een snelle identificatie van stamcellen in verschillende organen. In muizenexperimenten, die in vakjargon ‘lineage tracing’ (stamboom volgen) heten, wordt door genetische modificatie aan specifieke groepen cellen een kleurtje gegeven die ze als marker doorgeven aan dochtercellen. Cellen die dit gedurende het hele leven blijven doen – en deze kleur als het ware altijd aanwezig blijft in alle cellen van het orgaan – zijn de echte stamcellen. Niet-stamcellen kunnen niet voor altijd delen, en gaan uiteindelijk dood waardoor de kleur verdwijnt.

De muis is lang het beste model geweest voor veel takken van biologie, en in het bijzonder voor de stamcelbiologie. Het is echter lastig om proeven te doen in muizen, omdat er erg veel variabelen zijn en stamcellen vaak relatief zeldzaam zijn. Er zijn wel zogenaamde cellijnen die gekweekt kunnen worden in het lab, maar die hebben vaak nog maar weinig karakteristieken van de hiërarchie van de oorspronkelijke organen. Deze cellijnen zijn meestal afgeleid van tumoren en gezonde stamcellen ontbreken daarom. De identificatie van stamcelpopulaties via lineage tracing maakte het mogelijk deze cellen te isoleren uit muizen om te pogen deze te kweken. In 2009 werd in *Nature* onderzoek uit het Hubrecht Instituut gepubliceerd waarin voor het eerst gelukt was om adulte stamcellen uit een orgaan te isoleren en die op te groeien. Deze kweken groeien in 3 dimensies en bevatten functionele celtypen uit het corresponderende orgaan. De kweken – omgedoopt tot organoïden - werden in de jaren die volgden voor bijna alle organen opgezet, maar ook van ziek weefsel zoals tumoren. Uitzonderingen van organen die niet kunnen groeien als organoïden zijn het hart en de hersenen, beide organen waar waarschijnlijk geen stamcellen in een adult stadium aanwezig zijn.

Organoïden zijn in het afgelopen decennium uitgebreid gebruikt om ziekteprocessen te bestuderen. Door middel van genetische modificatie, in het bijzonder via het CRISPR/Cas9 gereedschap wat in diezelfde periode ontwikkelde, kan een organoïde gebruikt worden als model van ziekten als kanker. Organoïden gekweekt uit ziek materiaal, zoals kwaadaardige biopten van patiënten, maken het mogelijk om medicijnen te testen en hun effectiviteit te voorspellen voordat iemand hiermee daadwerkelijk behandeld wordt. Dit is een belangrijke doorbraak in de behandeling van kanker, omdat medicatie vaak niet werkt en de patiënt wel onnodige bijwerkingen ervaart. Een ander voorbeeld van de toepassing van organoïden is

I

II

III

IV

V

VI

VII

VIII

&

het bestuderen van de interactie tussen een pathogeen en het menselijke weefsel. Organoïden kunnen geïnfecteerd worden met een virus (bijvoorbeeld influenza of een coronavirus in long organoïden) om te bestuderen wat hiervan de gevolgen zijn en hoe een virus een cel binnen kan komen. Dit biedt vervolgens mogelijkheden om stoffen te testen die binnenkomst van een virus kunnen voorkomen. De darm van mensen zit vol met bacteriën, maar de grote hoeveelheid en verschillende soorten maken het lastig om erachter te komen wat het effect is van ieder soort bacterie op de darm. Individuele bacteriesoorten kunnen geïnjecteerd worden in darm organoïden, waarna het effect op de darmcellen specifiek bestudeerd wordt. Een studie, gepubliceerd dit jaar in *Nature*, kon zo laten zien dat een type darmbacterie fouten kan induceren in het erfelijke materiaal van darmcellen, wat mogelijk tot kanker kan leiden.

De studie van stamcelbiologie, die in de eerste plaats de ontwikkeling van organoïden mogelijk maakte, profiteert ook van deze nieuwe tool in het wapenarsenaal van een bioloog. Groeisignalen kunnen in organoïden beïnvloed worden om te kijken hoe het gedrag van een stamcel verandert. Een stamcel moet vaak niet één maar meerdere celtypen in een orgaan maken. Het is niet voor ieder orgaan bekend welke signalen precies een rol spelen bij zulke beslissingen. De meeste organoïde systemen bevatten daardoor vaak ook niet alle celtypen. Om deze reden zijn dit nog niet volledig volwassen en doorontwikkelde kweken om alle celtypen te bestuderen. We hebben met onderzoek, gepresenteerd in deze thesis, getracht deze beperkingen te beantwoorden. Dit werk is gefocust op de darm; het snelst vernieuwende orgaan in dieren. De mens maakt maar liefst 200 gram nieuwe darmcellen per dag, en vernieuwt de volledige darmbekleding binnen een week. De bekleding van de darm bestaat voornamelijk uit enterocyten, welke voedingsstoffen opnemen uit de darminhoud. De andere celtypen zijn secretoire cellen die stoffen afgeven; slijmbeker cellen maken mucus die de darm bekleedt en een bescherming is tegen bacteriën. Paneth cellen maken antimicrobiële stoffen en moleculen essentieel voor de identiteit van stamcellen. Als laatste zijn er enteroendocriene cellen die hormonen afgeven als reactie op voedsel. De hormonen van enteroendocriene cellen zijn erg belangrijk als eerste reactie op voedsel en reguleren je hongergevoel, afgifte van insuline en pancreasenzymen, en darmperistaltiek. Deze cellen zijn echter uitermate zeldzaam (<1% van het darmepitheel) en daarom niet goed bestudeerd, en het is niet goed bekend op welke stoffen deze cellen reageren of hoe ze gemaakt worden uit stamcellen.

In **hoofdstuk 1** van deze thesis geven we een samenvatting van de groeisignalen die stamcellen reguleren, en hoe stamcellen op basis daarvan beslissen welk celtype ze worden. Speciale aandacht wordt gegeven aan hoe de darm in staat is te reageren op schade. In een dergelijk geval zijn er gedifferentieerde cellen die weer stamcel kunnen worden om schade te compenseren. **Hoofdstuk 2** beschrijft de functie en het productieproces van de enteroendocriene cellen. Deze cellen, die samen zo'n 20 hormonen maken, zijn weer onder te verdelen in 5 subtypen die daardoor nog zeldzamer zijn (soms maar 0.01% van het darmepitheel).

Hoofdstuk 3 wordt het organoïde model gebruikt om regulatoren van celdeling van de darmstamcel te identificeren. We hebben gevonden dat remmers van EGF (epidermal growth factor) signalen stamcellen laten stoppen met delen, een staat waarin ze een week kunnen overleven. Een dergelijke proef zou in muizen onmogelijk zijn omdat de darm binnen hetzelfde

tijdsbestek verloren zou gaan, hetgeen niet compatibel is met overleving van de muis. De niet-delende stamcellen specialiseren echter niet automatisch, maar gaan bij teruggave van EGF signalen weer delen en hun normale functie vervullen. De gereactiveerde stamcellen maken alle celtypen, maar op een korte termijn met een sterke voorkeur voor enteroendocriene cellen. Deze verrassende vinding stelde ons in staat om met een combinatie van groeifactormodulaties (remmen van EGF, en remmen van Notch en Wnt signalen) organoïden sterk te verrijken met enteroendocriene cellen – tot wel 70% van de cellen (normaal <1%). Het mechanisme hoe de beperkte celdelingsactiviteit van stamcellen tot meer enteroendocriene cellen zou kunnen leiden, begrepen we toen nog niet. Ontdekkingen het afgelopen jaar hebben deze echter beter in een context geplaatst, toen ontdekt werd dat eiwitten actief tijdens celdeling transcriptiefactoren afbreken die normaal nodig zijn om enteroendocriene cel te worden.

In **hoofdstuk 4** hebben we geprobeerd factoren te ontdekken die bepalen welk hormoon enteroendocriene cellen maken. Het darmepitheel is georganiseerd in groepen van crypten (putjes in de darmwand) en villi (uitstulpingen uit de darmwand). Stamcellen liggen beschermd in de bodem van de crypten, en dochtercellen migreren gedurende hun leven van de bodem van de crypt naar de villus, waar ze uiteindelijk sterven aan de top van de villus. BMP is een zogenaamd morfogen; het BMP signaal is zwak in de bodem van de crypt bij de stamcellen en het sterkst in de top van de villus. We ontdekten in deze studie dat sommige hormonen uitsluitend in de crypt worden gemaakt en sommige uitsluitend in de villus. BMP signalen leiden in organoïden eveneens tot veranderingen in welk hormoon een enteroendocriene cellen maakt. Het blokkeren van BMP signalen in een muis zorgt ervoor dat hormonen die je normaal alleen in de crypt vindt, ineens ook in villi gemaakt worden. Aan de andere kant nemen villus hormonen sterk af. We konden op basis van dit werk concluderen dat enteroendocriene cellen gedurende hun leven en migratie andere hormonen maken in de crypt en villus, onder invloed van verschillende BMP signalen.

Niet alleen enteroendocriene cellen vervullen andere functies (in dit geval productie van hormonen) in de crypt en over de as van de villus, hetzelfde gebeurt bij de slijmbekercellen en enterocyten. In **hoofdstuk 5** beschrijven we dat BMP signalering ook deels verantwoordelijk is voor specialisatie van deze celtypen over de as van de crypt en villus. Enterocyten bijvoorbeeld produceren de machinerie om lipiden op te nemen, te verpakken en weer uit te scheiden in de bovenkant van de villus. Activatie van BMP signalering in organoïden is essentieel om dergelijke eiwitten onderdeel van die machinerie te produceren. Deze studie benadrukt ook dat het belangrijk is om stil te staan bij welke functionaliteiten de celtypen van je organoïden hebben, en hoe die samenhangen met welke vragen een onderzoeker probeert te beantwoorden met het systeem. Enterocyten hebben in dit geval verschillende functionaliteiten afhankelijk van weinig of veel BMP signalen, iets wat ze in de echte darm ook hebben.

In **hoofdstuk 6** focussen we op menselijke enteroendocriene cellen, en hun verschillen met dezelfde cellen in muizen. Tot dan toe was vrijwel al het werk aan deze zeldzame cellen in muizen gedaan. Mensen maken in de darm enkele hormonen die muizen niet hebben. Vanwege grote verschillen in het dieet tussen mensen en muizen vermoedden we eveneens dat de enteroendocriene cellen in mensen op andere stoffen kunnen reageren dan bij muizen

I
 II
 III
 IV
 V
 VI
 VII
 VIII
 &

het geval is. We beschrijven in dit manuscript een systeem in menselijke organoïden om grote hoeveelheden enteroendocriene cellen te maken, waarbij we verschillende hormonen kleuren hebben gegeven. Deze kleuren stellen ons in staat om de verschillende subtypen enteroendocriene cellen (die andere hormonen maken) te isoleren en in detail te bestuderen. We beschrijven op deze manier alle eiwitten die humane enteroendocriene cellen produceren, en vinden nieuwe receptoren (antennes op cellen die bijvoorbeeld voedingstoffen kunnen waarnemen) ten opzichte van muizen. Stimulatie van enkele van deze receptoren zorgt ervoor dat het corresponderende hormoon wordt uitgescheiden. We bestuderen daarnaast alle uitgescheiden producten van menselijke enteroendocriene cellen, en vinden hierbij nieuwe hormonen die niet bekend waren in de muisdarm. We hopen dat dit onderzoek ertoe kan leiden tot therapeutische moleculen die specifiek menselijke hormonen kunnen beïnvloeden, wat bruikbaar kan zijn bij suikerziekte of obesitas.

Tot nu toe waren alle organoïde systemen in de literatuur gefocust op zoogdieren, voornamelijk omdat ze als model dienen van menselijke ziekten. In **hoofdstuk 7** gaan we echter de evolutionaire boomstam af, en beschrijven we de eerste organoïde uit reptielen, van een gifklier van de slang. Het was tot dan toe niet bekend of reptielen ook stamcellen bevatten in volwassen organen. Ons systeem laat zien dat reptielen stamcellen bestaan en in veel opzichten lijken op de menselijke varianten. De gifklier organoïden kunnen actieve gifstoffen maken die ook in slangengif aanwezig zijn. Slangengif is een complex mengsel van tientallen soorten moleculen, en we vinden in deze studie dat deze verschillende stoffen niet door één maar verschillende celtypen worden gemaakt. We hebben individuele gifstoffen genetisch kunnen modificeren zodat ze aan een kleur zijn gekoppeld, waarmee dit de eerste erfelijke aanpassing is van slangencellen. Slangengif bevat veel therapeutisch interessante moleculen, en met dergelijke modificaties zouden we individuele gif componenten makkelijker kunnen isoleren of verbeteren. Daarnaast hopen we dat gifklier organoïden kunnen dienen als nieuwe bron om antigif te maken. Ieder jaar sterven meer dan 100.000 mensen aan slangengif, en dit komt deels door slecht werkend antigif.

In het laatste **hoofdstuk 8** worden de implicaties van de voorgaande hoofdstukken beschreven, en deze in de brede context van de literatuur besproken. We bediscussiëren de mogelijkheden van therapeutische interventies op basis van deze ontdekkingen en wat eventuele vervolgstappen zijn.

CURRICULUM VITAE

Joep Beumer was born on the 3rd of October 1992 in Ommen, The Netherlands. In 2010, he graduated from the Gymnasium Ceeleum in Zwolle, following the Nature and Health and Nature and Technology tracks. He continued his studies at the Utrecht University, where he completed the Bachelor Biomedical Sciences (*cum laude*) in 2013. Next, Joep enrolled in the Master Cancer, Stem Cells and Developmental Biology, that he finished in 2015 (*cum laude*). As part of the Master studies, Joep first performed an internship in the Clevers lab in the Hubrecht Institute working on the cell cycle regulation of intestinal stem cells. This exposure to fundamental stem cell research inspired Joep to later return to the Clevers lab for his PhD work. A second Master internship was performed in the lab of Inder Verma, in the Salk Institute in San Diego. Here, he worked on the identification of tumor suppressor genes in lung cancer. In October 2015, Joep started as a PhD student in the laboratory of Hans Clevers. The results of these research projects are presented in this thesis.

I

II

III

IV

V

VI

VII

VIII

&

LIST OF PUBLICATIONS

Basak, O., van de Born, M., Korving, J., **Beumer, J.**, van der Elst, S., van Es, J.H., and Clevers, H. (2014). Mapping early fate determination in Lgr5+ crypt stem cells using a novel Ki67-RFP allele. *EMBO J.* 33, 1–12.

Basak, O.*, **Beumer, J.***, Wiebrands, K.*, Seno, H., van Oudenaarden, A., and Clevers, H. (2017). Induced Quiescence of Lgr5+ Stem Cells in Intestinal Organoids Enables Differentiation of Hormone-Producing Enteroendocrine Cells. *Cell Stem Cell* 20, 177-190.e4.

Beumer, J., and Clevers, H. (2016). Regulation and plasticity of intestinal stem cells during homeostasis and regeneration. *Development* 143, 3639–3649.

Beumer, J., and Clevers, H. (2017). How the Gut Feels, Smells, and Talks. *Cell* 170, 10–11.

Beumer, J., and Clevers, H. (2018). ROCKin' Intestinal Cell Fate: A Potential Avenue to Improve Glucose Sensitivity. *Gastroenterology* 155, 974–976.

Beumer, J., Artegiani, B., Post, Y., Reimann, F., Gribble, F., Nguyen, T.N., Zeng, H., Van den Born, M., Van Es, J.H., and Clevers, H. (2018). Enteroendocrine cells switch hormone expression along the crypt-to-villus BMP signalling gradient. *Nat. Cell Biol.* 20, 909–916.

Gehart, H., van Es, J.H., Hamer, K., **Beumer, J.**, Kretzschmar, K., Dekkers, J.F., Rios, A., and Clevers, H. (2019). Identification of Enteroendocrine Regulators by Real-Time Single-Cell Differentiation Mapping. *Cell* 176, 1158–1173.e16.

Post, Y.*, Puschhof, J.*, **Beumer, J.***, Kerkkamp, H.M., de Bakker, M.A.G., Slagboom, J., de Barbanson, B., Wevers, N.R., Spijkers, X.M., Olivier, T., et al. (2020). Snake Venom Gland Organoids. *Cell* 180, 233–247.e21.

Yeddula, N., Xia, Y., Ke, E., **Beumer, J.**, and Verma, I.M. (2015). Screening for tumor suppressors: Loss of ephrin receptor A2 cooperates with oncogenic KRas in promoting lung adenocarcinoma. *Proc. Natl. Acad. Sci. U. S. A.* 112, E6476-85.

Pleguezuelos-Manzano, C., Puschhof, J., Huber, A.R., van Hoeck, A., Wood, H.M., Nomburg, J., Gurjao, C., Manders, F., Dalmaso, G., Stege, P.B., Paganelli, F.L., Geurts, M.H., **Beumer, J.**, Mizutani, T., Van der Linden, R., Van Elst, S., Genomics England Research Consortium, Top, J., Willems, R.J.L., Giannakis, M., Bonnet, R., Quirke, P., Meyerson, M., Cuppen, E., Van Boxten, R., Clevers, H. (2020). Mutational signature in colorectal cancer caused by genotoxic pks+ *E. coli*. *Nature*.

In press

Artegiani, B.*, Hendriks, D.*, **Beumer, J.**, Kok, R., Zheng, X., Joore, J., Chuva de Sousa Lopes, S., Van Zon, J., Tans, S., and Clevers, H. (2020). Fast and efficient generation of knock-in human organoids using homology-independent CRISPR/Cas9 precision genome editing. *Nat. Cell Biol.*

Battich, N., **Beumer, J.**, De Barbanson, B., Krenning, L., Baron, C., Tanenbaum, M., Clevers, H., and Van Oudenaarden, A. (2020). Sequencing metabolically labeled transcripts in single cells reveals mRNA turnover strategies. *Science.*

Under review

Beumer, J. and Clevers, H. (2020). Roadmap to the intestinal epithelium: cell fate specification and differentiation in the adult intestine. *Nat. Rev. Mol. Cell Biol.*

Beumer, J.*, Gehart, H.* and Clevers, H. (2020). Enteroendocrine dynamics – New tools reveal hormonal plasticity in the gut. *Endocr. Rev.*

Beumer, J.*, Puschhof, J.*, Bauza-Martinez, J.*, Martinez-Silgado, A., Elmentaite, R., James, K.R., Ross, A., Hendriks, D., Artigiani, B., Busslinger, G., Ponsioen, B., Andersson-Rolf, A., Kretschmar, K., Geurts, M.H., Bar-Ephraim, Y.E., Pleguezuelos Manzano, C., Post, Y., Van der Linden, F., Lopez Iglesias, C., Van de Wetering, W.J., Van der Linden, R., Peters, P.J., Heck, A.J.R., Goedhart, J., Snippert, S., Zilbauer, M., Teichmann, S.A., Wu, W., Clevers, H. (2020) High Resolution mRNA and Secretome Atlas of Human Enteroendocrine Cells. *Cell.* (in revision)

Patent

Improved differentiation method

International application number: PCT/EP2017/065101

International publication number: WO2017220586A1

Inventors: Johannes Carolus Clevers, Joep Beumer

Applicants: Koninklijke Nederlandse akademie van Wetenschappen; c/o Hubrecht Institute

I

II

III

IV

V

VI

VII

VIII

&

DANKWOORD

De afgelopen 5 jaar heb ik met ongelooflijk veel plezier gewerkt aan het werk in dit proefschrift, en ik kan me geen dag herinneren dat ik met tegenzin naar het lab kwam. Ik ben trots en vind het een enorm voorrecht dat ik onderdeel mag zijn van zo'n diverse groep mensen die stuk voor stuk excelleren, enorm gedreven en intelligent zijn. Ik ervaaarde het begin van dit traject als een spreekwoordelijk 'voor de leeuwen gooien', maar heb daarna voor mijn gevoel een steile leercurve ondergaan in diverse vaardigheden. Op de eerste plaats in onderzoek doen – proberen zo effectief en pragmatisch mogelijk te worden - maar ook het presenteren en opschrijven daarvan, samenwerken, een hele hoop papers reviewen, review artikelen schrijven, met juristen patenten opstellen, studenten begeleiden en tussen alles af en toe naar congressen gaan. Dit alles was niet mogelijk geweest zonder een hele groep betrokken mensen, die ik hierbij in het bijzonder wil bedanken.

Hans, mijn promotor, veel dank voor de mogelijkheid om onderzoek te mogen doen in jouw lab. Ik heb enorme bewondering hoe je zo'n goed-functionerende machine hebt opgebouwd. Met kleine stuurbewegingen lukt het je onderzoeksprojecten vaak een betere kant op te sturen. Door deze efficiëntie lukt het je het gigantische lab te leiden en daarbij ogenschijnlijk altijd ontspannen en joviaal te zijn. Soms heb je daardoor zelfs tijd over voor de minder belangrijke vragen des levens die je kunt stellen bij een bezoek aan ons kantoor onder het genot van een appel (waar komen die kauwen bij Genmab nou steeds vandaan?). Ik kan me herinneren dat we kort na het begin van mijn PhD een gesprek hadden (met een pils) hoe het zou uitpakken nu het lab zich over zoveel onderwerpen uitspreidde, en niet vooral meer aan de darm werkte. De productiviteit van het lab lijkt er na deze verstrooiing niet minder op geworden, integendeel. Ik heb genoten van de vrijheid die je geeft, en het type onderzoek dat je stimuleert in het lab. Geen hypotheses stellen, snel switchen tussen verschillende onderzoeksvelden waarbij gemeenschappelijke principes en eerder geleerde lessen makkelijk en snel kunt toegepast kunnen worden. En vooral grote vragen proberen te stellen. Ik wil je bedanken dat ik onderdeel mag zijn van dit lab en deze succesformule die je met iedereen hebt gecreëerd, en alle ervaringen die ik hier heb kunnen opdoen.

De leden van mijn leescommissie, Geert Kops, Madelon Maurice, Edward Nieuwenhuis, Eelco de Koning en Hugo Snippert. Heel veel dank voor het lezen en beoordelen van mijn proefschrift.

Jens en Fjodor. Ik ben in mijn noppen met jullie als paranimfen (be careful with Google translate, Jens). Jens' enthousiasme en wilde ideeën, gecombineerd met de realistische en hedonistische inbreng van Fjodor. I want to thank both of you for your support in organizing everything around the defence, but particularly for your useful input during more difficult phases of my PhD. **Jens** – although I recognize your Dutch has greatly improved – please excuse me choosing English vocabulary to avoid any miscommunication or -interpretation. We have shared a lot in the past few years! I am extremely glad having you as friend and collaborator

in multiple projects. Although my efficiency and attention levels are sometimes subjected to rather unpredictable patterns that display parallels to the Dutch weather, you master the art of being productive, organizing work, collaborations and many (!) meetings. I think we enhance each other in different ways, to name one example; thinking outside the box (no, I will not make it more specific than that). I particularly appreciate your humor and childish jokes you are willing to commit to with me, like driving around in the institute sitting on certain chairs. I think the lab would have been a lot less fun without (the memes, another art you control). I am looking forward to work with you on more cool science in the near future, and am very curious to see where these will develop into.

Fjodor, ik vind het erg leuk dat jij halverwege mijn PhD in het lab erbij bent gekomen. Je bent een levensgenieter *pur sang*, of hedonist zoals jij dat noemt, en dat is aanstekelijk in de positieve zin. Ik bewonder je onuitputtelijk enthousiasme en (realistisch) optimisme over experimenten. Je beheerst veel kennis en kunsten die ik bewonder, op het vlak van geneeskunde, maar met name op culinair gebied en in de wijnkunde. De facemerge van jou en Ilja Gort is toepasselijk genoeg denk ik het opus magnum van mijn tijd in het lab. Onze roadtrip in Californië was tot de nok gevuld met hedonistische praktijken en vind ik onvergetelijk. Voortreffelijk eten in overvloed (achteraf had je gelijk, we hadden 4G moeten nemen), af en toe een drankje, goede wandelingen in de nationale parken, net geen verkeersboetes, en tussendoor nog wetenschap. Ik vind het knap hoe je – met in de eerste plaats een achtergrond als arts– snel ontwikkelt in dit lab, je plek hebt gevonden en goede proeven doet. Veel dank dat je mijn paranimf wilt zijn!

Yorick, of Yopo, ik ben heel blij dat ik mijn promotietraject parallel met jou heb kunnen doen, en dat ik je paranimf mag zijn. De meeste mensen in ons vak hebben denk ik wel één of meer eigenaardige trekken die op een bepaalde manier een specifieke handleiding vereist. Ik denk dat jij hier een grote uitzondering op bent. Je bent altijd makkelijk, relaxed en ontspannen, ook wanneer de druk hoger is, en dat maakte dat ik altijd graag je kantoor in liep als ik me verveelde of om gewoon te praten. Ik heb bewondering voor hoe je na een misschien iets lastigere fase in je promotietraject snel de knop hebt omgezet en met een ijzeren discipline een aantal uitermate succesvolle projecten hebt opgetogen. Ik vond het heel gaaf om met je aan de slangenkweken te werken. Alhoewel ik je mis in het lab de afgelopen maanden, ben ik blij dat je nu bij Lina in Californië bent, en ik weet zeker dat je je werk daar ook tot een succes zult maken.

Kim, wij kennen elkaar nu écht inmiddels 10 jaar, een tijd waarin onze wegen geregeld overlapt. Ik ken je in het lab niet anders dan daarbuiten. Altijd enthousiast en gedreven, en een ontzettende drive om diverse zaken te regelen. Hier hoorde het voeden van mensen in het lab bij (dank hiervoor!). Ik vind het knap hoe je verschillende tegenslagen, waaronder fysieke, steeds hebt weerstaan en nu bijna een afgerond proefschrift hebt. Ik wens je het allerbeste met de laatste loodjes en je nieuwe avontuur in Duitsland!

I

II

III

IV

V

VI

VII

VIII

&

Else, ik heb in een brede zin enorme bewondering voor je. Je hebt een erg mooie thesis geproduceerd, terwijl je daarnaast een succesvolle zangcarrière onderhoudt met een grote vriendengroep. Ik vond naar Dekoor gaan altijd een gave ervaring! Daarnaast ben je chronisch ziek, wat geregeld onvoorspelbaar om de hoek kwam. Je hebt - misschien deels hierdoor - een groot vermogen om te relativiseren en in mogelijkheden te denken. Je hebt me met die eigenschappen vaak geholpen. Ik wil je bedanken hiervoor, en voor het feit dat je me op een namiddag onverwacht meenam naar de intervisie sessies. Ik weet zeker dat je met jouw brede set aan kwaliteiten overal succesvol zult zijn en toevoegt, en ik hoop dat onze paden elkaar vaker blijven kruisen.

Adriana, you were the first student I have supervised and I have greatly enjoyed this time! I particularly appreciate your no-nonsense attitude, and your extraordinary talent for graphic arts and presentation of your data. It would be great if we could get a Cell cover! Although you think you are a bit clumsy on the practical side of experiments, I think your eye for detail is also applicable here. Your experiments were always very reliable and reproducible. You have just started as a PhD student in the lab, and I am confident you will do very well.

Yotam, mijn fellow-Ajax-fan. Ik mis je wilde enthousiasme en aanwezigheid. Naar het schijnt ben ik nu de luidste van het lab. De reis naar Korea is mijn meest onvergetelijke vlucht, en we hebben een hoop gelachen in Seoul. Ik wens je het beste bij je huidige werkgever, en ben blij dat je het zo naar je zin hebt nu.

Maarten, beter bekend onder het pseudoniem 'CRISPR-Cas9' Marty. Ik bewonder je kennis en talent omtrent gene editing. Je stelt altijd goede vragen, kiest interessante onderzoeksvelden en voert je experimenten nauwkeurig uit. Als ik iets van jou krijg - van protocol tot plasmid - kan ik er altijd op vertrouwen dat het goed werkte. Ik vind het prettig met je over onderzoek, of onderzoek-gerelateerde zaken, te praten. Je hebt al een mooie paper op zak, en ik wens je het beste met de rest van je promotieonderzoek.

Cayetano, Cayeeeeeeee P.M, you are another reason to visit the other-side-office. I love your endless passion for science, and bacteria in particular. You have already finished a great study, and I think you will do more impressive things during your PhD work. I am looking forward.

Marie, the Breton, I enjoy having you in the lab, and notice that I undertake regular pilgrimages to your office even after Yorick had left. I think you have very nice science going on, and I am curious to see where these will develop to. I wish you all the best finishing these! I admire your pride of Brittany and Brest and believe me, I will definitely visit someday.

The other previous and current PhD students of the lab, Jelte, Carla, Evelyn, Margit, Frans and Luc, I want to thank you all for building such a nice community and environment to work

in. And I would like to particularly express my gratitude for contributions to the outstanding music in the cell culture room! The regular PhD activities and outings were always great fun, and I cherish the memories of Lisbon (also the bad part) and the Ardennes.

Mijn kamergenoten, Benedetta, Kadi, Kai, Delilah, en Lulu. Benedetta, thank you for being a great neighbor throughout my PhD journey – both on the left and right flank. I am still surprised you tolerated me endlessly scrolling through excel sheets. I always value your feedback and contributions to my work, and enjoyed constructing the EEC-NCB paper together with you. Good luck setting up your own lab! Kadi, our Estonian, I wish you the best with finishing your thesis! I appreciate your attentive gestures with birthdays and during the holidays. Kai, I have always been amazed by your endless willingness – taking into account your busy schedule – to help everyone with different things. Thank you for that. I wish you the best in Germany! Delilah, a.k.a. snubbull of een van de wederhelften van CRISPR-HOT, ik ken je nog niet zo lang maar was meteen onder de indruk van je snelheid en gedrevenheid tijdens het werk. Heel veel succes met je projecten! Lulu, I think you are a very nice and gentle person. I am impressed by your progress so far after you have moved to this other side of the globe, I am sure you will be successful during your PhD!

Wim, de nestor, of vader van het lab. Ik bewonder je liefde voor wetenschap en hoe je die onverminderd houdt. Ik vind het altijd prettig om over wetenschap – of persoonlijkere zaken – met je te praten.

Stieneke, moeder van de welpen, jouw aanpak en zorgzame controle over vrijwel alles in het lab zijn essentieel voor het goede functioneren hiervan. Veel dank hiervoor, en je nuchtere kijk op alles waarmee ik langs kon komen.

Amanda, we know each other for quite some time. I very much enjoy sharing our time in the lab in the past years. Your energy and positive attitude are inspiring. I wish you the best with your projects, we will keep in touch.

‘Circadian’ **Marrit,** ik vond het fijn om met je te werken aan twee endocriene organen. Ik zal het circadian experiment nooit vergeten, waarbij we tot 7 uur ’s ochtends op het lab mochten blijven om hormonen te meten. We hebben hier en daar een beetje pech gehad, maar ik vind het achteraf toch erg leerzame projecten!

Johan, ik was al vroeg in mijn studie onder de indruk van al je papers, een hele hoop ‘Van Es et al.’. Je bent denk ik een essentieel tandwiel in het lab met een ongelooflijk scherp oog voor goede uitvoering en conclusies van experimenten. Ik wil je bedanken voor al je hulp met de muizenproeven.

I

II

III

IV

V

VI

VII

VIII

&

Helmuth, thank you for your always critical attitude and questions during labmeetings. I enjoyed writing the enteroendocrine cell review with you. I wish you the best with building your science in your own lab.

Onur, I want to thank you for your supervision during my Master internship in the lab, and your help in the starting months of my PhD.

Annemieke, ik vind je een hele prettige aanwinst in het lab, altijd positief en behulpzaam. Ik denk dat Twitter een erg goed idee van je was!

Litha, heel veel dank voor al je hulp met 'MyPhd' en het herinneren van alle deadlines. Je lach en positieve houding hebben ervoor gezorgd dat ik nooit echt gestrest was met al het papierwerk omtrent het promoveren.

Harry en Jeroen, team histologie. Ik wil jullie erg bedanken voor al jullie hulp met kleuringen, en de onuitputtelijke toevoer van drop die jullie faciliteerden.

All other current and former members of the lab: Carola, Oded, Inha, Norman, Jasper, Aurelia, Charel, Georg, Jarno, Sigrid, Nobuo, Rosie, Janny, Karien, DJ, Mascha, Laura, Robert, Gijs, Mandy, Milou, Jochem, Sylvia, Lena, Huili, Priyanca, Veerle, Anjali, Sepide, Maaïke, Yoshi, Tomo, Dymph, Talya, Dominique, Florijn, Lisanne, Marc, Ana, Sangho, Gui-Wei and Matteo. Thank you all for your help and collectively creating this inspiring and nice working environment.

Julia, Wei and Albert, many thanks for your outstanding contribution to our human enteroendocrine cell paper. Your proteomic experiments have been a very important part of this work! I hope this will be published soon, and that we will stay in touch.

Michael and Merijn, thank you for your essential input on the snake venom gland work. It has been a fun ride! I wish you all the best with your ongoing projects, I am looking forward reading about these.

Matyas en Freek, veel dank voor jullie betrokkenheid bij het slangenwerk. Ik vond DWDD een geweldige ervaring met z'n allen. Ik kijk uit naar het toekomstige werk aan giklier-organoïden!

Reinier, ik vond het altijd leuk om met je te sorten en over van alles en nog wat te praten, zoals vakanties. Ik wil je heel erg bedanken voor al je hulp met het sort-werk.

Feline, we sprongen allebei recht van onze tijd in Amerika naar de PhD, wel een grote overgang. Onze lunches vond ik de afgelopen jaren altijd erg gezellig. Ik wil je bedanken voor al je adviezen en gezelligheid!

Lieve **Anja en Rob**, mama en papa, ik wil jullie bedanken voor alle steun. Ik ben me diep bewust van de geprivilegieerde omstandigheden waarin ik ben opgegroeid en alle mogelijkheden die jullie me hebben geboden. Zonder jullie had ik dit nooit kunnen bereiken. Ik vind het erg jammer dat we elkaar weinig zien en dat dit één van de opofferingen is van het promoveren. Gelukkig compenseerden we dit met onvergetelijke vakanties, zoals naar Sicilië en Amerika, om enkele voorbeelden te noemen. Het doet me een enorm plezier dat jullie de roadtrip-lijn enthousiast doortrekken.

Rik, Tom, Sanne, Eef, Noor, Saar en Milou, bedankt voor jullie betrokkenheid gedurende mijn promotietraject! Ik vind het altijd een geweldige ontspanning om de kinderen weer te zien en samen te spelen.

Familie De Koning en aanhang, Ton, Margreet, Celine, Patrick, Wouter en Laura, ik wil jullie bedanken voor alle gezelligheid en steun, de bereidheid om naar mijn gepraat over wetenschap te luisteren, en voor de onbeperkte mogelijkheid om lekker mee te komen eten. Ton, ik heb bewondering hoe je het wielrennen hebt opgepakt en hoop hier weer wat inspiratie uit op te doen! Misschien meer fietsvakanties?

Lieve **Joyce**, we leerden elkaar kennen vlak voor het begin van de PhD, en je bent snel onmisbaar voor mij geworden. Je liefde en zorgzaamheid, maar ook je weerbaarheid en passie voor sport zijn inspirerend voor me. Mijn excuses voor alle keren dat ik later kwam van het lab dan beloofd. Je had eens een vaste formule die dit benaderde, iets van met twee vermenigvuldigen plus 30 minuten? Ik wil je heel erg bedanken voor al je steun in de afgelopen jaren, en dat je altijd naar de leuke en minder leuke verhalen van het lab wilde luisteren. Ik kijk erg uit naar onze toekomst.

I

II

III

IV

V

VI

VII

VIII

&

